

**GEOMORPHOLOGY AND HYDROLOGY
OF THE COLVILLE RIVER DELTA, ALASKA, 1996**

Fifth Annual Report

Prepared for:
ARCO Alaska, Inc.
Kuukpik Unit Owners
P.O. Box 100360
Anchorage, AK 99510

Prepared by:

M. Torre Jorgenson
Erik R. Pullman
Thomas Zimmer
Yuri Shur
Alice Stickney

ABR, Inc.
P.O. Box 100360
Fairbanks, AK 99708

Shusun Li

Geophysical Institute
University of Alaska Fairbanks
Fairbanks, AK 99755

December 1997

TABLE OF CONTENTS

LIST OF TABLES	iii
LIST OF FIGURES	iii
LIST OF APPENDIX TABLES	vii
LIST OF APPENDIX FIGURES	vii
ACKNOWLEDGMENTS	vii
INTRODUCTION	1
STUDY AREA	1
PART I. FLOOD DISTRIBUTION	4
BACKGROUND	4
METHODS	5
AERIAL PHOTOGRAPHY AND MAPPING	5
RADARSAT IMAGERY	5
RESULTS AND DISCUSSION	8
AERIAL PHOTOGRAPHY AND MAPPING	8
RADARSAT IMAGERY	8
Overall Flood Distribution	8
Comparison of Photography and RADARSAT Imagery	18
Spatial Resolution and Backscatter Differentiation	26
RELATIONSHIP BETWEEN FLOODING AND TERRAIN UNITS	26
PART II. PALEOFLOOD HYDROLOGY	31
BACKGROUND	31
METHODS	32
SAMPLING DESIGN	32
SEDIMENTATION AND DATING	34
Field Methods	34
Laboratory Methods	34
Data Analysis	34
ESTIMATION OF RETURN PERIOD	35
PALEOSTAGE INDICATORS	35
COMPARISON WITH ESTIMATES FROM HYDROLOGIC MODELING	36
RESULTS AND DISCUSSION	36
CHARACTERISTICS OF SURFACE SEDIMENTS	36
SEDIMENT DISTRIBUTION	36
1989 Flooding Event	36
Total Mineral Accumulation	40
Vertical Ranking of Depositional Events	43
Accumulation Rates	43
ESTIMATED RETURN PERIOD FOR THE 1989 FLOOD EVENT	43
ELEVATIONS OF PALEOSTAGE INDICATORS	51
Driftlines	51
Slackwater Deposits	51
COMPARISON WITH ESTIMATES FROM HYDROLOGIC MODELING	57
PART III. SOIL STRATIGRAPHY AND PERMAFROST DEVELOPMENT	62
BACKGROUND	62
METHODS	63
CLASSIFICATION AND MAPPING	63

SOIL STRATIGRAPHY	64
RESULTS AND DISCUSSION	66
CLASSIFICATION AND MAPPING	66
Lithofacies	66
Ice Structures	66
Terrain Units	75
Relationships Among Terrain Components	75
SEDIMENT CHARACTERISTICS	91
Particle Size	91
Salinity	96
Thaw Depths	96
Ice Accumulation	96
Overall Accumulation Rates	105
CONCEPTUAL MODEL OF FLOODPLAIN EVOLUTION ON THE DELTA	105
Accumulation of Deltaic Deposits	105
Permafrost Development and Thaw Stability on Deltaic Floodplains	108
Delta Riverbed/Riverbar Deposits	108
Delta Active-floodplain Cover Deposits	108
Delta Inactive-floodplain Cover Deposits	110
Delta Abandoned-floodplain Cover Deposits	111
Delta Thaw Basin Deposits	111
External Factors	111
Implications for Development	112
PART IV. DRAINAGE NETWORK	113
BACKGROUND	113
METHODS	113
RESULTS AND DISCUSSION	113
PART V. DIGITAL ELEVATION MODEL USING SATELLITE RADAR DATA	117
BACKGROUND	117
METHODS	117
PRELIMINARY IMAGE PROCESSING	117
ASSESSMENT OF POTENTIAL ACCURACY	118
RESULTS AND DISCUSSION	118
SUMMARY AND CONCLUSIONS	124
FLOOD DISTRIBUTION	124
PALEOFLOOD HYDROLOGY	124
SOIL STRATIGRAPHY AND PERMAFROST DEVELOPMENT	124
DRAINAGE NETWORK	125
DIGITAL ELEVATION MODEL	125
LITERATURE CITED	126
APPENDICES	132

LIST OF TABLES

Table 1-1.	Summary of breakup data at the head of the Colville River Delta, 1962-1996.	9
Table 2-1.	Estimates of recurrence interval of 1989 flood event based on dating and ranking of flood events evident in soil profiles, Colville River Delta, Alaska, 1996. NP=not present.	49
Table 2-2.	Elevations and quality of driftlines related to the 1989 flood, Colville River Delta, Alaska. Measurements taken between 1992 and 1996. See Figure 2-12 for locations of driftlines surveyed.	52
Table 2-3.	Occurrence and description of slackwater deposits related to the 1989 flood, above or below driftlines near the Alpine development area, Colville River Delta, Alaska, 1996.	58
Table 3-1.	Classification and description of lithofacies observed in the Colville River Delta and adjacent coastal plain, Alaska, 1996. Structures less < 4 in. (10 cm) thick are not identified.	67
Table 3-2.	Description of terms used for classifying ground ice on the Colville River Delta, Alaska, 1996.	69
Table 3-3.	Descriptions of terrain units found within the Colville River Delta and adjacent coastal plain, Alaska, 1996.	76
Table 4-1.	Descriptions of stream orders for the drainage network in the Transportation Corridor adjacent to the Colville River Delta, 1996.	114

LIST OF FIGURES

Figure S-1.	Map of the area affected by the proposed Alpine Development, including the Facilities Area, Development Area, Transportation Corridor and the perimeter of the Colville River Delta, Alaska, 1996.	3
Figure 1-1.	Map of flooding study areas and flooding regions, Colville River Delta, Alaska, 1996.	6
Figure 1-2.	Percentage of total area covered by floodwater in five study areas in the Colville River Delta, Alaska, 1992-1996.	10
Figure 1-3.	Map of flood distribution in the Itkillik study area, Colville River Delta, Alaska, 1992-1996.	11
Figure 1-4.	Map of flood distribution in the Alpine study area, Colville River Delta, Alaska, 1992-1996.	12
Figure 1-5.	Map of flood distribution in the Tamayayak study area, Colville River Delta, Alaska, 1992-1996.	13
Figure 1-6.	Map of flood distribution in the Kupiguak study area, Colville River Delta, Alaska, 1992-1993.	14
Figure 1-7.	Map of flood distribution in the Cechelik study area, Colville River Delta, Alaska, 1992-1993.	15
Figure 1-8.	Map of flood distribution on 30 May 1943, Colville River Delta, Alaska.	16
Figure 1-9.	Flood distribution in early June 1971, Colville River Delta.	17
Figure 1-10.	RADARSAT Image of flood distribution within the alpine development area, 19 May 1996.	19
Figure 1-11.	RADARSAT image (standard-resolution) of flood distribution within the Alpine development area on 20 May 1996.	20
Figure 1-12.	RADARSAT image of flood distribution within the Alpine development area, 27 May 1996.	21

Figure 1-13.	Flood distribution visually delineated from 27 May RADARSAT IMAGERY, Colville River Delta, 1996.	22
Figure 1-14.	Flooding in the Alpine study area: RADARSAT and oblique methods.	23
Figure 1-15.	Percent agreement (top) and difference (bottom) in the distribution of floodwater within the Alpine area delineated from RADARSAT imagery acquired on 19 May (Fine-resolution image) and 27 May (standard-resolution image) 1996 when compared to mapping derived from oblique aerial photography, Colville River Delta, Alaska. A positive relative difference indicates more floodwater was mapped from RADARSAT imagery.	24
Figure 1-16.	Changes in flood stage at the head of the delta (Cross-section E27.09) in relation to times when RADARSAT imagery and oblique aerial photography were acquired in 1996, Colville River Delta, Alaska.	25
Figure 1-17.	Frequency of occurrence (%) of backscatter values for floodwater and nonflooded tundra for fine- (top) and standard- (bottom) resolutions of RADARSAT imagery used to map flooding on the Colville River Delta, Alaska, 1996.	27
Figure 1-18.	Percentage of each terrain unit covered by flooding in five study areas in the Colville River Delta, Alaska, 1992-1995.	29
Figure 1-19.	Relationship between percent area flooded and peak discharges (top) and stage (below) for the major terrain units, Colville River Delta, Alaska, 1992-1996.	30
Figure 2-1.	Map of locations of surface-sediments transects, Colville River Delta, Alaska, 1996.	33
Figure 2-2.	Photographs of soil profiles (with sample ID) at six distances away from the river bank at Transects 1 and 9, Colville River Delta, Alaska, 1996. Lines between photographs indicate the location of different flood events along the length of a transect.	37
Figure 2-3.	Relative composition (%) of sand, silt, and clay particles relative to distance from the riverbank within two terrain units, Colville River Delta, Alaska, 1996.	39
Figure 2-4.	Mean (+95% confidence interval) thickness of sediments deposited by the 1989 flood relative to distance from riverbank, terrain unit, and flood region, Colville River Delta, Alaska, 1996.	41
Figure 2-5.	Mean (+95% confidence interval) thickness of mineral sediments within the top 1 ft relative to distance from riverbank, terrain unit, and flood region, Colville River Delta, Alaska, 1996.	42
Figure 2-6.	Mean (+95% confidence interval) relative rank of 1989 sediment deposit relative to distance from riverbank, terrain unit and flood region, Colville River Delta, Alaska, 1996.	44
Figure 2-7.	Photographs of selected soil profiles with conventional radiocarbon dates from inactive- and abandoned-floodplain cover deposits, Colville River Delta, Alaska, 1996.	45
Figure 2-8.	Mean (+95% confidence interval) rates of sediment accumulation (mineral and organic) between inactive- and abandoned-floodplain cover deposits, Colville River Delta, Alaska, 1996.	47
Figure 2-9.	Estimated recurrence interval of 1989 flood within inactive- and abandoned- floodplain cover deposits, based on years to next larger event, ranking of depositional layers, and conservative ranking of layers, Colville River Delta, Alaska, 1996.	50
Figure 2-10.	Photographs of typical driftwood material associated with the 1989 flood before (top) and after (bottom) removal from moss mat, Colville River Delta, Alaska, 1996.	53
Figure 2-11.	Cross-sectional profile (with 1989 driftline) of Transect 19, located along the Sagoonang Channel, within the Alpine Development Area, Colville River Delta, Alaska, 1996.	55
Figure 2-12.	The locations and elevations (ft) surveyed driftlines that were associated with 1989 flood, Colville River Delta, Alaska, 1996.	56

Figure 2-13.	Photographs of soil profiles (with sample ID's) below and above driftlines associated with the 1989 flood near the proposed Alpine Facilities Area, Colville River Delta, Alaska, 1996.	59
Figure 2-14.	Mean elevations (\pm SD) of the highest slackwater deposits, the lowest sites where slackwater deposits were absent, and of driftlines associated with the 1989 flood (top graph) and the difference in elevations between the driftlines and where slackwater deposits were present (highest observed along transect) or absent (lowest point not observed)(bottom graph) within the Alpine Development Area, Colville River Delta, Alaska, 1996.	61
Figure 3-1.	Map of soil sampling locations in 1992, 1995, and 1996.	65
Figure 3-2.	Photographs of simple ice structures found in soils in the Colville River Delta, Alaska, 1996.	71
Figure 3-3.	Photographs of common composite ice structures found in soils in the Colville River Delta, Alaska, 1996.	73
Figure 3-4.	Photographs of typical depositional environments associated with lateral accretion deposits on riverbars (upper left), active-floodplain cover deposit (upper right), inactive-floodplain cover deposit (middle left), abandoned floodplain cover deposit (middle right), sand dunes (lower left), delta thaw lake deposits (lower right), Colville River Delta, Alaska, 1996.	79
Figure 3-5.	Map of the distribution of terrain units in the Colville River Delta and adjacent Transportation Corridor, Alaska, 1996.	81
Figure 3-6.	Representative soil profiles showing lithofacies and ice structures associated with six terrain units, Colville River Delta, 1996.	83
Figure 3-7.	Soil stratigraphy along a terrain sequence (Transect 12) along the upper Nechelik Channel, Colville River Delta, 1996.	84
Figure 3-8.	Soil Stratigraphy along a terrain sequence (Cross-section N7.46, 312) along the middle Nechelik Channel, Colville River Delta, 1996.	85
Figure 3-9.	Soil stratigraphy along a terrain sequence (Transect 13) along upper Sakoonang Channel, Colville River Delta, 1996.	86
Figure 3-10.	Soil stratigraphy along a terrain sequence (Cross-section S9.80, #11) along the middle Sakoonang Channel, Colville River Delta, 1996.	87
Figure 3-11.	Soil stratigraphy along a terrain sequence (Transect 19) along the middle Sakoonang Channel, Colville River Delta, 1996.	88
Figure 3-12.	Soil stratigraphy along a terrain sequence (Transect 18) along the East Channel, along the East Channel, Colville River Delta, 1996.	89
Figure 3-13.	Frequency of occurrence (% of total core length) of ice structures by lithofacies (top) and map terrain unit for profiles that extend down to riverbed/riverbar sediments (below) of the Colville River Delta, 1996.	90
Figure 3-14a.	Frequency of occurrence (% of observations) of ice structures by map terrain unit within a lithofacies allowing comparison of how structures change over time, Colville River Delta, 1996.	92
Figure 3-14b.	Mean (+ SD) relative elevations (relative to surface of inactive floodplain) or ice structures for terrain units (top) and within inactive-floodplain cover deposits, Colville River Delta, 1996.	93
Figure 3-15.	Mean (\pm SD) percentages of sand, silt, and clay of sediments associated with various lithofacies (top) and strata terrain units (bottom) on the Colville River Delta, 1996.	94

Figure 3-16.	Mean (\pm SD) thickness of the surface organic horizon and cumulative thickness of organic (organic and organic-mineral combined) layers in top 1 ft (right) for soils associated with various surface terrain units on the Colville River Delta and the adjacent Transportation Corridor, 1996.	95
Figure 3-17.	Mean (+ SD) salinity (electrical conductivity) values for sediments associated with various lithofacies and stratigraphic terrain units on the Colville River Delta and the adjacent coastal plain, Alaska, 1996.	97
Figure 3-18.	Mean (\pm SD) active-layer depths for various surface terrain units on the Colville River Delta and the adjacent Transportation Corridor, Alaska, 1996.	98
Figure 3-19.	Mean (+ SD) volumetric ice contents in near surface sediments grouped by lithofacies and surface terrain unit, Colville River Delta, Alaska, 1996.	99
Figure 3-20.	Mean (+ SD) volumetric ice contents in near surface sediments grouped by composite and primary (dominant structure within composite) ice/structures, Colville River Delta, Alaska, 1996.	100
Figure 3-21.	Volumetric ice contents by depth within stratigraphic terrain units (upper four graphs) and mean (+ SD) contents summarized by depth (lower left), Colville River Delta, 1995.	101
Figure 3-22.	Aerial photographs of development of ice-wedge polygons associated with nonpatterned (upper left), disjunct polygons (upper right), low-density polygons (lower left), and high-density polygons (lower right), Colville River Delta, Alaska, 1996.	103
Figure 3-23.	Mean (+ SD) density of ice wedges (top graph), mean polygon size (middle graph), and estimated percent of the volume of the top 7ft. of permafrost occupied by ice wedges (bottom graph), Colville River Delta, Alaska, 1996.	106
Figure 3-24.	Mean (+SD) rates of accumulation of material (sediments, organics, and ice) for various surface terrain units on the Colville River Delta, 1996.	107
Figure 3-25.	Relative importance of the processes of fluvial and eolian deposition, and organic matter and ice accumulation in common floodplain deposits on the Colville River Delta, 1996.	107
Figure 3-26.	A conceptual model of changes in lithofacies, ice structures, and active-layer thicknesses during evolution of floodplain deposits on the Colville River Delta, Alaska, 1996.	109
Figure 4-1.	Drainage network for the Transportation Corridor, 1996.	115
Figure 5-1.	Image processing steps utilized for generation of digital elevation model (DEM) from synthetic aperture radar images.	119
Figure 5-2.	Interferogram of ERS-SAR images of the Alpine Development Area, Colville River Delta, 1996.	120
Figure 5-3.	Comparison of ground elevations with interferogram index values generated from synthetic aperture radar imagery along Cross-sections 11, 12, and 14, Colville River Delta, Alaska, 1996.	121
Figure 5-4.	Comparison of ground elevations with interferogram index values generated from synthetic aperture imagery along two Cross-sections 1 and 6, Colville River Delta, 1996.	122

LIST OF APPENDIX TABLES

Appendix Table A-1.	Data file listing for geodetic control points on the Colville River Delta, Alaska, 1996.	133
Appendix Table B-1.	Data file listings for soil profile and SIPRE core locations along sediment transects, Colville River Delta, Alaska, 1996.	136
Appendix Table B-2.	Results from multi-factor analysis of variance for 1989 flood deposits, Colville River Delta, Alaska, 1996	140
Appendix Table B-3.	Results from multi-factor analysis of variance for total mineral accumulation, Colville River Delta, Alaska, 1996.	140
Appendix Table B-4.	Results from a multi-factor analysis of variance for ranking of flood deposits, Colville River Delta, 1996.	141
Appendix Table B-5.	Data file listing for samples with radiocarbon aging, Colville River Delta, 1996.	142
Appendix Table C-1.	System for classifying ground ice structures observed on the Colville River Delta, 1996.	146
Appendix Table C-2.	Integrated terrain units for ecological land classification system of the Colville River Delta, 1996.	148

LIST OF APPENDIX FIGURES

Appendix Figure A-1.	Location of geodetic control monuments, Colville River Delta, Alaska, 1996.	135
Appendix Figure B-1.	Profiles of vertical sediment distribution along Transect S1, Colville River Delta, Alaska, 1996.	143
Appendix Figure B-2.	Profiles of vertical sediment distribution along Transect S3, Colville River Delta, Alaska, 1996.	144
Appendix Figure B-3.	Profiles of vertical sediment distribution along Transect S5, Colville River Delta, Alaska, 1996.	145

ACKNOWLEDGMENTS

We acknowledge the many participants who contributed to this project. The project was funded by ARCO, Alaska, Inc., and the Kuukpik Unit Owners and was managed by Stan Pavlos, Senior Project Engineer for ARCO. We also thank Mike Joyce, Senior Consultant Biological Sciences, ARCO, for his interest and guidance in this project early on. Numerous individuals helped with the fieldwork. Mark Prins, of Imanda Placer, helped with soil coring. Many villagers in Nuiqsut also contributed to this study. Jobe Woods performed ably as a boatman during long days. Lanston Chinn, Manager of Kuukpik Corporation, helped arrange field personnel and contractual arrangements. Numerous people from ABR contributed to this study: Tom DeLong and George Zusi-Cobb helped with field logistics and coordinated services provided by Kuukpik Corporation. Allison Zusi-Cob, Will Lentz, and Mike Smith helped with GIS analysis. Stephen Murphy provided editorial review, and Devonee Harshburger and Cecilia Barkley provided clerical work.

INTRODUCTION

The Colville River drains ~29% of the North Slope of Alaska and its delta is the largest in arctic Alaska. The river's volume and heavy sediment load produces a dynamic deltaic system with diverse geomorphic, hydrologic, and ecological systems. In recognition of these characteristics and in preparation for oil development on the Colville River Delta, ARCO Alaska, Inc. (ARCO), and the Kuukpik Unit Owners, contracted ABR, Inc. to conduct both this study on geomorphology and hydrology and a companion study on wildlife and their habitats. The geomorphology and hydrology studies were designed to provide essential information for designing bridge and pipeline crossings and for locating roads and pads to minimize problems associated with flooding and terrain stability. The studies mainly focused on the delta, but also included some work in the proposed Transportation Corridor.

The remarkable environment of the delta has been the subject of numerous studies conducted over the last four decades. Most information on the geomorphology and hydrology of the delta was gathered by H. J. Walker and his associates during the 1960s and 1970s (Walker 1983a). Other important studies on the geomorphology of the delta and nearby coast have been done by Carter and Galloway (1982, 1985), Reimnitz et al. (1985), and Rawlinson (1993). In addition, several major multi-disciplinary research efforts have been conducted, including a study of nearshore aquatic and marine environments by the University of Alaska (UAF 1972), the investigation of the coast and shelf of the Beaufort Sea by numerous organizations during the early 1970s (Reed and Sater 1974), and numerous studies conducted under the Outer Continental Shelf Environmental Assessment Program of the National Oceanic and Atmospheric Administration. Pertinent information from these and other studies are included in the background portions of each section of this report.

This report contributes to this information by providing results from the fifth year of our investigation of the geomorphology and hydrology of the delta. The data collected each year were intended to provide a long-term database upon which detailed engineering and facility planning analyses could be made. In 1992, this project investigated the geometry of selected channels, mapped the distribution of terrain units, analyzed the flooding regime, and quantified the rate of landscape change (Jorgenson et al. 1993). In 1993, the

project was limited to measuring peak discharge after snowmelt and mapping the distribution of floodwater within five small study areas (Jorgenson et al. 1994a). In 1994, only spring breakup was monitored (Jorgenson et al. 1994b). In 1995, an expanded effort included a wide range of studies that investigated channel geometry within the delta and offshore, analyzed the flooding regime, mapped drainage networks for route alignment and oil spill contingency planning, evaluated soil and permafrost development, quantified the rate of landscape change over a broader area, and generated a satellite image base map for engineering and environmental studies (Jorgenson et al. 1996).

In 1996, we continued many of these studies, although the channel assessment, analysis of flood frequency, and monitoring of spring breakup were split off into separate studies (Shannon and Wilson 1996a, 1996b, 1996c). This report is divided into five parts and focuses on work conducted by ABR, Inc. In Part I, we focus on monitoring the distribution of floodwater during spring breakup to provide information for facility design, and we evaluate the use of satellite radar imagery for mapping floodwater. In Part II, we present results from the paleohydrologic assessment of past flooding to provide information for the development of flood-design criteria. In Part III, we synthesize information collected on soil stratigraphy and permafrost development that is needed to aid geotechnical design, evaluate terrain stability, and analyze ecosystem development. In Part IV, we update the drainage network map developed for facility alignment and oil spill contingency planning by completing the network of drainages downstream of the Transportation Corridor. Finally, in Part V, we evaluate an experimental approach to developing of a digital elevation model using satellite radar imagery.

STUDY AREA

This study focuses on the Colville River Delta and the proposed Transportation Corridor (hereafter referred to as the Transportation Corridor) adjacent to the delta (Figure S-1). Current plans for oil development on the delta include a road and two drill sites within the proposed Development Area (hereafter referred to as the Development Area) and a pipeline to the Kuparuk Oilfield. Various alternative development

scenarios also are being considered, although the preferred ARCO alternative is depicted and discussed here (Parametrix 1996). The village of Nuiqsut, established in 1971, is near the head of the delta.

The Colville River is the largest river on Alaska's North Slope and is one of eight major rivers with significant freshwater input to the Arctic Ocean (Walker 1983a). The Colville enters the Beaufort Sea just west of the Kuparuk Oilfield and midway between Barrow and Kaktovik. The Colville River drains about 20,700 mi² (29%) of the North Slope. Most of the watershed is situated in the foothills (64%), with smaller amounts situated in the Brooks Range (26%) and coastal plain (10%, Walker 1976). The head of the delta is located about 2 mi upstream from the mouth of the Itkillik River (Arnborg et al. 1966). Below the Itkillik River, the area encompassed by the floodplain of the delta and water within the fringe of the delta covers 257 mi².

The delta is bounded on both sides by old alluvial terraces that are traceable from the coast to above the Itkillik River (Carter and Galloway 1982). Fossil wood collected at the base of exposures yielded ages of 48,000–50,600 ybp, suggesting that the terraces and underlying deposits of gravelly sand were formed during the last interglacial period (Carter and Galloway 1982). These deposits are part of the Gubik Formation (Black 1964, Carter et al. 1977), a series of unconsolidated deposits that record a complex marine and alluvial history spanning ~3.5 million years (Carter et al. 1986). Modern sandy deltaic sediments in the delta generally range from 15–30 ft below sea level and are underlain by 20–40 ft of gravelly riverbed material (glaciofluvial outwash) and 60 or more ft of interbedded silts, clays, and organics indicative of marine or deltaic sediments associated with the Gubik Formation (Miller and Phillips 1996). Sand dunes are common throughout the delta (Walker 1983). The surficial geology of the central Arctic Coastal Plain has been mapped (1:63,360 scale) by Rawlinson (1993).

The delta has two main distributaries, the Nechelik (western) Channel and the Colville East Channel (Figure S-1). These two channels carry about 90% of the water through the delta during flooding and 99% during low water (Walker 1983a). Smaller channels branching from the East Channel include the Sakoonang, Tamayayak, and Elaktoveach channels. The delta also is characterized by numerous lakes and

ponds, riverbars, mud flats, sand dunes, and low- and high-centered polygons (Walker 1976). Most water bodies are shallow (<6 ft deep) ponds that freeze to the bottom in winter and thaw by June. Larger lakes typically are deeper (up to 33 ft) and freeze only in the upper 6 ft.

The delta study area has a typical arctic maritime climate. Winters last about eight months and are generally cold and windy. Summers are cool, with temperatures ranging from 12° F in mid-May to 60° F in July and August (Simpson et al. 1982); summers also are characterized by low precipitation, overcast skies, fog, and persistent winds from the northeast. Occasional northwesterly winds usually bring storms, with high, wind-driven tides and rain (Walker and Morgan 1964).

Integrated-terrain-unit maps (based on 1:18,000-scale photography) that classified and delineated terrain units, surface-forms, and vegetation components of the landscape were produced for the delta by Jorgenson et al. (1993) and revised in 1995 (Jorgenson et al. 1996). In addition, land-cover maps (1:30,000 scale) of the delta have been generated by the U.S. Fish and Wildlife Service (USFWS) (Rothe et al. 1983). Wetlands (1:63,360 scale) classified under the National Wetlands Inventory system also have been mapped by the USFWS. The North Slope Borough has mapped the delta for vegetation, surface form, and landforms (1:250,000 scale). Vegetation-soil-landform associations have been described for the Prudhoe Bay region (Walker et al. 1980).

The delta has been long recognized as one of the most productive deltas for fish and wildlife on the Arctic Coast of Alaska (Gilliam and Lent 1982, Divoky 1983). The area is important for Tundra Swans, Brant, Yellow-billed Loons, and Greater White-fronted Geese and a variety of other migratory birds (Rothe et al. 1983, Johnson et al. 1996). Arctic and least cisco overwinter in the delta and support the only commercial fishery on the North Slope (NOAA/OCSEAP 1983, Moulton 1996). Caribou from both the Central Arctic Herd and the Teshekpuk Herd use the delta (Gilliam and Lent 1982). Finally, the area's resources are important to the subsistence economy of the Nuiqsut villagers.

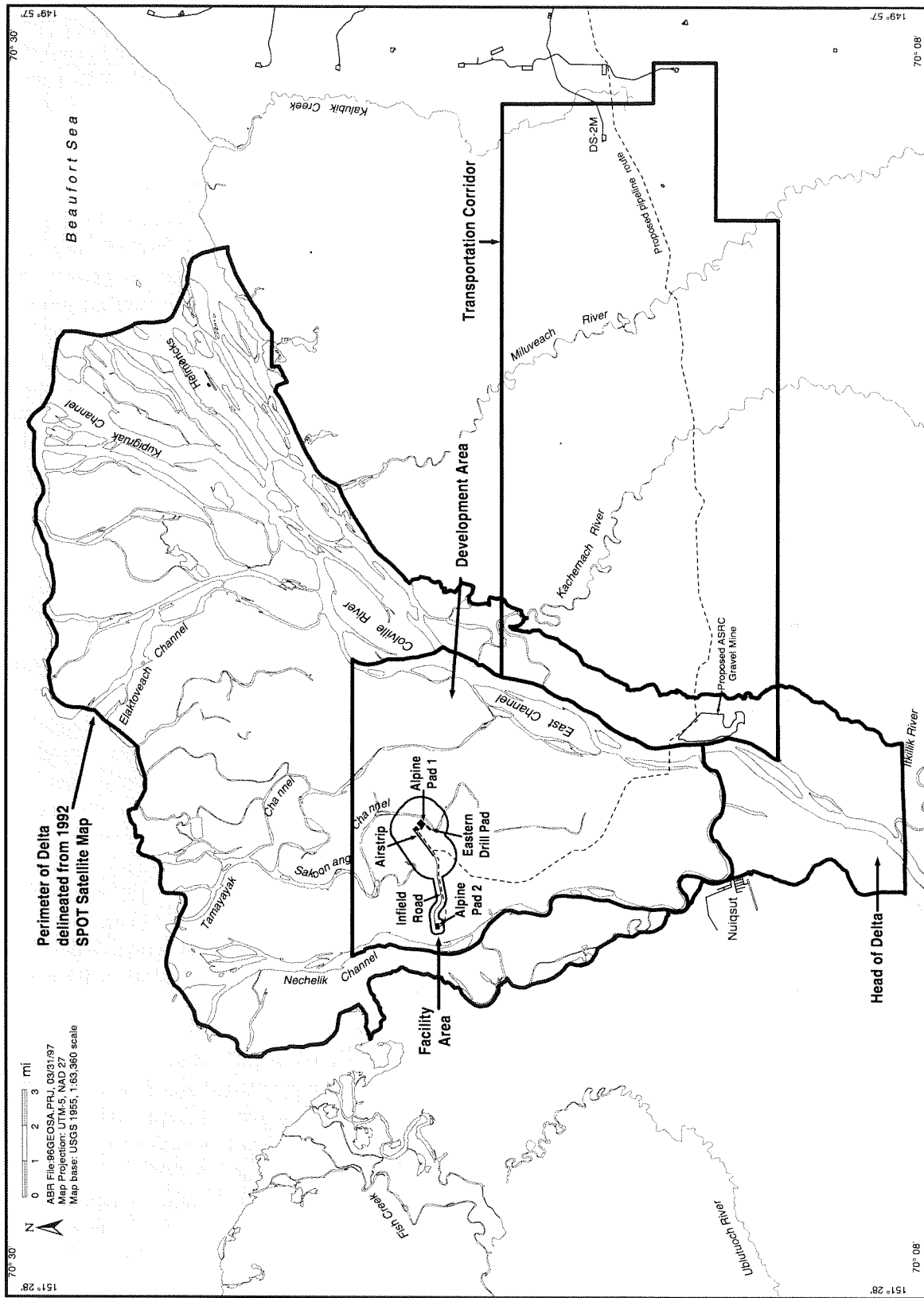


Figure S-1. Map of the area affected by the proposed Alpine Development, including the Facilities Area, Development Area, Transportation Corridor and the perimeter of the Colville River Delta, Alaska, 1996.

PART I. FLOOD DISTRIBUTION

BACKGROUND

The distribution of floodwater during spring breakup was monitored within small, representative study areas on the Colville River Delta from 1992 to 1996, and over the entire delta in 1996. This information was used to delineate the extent of annual flooding and to analyze the patterns of flooding across the delta. Such information will aid in siting oilfield facilities to avoid frequently flooded areas and the obstruction of floodwater.

Despite the numerous geomorphic studies conducted on the delta, few data are available to characterize the magnitude and distribution of flooding. The record of discharge measurements is short, particularly at the head of the delta. Arnborg et al. (1966, 1967) collected stage-discharge information in 1962, as did the U. S. Geological Survey (USGS 1978) in 1977. The USGS also collected selected discharge measurements in 1979, 1980, and 1981 (USGS 1980, 1981, 1982). Discharge measurements were made during 1992–1995 by Jorgenson et al. (1996) and in 1996 by Shannon and Wilson (1996a). Small-scale maps of the distribution of floodwater across the delta in 1943 and 1971 were developed by Walker (1974). Relative frequencies of flooding have been mapped on a small scale for the delta by using geomorphic characteristics to delineate active and inactive portions of the floodplain (Cannon and Rawlinson 1981, Cannon and Mortensen 1982). However, those maps were not sufficiently detailed to be useful to this project.

To improve the analysis of flood distribution, we monitored the floodwaters near peak stage during breakup using oblique photography taken from small aircraft during the years 1992–1996. Due to the large area of the delta, the photography and subsequent mapping were limited to small study areas representative of different portions of the delta. These study areas have changed over the years, however, as the oil reservoir underlying the delta was delineated. Initially, oil exploration focused on the outer delta, whereas subsequent exploration and development planning has focused on the central delta.

In 1996, we also evaluated the use of synthetic aperture radar (SAR) imagery to map flooding because it is not affected by cloud cover, can be acquired al-

most daily, and avoids the safety risks associated with obtaining aerial photography under poor weather conditions. We obtained imagery acquired by RADARSAT International, Inc., Richmond, BC (hereafter referred to as RADARSAT imagery) using a newly deployed Canadian satellite specifically designed for monitoring ice conditions in the polar region. RADARSAT became fully operational on 23 May 1996 and has been used as a tool for imaging sea ice, flooding events, and geological features. The high resolution of the images and the ability to acquire images daily make this method attractive for monitoring time-sensitive events such as breakup on the Colville Delta. Previous studies have shown SAR imagery to be useful for a variety of hydrologic and climatic studies, including flood monitoring on the MacKenzie River Delta (Searcy et al. 1995), classifying lake depths on the North Slope (Mellor 1983), and monitoring freeze-thaw cycles in soil (Rignot and Way 1994). We evaluated the accuracy of flood-distribution maps produced from RADARSAT imagery by comparing them with maps produced from oblique aerial photography taken within 12 hours or less of the acquired image.

Because the delta is virtually flat with only small changes in topography, our analyses of flood distribution have focused on determining relationships between flooding and terrain units rather than actual elevations. High-resolution (e.g., 2-ft interval) contour mapping has not been done across the entire delta and, may not be adequate for delineating small differences in floodplain steps that effect distribution of floodwater at high-flood stages. Instead, we analyzed flood distribution relative to terrain units because they reflect environments that differ in sediment deposition and in relative heights above the surface of the river. Information on the frequency of flooding among various terrain units is useful for planning facility locations in areas least prone to flooding.

As this study has progressed, geodetic control for our spatial data have changed. Initially, vertical control was obtained from a few U.S. Coast and Geodetic Survey (USCGS) monuments. In 1995, a limited set of temporary benchmarks was established using GPS technology and referenced to the USCGS monument "River" (Loundsbury and Associates, Inc. 1995). In 1996, more monuments were established, which were horizontally referenced to USCGS monument "Bite"

(western Colville River Delta) and “Maxie” (west portion of Kuparuk oilfield) and vertically referenced to the British Petroleum Mean Sea Level datum (BPMSL). When possible, we report elevation using the BPMSL datum (Appendix Table A-1).

METHODS

AERIAL PHOTOGRAPHY AND MAPPING

Mapping of flood distribution within five small study areas on the delta was conducted annually during 1992–1996 (Figure 1–1). The study areas changed over the years as oil exploration activities were redirected during that period. Aerial photography and mapping methods were similar for all years. Oblique photographs were taken with a 35-mm camera using true-color film, from a small fixed-wing aircraft (Cessna 185) flown at 500–700 ft above ground level (agl), or just below the lowest cloud layer. Minor modifications were sometimes necessary, depending on the effects of weather on our aerial photo flights. Specific details for each year are provided below.

In 1992, the extent of floodwater coverage of three study areas (Nechelik, Tamayayak, and Kupigruak) was mapped using aerial photographs taken on 4 and 8 June. Oblique photographs were taken on 4 June, two days after peak stage occurred at the head of the delta. On 8 June, when weather improved, vertical color photographs (1:17,000 scale) were taken at 11,000 ft agl with a large-format camera (6 x 7-cm Pentax). Complete photographic coverage of all study areas was obtained on this flight.

In 1993, oblique aerial photographs of four study areas (Tamayayak, Kupigruak, Kachemach, and Itkillik) were obtained on 1 June and a fifth study area (Nechelik) was photographed on 2 June. Thus, most of the photography was acquired one day after peak stage occurred at the head of the delta. Because of poor weather, vertical photographs could not be obtained with the large-format camera. The photography obtained that year was incomplete (approximately 20–30% of each study area), because of lack of overlapping coverage between flight lines. Flooding was estimated in each study area by interpolating floodwater extent along terrain boundaries across unphotographed section of flight lines.

In 1994, oblique aerial photography was obtained only for the Itkillik area because of reduced monitoring efforts that year. Photographs were taken on 25 May, the day of peak stage. In 1995, oblique aerial photography was obtained for the Itkillik, Alpine, and Tamayayak areas on 16 May, the day of peak stage. No vertical photographs were taken in either year.

In 1996, oblique aerial photography was obtained for the Alpine area on 20 May and for the Itkillik, Alpine, and Tamayayak study areas on 28 May. Peak stage occurred on 26 May, two days before aerial photography.

For each year, we examined oblique photographs to determine the extent of flooding in the study areas, which then was delineated on vertical color-infrared photography (1:18,000 scale) by referencing identifiable landmarks (e.g., riverbanks, polygonal rims). Floodwater appeared light brown in color, due to the presence of suspended sediments, whereas standing water from snowmelt in depressions and ponds typically appeared clear or black. Ice-covered lakes and channels that were partially flooded were mapped as entirely flooded because we assumed that floodwater was present under the ice. In 1992, 1994, 1995, and 1996, floodwater in the study areas was mapped entirely from the oblique aerial photography. In 1993, flood distribution was mapped in two phases because of the incomplete photographic coverage. First, the extent of floodwater was delineated within those areas covered by the aerial photography. Then, the distribution of floodwaters in the intervening gaps was interpolated along integrated-terrain-unit (ITU) boundaries. The lines were digitized with a geographic information system (*AtlasGIS*, San Jose, CA) and were rectified to the ITU map initially produced in 1992 and later revised in 1995.

RADARSAT IMAGERY

In 1996, SAR imagery was acquired by RADARSAT for the entire delta on 19 May, 20 May, and 27 May. The high-resolution image acquired on 19 May (17:42 AST) had an effective pixel size of 8 m (fine beam mode) and incidence angle of 47°. The standard-resolution images acquired on 20 May (20:13 AST) and 27 May (17:09 AST) had an effective pixel resolution of 27 m (standard beam mode) and incidence angles of 36° and 39°, respectively. Images were rectified individually using control points from the

PART I. Flood Distribution

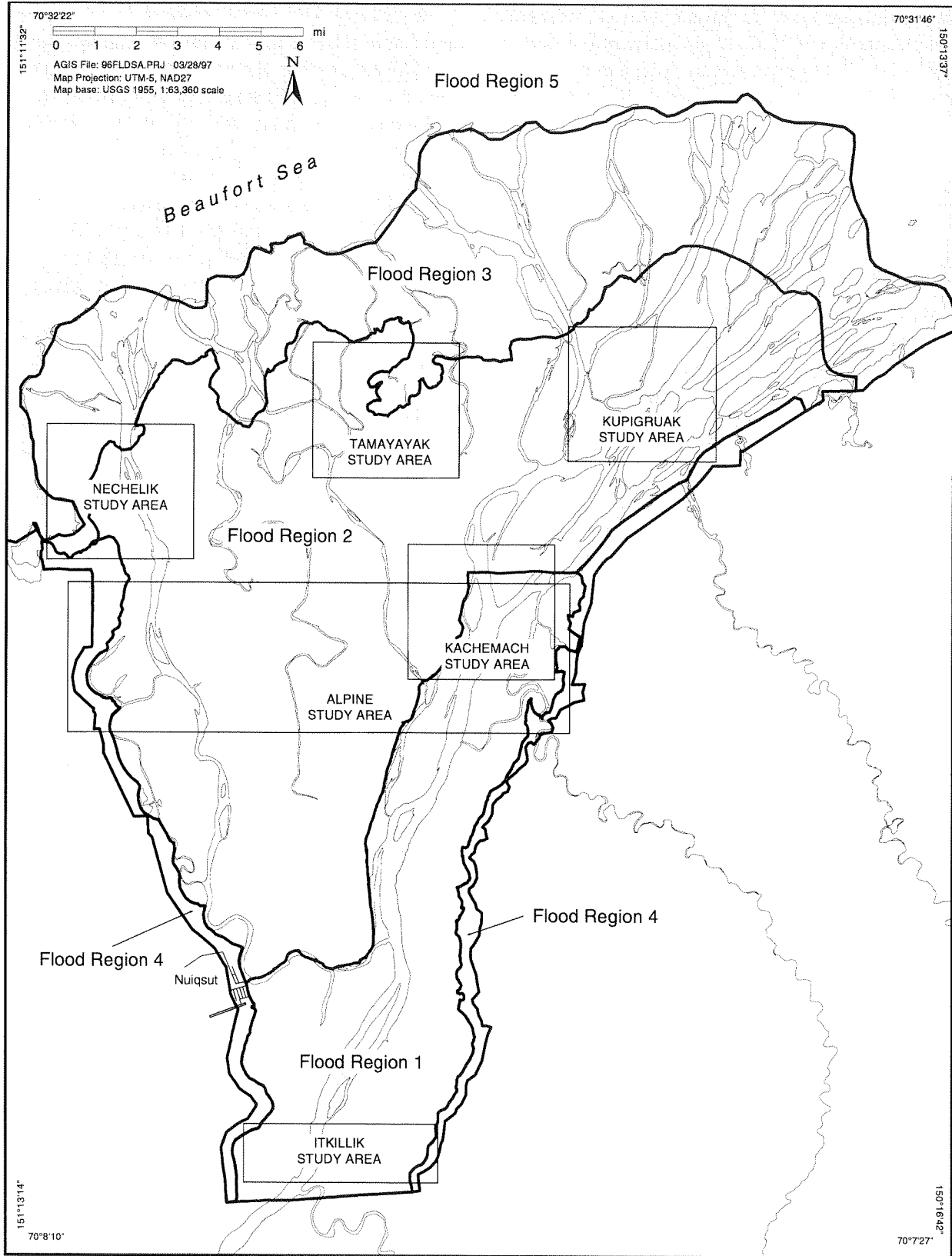


Figure 1-1. Map of flooding study areas and flooding regions, Colville River Delta, Alaska, 1996.

SPOT base map (Jorgenson et al. 1996) and printed at 1:63,360 scale for visual interpretation of flood distribution.

Flood distribution over the entire delta was mapped using the 27 May image and the 19 and 20 May images were used within the Alpine study area. The extent of flooding was determined visually in the RADARSAT images by associating grayscale values (equating to the signal's backscatter intensity) of river channels with signatures of lakes and tundra. Areas mapped as flooded exhibited a similar signal to that of the open river and had visible connections to a flooded channel. SPOT images acquired on 29 August 1992 were used in conjunction with RADARSAT images to assess flooding in lakes and basins that exhibited grayscale values similar to open water. These areas were delineated as flooded if a clear high-water connection existed to the flooded channel.

To assess the accuracy of flood maps produced from RADARSAT images and to evaluate differences in delineation based on image resolution, flooding interpretations were performed on both standard- and high-resolution RADARSAT images. These delineations were done independently, without reference to the oblique aerial photography. Two indices then were used to evaluate the accuracy of flood distribution maps produced from RADARSAT images. First, the maps were compared with flood-distribution maps produced using aerial photography to evaluate classification agreement errors of omission and commission. Second, the relative difference in overall flood extent, which ignores registration errors, was compared. These comparisons were done for the map produced from the high-resolution image (19 May) and the standard-resolution images (on 20 May and 27 May). The analysis was performed within the Alpine study area for the high-resolution image and standard-resolution image acquired on 19–20 May, and within the Alpine, Itkillik, and Tamayayak study areas for the standard-resolution image taken on 27 May. We assumed the map produced using the oblique aerial photos was more accurate because it had higher spatial resolution and the true-color photos facilitated differentiation of floodwater from *in situ* meltwater. Therefore, that map formed the basis for comparison with the RADARSAT-based map, using the following formulas:

Classification Agreement (%)

$$A = (1 - (R + P) / B) \cdot 100$$

Where:

A = Agreement (%)

R = Area flooded only on RADARSAT
(commission error)

P = Area flooded only on aerial
photography (omission error)

B = Area delineated on both the RADARSAT image
and aerial photos

Relative Difference (%)

$$D = ((R - P) / P) \cdot 100$$

Where:

D = Relative difference from aerial
photography (%)

R = Area delineated using RADARSAT
image

P = Area delineated on aerial photos

RELATIONSHIP BETWEEN FLOODING AND TERRAIN UNITS

To analyze flood distribution in relation to terrain units, the flood distribution map produced from oblique aerial photography was overlaid on the integrated-terrain-unit (ITU) map (Jorgenson et al. 1996), and the percentage of each terrain unit covered by floodwater was determined. Although the ITU classification consists of terrain unit, surface form and vegetation components, the analysis was done only for the terrain unit component to reduce the complexity of analysis and because terrain units accounted for most of the variation in flood distribution. In 1993, however, only those areas mapped directly with the aerial photography in the first phase of mapping as described above were used for this analysis. For all years, data were summarized within each study area and for all areas combined.

RESULTS AND DISCUSSION

AERIAL PHOTOGRAPHY AND MAPPING

Differences in monitoring effort among study areas did not allow reliable calculation of overall flooding among all years. Therefore, we examined differences in the amount of flooding among study areas within years, and among years within study areas. The stage and discharge of peak flooding associated with spring breakup for seven years of record are provided in Table 1-1.

Within any given year, the amount of flooding varied considerably among areas (Figures 1-2 to 1-7). In 1993, when peak discharge at the head of the delta was greatest, the amount of flooding ranged from 39% in the Tamayayak area in the central delta to 69% in the Kachemach area which encompassed the East Channel and was later incorporated into the Alpine study area. In 1996, when discharge was least, the amount of flooding ranged from 28% in the Alpine area to 36% in the Tamayayak area on the central delta.

The amount of flooding also varied considerably among years for any given area. In the Itkillik area at the head of the delta, where the floodplain is narrow and constrained by high banks, there was large variation in the percentage of area flooded, from 13% in 1994 to 52% in 1993 (Figures 1-2 and 1-3). In 1996, the flooded area covered 21% of the Itkillik area even though discharge (160,000 cfs) was the lowest on record.

In the Alpine area, flooding ranged from 28% in 1996 to 69% in 1993 (Figures 1-2 and 1-4). The value for 1993, however, was high because only a small portion of the area (the Kachemach area, centered on the East Channel) was mapped that year, thus amplifying the flood coverage. Of particular interest in the Alpine area is the extensive flooding around the Alpine #1 exploratory well site in 1995 and 1996. We attribute this extensive flooding to the tapping of Nanuk Lake (prior to 1943) at an outside bend of the Nechelik Channel. During breakup, floodwaters are directed into this lake, overflowing the bank even at relatively low flood stages.

In the Tamayayak area of the central delta, flooding only varied between 34% in 1996 and 40% in 1995 (Figures 1-2 and 1-5), a much smaller range than in the Itkillik or Alpine study areas. This area is in one of the oldest portions of the delta and encompasses only one small distributary, the Tamayayak channel.

In the Kupiguak area, centered on a portion of the East Channel in the outer delta, flood coverage ranged from 49% in 1992 to 62% in 1993 (Figures 1-2 and 1-6). Similarly, in the Nechelik area, encompassing an extensive area of tidal flats on the outer delta, flooding coverage ranged from 41% in 1992 to 65% in 1993 (Figure 1-7).

For comparison, we have included maps of flood distribution in 30 May 1943 (Walker, unpubl. data) and early June 1971 (Walker 1976) which we rectified to our base map (Figures 1-8 and 1-9). The percentage of the delta covered by flooding was 46% in 1943 and 58% in 1971. These values fall within the range of coverage that we observed from 1992 to 1996. Although the flood maps do not have associated discharge data and are not of sufficient resolution to include in our analysis of terrain relationships, they nevertheless provide a useful overview of flooding across the entire delta in earlier years.

In summary, floodplains along the East Channel experienced the most extensive flooding in 1993; the year of highest observed peak discharge. In particular, extensive overbank flooding occurred at the head of the delta (Itkillik area) and near the mouth of the Kachemach River (Kachemach area), where most of the flow is constrained by high banks on the eastern side of the floodplain and by high sand dunes on the western side of the East Channel. Frequent overbank flooding also occurred near Nanuk Lake at the Alpine #1 exploratory well site. We attributed the flooding of that well site, which occurred at fairly low flood stages, to the tapping of Nanuk Lake; to the occurrence of a low-lying, ice-rich thaw basin around the exploratory well site; and to the occurrence of low-lying, ice-poor thaw basins east of this well site. In contrast, most of the central portion of the delta west of the sand dunes bordering the East Channel did not flood during our monitoring in 1992-1996. The central portion is the oldest part of the delta and is characterized by numerous abandoned-floodplain cover deposits.

RADARSAT IMAGERY

Overall Flood Distribution

In 1996, RADARSAT images were acquired on 19 and 20 May near the initial false peak (17 May) and on 27 May, soon after the actual peak stage on 26

Table 1-1. Summary of breakup data at the head of the Colville River Delta, 1962-1996.

Year	Approximate Date Water Began To Flow	Peak Water-Surface Elevation ^a (ft)	Peak Breakup Discharge (cfs)	Date of Peak Water-Surface Elevation	Date of First Clear Channel/Open Water ^b
1996 ^c	15 May	17.2	160,000	26 May	27 May
1995 ^d	8 May	14.9	233,000	16 May	30 May
1994 ^e	16 May	12.2	159,000	25 May	9 June
1993 ^f	—	19.2	379,000	31 May	1 June
1992 ^g	—	13.9	188,000	2 June	4 June
1977 ^h	—	19.1	407,000	7 June	9 June
1973 ⁱ	25 May	—	—	8 June	8 June
1971 ⁱ	23 May	—	—	2 June	2 June
1964 ⁱ	28 May	—	—	3 June	5 June
1962 ^j	19 May	12.4	215,000	14 June	10 June

^aWater-surface elevations are based on British Petroleum Mean Sea Level Datum.

^bApproximate date the main channel was generally clear of ice.

^cData from Shannon and Wilson (1996a).

^dData from Jorgenson et al. (1996).

^eData from Jorgenson et al. (1994b).

^fData from Jorgenson et al. (1994a).

^gData from Jorgenson et al. (1993).

^hData from U. S. Geological Survey (1978).

ⁱBased on data collected near Nuiqsut (Walker 1974).

^jData from Arnborg et al. (1966).

PART I. Flood Distribution

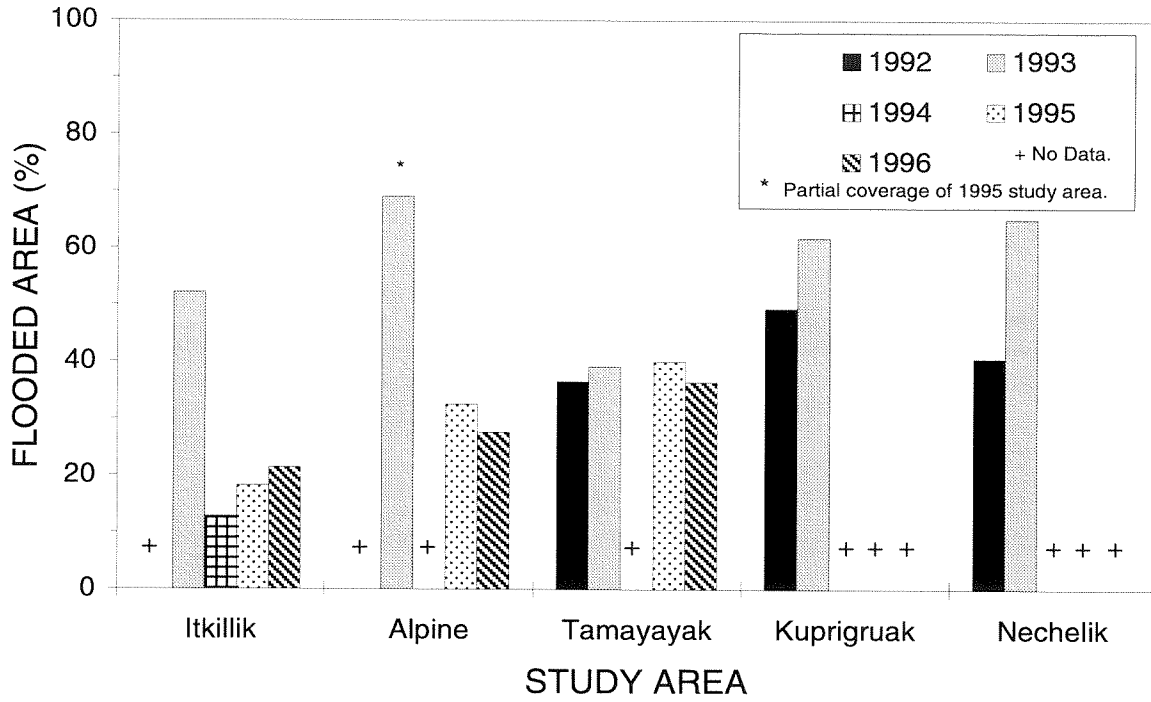


Figure 1-2. Percentage of total area covered by floodwater in five study areas in the Colville River Delta, Alaska, 1992-1996.

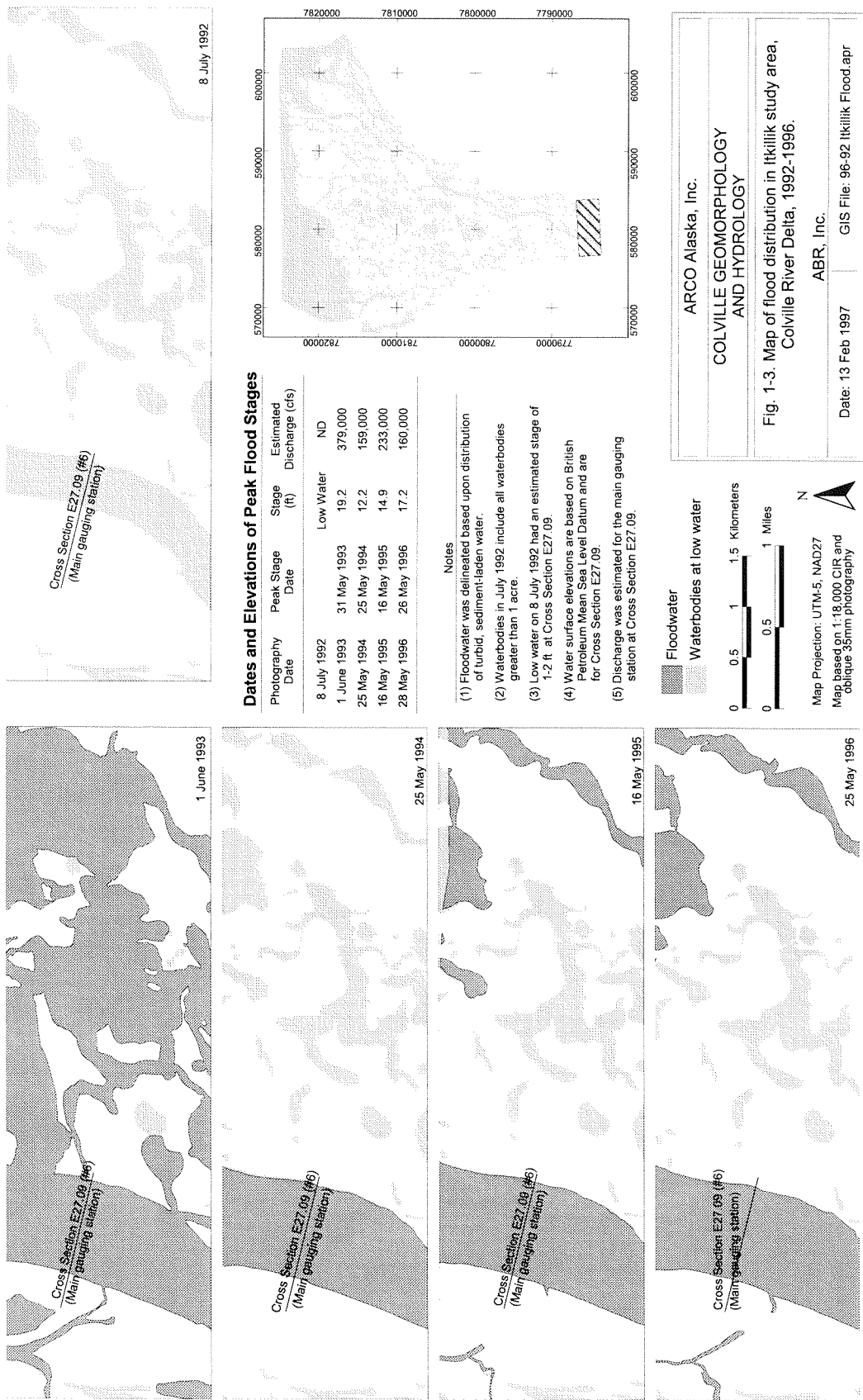


Figure 1-3. Map of flood distribution in the Iktiklik study area, Colville River Delta, Alaska, 1992-1996.

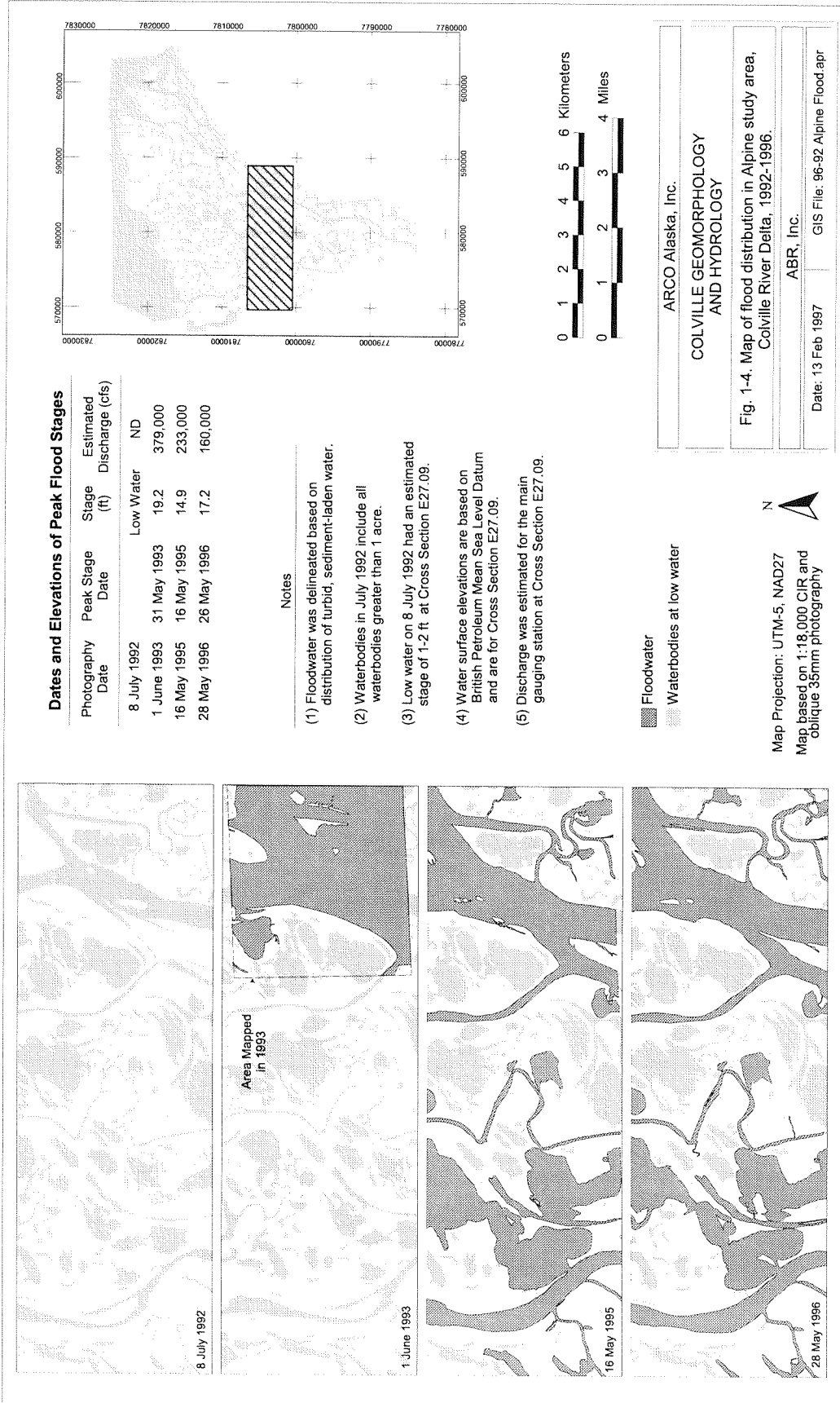


Figure 1-4. Map of flood distribution in the Alpine study area, Colville River Delta, Alaska, 1992-1996.

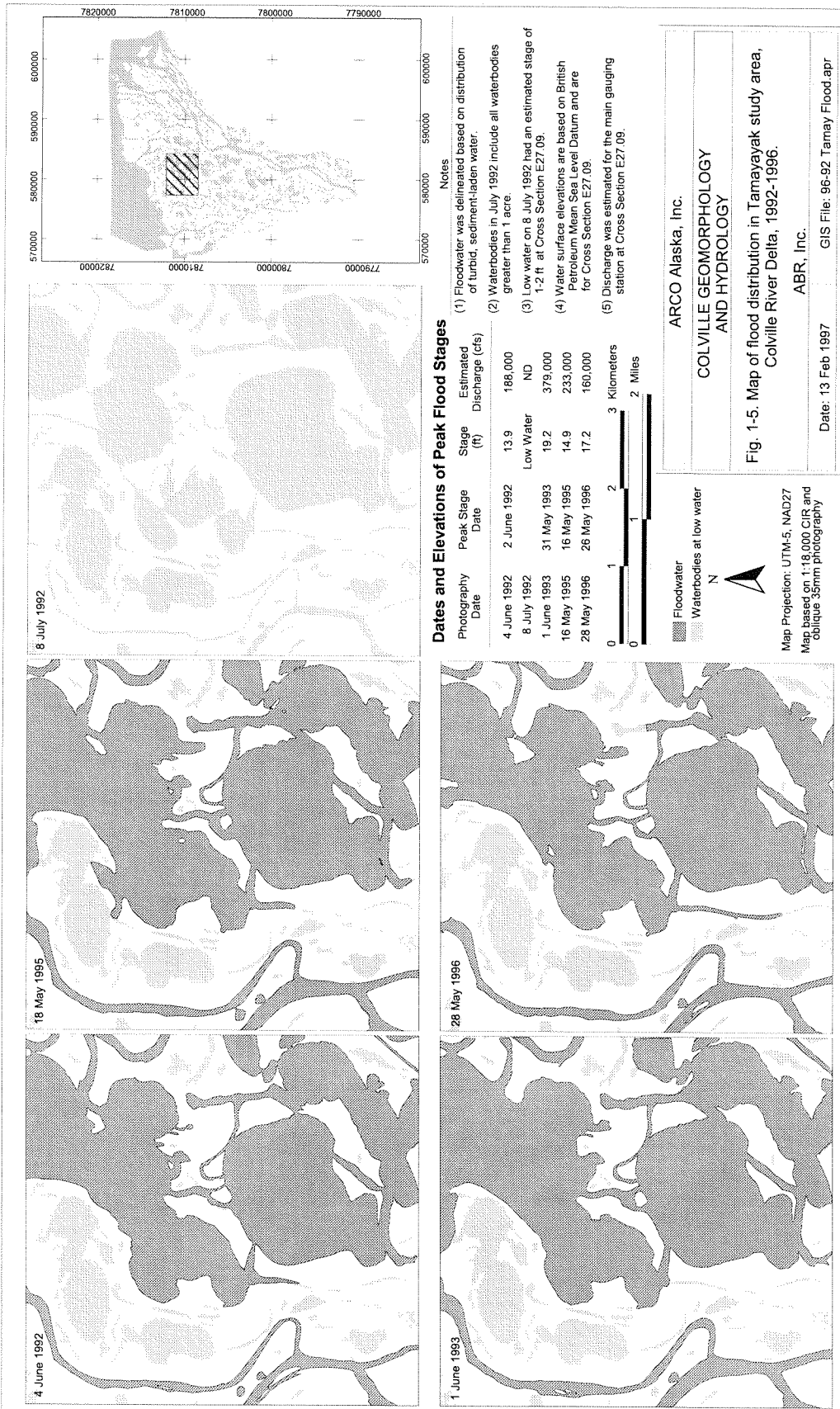


Figure 1-5. Map of flood distribution in the Tamayyak study area, Colville River Delta, Alaska, 1992-1996.

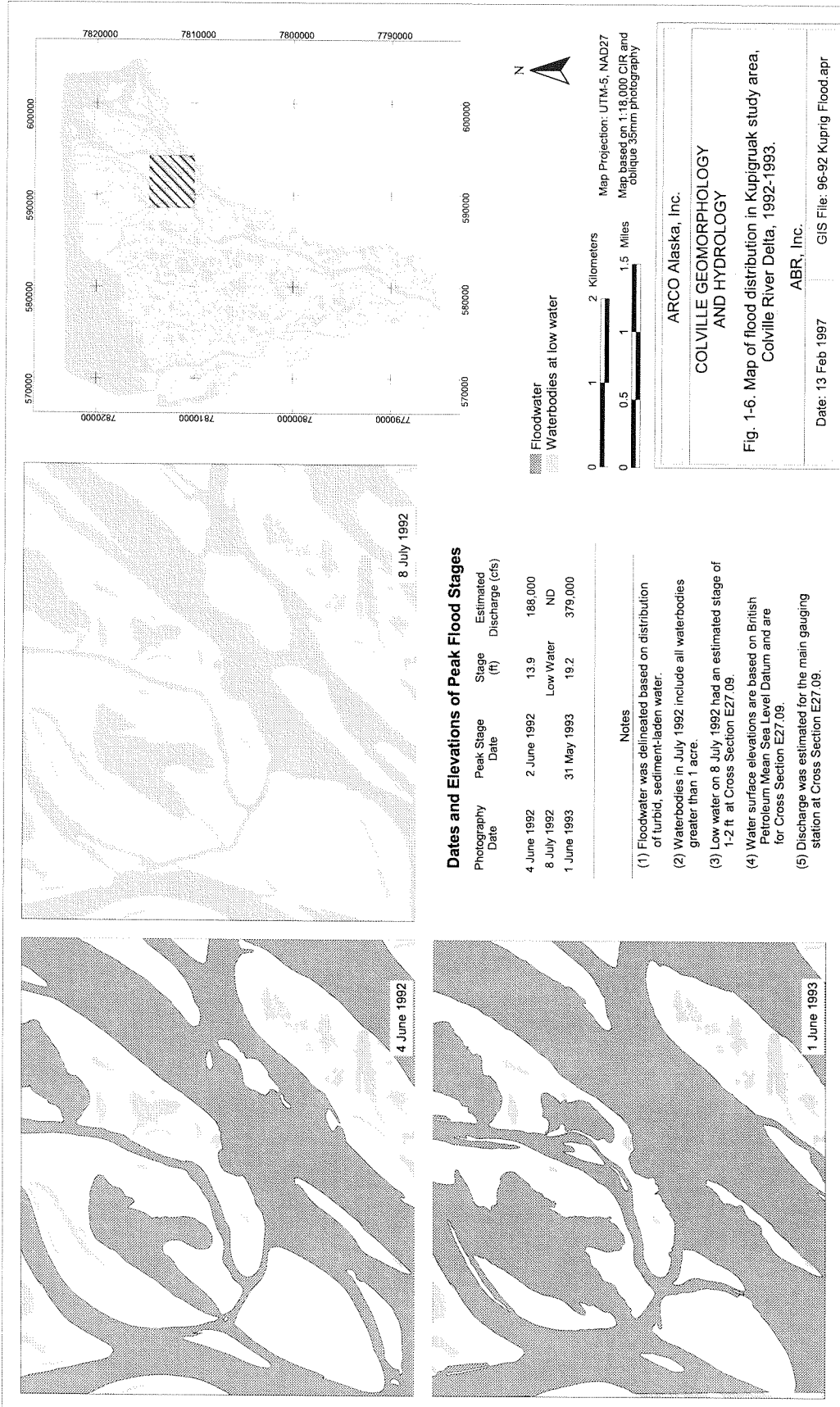


Figure 1-6. Map of flood distribution in the Kupiguak study area, Colville River Delta, Alaska, 1992-1993.

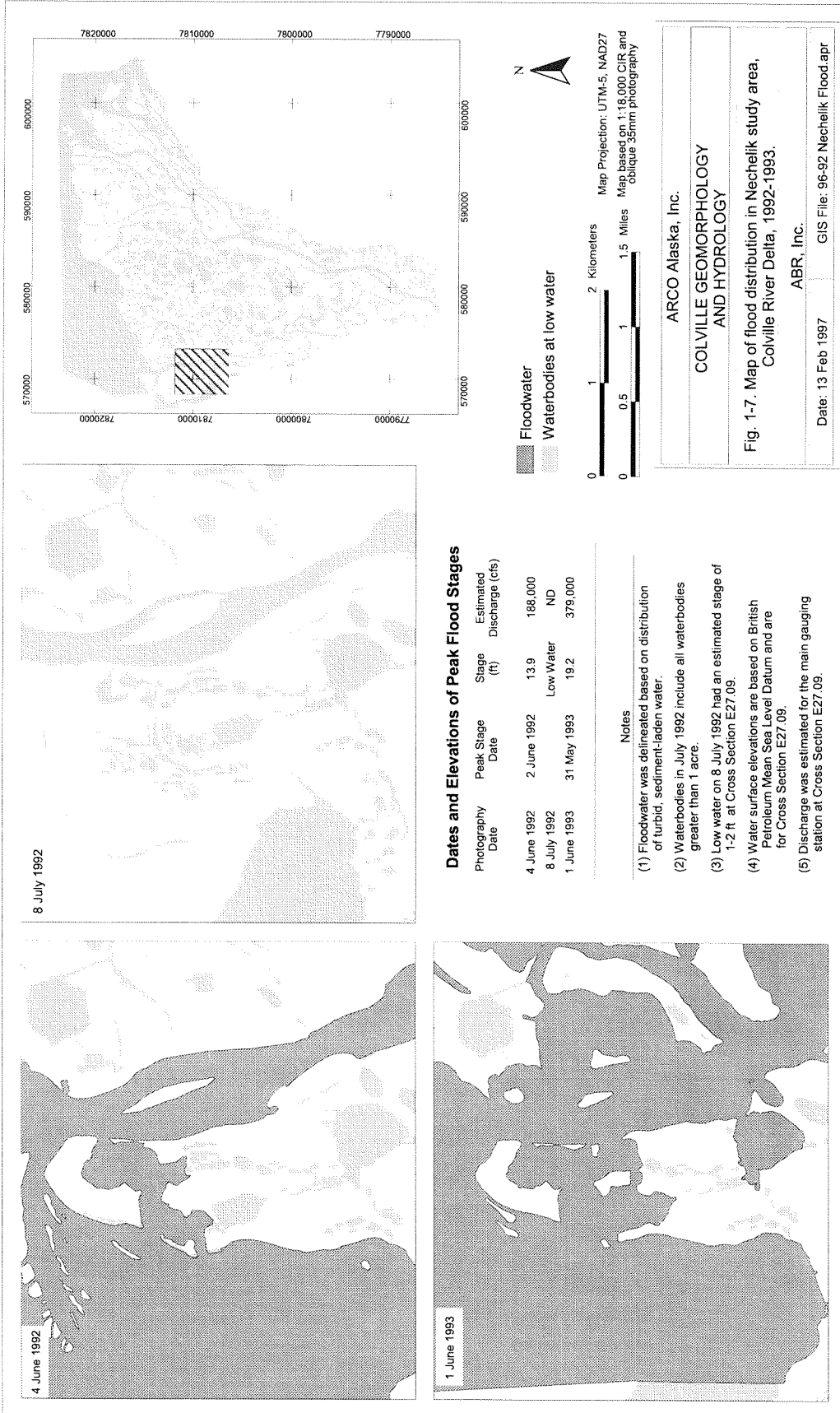


Figure 1-7. Map of flood distribution in the Cechelik study area, Colville River Delta, Alaska, 1992-1993.

PART I. Flood Distribution



2 0 2 4 6 Kilometers



2 0 2 4 Miles






Map Projection: UTM-5, NAD27

Flood distribution based on unpublished data from H. J. Walker.

Registration based on 1995 SPOT base map, USGS control points and ground DGPS surveys.



-  Floodwater
-  Nonflooded waterbodies
-  Nonflooded tundra

ARCO Alaska, Inc.	
COLVILLE GEOMORPHOLOGY AND HYDROLOGY	
Figure 1-8. Flood distribution on 30 May 1943, Colville River Delta.	
ABR, Inc.	
Date: 12/20/96	File: radarsatfld.apr



Map Projection: UTM-5, NAD27

Flood distribution based on Walker (1976)

Registration based on 1995 SPOT base map, USGS control points and ground DGPS surveys.



- Floodwater
- Nonflooded waterbodies
- Nonflooded tundra

ARCO Alaska, Inc.	
COLVILLE GEOMORPHOLOGY AND HYDROLOGY	
Figure 1-9. Flood distribution in early June 1971, Colville River Delta.	
ABR, Inc.	
Date: 12/20/96	File: radarsatfid.apr

May (Figures 1-10 to 1-12). Using the RADARSAT image acquired on 27 May, visual image interpretation was used to map flood distribution across the entire delta (Figure 1-13). Overall, the floodwater covered 39% of the delta in 1996. This value is lower than those obtained for flooding in 1943 (46%) and 1971 (58%) (Figures 1-8 and 1-9).

Using RADARSAT imagery to map flood distribution has several advantages: An image of the entire delta can be acquired almost daily in a single frame, image quality is unaffected by weather conditions, safety hazards associated with acquiring aerial photography under marginal weather conditions can be avoided, and the cost to delineate and georeference the data is lower. However, acquiring an image in 1996 that coincided with peak discharge was problematic, mainly due to RADARSAT International's administrative procedures in effect at the time (the office was closed during the weekend when peak flooding occurred). In general, the timing of peak stage is unknown until it passes. In 1996, we did not know peak stage had occurred until the second week of June, when it became clear that no more peaks were likely. During peak events, such as on 17 and 26 May 1996, it was difficult to predict when floodwaters were going to peak and to have RADARSAT, Inc. acquire the images in a timely manner. This difficulty could be avoided by scheduling image acquisition during the entire period that is most likely encompassing the peak event (20 May-5 June). Currently, however, this imagery costs \$3000 per day, plus some added costs for processing the scenes of interest. The optimal approach would be to have RADARSAT acquire all the images but only have the user pay for a few dates of interest. They were not agreeable to this approach in 1996, but may be in the future.

Comparison of Photography and RADARSAT Imagery

The distribution of floodwater interpreted and mapped from RADARSAT images compared well with delineations from oblique aerial photography (Figure 1-14). Classification agreement (2 classes: flooded and nonflooded) between the delineation from aerial photography on 20 May and RADARSAT images acquired on 19 and 20 May were 94.6% and 94.2%, respectively (Figure 1-15). Classification agreement between flood distribution delineated on the 27 May

RADARSAT image and 28 May aerial photography in the three study areas was 91% for the Alpine area, 99% for the Ikillik area, and 88% for the Tamayyak area.





The relative difference in total flood extent between the two methods also indicated that interpretation of RADARSAT images produced similar results (Figure 1-15). For 19 and 20 May, the relative difference was 1.6% and -5.7%, respectively. For the later dates of 27-28 May, relative differences were 13.9% in the Alpine, 7.1% in the Ikillik, and -2.6% in the Tamayyak study areas.

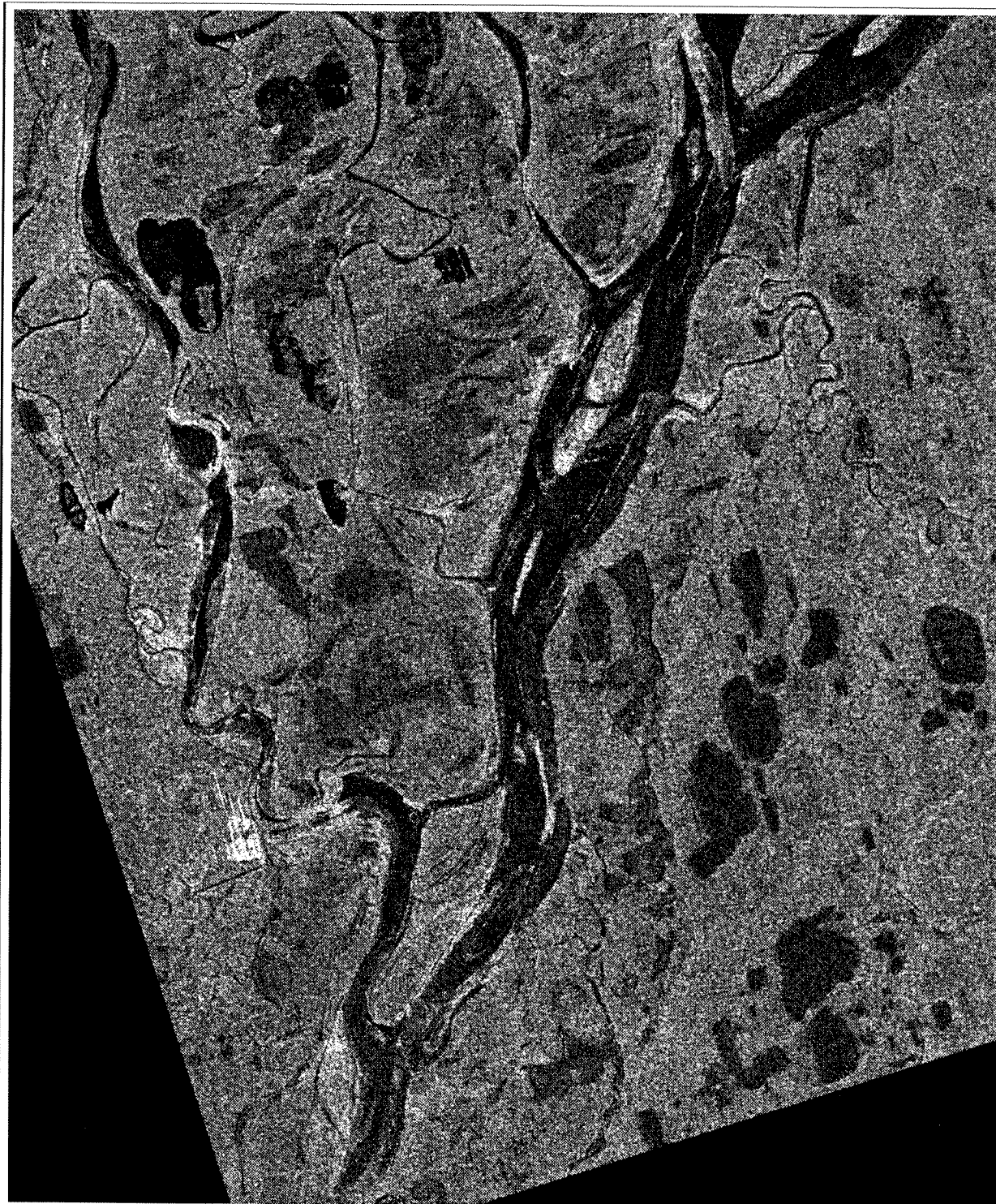
Delineation errors on RADARSAT images can originate from three sources: misidentification of flooding signatures, registration errors with aerial photography, and changes in river stage between the time of oblique aerial photography and imagery acquisition. Misidentification of flood signatures is a substantial problem. Generally, backscatter signatures (see below) were not consistent enough to allow us to clearly distinguish flooded areas from nonflooded areas. For example, dark signatures occurred both within the flooded channel and within deep nonflooded lakes covered by ice. Similarly, mixed gray speckling occurred within ice-choked channels and on nonflooded tundra. Instead of relying entirely on signatures, we frequently relied on continuity of floodwater margins and connectivity to features with similar spectral characteristics to interpret floodwater distribution.


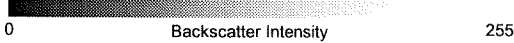


Registration errors between the two layers was minimized by geocoding both RADARSAT images and aerial photographs using the SPOT base map. Registration error using this technique typically is <20 m within the delta (Jorgenson et al. 1996).

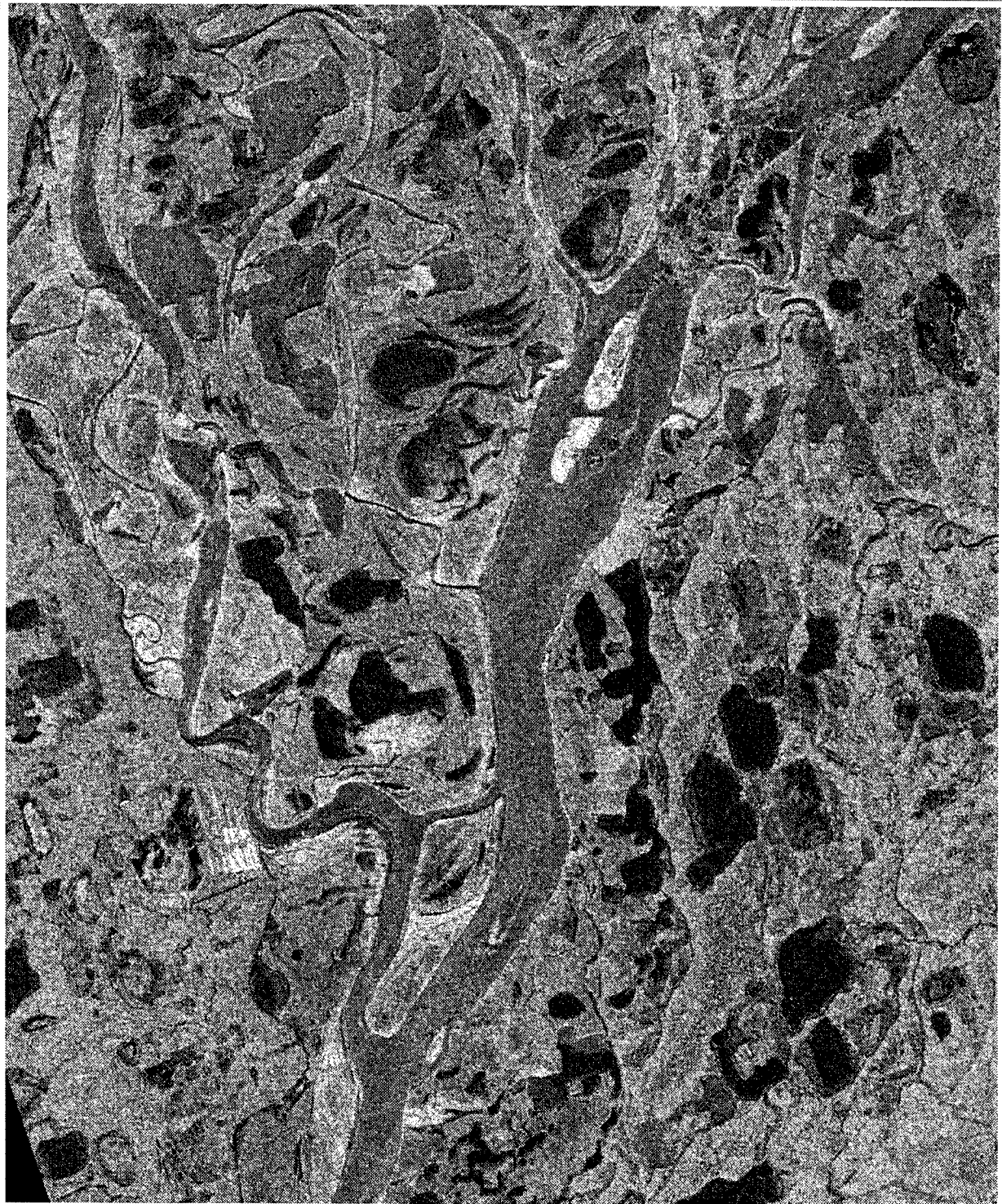
We attributed much of the difference in flood distribution resulting from the two methods to differences in water level, particularly for the 27-28 May time period (Figure 1-16). Measurements of river stage on the outer delta at the Helmericks residence (J. Helmerick, pers. comm.) and at the head of the delta (Cross-section E27.09, Shannon and Wilson, 1996) indicated a negligible decrease in flood stage during 19-21 May, but nearly a two ft decrease during 27-28 May. Differences in delineation between 19-20 May maps primarily resulted from a change in floodwater distribution within a connected lake east of Nanuk Lake and from small differences in delineation of river channels and basin margins. The decrease in flooded area from 34% on 27 May (RADARSAT image) to 28%




<p style="text-align: center;">N</p>  <p>Map Projection: UTM-5, NAD27 RADARSAT 1 Image 19 May 1996; 5:42 PM AST Fine 5 Beam Mode</p> <p>Registration based on 1995 SPOT base map, USGS control points and ground DGPS surveys.</p>	<p style="text-align: center;">0 255</p> <p style="text-align: center;">Backscatter Intensity</p> 	<p style="text-align: center;">2 0 2 4 Kilometers</p> 		<p style="text-align: center;">1 0 1 2 Miles</p> 		<p>ARCO Alaska, Inc.</p> <p>COLVILLE GEOMORPHOLOGY AND HYDROLOGY</p> <p>Figure 1-10. RADARSAT image of flood distribution within the Alpine development area, 19 May 1996.</p> <p>ABR, Inc.</p>	
						<p>Date: 12/20/96 File: Radarsatfld.apr</p>	

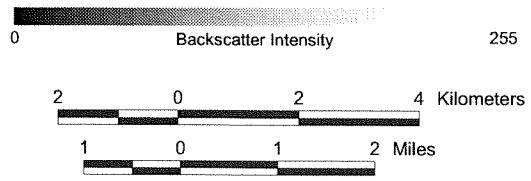


												
<p>Map Projection: UTM-5, NAD27 RADARSAT 1 Image 20 May 1996; 5:42 PM AST Standard 3 Beam Mode</p> <p>Registration based on 1995 SPOT base map, USGS control points and ground DGPS surveys.</p>												
<table border="1" style="width: 100%; border-collapse: collapse;"> <tr> <td colspan="2" style="text-align: center;">ARCO Alaska, Inc.</td> </tr> <tr> <td colspan="2" style="text-align: center;">COLVILLE GEOMORPHOLOGY AND HYDROLOGY</td> </tr> <tr> <td colspan="2" style="text-align: center;">Figure 1-11. RADARSAT image of flood distribution within the Alpine development area, 20 May 1996.</td> </tr> <tr> <td colspan="2" style="text-align: center;">ABR, Inc.</td> </tr> <tr> <td style="width: 50%; text-align: center;">Date: 12/20/96</td> <td style="width: 50%; text-align: center;">File: Radarsatfld.apr</td> </tr> </table>			ARCO Alaska, Inc.		COLVILLE GEOMORPHOLOGY AND HYDROLOGY		Figure 1-11. RADARSAT image of flood distribution within the Alpine development area, 20 May 1996.		ABR, Inc.		Date: 12/20/96	File: Radarsatfld.apr
ARCO Alaska, Inc.												
COLVILLE GEOMORPHOLOGY AND HYDROLOGY												
Figure 1-11. RADARSAT image of flood distribution within the Alpine development area, 20 May 1996.												
ABR, Inc.												
Date: 12/20/96	File: Radarsatfld.apr											




 Map Projection: UTM-5, NAD27
 RADARSAT 1 Image
 27 May 1996; 6:09 PM AST
 Standard 2 Beam Mode

 Registration based on 1995
 SPOT base map, USGS control
 points and ground DGPS surveys.



ARCO Alaska, Inc.	
COLVILLE GEOMORPHOLOGY AND HYDROLOGY	
Figure 1-12. RADARSAT image of flood distribution within the Alpine development area, 27 May 1996.	
ABR, Inc.	
Date: 12/20/96	File: Radarsatfid.apr

PART I. Flood Distribution



- Floodwater
- Nonflooded waterbodies
- Nonflooded tundra



Map Projection: UTM-5, NAD27
 Registration based on 1995 SPOT base map, USGS control points and ground DGPS surveys.

ARCO Alaska , Inc.	
COLVILLE GEOMORPHOLOGY AND HYDROLOGY	
Figure 1-13. Flood distribution visually delineated from 27 May RADARSAT imagery, Colville River Delta, 1996.	
ABR, Inc.	
Date: 12/20/96	File: radarsatfid.apr



Figure 1-14. Flooding in the Alpine study area: RADARSAT and oblique methods.

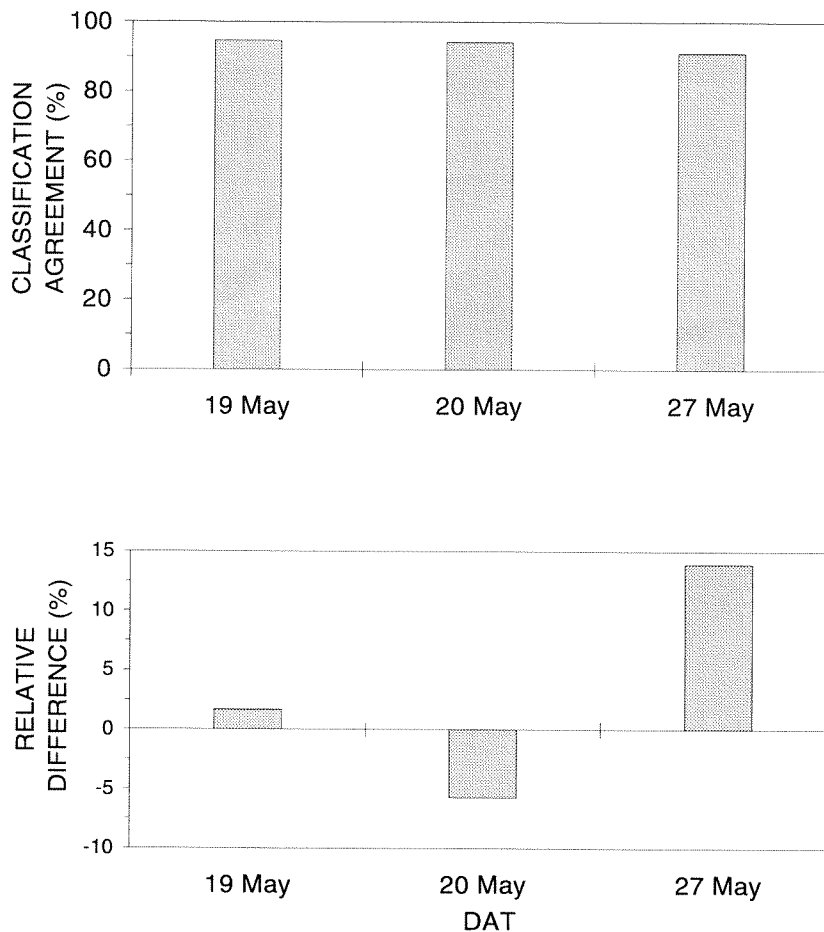


Figure 1-15. Percent agreement (top) and difference (bottom) in the distribution of floodwater within the Alpine area delineated from RADARSAT imagery acquired on 19 May (Fine-resolution image) and 27 May (standard-resolution image) 1996 when compared to mapping derived from oblique aerial photography, Colville River Delta, Alaska. A positive relative difference indicates more floodwater was mapped from RADARSAT imagery.

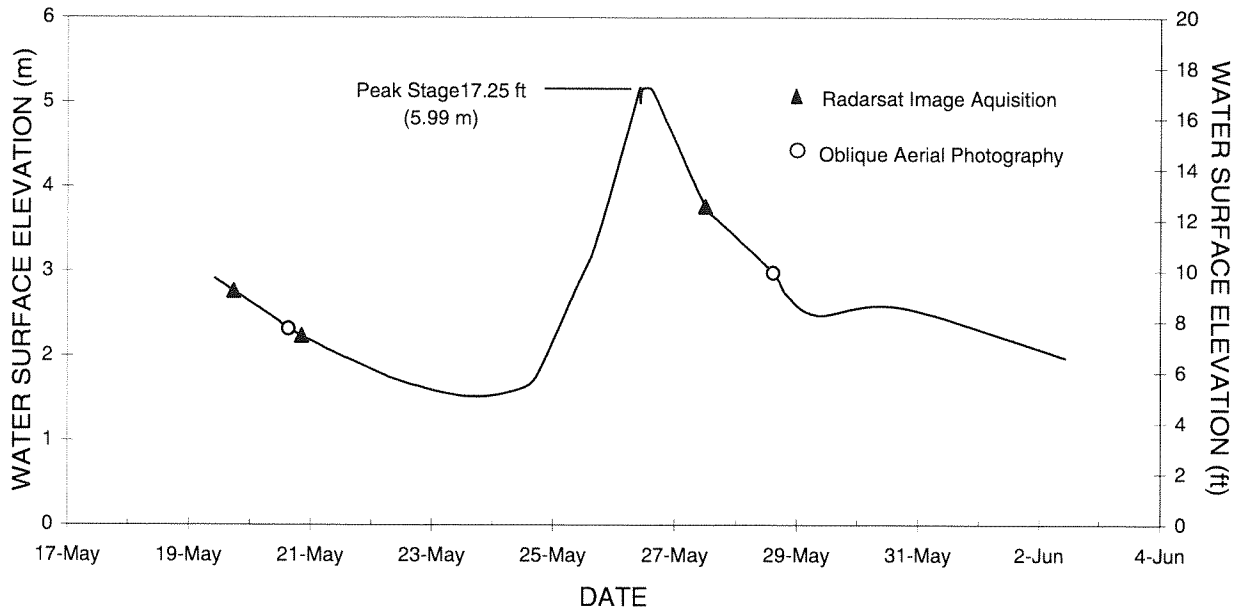


Figure 1-16. Changes in flood stage at the head of the delta (Cross-section E27.09) in relation to times when RADARSAT imagery and oblique aerial photography were acquired in 1996, Colville River Delta, Alaska.

on 28 May (aerial photography) appears consistent with the measured decrease in water levels (2 ft) during that period. Over the entire period of 19–28 May, floodwater coverage in the Alpine area was closely related to the river stage at Cross-section E27.09 ('6) if each of the delineations (either RADARSAT-based or aerial photo-based) is considered an individual observation ($r^2 = 0.90$, $n = 5$).

Spatial Resolution and Backscatter Differentiation

Differences in image quality between the high- and standard-resolution images are apparent by comparing Figures 1–10 and 1–11. The contrast between open water, ice, and land is much greater in the high-resolution image of 19 May, allowing more precise determination of shorelines and basin edges. In addition, the greater angle of incidence of the 20 May standard-resolution image (Figure 1–11) results in greater contrast of water, ice and land than was seen in the 27 May image (Figure 1–12).

We found the standard-resolution image to be adequate for flood extent mapping. This image type is more readily available for time-sensitive monitoring due to the greater area of coverage and more frequent satellite return times. When available, however, high-resolution images are preferable because the higher spatial resolution allows better definition of water margins and interpretation of connections between waterbodies. Higher incidence angles are preferable, because they provide increased contrast between open water, ice, and land. In January 1997, 10 new high-resolution positions were made available by RADARSAT due to the high demand for high-resolution imagery. This increase will result in greater image availability, and should allow a high-resolution image of the delta to be available every other day.

Differentiation of backscatter intensity (represented by grayscale values ranging between 0 and 255) between flooded and nonflooded areas varied between the high- and standard-resolution images (Figure 1–17). The distribution of backscatter values in the high-resolution image show a greater separation between flood areas, with values from flood areas heavily skewed towards zero. The substantial overlap between terrain types, particularly for the standard-resolution images, reduces their usefulness for classifying floodwater, however. Because backscatter characteristics of flooded and nonflooded areas were similar, it was important to note connectivity of floodwater during the interpretation process.

We briefly investigated the feasibility of using computer algorithms to classify floodwater. Because the images have only one band and there is high degree of overlap in backscatter values among terrain types, direct conversion of reflectance values to flood coverages was not successful. We next tried to develop a flood classification model using three visible bands of a SPOT image (obtained 29 August 1992) and the 27 May RADARSAT images. The RADARSAT image was filtered to reduce speckle and enhance contrast between land, ice and open water using a majority algorithm (Earth Resource Mapping, San Diego, CA) and was added as a layer to the three-band SPOT image. A supervised classification scheme was set up with representative regions defined to cover dominant terrain types.

Initial results of this method varied across the delta and in some places looked reasonable. However, the results were driven too much by characteristics of the SPOT image (thus proving useful for low-flood stages but probably not good for high-flood stages) and suffered from poor resolution of flooded and nonflooded surfaces in the RADARSAT image (Figure 1–17). Based on this evaluation, we believe automated computer classification is not reliable enough for achieving the level of detail needed for facilities planning and flood modeling, given the satellite imagery currently available. Use of images produced by the high-resolution mode will improve the output of this method, but accuracy will be significantly lower than with current methods. Given the relative ease of visual classification of RADARSAT imagery and its good agreement with mapping from oblique aerial photography, we conclude that visual classification is the best approach.

RELATIONSHIP BETWEEN FLOODING AND TERRAIN UNITS

Patterns of flood distribution are strongly related to the distribution of terrain units and show considerable annual variability among years: 1994 showed the least flooding and 1993 the most flooding overall in five years of observations (Figure 1–18). Delta riverbed/riverbar deposits were nearly entirely flooded (82–95%) every year. Active-floodplain cover deposits experienced up to 47% flood coverage at the highest flood stage. In contrast, flood coverage on abandoned and inactive-floodplain cover deposits was relatively

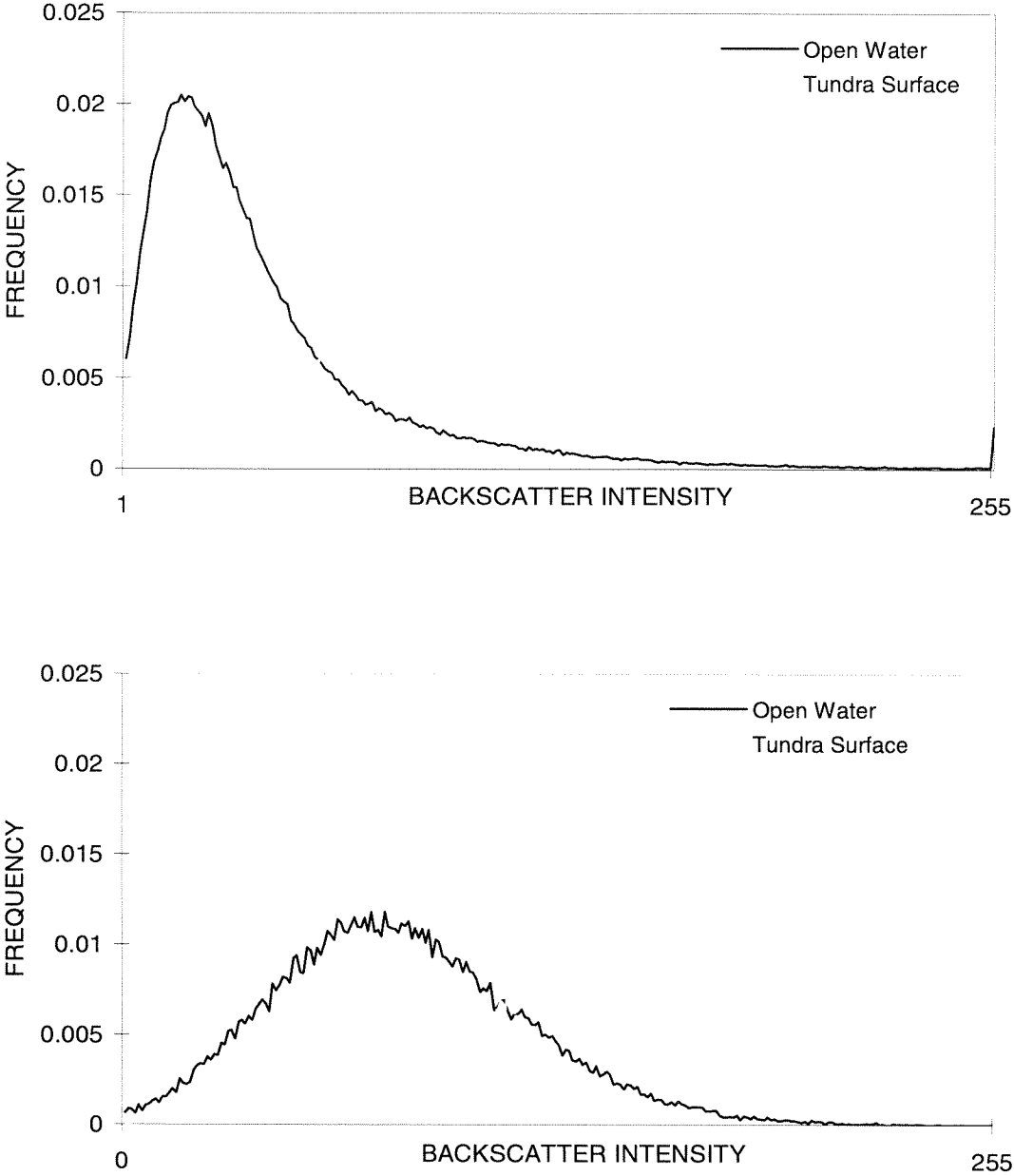


Figure 1-17. Frequency of occurrence (%) of backscatter values for floodwater and nonflooded tundra for fine- (top) and standard- (bottom) resolutions of RADARSAT imagery used to map flooding on the Colville River Delta, Alaska, 1996.

PART I. Flood Distribution

low, at 11% and 16%, respectively. Terrain units that were not considered to be affected by the current fluvial regime, such as sand dunes and alluvial terraces, also had minor amounts of flooding along their margins (5% and 6%, respectively).

Among years, the 1996 data suggest an intermediate level of flooding, although the discharge estimate was the second lowest on record (Table 1-1). Flood extent in 1996 offers a better estimate of terrain unit coverage at a low flood stage than does data from 1994, when only observations from the Ikillik area were available. During our five years of observation, we have yet to see substantial overbank flooding, other than isolated events in 1993 near the head of the delta, and within the Kupiguak area.

The amount of flooding in each terrain unit also was strongly related to discharge (Figure 1-19). Riverbed/riverbar deposits were nearly entirely flooded at intermediate stages of discharge. In contrast, the inactive- and abandoned-floodplain cover deposits showed only small, but consistent, increases in flood coverage at the discharge rates (up to 379,000 cfs) observed in this study (1992-1996). The relationship between terrain unit flooding and flood stage was similar to the flooding-discharge relationship, but revealed some small differences that may be due to difficulties in estimating discharge during breakup because of ice-jamming.

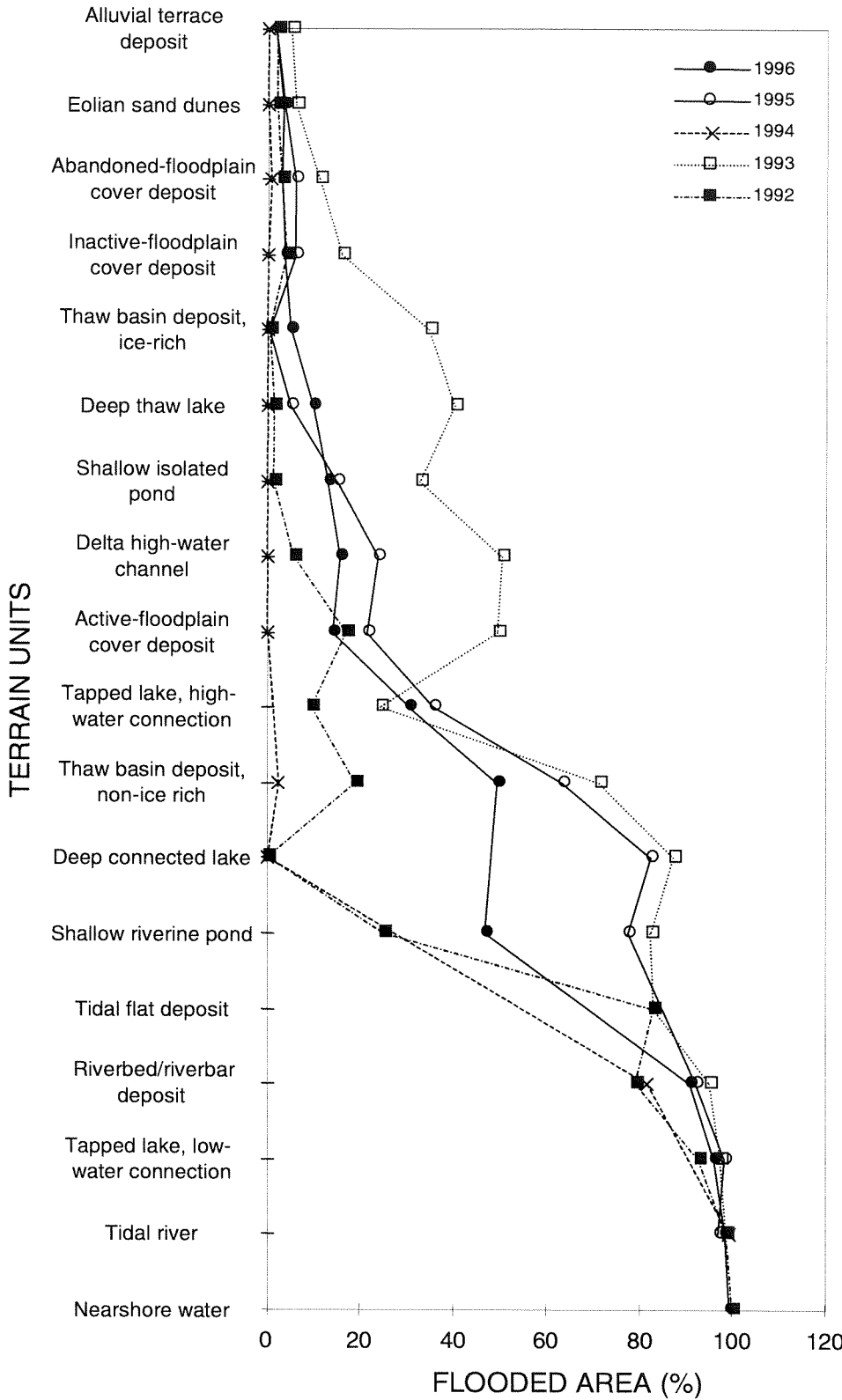


Figure 1-18. Percentage of each terrain unit covered by flooding in five study areas in the Colville River Delta, Alaska, 1992-1995.

PART I. Flood Distribution

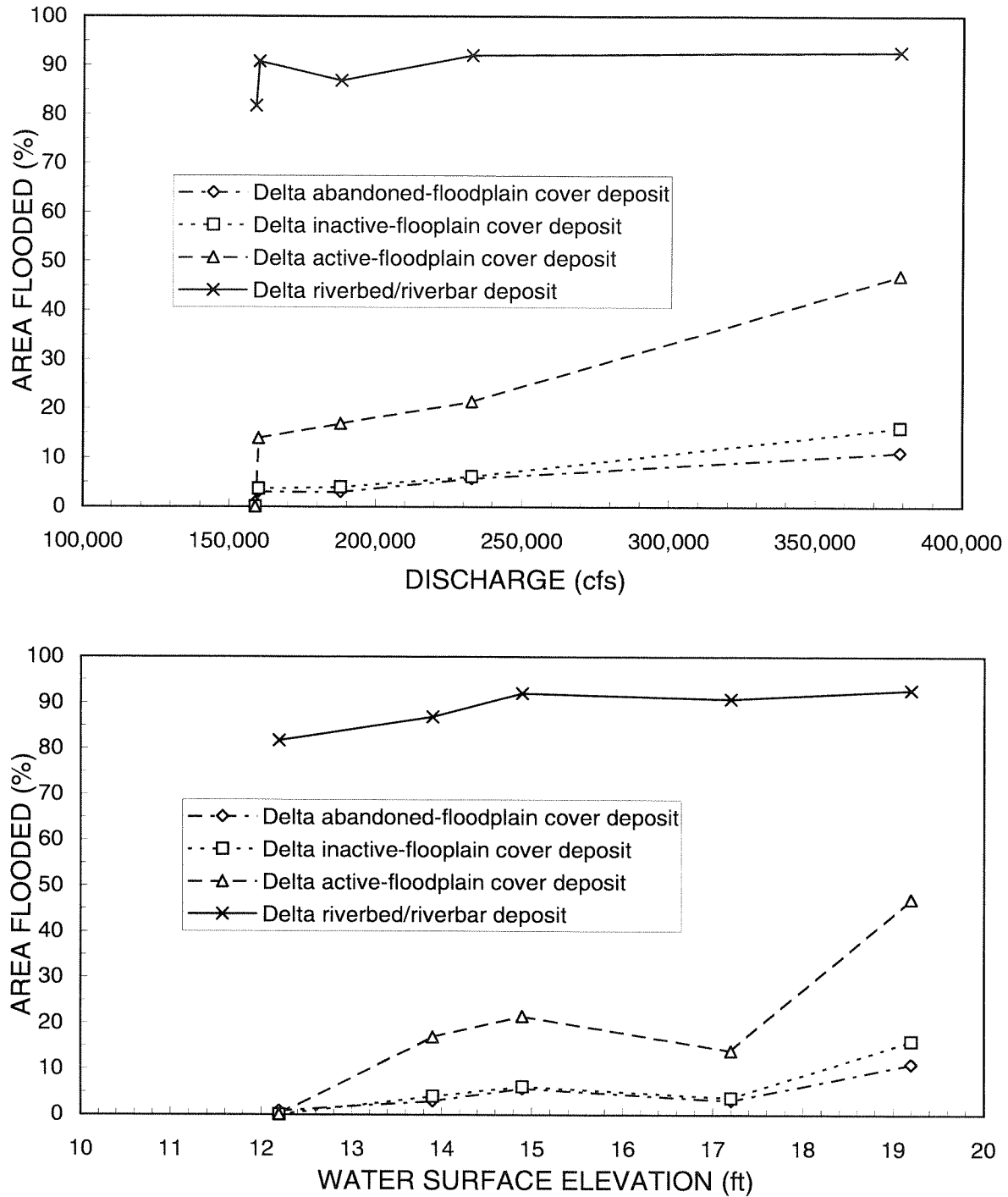


Figure 1-19. Relationship between percent area flooded and peak discharges (top) and stage (below) for the major terrain units, Colville River Delta, Alaska, 1992-1996.

PART II. PALEOFLOOD HYDROLOGY

BACKGROUND

Given the scant historical data on the magnitude and distribution of flooding on the Colville River Delta, there is substantial uncertainty concerning the flood stage and discharge criteria that should be used for the design of facilities for the Alpine Development Project. This study was designed to reduce this uncertainty by evaluating paleoflood indicators to determine the magnitude, distribution, and frequency of large flooding events. In particular, this study focuses on paleoflood indicators from a large flood in 1989 to characterize the nature, distribution and frequency of these unusual events.

Paleoflood hydrology is the study of past or ancient flood events involving the analysis of slackwater, or overbanks, deposits and other paleostage indicators (Baker 1987, Baker et al. 1988, Hupp 1988). Slackwater deposits are fine-grained material (fine sand, silt, and clay) dropped from suspension in the water column due to large decreases in water velocity, which occur in places such as mouths of tributaries, areas of abrupt constriction or expansion of channels, small niches in bedrock or other material, high floodplain steps, and densely vegetated areas. Slackwater deposits are useful indicators because they can be widespread across the floodplain, but they often underestimate the stage of flood peaks (CH2M Hill 1994). Other paleoflood indicators that can be used to establish peak stage include organic driftlines or driftwood, silt lines, and scour marks in soil or regolith (bedrock or weathered material). Although high-water marks indicative of peak stage are much less common than slackwater deposits, their potential for evaluating stage and discharge make them extremely valuable. To be useful, the chronology of these paleoflood indicators needs to be established, for which radiocarbon dating of organic material has become one of the most common methods (Tornqvist et al. 1993). The principal concerns regarding paleoflood indicators are the degree of preservation, the degree to which slackwater deposits underrepresent peak stages, and the reliability of other paleoflood indicators in marking peak stage.

On the Colville River Delta, we examined slackwater deposits to assess the frequency of large

events and examined driftwood deposits to establish the stage of the latest large flood event. We were fortunate to conduct this study only seven years after a large event, because abundant sediment and driftwood that had been deposited by that event has appeared to remain stable and easily observable. We used the slackwater deposits to assess the relative magnitude of the 1989 event by comparing the size of various depositional layers in the stratigraphic record over a time period established through radiocarbon dating of organic material. We surveyed driftlines to establish the peak stage of the 1989 event and used measurements from numerous driftlines scattered over the delta to assess the quality of the driftline information. Finally, these data were used for comparison with the results of the hydraulic modeling of 100- and 200-yr flood events performed by Shannon and Wilson, Inc. (1997).

The flood during spring breakup in 1989 is considered by Jim Helmericks, who lives near the mouth of the East Channel, to be the largest flood that he has seen in 39 yrs. He observed ice floes that had gone over the bank in some places near the head of the delta, and we obtained photographs of ice floes deposited over the bank south of the Itkillik River mouth, indicating a highly unusual event. During 1992–1995, we observed widespread distribution of organic debris and thin slackwater deposits, which we attributed to the 1989 flood, on top of organic soils across most of the delta, also indicating the unusual nature of the event.

To assess the relative magnitude of the 1989 flood, we evaluated several factors (distance from bank, terrain units, and flood regions) potentially affecting the geographic variability of sediment deposition. Understanding such factors is necessary to identify the appropriate conditions for which samples can be used in analyzing the return period (average period of years expected between similar-sized events) for the 1989 flood and in evaluating changes in flood regime across the delta. The rationale for selecting these geographic factors is described below.

Large decreases in sedimentation with increasing distance from the riverbank were evident during our previous sampling, but we had not collected sufficient data to analyze this effect. This increased sedimentation along riverbanks is evidenced by thick accumulations of mineral material, lack of organic matter at the surface, and vigorous growth of willows, which respond to the nutrients associated with sediments.

Accounting for the effect of distance is important because channel migration over time may affect the relative size of deposits from various floods.

Our previous studies revealed large differences in sedimentation rates among the terrain units we mapped in 1992, but we needed more data on sediment deposition on inactive-floodplain and abandoned-floodplain cover deposits (hereafter referred to as inactive and abandoned floodplains). We focused on these two terrain units because (1) they are the highest floodplain steps and thus are affected only by large floods, (2) they typically have interbedded mineral and organic layers that are ideal for radiocarbon dating, and (3) they are widely distributed across the floodplain, so they can be used to analyze the effect of distance. We define inactive floodplains as areas having interbedded mineral and organic layers near the surface and surface morphology that vary from nonpatterned to low-density, low-centered polygons. The most common vegetation type on this deposit is wet sedge-willow meadows. Vegetation on inactive floodplains appears to be more productive than vegetation on abandoned floodplains due to occasional sediment input. In contrast, abandoned floodplains typically have massive organic deposits (lacking interbedded mineral layers at the surface but with interbedded layers at depth); evidence of cryoturbation in the sediments, which is indicative of slow sediment accumulation; and high-density, low-relief polygons. The vegetation on abandoned floodplains is a complex association of wet and moist tundra types, with a prevalence of dwarf evergreen shrubs that typically occur in areas of low disturbance and low nutrient input. The height of abandoned floodplains averages 15% more than inactive floodplains (Jorgenson et al. 1996). Because of the large differences in sediment stratigraphy and vegetation composition between these two types of floodplain deposits, we hypothesized that they had different flooding regimes. The differences in surface-form associated with formation of ice-wedge polygons were used to differentiate these types on aerial photographs.

Finally, we hypothesized that there are differences in the magnitude of flooding between the floodplain along the East Channel, which is confined to the west by large, nearly continuous sand dunes, and the floodplain along the lower Nechelik Channel; we based this hypothesis on differences in soil stratigraphy and surface patterns between the two areas. One reason that we suspect the difference in flood regions (subdivi-

sions of the delta) may be important is the effect of ice jamming at the head of distributaries, which forces more flow, and consequently higher flood stages, along the East Channel than would otherwise occur.

The goals of this study were to use paleoflood indicators to evaluate the magnitude, distribution, and frequency of large flooding events. Specific objectives of this study were to:

- 1) characterize the nature (structure and particle size) of slackwater deposits,
- 2) evaluate whether sediments from the 1989 flood could distinguished from other deposits,
- 3) evaluate differences in sediment deposition away from the riverbank, between terrain units and between flood regions, to identify which stratigraphic conditions are best for estimating return periods,
- 4) estimate the return period for the 1989 flood by dating the depositional sequence and ranking the relative magnitude of the event, and
- 5) estimate the stage of the 1989 event using paleostage indicators such as driftlines and the occurrence of slackwater deposits.

METHODS

SAMPLING DESIGN

To analyze the geographic variability in sediment distribution, we allocated sample locations according to a three-factor design that incorporated six distances (7, 66, 164, 328, 656, and 1640 ft) from the riverbank, two terrain units (inactive- and abandoned-floodplain cover deposits), and two flood regions (1 and 2) (Figure 2-1). The initial design specified that each treatment be replicated five times for a total of 120 samples along 20 transects. During sampling, however, some conditions could not be met, resulting in a total of 101 profiles along 19 transects (Appendix Table B-1). Distances perpendicular from the riverbank were measured with a tape measure. Due to the complex drainage patterns on the delta, transect length often was shortened to avoid back channels. Our integrated-terrain-

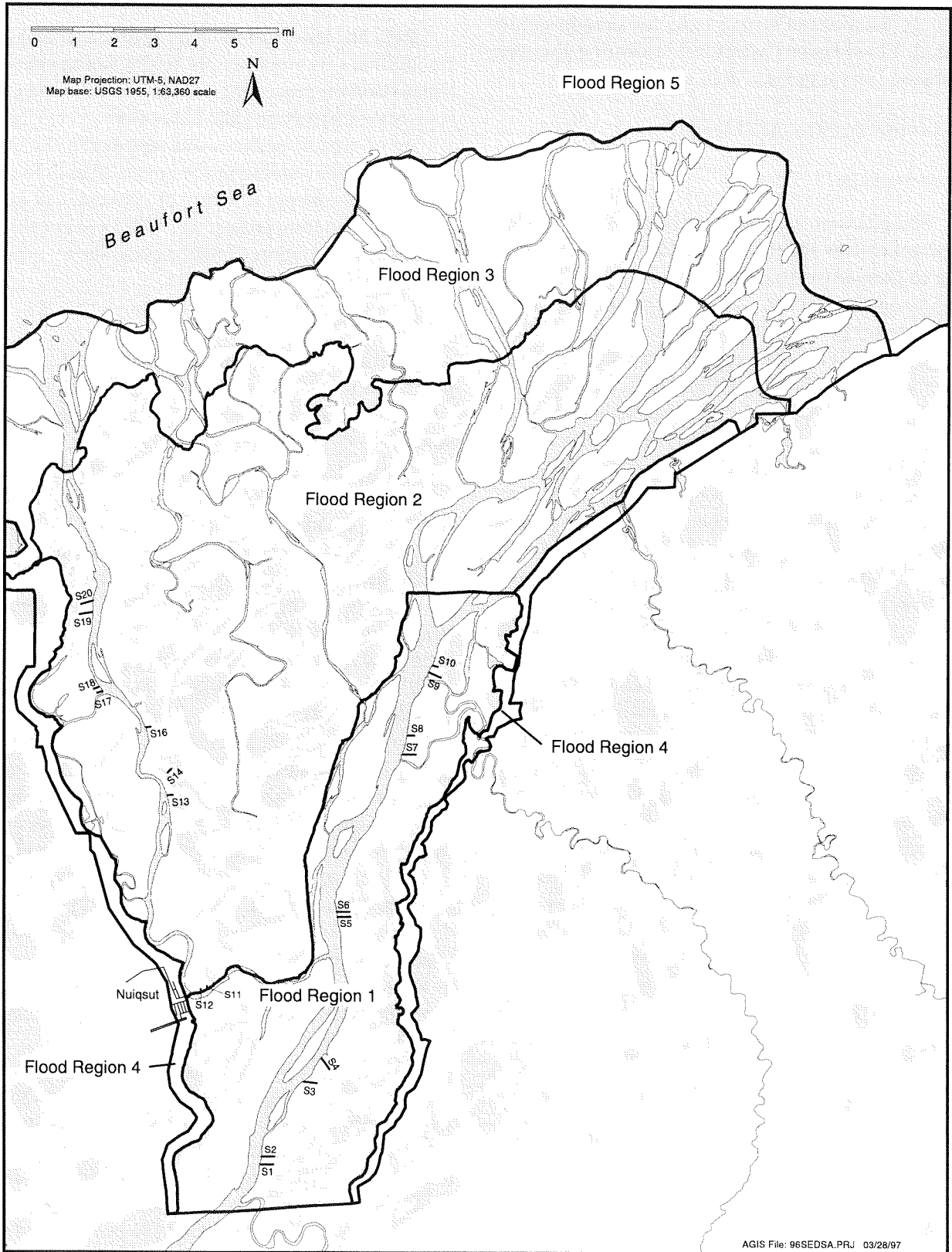


Figure 2-1. Map of locations of surface-sediments transects, Colville River Delta, Alaska, 1996.

unit (ITU) map (Jorgenson et al. 1996) was used to identify locations of terrain units for sample stratification. Flood regions used for stratification also were obtained from Jorgenson et al. (1996).

SEDIMENTATION AND DATING

Field Methods

Soil pits were located in polygon centers or in the appropriate low sediment catchment areas and were dug to permafrost, approximately 1.2–1.5 ft (35–45 cm), to obtain an intact core for description. Descriptions of soil profiles emphasized mineral sediments interbedded between the organic horizons. Field textures were described for all horizons. Taste testing and hand lenses frequently were used to find trace levels of mineral particles in organic material. Grab samples and volumetric (2 x 2 x 2 in.) samples were taken from the horizons ascribed to the 1989 flood event. These samples later were analyzed for particle size and organic matter content (loss on ignition). For a limited number of profiles, organic samples were removed from the permafrost horizon (at approximately 1.5-ft depth) so that radiocarbon dates could be determined for the bottom of the described profile.

After river freeze-up during October 1996, a series of cores were obtained with a SIPRE corer in Flood Region 1. Cores were taken at the 328-ft (100 m) and a 1640-ft (500 m) distance on sediment transects 1, 3, and 9. The objective was to retrieve an undisturbed volumetric sample with an associated organic subhorizon for radiocarbon dating. Cores were drilled to 2 ft (60 cm). Unfortunately, incomplete cores were retrieved due to incomplete freeze-back at the time of drilling. Freeze-back had reached the 10–14 inch (25–35 cm) range, thus leaving a thin, unfrozen zone. The recovered cores were labeled and returned to Fairbanks for soil description and sample preparation. All horizons above 1.6 ft (50 cm) were analyzed for mineral content by loss on ignition tests, and the bottom organic horizon at 1.6–2.0 ft (50–60 cm) was used for radiocarbon dating.

Laboratory Methods

Particle-size distribution by hydrometer and loss-on-ignition (on a subsample basis) were performed using standard procedures (Klute 1986) by the Colorado State University Soils Laboratory in Ft. Collins. Dating of organic samples was obtained by standard radiometric analysis by Beta Analytic, Miami, Florida. Dates were reported in terms of conventional radiocarbon years before present (RCYBP) and as calendar years after calibration of radiocarbon age to calendar year.

Data Analysis

Soil descriptions were compared with close-up photographs to ensure that textural classes (particularly, Oi w/s Si versus Si w/s Oi) (For textual abbreviation: Oi=Fibric organic, Si=Silt, Sa=Sand, L=Loam) were consistent among profiles. For analysis, field textures were grouped into mineral (Sa, Si, SiSa, SiL, Si w/t Oi), organic–mineral mixtures (Si w/s Oi, Oi w/s Si, Oi w/s Sa), or organic (Oi, Oi w/t Si) layers.

To help identify sediments deposited by the 1989 flood event, photographs of profiles at different distances were compared within transects and distinctive layers that could be followed across the transects were identified. The mineral or organic–mineral layers at or near the surface (0–4 in., most cases within 1 in.) were assumed to have been deposited by the 1989 flood. In a few cases next to the riverbank, a thin silt layer above a massive underlying silt layer was assigned to the 1993 flood, based on flood maps delineating overbank flooding during that minor flood. We ranked the relative size of the sediment deposits within a profile by comparing the thickness and grayness of the various layers. This process required subjective appraisals because some sediments were washed down or diluted into underlying organic layers and, therefore, thickness was not always a reliable means of ranking the mass of deposited sediments.

A simple, factorial general linear model (multivariate analysis of variance [MANOVA]; SPSS software, SPSS, Inc.) was used to test the significance of distance, terrain units, and flood regions on (1) the thickness of the 1989 deposit, (2) total mineral accumulation (sum of mineral layers), and (3) the rank of the 1989 flood. The mean and 95% confidence intervals were calculated for each dependent variable.

ESTIMATION OF RETURN PERIOD

The return period (average period of years expected between similar-sized events) for the 1989 flood event was calculated in three ways. The first approach used the average accumulation rate (depth to radiocarbon sample, age of sample) to estimate the age of the next older sediment deposit that was larger than the 1989 flood. Restated, this approach calculates the 1989 event to be the largest flood in x number of years, assuming that material (mineral and organic) accumulation rates are constant and that the amount of sediment is proportional to the magnitude of the flood. The number of years (x) present varied by sample location. We did not date the next larger flood directly (i.e., by dating the organic layer immediately below the mineral layer) because samples from the middle of the active layer probably would have been contaminated by live roots and because the ages would be too young for reliable radiocarbon analysis.

The second approach for determining the return period used the Weibull formula for calculating exceedence probabilities (Maidment 1992):

$$R = 1 \div (i \div (n + 1))$$

where:

R = return period (years)

i = rank of observation

n = number of observations (years)

This formula differed from the standard approach of examining the statistical distribution of observations because small events were not evident in the sedimentary record. Instead, we used the radiocarbon date for the observation period. Standard approaches to calculation exceedence probabilities could not be used because (1) the mass of sediment associated with each event was not quantified and (2) the depositional layers in the sediments were associated only with larger events, and thus did not contain a record of high-frequency events. We evaluated other formulas (Hazen, Cunnane, and Gringorten formulas in Maidment 1993), but chose the Weibull formula because it gave the youngest estimates of return period and because the observation period established by the radiocarbon dating was relatively long (hundreds of years). The advantage of this approach was that it did not require calculation of accumulation rates; the disadvantage was that it was sensitive to ranking.

The third and most conservative approach was similar to the second approach but added 1 to the rank of the deposits. Adding one rank was done to compensate for errors inherent in ranking and to compensate for the chance that another large flood may happen in the next few years.

PALEOSTAGE INDICATORS

During fieldwork from 1992 to 1996, the elevation of driftlines were measured along cross sections established for hydrologic studies and along transects established for ecological land survey studies (Jorgenson et al., 1997.). We conducted an additional search for driftlines near Cross-section E27.09. When possible, driftwood lines were surveyed with reference to temporary bench marks (TBM) established in 1995. The elevations were adjusted to conform to the elevations of new monuments established in 1996 using the BPMSL datum (Appendix Table A-1). When no TBM was nearby, the driftline was surveyed relative to the water level in the tidal river. Due to small tidal variation during low water and the effect of wind-driven tides, the accuracy of this method is approximately ± 1 ft.

A driftline was defined as a collection of driftwood or debris (human debris and other flotsam) judged to have been transported and deposited by a flood event. Single pieces of driftwood were not considered because their mode of transport could not be ascertained. The driftline associated with the 1989 flood was identified by several characteristics (1) it was gray from moderate weathering, (2) it was imbedded 1–3 in. into the moss mat, indicating an approximate age of 5–15 yr, (3) it was the highest driftline evident, and (4) on a few occasions, the ages of willow stems growing under the driftwood were estimated by counting growth rings or stem nodes to reveal the number of years of growth since the stem was covered. Because the 1989 flood was the largest flood in at least 39 years and because it is likely that older driftwood would be covered by moss growth, we are confident that the highest driftline was associated with the 1989 flood. Only the maximum elevations of driftlines found at a site were used for analysis.

We also used soil stratigraphy and elevation data from the ecological land survey to identify the highest elevations where slackwater deposits were present and the lowest elevations where slackwater deposits were

absent. Slackwater deposits that were at or near the surface (0–3 in.) were attributed to the 1989 flood.

COMPARISON WITH ESTIMATES FROM HYDROLOGIC MODELING

We compared the results from our paleoflood analysis to those from modeling of hydrologic flow across the delta to assess the amount of agreement between the two approaches. We compared our data from one large event, the 1989 flood, with outputs from a two-dimensional physical model of hydrologic flow in the delta (Shannon and Wilson, 1997). To assess agreement, we first compared the elevations of driftlines around the proposed Alpine facilities with water-surface elevations predicted by the model for floods of three magnitudes (50-, 100-, and 200-yr return periods). Then the discharge associated with the 1989 flood was estimated by determining the discharge for the stage that best fit the distribution of driftlines.

In our comparison, we examined discharges associated with the flood-frequency relationship for both the base flow-frequency curve (average discharge associated with a given probability of occurrence) and the flow-frequency curve that incorporates expected probabilities (average probability associated with a given discharge). We include both here because the base curve provides estimates for average relationships, which are similar in concept to our estimate of return period for the 1989 event, whereas the estimates that incorporate the expected probabilities are more appropriate for facility design.

RESULTS AND DISCUSSION

CHARACTERISTICS OF SURFACE SEDIMENTS

Sediments from the 1989 and other flood events formed distinctive interbedded deposits near the riverbank, and formed massive nonbedded deposits away from the riverbank; these latter deposits were comprised of fine sand, silts, and clays interbedded with organic material (Figure 2–2, Appendix Figures 2-1 to B2-3 for representative profiles). The 1989 deposit was distinguished by its large size and proximity (0–3 in., usually <1 in.) to the surface. In addition, it was nearly always the thickest layer in the top half of the active layer, supporting the assumption that it was deposited by the largest flood in at least 39 years. Finally, this deposit always was found below the high-

est driftlines, indicating that it was associated with the same event that left the driftlines. In some locations near the riverbank, a thin layer (1–5 mm) of sediments was found above the thicker 1989 deposit, and was attributed to flooding in 1993. Usually, the mineral deposits in the upper portion had distinct lower boundaries, although occasionally an illuvial zone was evident where mineral material was washed down into the underlying organics. For deeper sediment layers, the boundaries often were indistinct or gradual, indicating more translocation of sediments. Differences in particle-size characteristics due to distance from the riverbank and terrain units are described below.

Distance from riverbank appeared to have a strong effect on particle-size distribution (sand-silt-clay) within 164 ft (50 m) of the bank and possibly smaller effects farther away (Figure 2–3). Fine sand dropped substantially within 164 ft (50 m) but changed little thereafter. Silt increased substantially within 164 ft (50 m), but changed little thereafter. Clay showed little change throughout the 1640-ft (500 m) measurement length.

Small sample size prevented more rigorous analysis of particle-size changes. The data are sufficient, however, to conclude that the effect of distance is negligible, in comparison to other factors, for samples taken at distances >328 ft (100 m) from the riverbank. The lack of difference in particle-size composition at distances >328 ft also indicates that the velocity of water flow, and the composition of suspended sediments, was fairly uniform.

SEDIMENT DISTRIBUTION

An understanding of the factors affecting the geographic variability of fluvial sediments is important to assess the reliability of analytical techniques used to analyze flood frequency and elevations associated with paleostage indicators. The effects of distance, terrain units and flood region (MANOVA procedure) on 1989 sediment deposition, total mineral accumulation, and ranking of the 1989 deposit (relative to other slackwater deposits) are described below.

1989 Flooding Event

The thickness of 1989 flood sediments differed significantly ($P = 0.002$, $df = 22$, $F = 2.45$) with respect to distance, terrain units, and flood regions (Appendix Table B–2). Differences related to the indi-

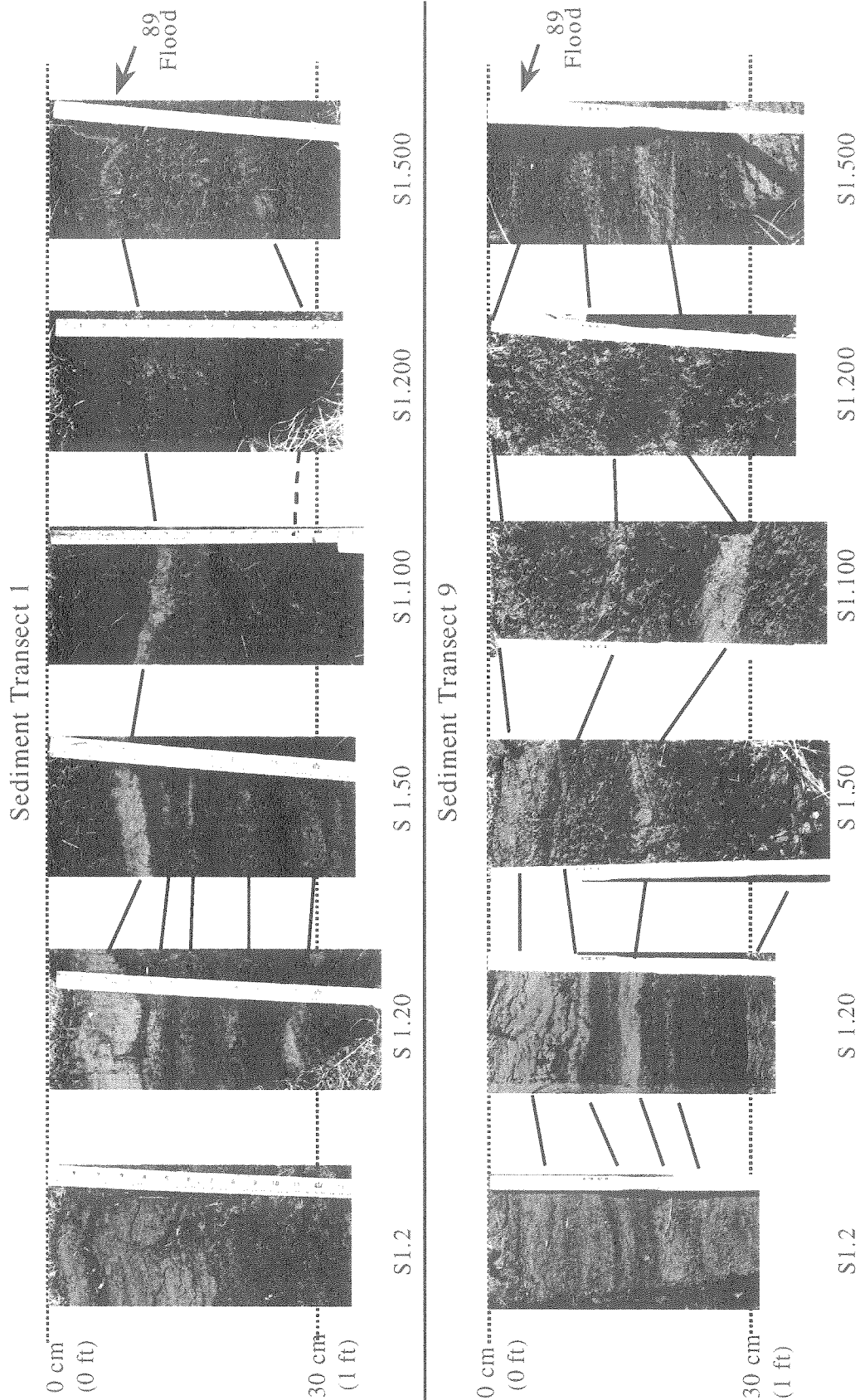


Figure 2-2. Photographs of soil profiles (with sample ID) at six distances away from the river bank at Transects 1 and 9, Colville River Delta, Alaska, 1996. Lines between photographs indicate the location of different flood events along the length of a transect.

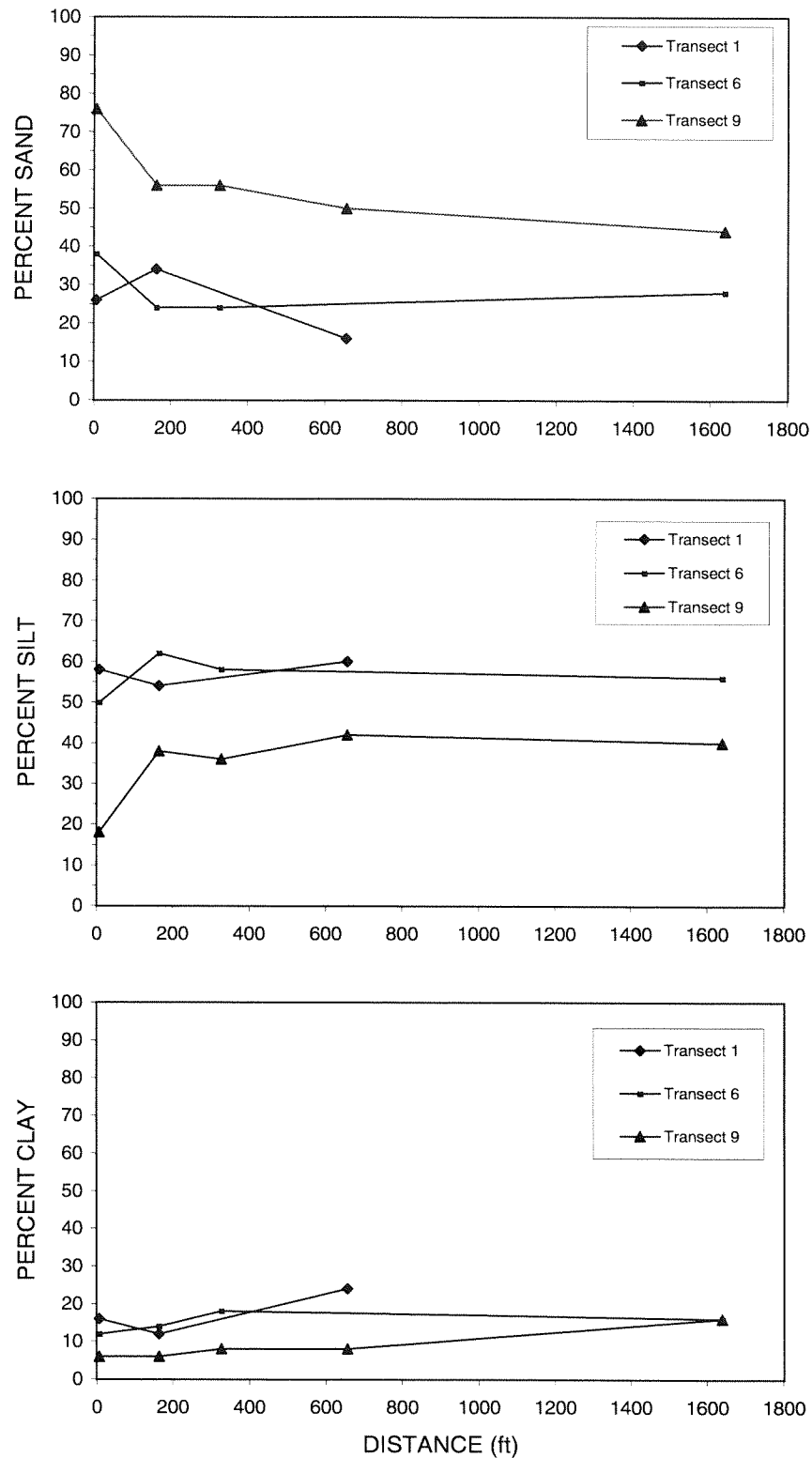


Figure 2-3. Relative composition (%) of sand, silt, and clay particles relative to distance from the riverbank within two terrain units, Colville River Delta, Alaska, 1996.

vidual factors are discussed below.

Distance had a highly significant ($P = 0.002$) effect on the distribution of 1989 flood sediments with the greatest accumulation occurring near the riverbank (Figure 2-4). Mean sediment thickness at 7 ft (0.24 ft, 7.4 cm) was significantly ($P = 0.002$) greater than the thickness at 164 ft (0.14 ft, 4.3 cm), but sediment thickness at distances from 328 to 1640 ft (0.12 ft to 0.08 ft, or 3.8 to 2.5 cm, respectively) did not differ significantly from the thickness at 164 ft.

In contrast, there was no significant ($P = 0.221$) difference between terrain units in the mean thickness of 1989 sediments (0.15 vs. 0.16 ft, or 4.6 vs. 4.8 cm, for abandoned and inactive floodplains, respectively)(Figure 2-4). Differences between terrain units within flood regions, however, did reveal trends that may indicate changes in flooding regime. Within Flood Region 1, the mean thickness of the 1989 flood sediments on abandoned floodplains (0.19 ft, 5.8 cm) was similar to that on inactive floodplains (0.18 ft, 5.6 cm), whereas within Flood Region 2, mean thickness of sediments on abandoned floodplains (0.07 ft, 2.2 cm) was 42% less than on inactive floodplains (0.13 ft, 3.9 cm)(Appendix Figure B-2).

The difference in the distribution of slackwater deposits between flood regions was highly significant ($P < 0.001$) (Figure 2-4). Mean thickness of 1989 sediments within Flood Region 2 (0.11 ft, 3.3 cm) was 42% lower than in Flood Region 1 (0.19 ft, 5.7 cm).

These results have several important implications. First, because deposits from the flood events of 1989 and other years formed distinctive layers that generally could be traced continuously away from the bank, the presence of slackwater deposits appears to be a reliable indicator of large floods. Second, the rapid decrease in thickness of the 1989 flood deposits at distances within 164 ft (50 m) of the bank indicates that samples from this zone should not be used to analyze return periods. Third, the difference in sediment thickness between flood regions indicates that there were substantial differences in the depth of floodwater over the bank. Moreover, the data suggest that the depth of flooding in Flood Region 1 was high enough that the small difference in relative elevations (15%) between the two terrain units had little effect on sedimentation. In contrast, the small differences in elevations between the two terrain units in Flood Region 2 appeared to have a substantial effect on sedimentation, presumably due to shallower floodwater.

Total Mineral Accumulation

Analysis of differences in total mineral accumulation (sum of thickness of visually distinct layers dominated by mineral material) was used to assess the cumulative effects of flooding over time. Differences in total mineral accumulation due to the effects of distance, terrain units, and flood regions were highly significant ($P < 0.001$, $df = 23$, $F = 6.41$) (Appendix Table B-3). Differences related to the individual factors are discussed below.

Total mineral accumulation was significantly greater ($P < 0.001$) near the riverbank (Figure 2-5). Mean thickness dropped significantly ($P < 0.001$) from the 7-ft distance (0.50 ft, 15.2 cm) to the 328-ft distance (0.12 ft, 3.8 cm), but not between 328-ft and 1640-ft (0.11 ft, 3.5 cm, $P > 0.91$). In general, total mineral accumulation decreased more consistently with distance on inactive floodplains than on abandoned floodplains (Appendix Figure B-3).

Within terrain units (flood regions and distances combined), mean thickness in total mineral accumulation was 28% less ($P = 0.001$) on abandoned floodplains (0.20 ft, 6.2 cm) than on inactive floodplains (0.28 ft, 8.6 cm) (Figure 2-5). Both deposits, however, had highly variable (0-0.8 ft, 0-24 cm range) mineral accumulations.

Within flood regions (terrain units and distances combined), mean total mineral accumulation in Flood Region 1 (0.26 ft, 7.9 cm) was not significantly ($P = 0.180$) different from Flood Region 2 (0.23 ft, 7.1 cm) (Figure 2-5). Within terrain units, however, total mineral accumulation differed between the flood regions on abandoned floodplains (0.25 vs. 0.15 ft, 7.5 vs. 4.5 cm, respectively) but not on inactive floodplains (0.27 vs. 0.31 ft, 8.3 vs. 9.6 cm, respectively).

The distribution of total mineral accumulation generally is similar to that obtained for the 1989 flood deposits. Both the 1989 flood deposits and total mineral accumulations reveal that sedimentation decreases sharply away from the bank, indicating that there is a rapid decrease in water velocity as the floodwater overtops the banks and heavier suspended particles drop out. In addition, both analyses support our conclusion that samples taken at distances of 328 ft (100 m) away from the bank provide the best data for comparing the relative thicknesses of sediment deposited by individual flooding events.

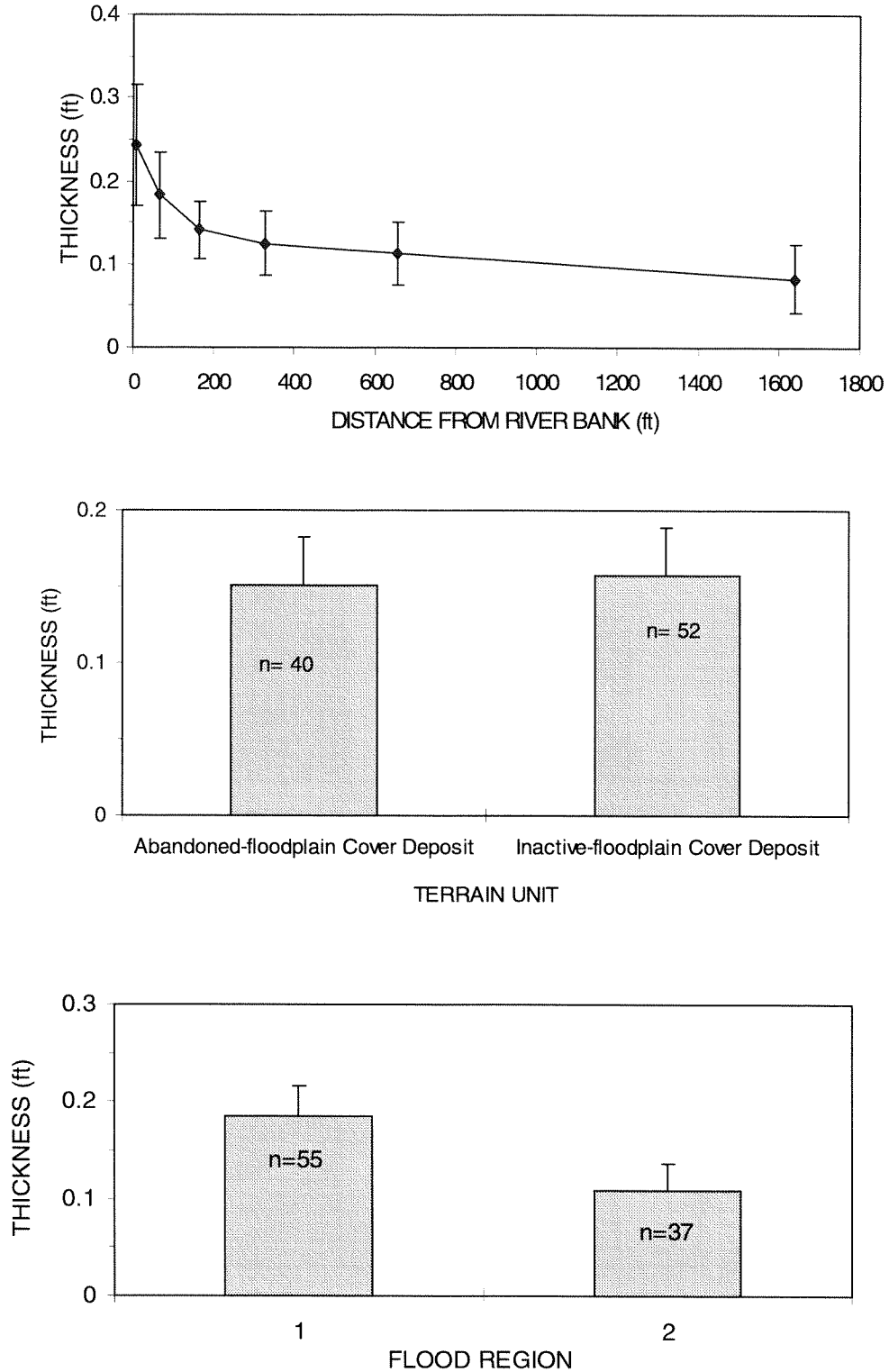


Figure 2-4. Mean ($\pm 95\%$ confidence interval) thickness of sediments deposited by the 1989 flood relative to distance from riverbank, terrain unit, and flood region, Colville River Delta, Alaska, 1996.

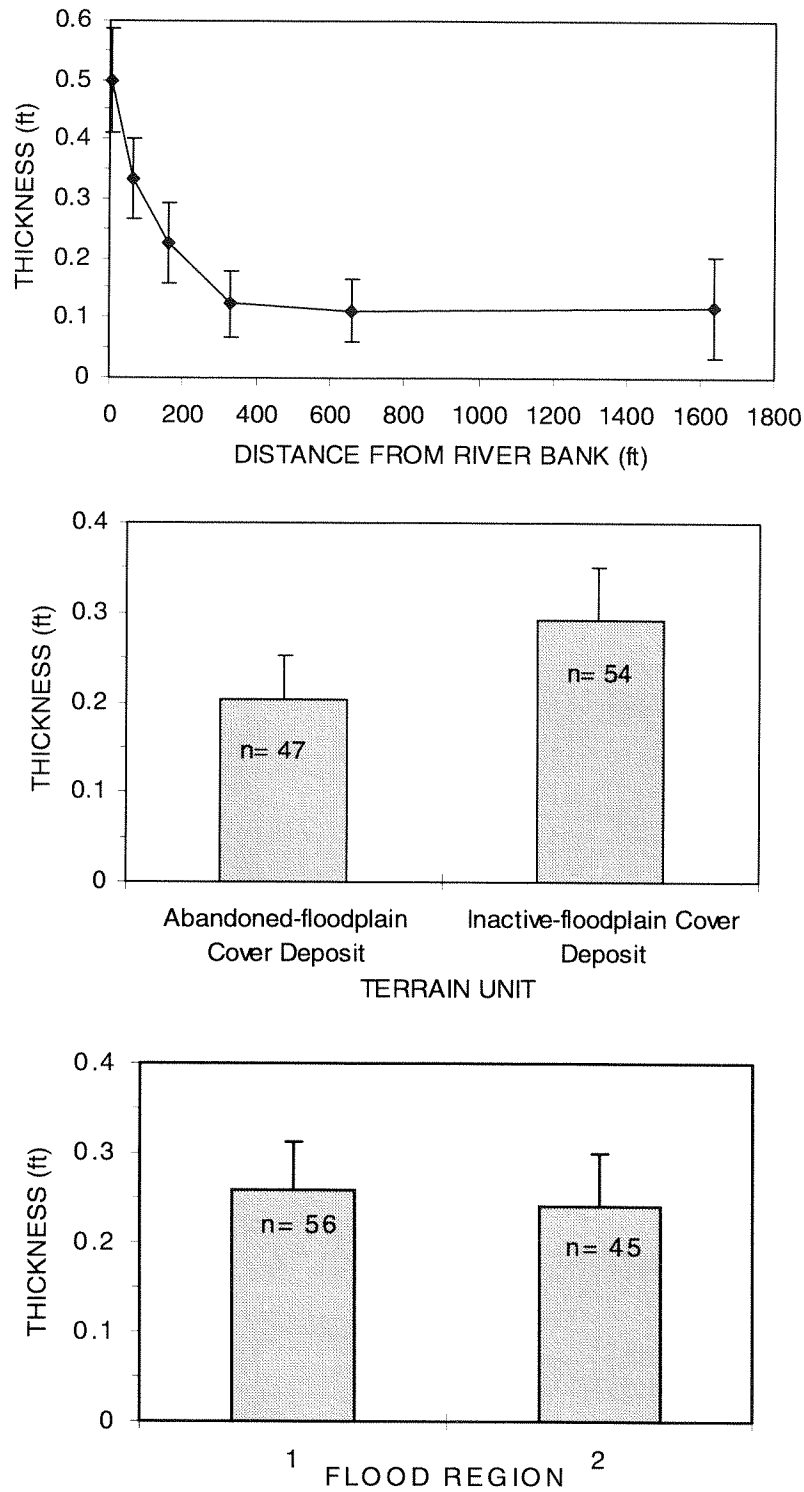


Figure 2-5. Mean ($\pm 95\%$ confidence interval) thickness of mineral sediments within the top 1 ft relative to distance from riverbank, terrain unit, and flood region, Colville River Delta, Alaska, 1996.

The greater accumulation of total mineral sediments on inactive floodplains in comparison to abandoned floodplains also is supported in part by the differences found for the 1989 flood deposits. While there was no overall difference in mean thickness of 1989 flood deposits between terrain units, there were substantial differences within Flood Region 2. This suggests that flood water was deep enough in Flood Region 1 that the small difference (15%) in relative elevation between the two terrain units did not have much effect on sedimentation. In Flood Region 2, small differences in elevation appeared to have substantial effect.

Vertical Ranking of Depositional Events

The size of the individual flood deposits were ranked visually according to their thickness and grayness (a subjective interpretation of sediment mass) and were cross-referenced with distance along a transect (Figure 2-2, Appendix Figures B-1). Overall, the mean ranking (2.2) of the 1989 flood event indicates that it was the second largest event with the period delimited by the radiocarbon dating. Differences in ranking due to distance, terrain units, and flood regions were highly significant ($P = 0.003$, $df = 22$, $F = 2.43$) (Appendix Table B-4). Differences in ranking due to individual factors are discussed below.

Distance had only a marginally significant effect on ranking of the 1989 flood event ($P = 0.054$) (Figure 2-6). Multiple comparison tests revealed significant increases ($P = 0.046$) in rank within the first 164 ft (from 1.7 to 2.4), although differences between 164 ft and distances >164 ft (2.4 to 2.9) were not significant.

Terrain units had no significant ($P = 0.286$) effect on ranking (Figure 2-6). The mean ranks of the 1989 event within abandoned and inactive floodplains were identical.

Flood region did have a significant effect on ranking ($P < 0.001$) (Figure 2-6). The ranking revealed that the 1989 flood was the second largest event (mean rank = 1.8) in Flood Region 1 and the third largest event (mean rank = 2.9) in Flood Region 2 over the observation period established by radiocarbon dates.

The ranking results are consistent with those from the other sediment analyses. First, at close distances, channel migration and increased deposition near the bank affects ranking (e.g., deposits next to the bank from a small flood could appear larger than the depos-

its from a large flood at long distances from the bank). Thus, samples taken from distances of 328 ft (100 m) are most reliable for analysis of flood frequency. Second, the effects of terrain units are negligible for the purposes of ranking magnitudes of large events. Third, differences between flood regions indicates that flooding historically has been greater in Flood Region 2 and that the proportion of flow going down the Nechelik Channel has decreased in recent times. This conclusion is supported by observation of infilling of the Nechelik Channel and the recent inability of Nuiqsut residents to use the head of the channel during low water.

Accumulation Rates

The highly organic nature of floodplain cover deposits was ideal for estimating rates of accumulation of mineral sediments and organics (Figure 2-7). All radiocarbon samples in 1996 were taken from the top of the permafrost to avoid contamination by roots, whereas a few samples in earlier years were obtained at shallower depths within the active layer (Appendix Table B-5).

The overall mean accumulation rate for sediments (mineral sediments and organics combined) near the surface (active layer and top of permafrost) was estimated to be 0.33 ft/100 yr, but varied widely between terrain units. Within Flood Region 1, the accumulation rate for abandoned floodplains (0.15 ft/100 yr) was about a quarter of the rate on inactive floodplains (0.66 ft/100 yr) (Figure 2-8). Similarly, within Flood Region 2, the accumulation rate for abandoned floodplains (0.10 ft/100 yr) was about a third of the rate on inactive floodplains (0.29 ft/100 yr). Accumulation rates were twice as high in Flood Region 1 (0.39 ft/100 yr) than in Flood Region 2 (0.18 ft/100 yr).

These large differences in accumulation rates potentially could have a large effect on our estimates of return periods, because the estimate of years to the next largest event depends on the rate of accumulation. The difference suggests that estimates of return periods should be calculated separately for each terrain unit.

ESTIMATED RETURN PERIOD FOR THE 1989 FLOOD EVENT

Material accumulation rates, determined by radiocarbon dating of organic material interbedded with

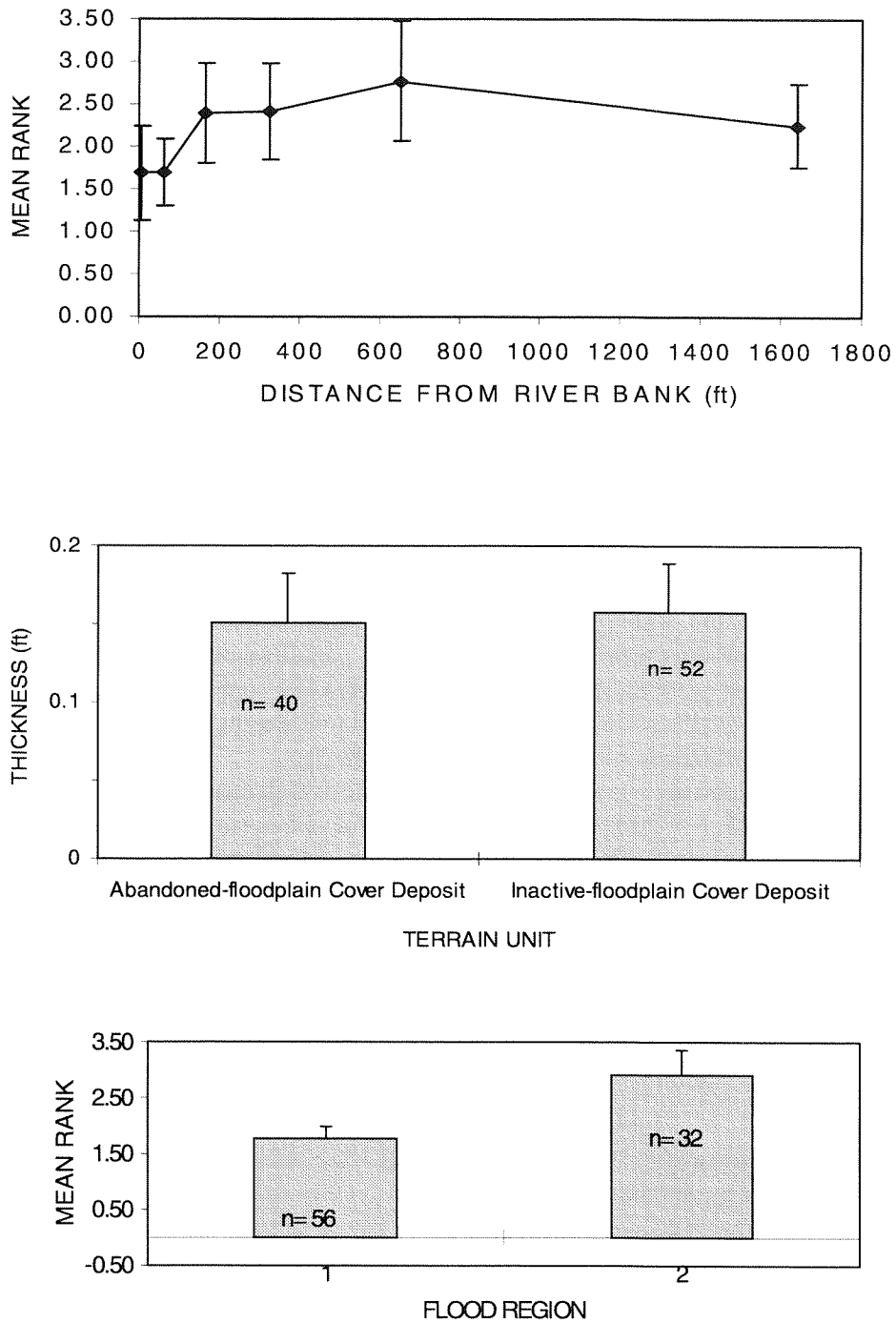


Figure 2-6. Mean ($\pm 95\%$ confidence interval) relative rank of 1989 sediment deposit relative to distance from riverbank, terrain unit and flood region, Colville River Delta, Alaska, 1996.

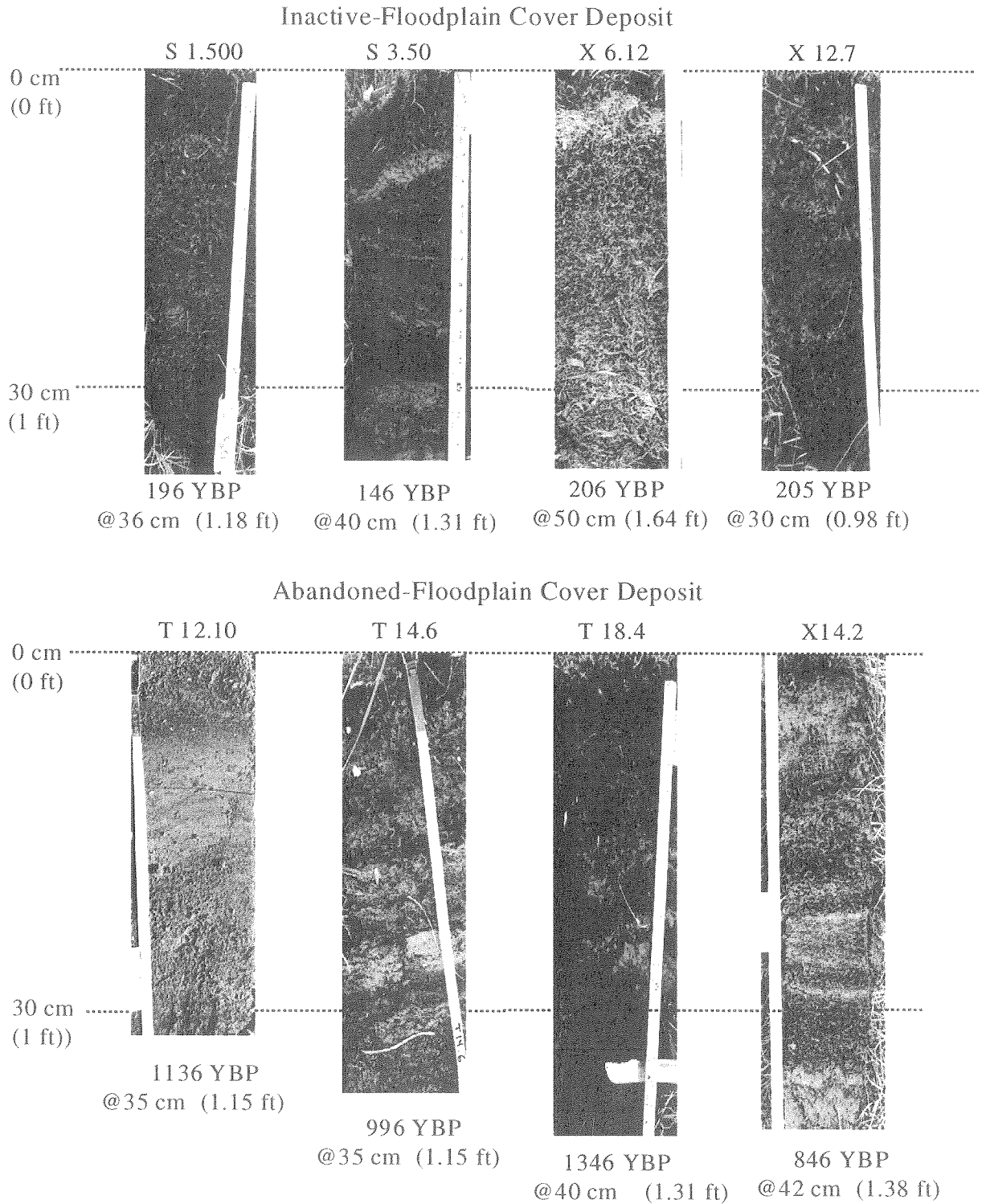


Figure 2-7. Photographs of selected soil profiles with conventional radiocarbon dates from inactive- and abandoned-floodplain cover deposits, Colville River Delta, Alaska, 1996.

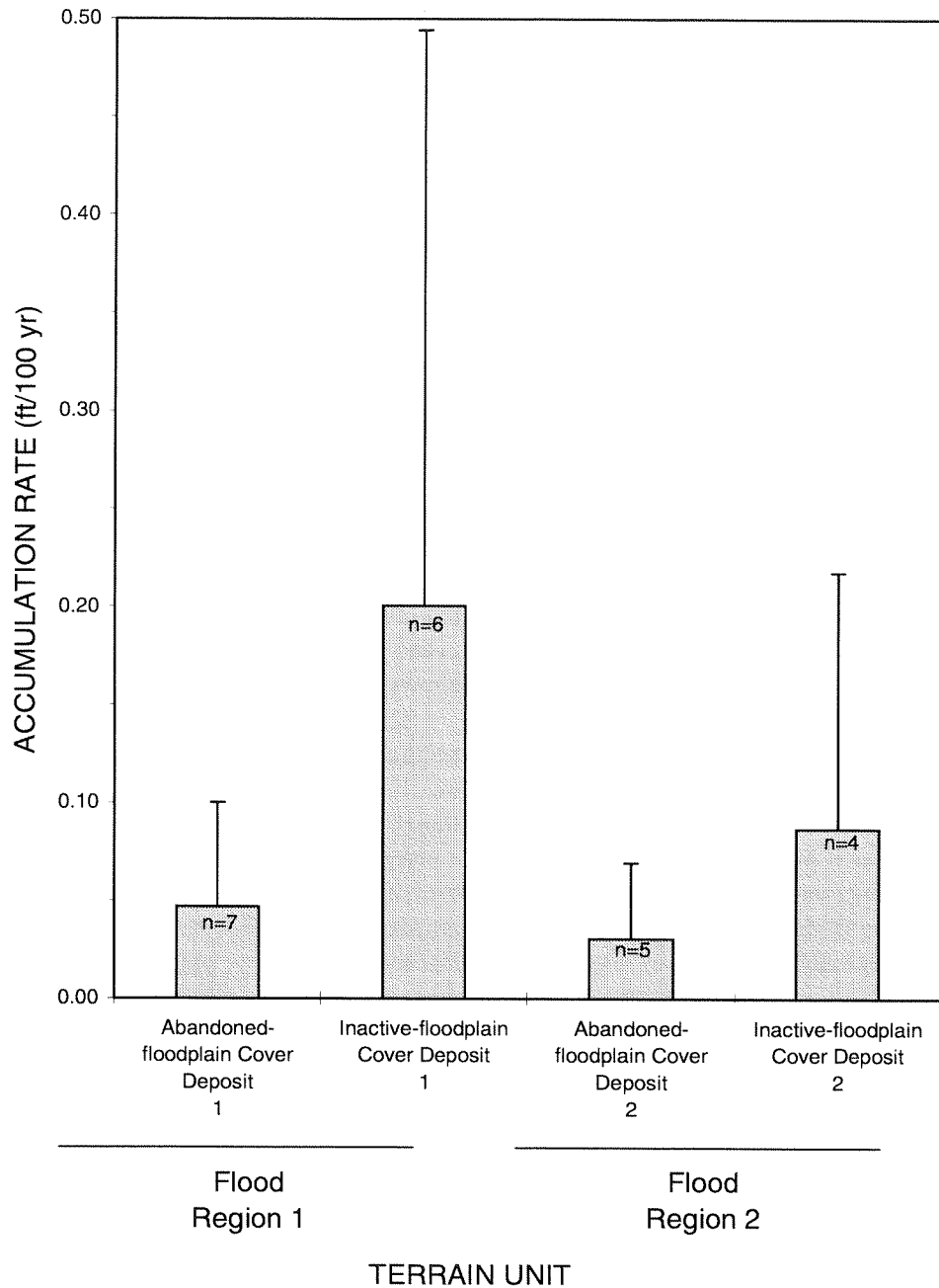


Figure 2-8. Mean ($\pm 95\%$ confidence interval) rates of sediment accumulation (mineral and organic) between inactive- and abandoned-floodplain cover deposits, Colville River Delta, Alaska, 1996.

fluvial sediments, were used to date various flooding events and to establish the period of observation over which depositional events were ranked (Table 2-1, Appendix Table B-5). In these analyses, estimates of the return period were calculated for both abandoned and inactive floodplains because of large differences in sediment accumulation rates. Results from three different approaches were used to determine the return period for the 1989 flood (using sites at 328 ft from the riverbank), as described below.

The most straightforward technique for estimating return period used rates of sediment accumulation (mineral and organic combined) to estimate the age of the next larger flooding event older than the 1989 flood (assuming that thickness of depositional layer is proportional to flood magnitude and that accumulation rates are constant over time). Mean estimated age to the next larger event was 468 yr (± 156 yr) on abandoned floodplains and 150 yr (± 31 yr) on inactive floodplains, with a combined mean of 289 yrs (± 104 yrs) (Figure 2-9). The most conservative interpretation of the data used the lower confidence limit of the mean on the inactive floodplain, giving an estimated return period of 119 years.

The second approach was to rank the 1989 flood relative to other depositional events, thereby providing a way to assess the flood frequency over a longer time period. On abandoned floodplains, the mean rank of the 1989 flood was 3.5 over a mean time period of 1074 years, for a mean return period of 361 years (± 121 yrs) (Figure 2-9). On inactive floodplains, the mean rank of the 1989 flood was 2.7 over a mean time period of 308 years, for a mean return period of 128 years (± 32 yrs). In the most conservative interpretation of the data using the lower confidence limit of the mean on the inactive floodplain, the estimated return period was 96 years.

In the third, most conservative approach to ranking of the 1989 flood relative to other depositional events, the rank of the 1989 flood was increased by 1 to compensate for errors associated with ranking and for the chance that a similar-sized flood may happen in the next few years. On abandoned floodplains, the mean return period estimated with this approach was 253 years (± 55 yrs), whereas on inactive floodplains the estimate was 85 years (± 18 yrs) (Figure 2-9). In the most conservative interpretation of the data using the lower confidence limit of the mean on inactive floodplains, the estimated return period was 67 years.

Each of the different approaches for estimating return periods has advantages and disadvantages. Estimating years to the next larger event (the first approach) avoids ranking of depositional layers that may or may not have been altered by washing or organic expansion, but relies on the assumption that material accumulation is constant over the time period. This approach may overestimate the return period because the interval between the last larger event could have been unusually long and a similar-sized event may happen in the next few years. In contrast, ranking of depositional layers (the second approach) has the advantage of averaging events over a longer time period and avoids the assumption of constant accumulation rates, but relies on subjective characterization of ranks. Fortunately, the second approach is not very sensitive to being one rank off. The third approach probably is too conservative because we do not observe as many events in the sedimentary record as indicated by this approach.

This analysis of return period also relies on the accuracy of radiocarbon dating, which is known to be unreliable for periods less than 300 years. Conventional radiocarbon dates (years before 1950) can be converted to calendar years using calibration curves to compensate for contamination caused by large-scale burning of fossil fuels and testing of nuclear devices. For samples <300 yr old, this calibration yields intercepts and confidence intervals that range from approximately 1650 to 1950 A.D. (Appendix Table B-5). We used conventional radiocarbon dates because they provided single dates, instead of multiple intercepts and ranges, and because they tend to underestimate, the age for samples <500 yr, a conservative approach for our analysis. Thus, the dates associated with the older samples typical of abandoned floodplains are more reliable than samples from inactive floodplains. This interpretation imposes a paradox, however; the abandoned floodplains provide more accurate dates but poorer resolution of depositional events, whereas inactive floodplains have less accurate dates but better resolution. We decided to rely more on return-period estimates obtained from inactive floodplains because they were lower than those obtained from abandoned floodplains, and thus, more conservative.

In summary, for the purposes of facility design we conclude that the 1989 flood was on the order of a 100-yr event (e.g., 128 ± 32 yr). This estimate incorporates conservative biases by using conventional

Table 2-1. Estimates of recurrence interval of 1989 flood event based on dating and ranking of flood events evident in soil profiles, Colville River Delta, Alaska, 1996. NP=not present.

Location	Terrain Unit ^a	Flood Region	Sample Depth (ft)	Years before 1996 ^b	Distance from river (ft)	Material Accumulation Rate (ft/100 yr) ^c	Depth to top of 1989 Deposit (ft)	Thickness of 1989 Flood (ft)	Thickness of next largest deposit (ft)	Depth to middle of bigger deposit (ft)	Estimated Age of Next Bigger Deposit (yr) ^d	Rank of 1989 deposit within date	Return Period Based on Rank ^e	Conservative Return on Rank ^f	Resolution of Sediment Layers ^g
X12.5	Fdci	2	0.56	316	4265	0.18	0.07	0.03	0.03	0.20	112	2	158	105	G
X13.5	Fdci	2	1.64	686	3609	0.24	0.03	0.07	0.03	0.43	178	5	137	114	G
T14.6	Fda	1	1.35	996	2297	0.14	0.10	0.10	0.10	0.82	607	3	332	249	G
T4.05(NS)	Fdci	2	1.05	396	1641	0.27	0.07	0.03	0.10	0.30	111	6	66	57	G
S1.500	Fdci	1	1.28	196	1641	0.65	0.13	0.03	0.10	0.75	116	2	98	65	G
S3.500 ^h	Fdci	1	1.80	296	1641	0.61	0.16	0.03	0.07	0.98	161	2	148	99	G
X12.7	Fdci	2	0.92	205	1641	0.45	0.10	0.07	0.20	1.08	242	2	103	68	G
S9.500 ⁱ	Fda	1	1.80	876	1641	0.21	0.03	0.03	0.03	0.59	287	3	292	219	G
T18.4	Fda	1	1.48	1346	1312	0.11	0.03	0.03	0.10	0.36	329	6	224	192	G
S1.100	Fdci	1	1.80	126	328	1.43	0.36	0.16	0.43	1.08	76	2	63	42	G
X6.12	Fdci	1	1.80	206	328	0.88	0.13	0.13	0.10	1.12	127	1	206	103	G
S3.100	Fdci	1	1.80	346	328	0.52	0.20	0.07	0.10	0.85	164	2	173	115	G
S7.100	Fda	1	1.64	596	328	0.28	0.07	0.10	0.16	0.56	203	1	596	298	G
X6.13b	Fda	1	1.05	1156	328	0.09	0.07	0.03	0.07	0.33	361	5	231	193	G
S9.100	Fda	1	1.80	1476	328	0.12	0.03	0.13	0.10	0.89	725	3	492	369	G
X13.7	Fda	2	1.54	796	7874	0.19	NP	0.00	0.16	0.75	390	NP	NP	NP	G
S3.50	Fdci	1	1.35	146	164	0.92	0.20	0.10	0.16	1.05	114	2	73	49	G
X14.2	Fda	1	1.54	846	164	0.18	0.10	0.16	0.13	1.31	720	1	846	423	G
T2.16(T16)	Fdci	2	0.89	466	0	0.19	0.00	0.07	NP	NP	NP	1	466	233	G
T13.7	Fda	2	1.48	1576	8859	0.09	0.03	0.07	0.16	0.33	350	4	394	315	P
X11.9A	Fda	2	1.90	1996	4265	0.10	NP	0.00	0.75	0.85	895	NP	NP	NP	P
T12.10	Fda	2	1.41	1136	2625	0.12	0.03	0.03	0.30	0.36	291	4	284	227	P
S1.500	Fdci	1	1.80	746	1641	0.24	0.10	0.07	0.13	0.79	326	2	373	249	P
S8.200	Fda	1	1.18	436	656	0.27	0.03	0.13	0.16	0.49	182	2	218	145	P
G1.5	Fda	2	1.41	2216	492	0.06	NP	0.00	0.07	0.30	464	NP	NP	NP	P
S18.50	Fdci	2	1.25	136	164	0.92	0.03	0.07	0.10	0.36	39	4	34	27	P
N23A	Fdci	2	0.43	386	0	0.11	0.00	0.10	0.07	0.30	267	2	193	129	P

^aTerrain Units: Inactive-floodplain cover deposit (Fdci), Abandoned-floodplain cover deposit (Fda).

^bYears before 1996 = conventional radiocarbon years before present (base 1950) of sample + 46.

^cMaterial accumulation rate = (radiocarbon sample depth)/(years before 1996).

^dEstimated age of next bigger deposit = (depth to middle of next bigger deposit)/(material accumulation rate).

^eRecurrence interval based on rank (using Weibull formula for exceedence probability) = 1/(rank/(years before 1996)+ 1).

^fConservative recurrence interval based on rank = 1/((rank + 1)/(years before 1996) + 1).

^gResolution of layers: G - good resolution with distinct mineral layers, P - poor resolution with substantial redistribution of sediments.

^hStratigraphy of S3.500 profile taken from summer profile, radiocarbon date from winter sampling because disruption of sample from 17-33 cm.

ⁱTerrain units mapped as Fdci but reclassified as Fda for this analysis because of cryoturbation features and accumulation rates indicative of Fda.

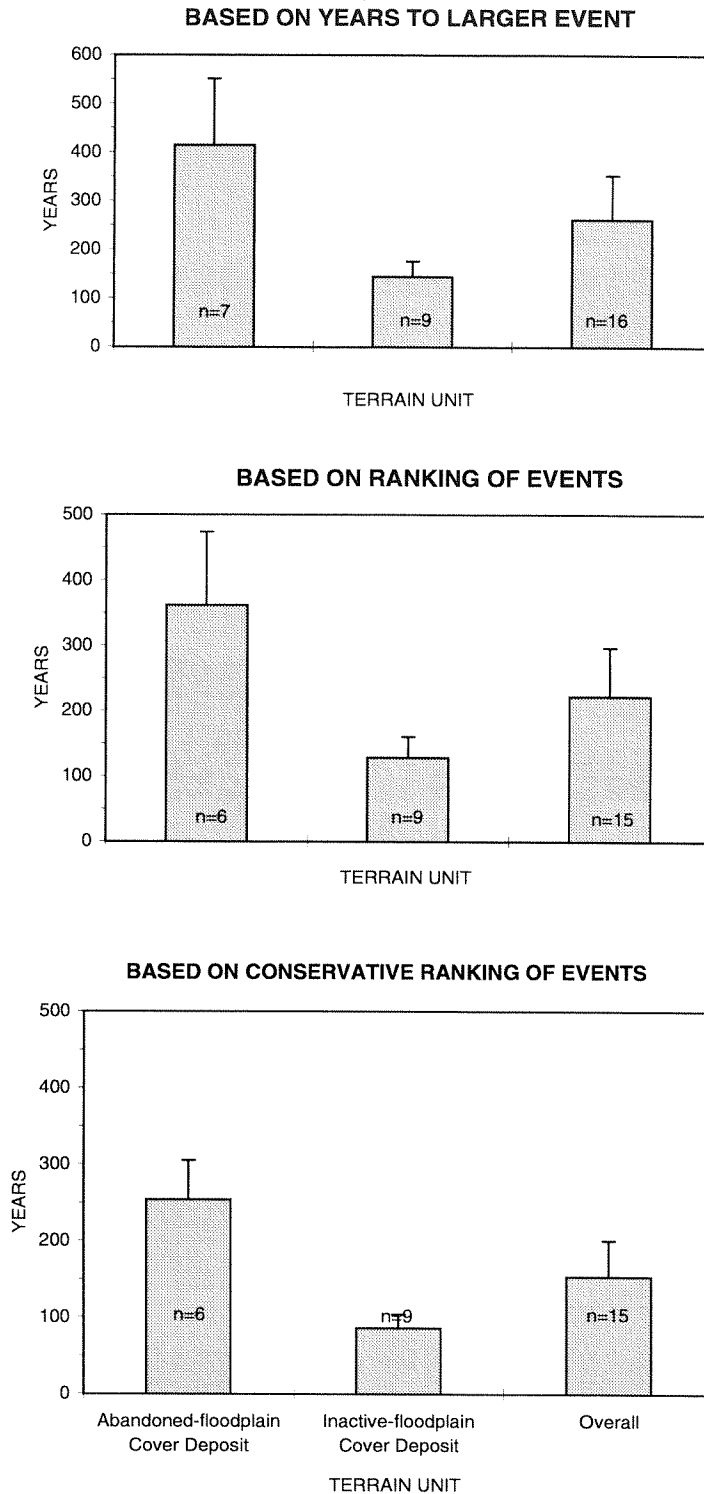


Figure 2-9. Estimated recurrence interval of 1989 flood within inactive- and abandoned-floodplain cover deposits, based on years to next larger event, ranking of depositional layers, and conservative ranking of layers, Colville River Delta, Alaska, 1996.

radiocarbon ages, data sets selected from inactive floodplains, and statistical interpretations using the lower limit of 95% CI, all of which provide the youngest dates. Without these biases, our data suggest that the 1989 event was on the order of a 150–300-yr event.

ELEVATIONS OF PALEOSTAGE INDICATORS

Driftlines and the occurrence of slackwater deposits were used to estimate the elevations of peak stage of the 1989 flood. Each of these indicators has its advantages and disadvantages, as discussed below.

Driftlines

Driftlines associated with the 1989 event were readily identifiable by the moderate weathering (gray wood without lichens) and by their slight embedding in the moss mat (Figure 2–10). A cross-section (T19) along the Sakoonang Channel near the proposed Alpine facilities illustrates the location of a driftline in a typical floodplain landscape (Figure 2–11). During our 1992–1996 field studies, we identified and surveyed 27 driftlines (Figure 2–12). As indicators of peak stage of the 1989 flood event, the driftlines provide data of variable quality in terms of their distinctness, whether they were the highest driftline, whether they were deposited by waning floodwater, and the accuracy of the elevational data (Table 2–2).

Near the proposed Alpine facilities, the mean elevation of the highest good driftlines was 10.6 ft (± 0.67 ft, maximum = 11.2 ft, $n = 7$). We are confident of the quality of the data from the driftlines near the facilities because (1) no driftwood was found above these driftlines, despite a substantial search, (2) the data are well-replicated across a broad area, and (3) all but one of the driftlines were surveyed relative to established monuments, so elevational accuracy should be 0.5 ft given that driftlines vary. Using the maximum elevation of 11.2 ft, the flood water in 1989 probably was 2–3 ft higher than the surface of inactive floodplains in the area and was even with the surface of abandoned floodplains.

At the head of the delta, near Cross-section E27.09 (#6), the mean elevation was 19.1 ft (± 0.8 ft, maximum = 22.9 ft, $n = 4$). We have low confidence in these data because we did not find distinct, continuous driftlines, and because the maximum value of 22.9 ft was poorly replicated (three other driftlines surveyed ranged from 17.8–18 ft). Although the 22.9-ft elevation may be a reasonable estimate, we cannot rule out

the possibility of having missed higher driftlines. The 22.9-ft peak stage was approximately 3.6 ft higher than the average riverbank elevation (19.3 ft on inactive floodplains on the east bank of Cross-section E27.09 [#6]).

Slackwater Deposits

We examined the occurrence of slackwater deposits relative to the driftlines near the proposed Alpine facilities to determine whether their presence could be used to determine stages of large floods (Table 2–3, Figure 2–13). This analysis focused on the Alpine Facilities Area because of gentle differences in slopes and elevations and because the 1989 flood did not cover the entire area. In contrast, at the head of the delta, the 1989 flood covered all of the inactive and abandoned floodplains deposits that we examined.

At five sites situated above the 1989 driftlines, no evidence of surface sedimentation attributable to the 1989 flood was observed. In addition, in all five profiles no other slackwater deposits were found within the top 1 ft, although some fine sand sediments were found in trace amounts or in indistinct layers that were attributed to eolian input (Figure 2–14). At one site (T19.6) below the driftline, no 1989-related deposit was evident at the surface, although three other fluvial layers were evident. At the other four sites just below the driftline, 1989 slackwater deposits were evident, as were other depositional events.

The distribution of slackwater deposits reinforces the contention that the 1989 flood was a very large event. In the area around the proposed Alpine facilities, we found no sedimentary evidence of flooding within 1 ft of the surface at sites above the driftline associated with the 1989 event. Most of these sites were on abandoned floodplains, which have very slow rates of material accumulation (mean of 1 ft/733 yr). The soil profiles near the proposed Alpine facilities also revealed that slackwater deposits usually are evident even when overbank water depths are relatively shallow (<2 ft) (Figure 2–14). Thus, the possibility that there could have been large floods (>2 ft overbank) which left no sedimentary evidence is unlikely (four of five sites within 2.1 ft below driftline showed slackwater deposits). In summary, the lack of slackwater deposits near the surface at sites above the highest driftline (11.2 ft) stage higher than indicated that floods with a stage of 13.3 ft have not occurred for hundreds of years within the Alpine Facilities Area.

Table 2-2. Elevations and quality of driftlines related to the 1989 flood, Colville River Delta, Alaska. Measurements taken between 1992 and 1996. See Figure 2-12 for locations of driftlines surveyed.

Location	Nearest Profile	Year of Observation	Elevation in		Reference Used For Elevation	Elevation Relative to BPMSL datum (ft)	Estimated Accuracy of Driftline (ft)	Field Observations ^a
			1992 or 1995 (ft)	1992 or 1995 (ft)				
XSEC1-W	T4	1992	14.5	14.3	92-TBM1B/RIVER	14.3	1.0	None
XSEC2-W	T5	1992	13.1	12.7	92-TBM2B/DUNE	12.7	1.0	None
XSEC3-W	T3	1992	9.8	9.4	92-TBM3B/DUNE	9.4	1.0	None
XSEC4-E	T7	1992	4.4	5.1	92-TBM4A/SALVO	5.1	Poor	May not be highest driftline
XSEC4-W	T4	1992	>5.6	>6.3	92-TBM4A/SALVO	>6.3	Poor	Soil profile has 1 cm of Si at 0-1 cm
XSEC5-W	None	1992	4.1	4.8	92-TBM5A/SALVO	4.8	Poor	May not be highest driftline
XSEC6-W	T5	1992	18.8	19.3	92-TBM1A/RIVER	19.3	Poor	Probably not highest driftline
XSEC6-W	T9	1992	19.0	19.5	92-TBM1A/RIVER	19.5	Poor	Driftline noted upslope of soil profile (16.7 ft), soil profile has Oi w/s SiSa at 2-5 cm, probably not highest driftline
Helmericks		1992	5.4		River level, 2 Aug		1.0	Water 1.5 ft above runway, 5.4 ft above sea level on 2 Aug 92
T1	T1.8	1992	9.8		River level, 16 July		1.0	No flood sediment at top of T1.9 profile which was slightly upslope of driftline.
T2	T2.14	1992	10.1		River level 16 July		1.0	T2.16 has Si w/s Oi at 0-2 cm probably from 1989 flood. Driftline measured at 9.06 ft.
T3	T2.19	1992	10.0		River level 17 July		1.0	None
T4	T4.5	1992	8.7		River level, 19 July		1.0	1 cm of vf to f sand found on top of nearby profile.
N3	N3.17	1992	4.5		River level, 20 July		1.0	Large driftline
XSEC11	X11.3	1995	11.5	11.2	30P	11.2	0.5	Silt at 0-3 cm related to 1989 event. At X11.4 and X11.5, slightly upslope, no 1989 flood sedimentation evident.
XSEC12	X12.9	1995	11.5	11.1	40P	11.1	0.5	Silt at 1-2 cm depth, related to 1989 flood.
XSEC13	x13.5	1995	13.3	>13.1	RIVER	>13.1	Poor	No driftwood lines measured above 13.1 ft, but driftwood not located above 15.5 ft. Sediment observed at 2-3 cm depth at X13.6 (14.9 ft).
XSEC14	X14.2	1995	>19.3	>18.5	60P	>18.5	Poor	Silt from 1989 flood at 3-8 cm depth, driftwood scattered across site, probably not highest driftline
T10	T10.4	1995	8.3	8.1	Alpine (1B)	8.1	Poor	Indistinct driftline (elevation change based on correction to RIVER)
T10	T10.7	1995	9.6	9.4	Alpine (1B)	9.4	Poor	Driftwood scattered across site, probably not highest
T11	T11.3	1995	9.9		river level		1.0	No 1989 sediment evident at T11.3 at 10.3 ft
T12	T12.5	1995	15.9		river level		1.0	Silt from 1989 flood evident at 0-1 cm depth at T12.5 and at 1-2 cm depth at T12.10 (16.1 ft)
X6		1996		22.9	MON01	22.9	0.5	Highest driftline of a series.
T14		1996		>18.4	MON02	>18.4	Poor	Stranded driftwood on Fda, probably not highest driftline
T19	T19.6	1996		10.1	MON16	10.1	0.5	Well defined driftline at base of terrain bench.
X10	On Bank	1996		>16.1	MON20	>16.1	Poor	Probably not highest driftline

^a See Table 3-1 for definition of sediment abbreviations.

Textual abbreviations: Oi=Fibric organics, Si=Silt, Sa=Sand.

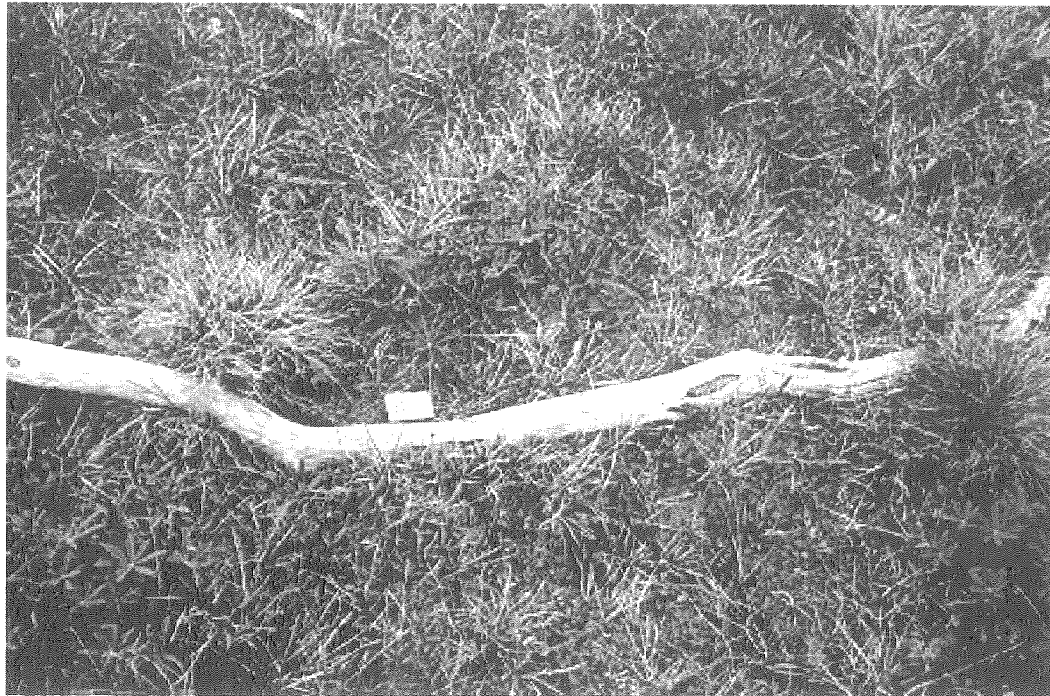


Figure 2-10. Photographs of typical driftwood material associated with the 1989 flood before (top) and after (bottom) removal from moss mat, Colville River Delta, Alaska, 1996.

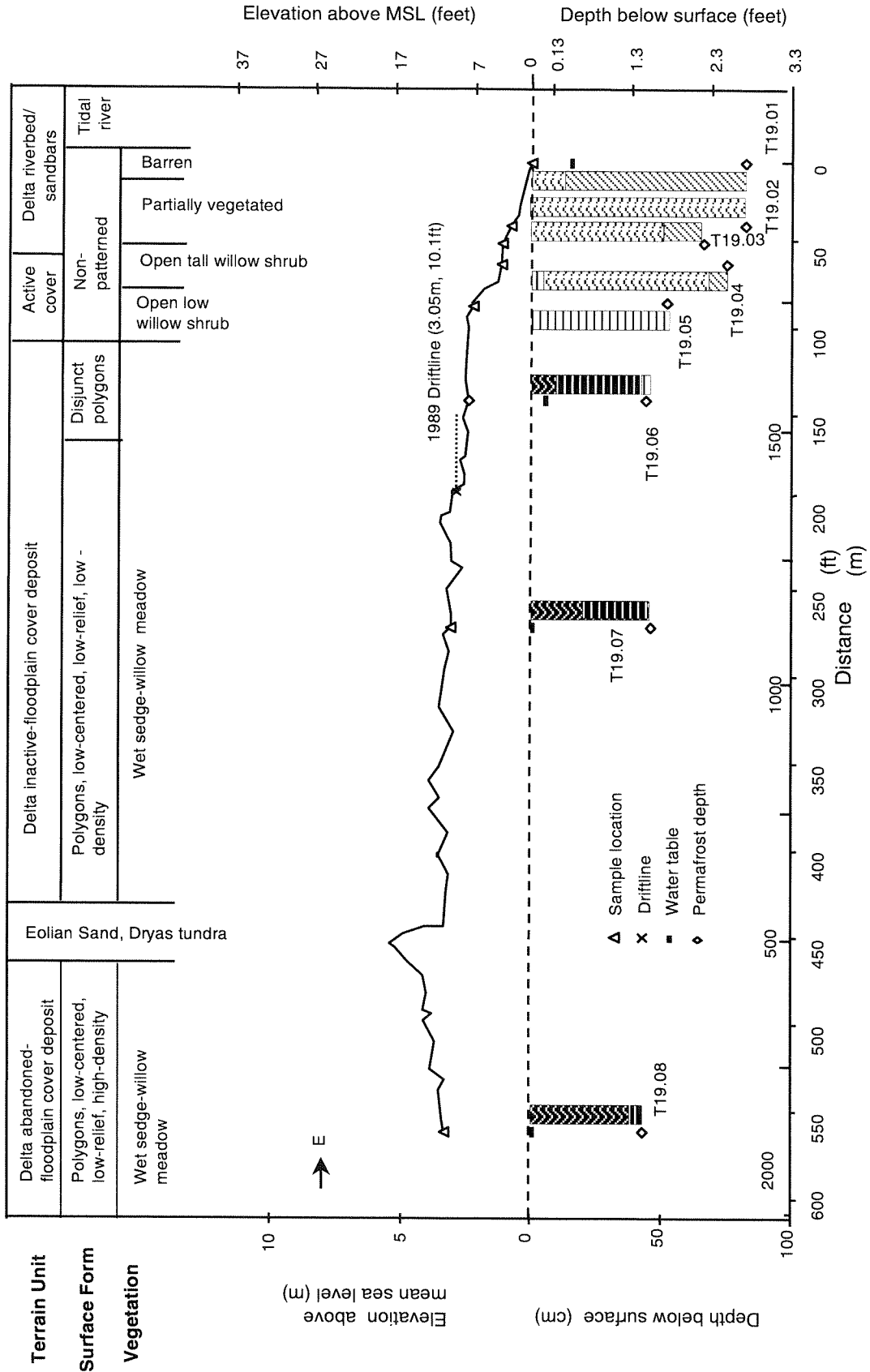


Figure 2-11. Cross-sectional profile (with 1989 driftline) of Transect 19, located along the Sakoong Channel, within the Alpine Development Area, Colville River Delta, Alaska, 1996.

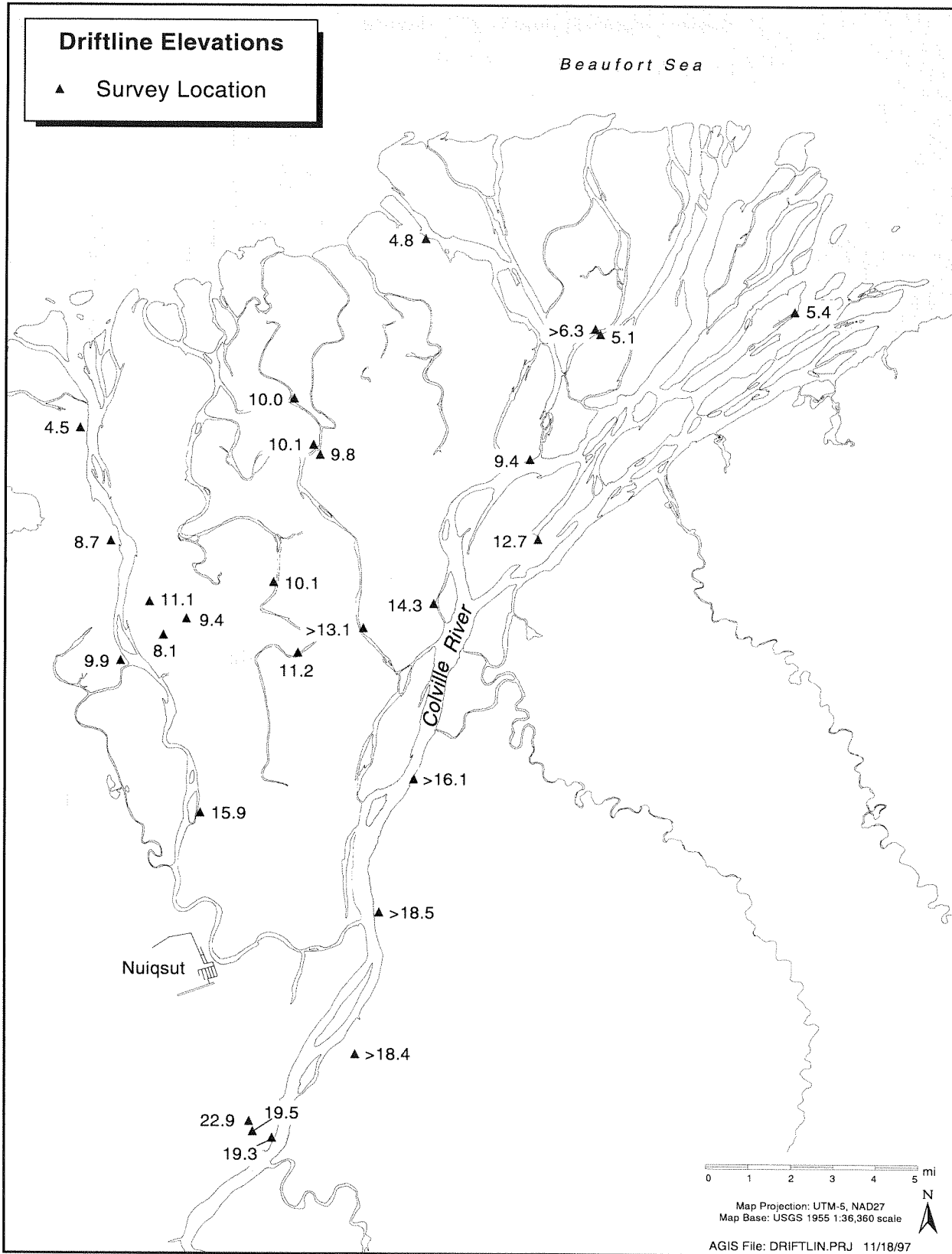


Figure 2-12. The locations and elevations (ft) surveyed driflines that were associated with 1989 flood, Colville River Delta, Alaska, 1996.

COMPARISON WITH ESTIMATES FROM HYDROLOGIC MODELING

When comparing our results with outputs from a two-dimensional physical model of hydrologic flow on the delta (Shannon and Wilson, 1997), the elevations of four good driftlines (mean = 10.6 ft, range = 9.9–11.2 ft) around the Alpine Facilities Area were similar to the water-surface elevations for the 50-yr (range = 10.7–11.5 ft), 100-yr (range = 11.6–12.6 ft) and 200-yr (range = 12.3–14.4 ft) flood events predicted for the six locations by the hydrologic model. The mean elevation of the driftlines, is similar to the stage estimated for the 50-yr event (using expected probabilities) and the maximum elevation of the driftlines approaches the lower range of the 100-yr flood stage.

Based on regressions of the stage-discharge curves obtained from the hydrologic model for locations with good driftline data ($n = 17$), Shannon and Wilson made a preliminary estimate that the 1989 flood had a discharge of 775,000 cfs (range = 665,000–930,000 cfs, based on a SD of 0.9 ft). When considering the base curve (without expected probability), this estimated discharge is closer to the discharge for the 100-yr event (774,000 cfs) than for the 50-yr (670,000 cfs) and the 200-yr (880,000 cfs). When considering the flow frequency with expected probabilities, the estimated discharge of the 1989 flood is closer to the discharge for the 50-yr event (726,000 cfs) than for the 100-yr (862,000 cfs) and 200-yr (1,020,000 cfs) events.

Overall, our estimate of the stage and return period of the 1989 flood are in close agreement with the stage of the 50-yr event, only slightly below the stage of the 100-yr event, predicted for the area around the Alpine facilities by the hydrologic model. In addition, the small differences in the estimates are well within the errors associated with the methods and the confidence limits of the data.

PART II. Paleoflood Hydrology

Table 2-3. Occurrence and description of slackwater deposits related to the 1989 flood, above or below driftlines near the Alpine development area, Colville River Delta, Alaska, 1996.

Site ID	1989 Slackwater Deposit	Terrain Unit ^a	Depth (ft)	Sediments ^b	Slackwater Deposits within 1 ft	Sediment Origin ^c	Elevation of Surface (ft)	Elevation of Nearest Driftline (ft)	Height Above or (Below) Driftline
X11.8	Absent	Fda	0-1.21	Oi w/t fSa	None	Eolian	13.9	11.2	2.7
T11.3	Absent	Fda	0-0.95	Oi w/s fSa and Oi w/t fSa	None	Eolian	9.9	9.9	(0.0)
T19.7	Absent	Fda	0-0.75	Oi and Oi w/t fSa and Oi w/s fSa)	1 layer fSa at 24 cm	May be eolian	10.2	10.1	0.1
T19.8	Absent	Fda	0-1.25	Oi w/t fSa	None	Eolian	11.0	10.1	0.9
X11.5	Absent	Fdci	0-1.02	Oi w/t fSa	None	Eolian	12.1	11.2	0.9
T19.6	Absent	Fdci	0.33-0.43	Oi w/s Si	3 layers	Fluvial	8.0	10.1	(2.1)
X11.4	Present	Fdci	0.07-0.10	Oi w/s SiSa	>4	Fluvial	10.6	11.2	(0.6)
T19.5	Present	Fdca	0-0.13	Si w/s Oi	>4	Fluvial	7.6	10.1	(2.5)
T10.3	Present	Fdci	0-0.26	Si w/s Oi	2 layers	Fluvial	7.1	8.1	(1.0)
T10.7	Present	Fda	0-0.03	Si	Indistinct	Uncertain	9.4	9.4	(0.0)
X12.9	Present	Fda	0.03-0.07	Oi w/s Si	2 layers	Fluvial	9.1	11.1	(2.0)
T11.7	Present	Fdci	0.10-0.13	Si w/s Oi	2 layers	Fluvial	9.1	9.9	(0.8)
X12.9	Present	Fda	0.03-0.07	Oi w/s Si	2 layers	Fluvial	9.2	11.1	(1.9)

^a Terrain Units: Fda = abandoned-floodplain cover deposit, Fdci = inactive-floodplain cover deposit.

^b Textual abbreviations: Oi=Fibric organics, F=Fine, Si=Silt, Sa=Sand.

^c Sediments were interpreted to be fluvial if they were dominated by silt and clays and eolian if they had trace amounts of fine sand without silts and clays.

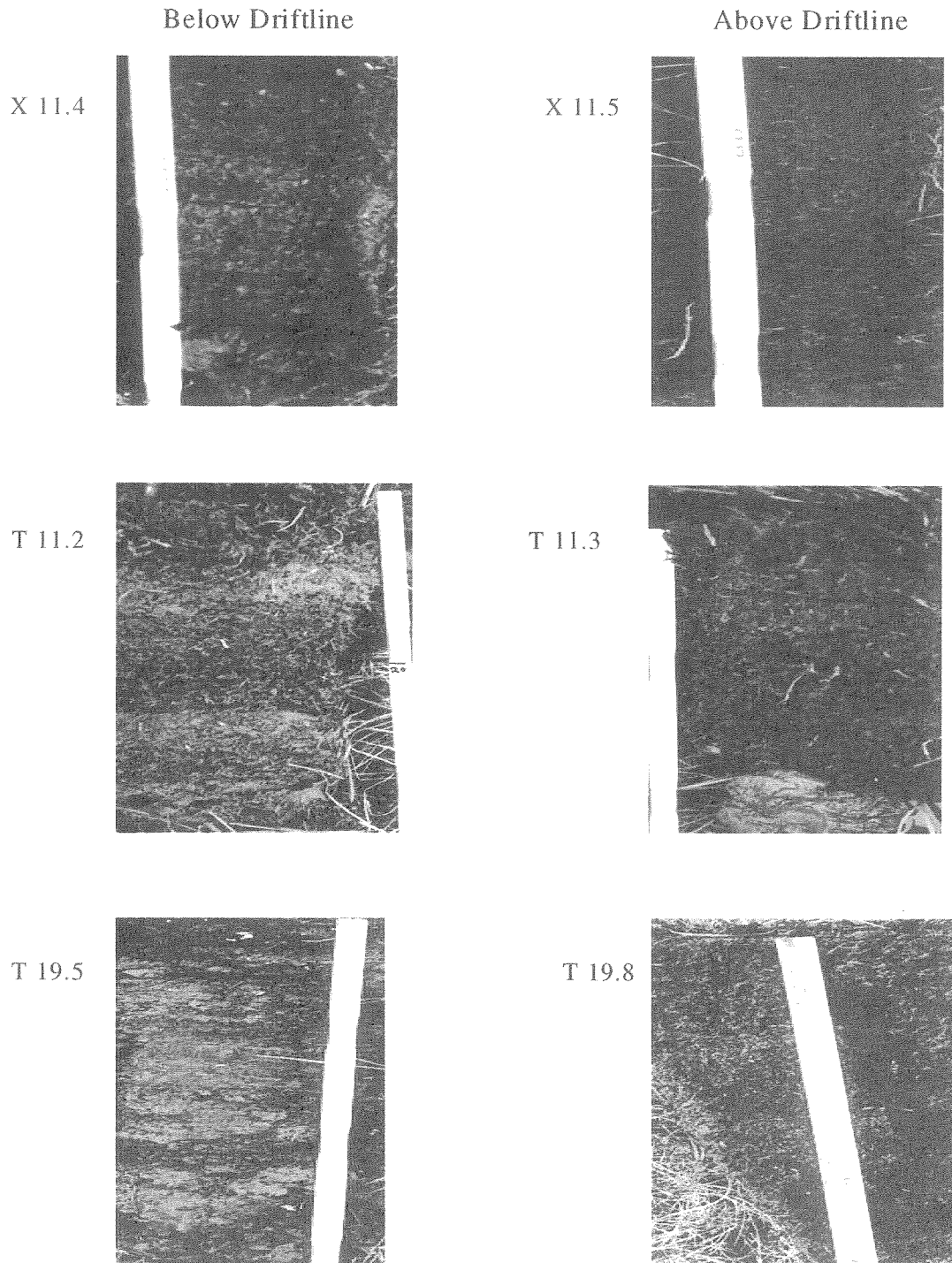


Figure 2-13. Photographs of soil profiles (with sample ID's) below and above driftlines associated with the 1989 flood near the proposed Alpine Facilities Area, Colville River Delta, Alaska, 1996.

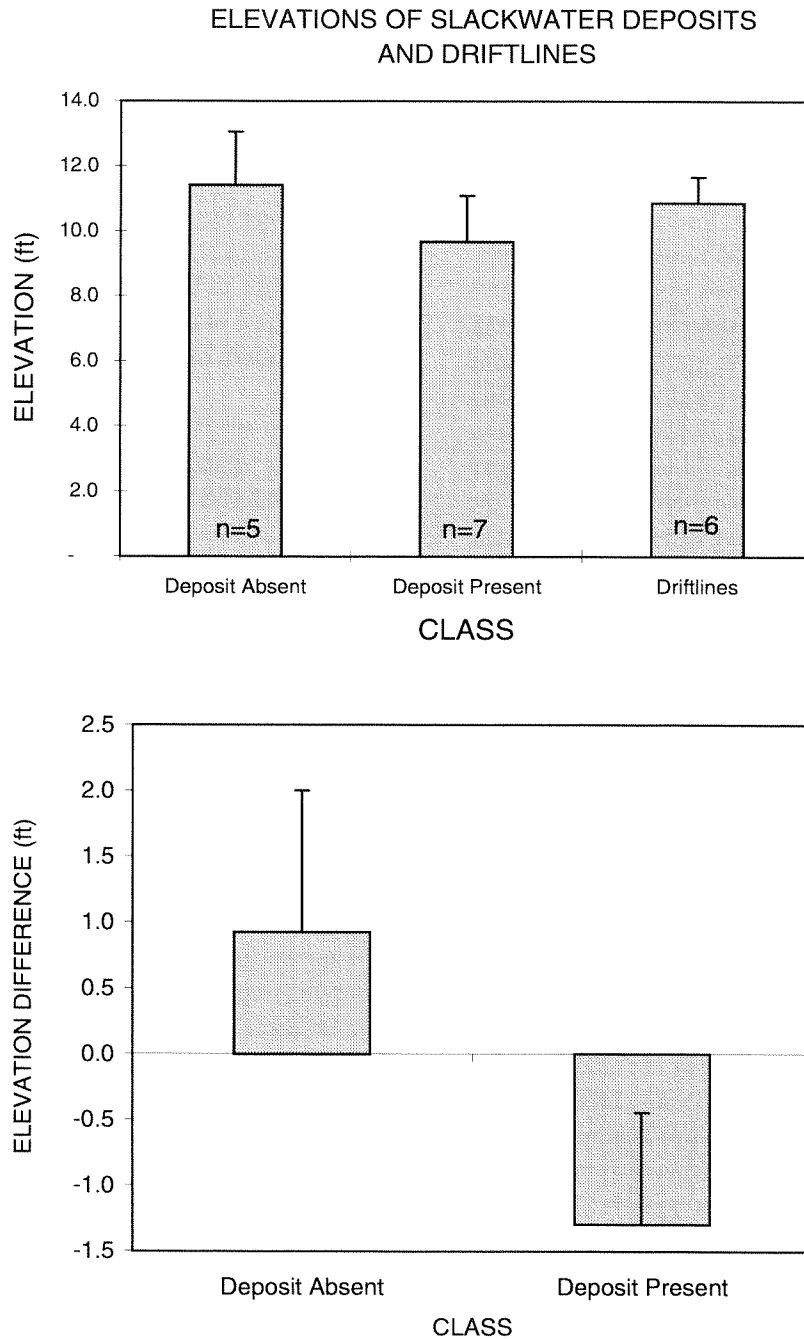


Figure 2-14. Mean elevations (\pm SD) of the highest slackwater deposits, the lowest sites where slackwater deposits were absent, and of driftlines associated with the 1989 flood (top graph) and the difference in elevations between the driftlines and where slackwater deposits were present (highest observed along transect) or absent (lowest point not observed)(bottom graph) within the Alpine Development Area, Colville River Delta, Alaska, 1996.

PART III. SOIL STRATIGRAPHY AND PERMAFROST DEVELOPMENT

BACKGROUND

Similar to other deltas around the world, the Colville River Delta is a complex environment that is characterized by migrating distributary channels, waterbodies of various origins, natural levees, sand dunes, riverbars, and mudflats (Walker 1976, 1983a). Unlike temperate and tropical deltas, however, it is greatly influenced by two other factors: (1) low temperatures that prevent the movement of most of the annual precipitation until spring breakup, and (2) the presence of permafrost (Walker 1976). Because of permafrost, the delta has ice wedges, ice-wedge polygons, frost mounds, and pingos. Permafrost also alters the character of river discharge and erosional processes on the delta (Walker 1976).

The geomorphology and surficial geology of the delta have been studied intensively by Walker (1966, 1976, 1978) and Walker and Matsukara (1979). In addition, regional studies that included the delta have been conducted by Black (1964), Naidu and Mowatt (1975), Williams et al. (1978), Cannon and Rawlinson (1979), Carter (1981), Craig and Thrasher (1982), Carter and Galloway (1982, 1985), Foster (1988), Reimnitz et al. (1988), and Rawlinson (1993). Deeper stratigraphy (up to 125 ft deep) has recently been investigated by Miller and Phillips (1996). Of these studies, the field investigations and geological mapping done by Rawlinson (1993) are particularly relevant to this study, and were relied upon heavily during the mapping of surficial deposits in the proposed Transportation Corridor.

This component of the geomorphology study investigated the nature and distribution of surficial deposits in the delta to provide information for facility siting and engineering design. This effort included both mapping of "integrated terrain units" (ITUs) across the landscape and field investigation of the stratigraphy of surficial materials. Results of these surveys were used to evaluate permafrost development and thaw stability and to help analyze the flooding regime on the delta. The field effort focused on the delta, although a limited amount of work also was conducted in the Transportation Corridor. Specific

objectives of this study were:

1. to classify surface terrain units within the delta and Transportation Corridor;
2. to describe the stratigraphy of near-surface materials near the proposed oil facilities;
3. to evaluate ice structures and ice contents in near-surface soils; and
4. to evaluate differences in soil stratigraphy among terrain units in terms of permafrost development and thaw stability.

Mapping of ITUs incorporates several standard classification systems for terrain units (surficial deposits and waterbodies), surface forms (ice- and frost-related features), and vegetation (Jorgenson et al. 1993). Delineating the landscape in terms of terrain units is useful for identifying areas with different soil genesis and properties relevant to engineering applications. Surface forms, particularly those that reflect various stages of ice-wedge development, are indicative of areas with different ice contents, ages, elevations, and flooding regimes. Vegetation is sensitive to flooding and salinity, and therefore is useful for differentiating among areas with different sedimentation rates and areas inundated by storm surges. Thus, the mapping system was designed to provide information that is useful for a wide range of applications regarding flooding regime, geotechnical properties, thaw stability, landscape change, soil productivity, fish and wildlife habitats, and sensitivity to oil spills. The original mapping was done in 1992, using results from preliminary field investigations, and was revised in 1995 under an ecological land classification framework which provided additional information on wildlife habitat characteristics and incorporated new information on soils. The ecological land classification effort is described by Jorgenson et al. (1997); however, the terrain-unit mapping component of that work is summarized in this study and was used in the analyses presented in this section.

The soil stratigraphy work was designed to identify changes with depth across the landscape for mineral sediments, organic matter, ice structure and volumes, and ages of materials. The work in 1995 and 1996 also was designed to further describe and evaluate the terrain units that were mapped initially in 1992. To describe and analyze soil and permafrost development, we used a multi-scale approach that evaluated

surface materials by describing microscale differences in sediment texture and ice structures (ice structures), then organized them into vertical sequences of related textures and structures (lithofacies), and finally grouped these lithofacies into three-dimensional structural elements with a characteristic surface form (terrain units) related to particular depositional or cryogenic environments. For analysis, we also differentiated stratigraphic terrain units (terrain units within a vertical profile) from surface terrain units (terrain units at the surface) to assess how well surface characteristics represented subsurface properties. Because we mapped terrain units over a large area with little subsurface information, we mapped only the surface terrain units, relying on conceptual models we developed of the relationships of stratigraphic terrain units to surface terrain units to represent subsurface characteristics.

Examination of soil properties at various spatial scales helped identify the processes that are responsible for the distribution of surficial materials across the landscape and the spatial scale that is best for differentiating soil properties. After detailed classification and analysis of the microscale and macroscale differences in soil properties across the complex landscape of the delta, we synthesize the unifying patterns and processes into a conceptual model of floodplain evolution. We then use the model as the basis for assessing the environmental and engineering constraints on development in the delta.

METHODS

CLASSIFICATION AND MAPPING

Classification and mapping of terrain units was done initially in 1992 based on results of preliminary fieldwork. The mapping then provided a base for stratifying additional fieldwork and was revised in 1995. The classification and mapping procedures used in this iterative approach are described below.

The microscale soil textures and structures described from the field profiles were grouped into lithofacies (distinctive suites of sedimentary structures related to a particular depositional environment), ice structures (repeating patterns of ice characteristics), and terrain units (three dimensional architectural elements expressed within a profile). Lithofacies and cryogenic structures of the cores were classified in the

office using field descriptions and photographs of cores. Lithofacies were classified according to systems of facies analysis for fluvial deposits developed by Miall (1978, 1985) and Brierley (1991). We added several new classes to these systems to incorporate features of a permafrost environment.

Cryogenic structure (form, distribution, and volume of ice) was classified in the field in 1995 according to Russian (Katasonov 1969) and North American systems (Philainen and Johnston 1963), but were reclassified following Murton and French (1994) after review of field descriptions and examination of close-up photography. In 1996, we modified the Murton and French classification system to better differentiate the structures that we observed in the delta (Appendix Table C-1).

During classification, primary structures were further subdivided by secondary structural characteristics such as shape and size. Frequently, structures occurred in assemblages in which the individual structures were too small to differentiate; consequently, they were grouped into composite structures. Based on this subdivision of ice structures and grouping of associated structures into composites, we described a total of 102 combinations in the field. Because this number was too large for practical application, we aggregated classes through a two-step process. First, we aggregated the 102 combinations into 8 simple primary structures (by dropping secondary subdivisions) and 6 composite primary structures. Second, we further combined the composite structures with the simple structures according to the developmental stage of the ice structures (in descending order of complexity: solid > ataxitic > reticulate > vein > layered > lenticular > organic-matrix > pore) that were present in the composite structure. For example, a composite structure that had ataxitic, reticulate, and layered ice was grouped with the simple ataxitic structure. Vertical trending ice structures (vein, reticulate, ataxitic) were considered to be more advanced or complex than horizontal structures (pore, lenticular, layered).

The terrain-unit classification system that we used was adapted from the systems developed by Kreig and Reger (1982) and the Alaska Division of Geological and Geophysical Surveys for their engineering-geology mapping scheme. This classification system was modified to incorporate surficial geology units in the Transportation Corridor (following Rawlinson 1993) and to better differentiate deltaic sediments related to flooding regimes.

For mapping we used a compound classification system that combined information about terrain units, surface forms, and vegetation into ITUs (Appendix Table C-2). The ITU classification and mapping is presented here, but a more complete description of the entire ecological land classification system is presented in Jorgenson et al. (1997). During mapping only the surface terrain unit was mapped because of the lack of information about subsurface layers. Surface forms were classified using the scheme developed by Washburn (1973), which was modified to include surface forms described by Everett (1980) and the National Wetlands Group (1988). Vegetation was classified using the Alaska Vegetation Classification system developed by Viereck et al. (1992), which was modified to include information from Walker and Acevedo (1987) and additional salt-affected classes prevalent on the delta.

ITUs were delineated on acetate overlays of color-infrared (CIR) photographs (1:18,000 scale) taken on 8 July 1992 by AeroMap, Inc., (Anchorage, AK). Minimal mapping size for features was 1 acre (0.4 ha), although waterbodies as small as 0.5 acre occasionally were mapped to provide additional geodetic reference points. Lines and codes were digitized and encoded using Atlas GIS software (Strategic Mapping, Inc., Santa Clara, CA). During digitizing, photos were registered to UTM coordinates obtained from prominent features along waterbody shorelines identified on a base map developed from SPOT imagery (Jorgenson et al. 1996). After digitizing, the digital features on each photo were rectified geometrically by performing a three-point transformation ("rubber-sheeting") to match waterbodies on the SPOT base map, and thus compensate for distortion caused by tilt. After rectification, features on adjacent photos were joined to create a seamless map of the entire area.

SOIL STRATIGRAPHY

Field surveys were conducted during 8 July–3 August 1992, 28 July–8 August 1995, and 28 July–14 August 1996 to collect data on soil stratigraphy along toposequences related to 11 hydrologic cross sections (including ground surface below channels) and along 13 additional transects (including areas adjacent to rivers) chosen subjectively to sample a variety of terrain units on the delta (Figure 3-1, Appendix Table C-3). The cross sections initially were numbered consecu-

tively in the field, but the numbering system was changed after the field work to denote river miles from the ocean. Transects were numbered consecutively. Sampling stations along the cross sections and transects were labeled with a letter denoting the field cross-section or transect number followed by a consecutive number to indicate position along the toposequence (e.g., X11.9 or T12.3).

The stratigraphy of the near-surface soil (i.e., the active layer) was described in 1995 and 1996 from soil cores and soil pits to assess the occurrence of flood-deposited sediments (Appendix Table C-3). For sampling frozen soils below the active layer, a 3-in.-diameter SIPRE corer with a portable power head was used to obtain cores to depth of 10 ft (3 m). Several profiles also were described from cutbanks after unfrozen material was removed with a shovel to expose undisturbed frozen sediments. Descriptions for each profile included the texture of each horizon, the depth of organic matter, depth of thaw, and ice volume and structure. In the field, soil texture was classified according to the Soil Conservation Service system (SSDS 1993). Similar data were collected from soil pits and bank exposures in 1992 (Jorgenson et al. 1993), although ice descriptions were not included.

During field sampling, the occurrence of thin fluvial and organic layers was noted and two measures of organic accumulation were analyzed to assess differences among terrain units and to evaluate differences in the frequency of flooding. First, the thickness of organic material above the uppermost distinct mineral horizon of fluvial origin was measured to evaluate how much material had accumulated since the previous major flood. Then, the total amount of organic material that had accumulated in the top 1 ft of soil was calculated by summing the thicknesses of all the individual organic layers; these data were used to assess rates of sediment accumulation. The first approach provides a short-term measure of flood frequency by identifying those areas affected by the 1989 flood (see Part II for description of that flood), whereas the second approach is a long-term indicator of flood frequency (e.g., more organics indicate less flooding and sediment deposition, whereas, less organics indicate more frequent flooding).

Soil samples were taken from the profiles for analysis of gravimetric water content, particle size, and electrical conductivity. In 1992, samples taken from the active layer were analyzed for particle-size distri-

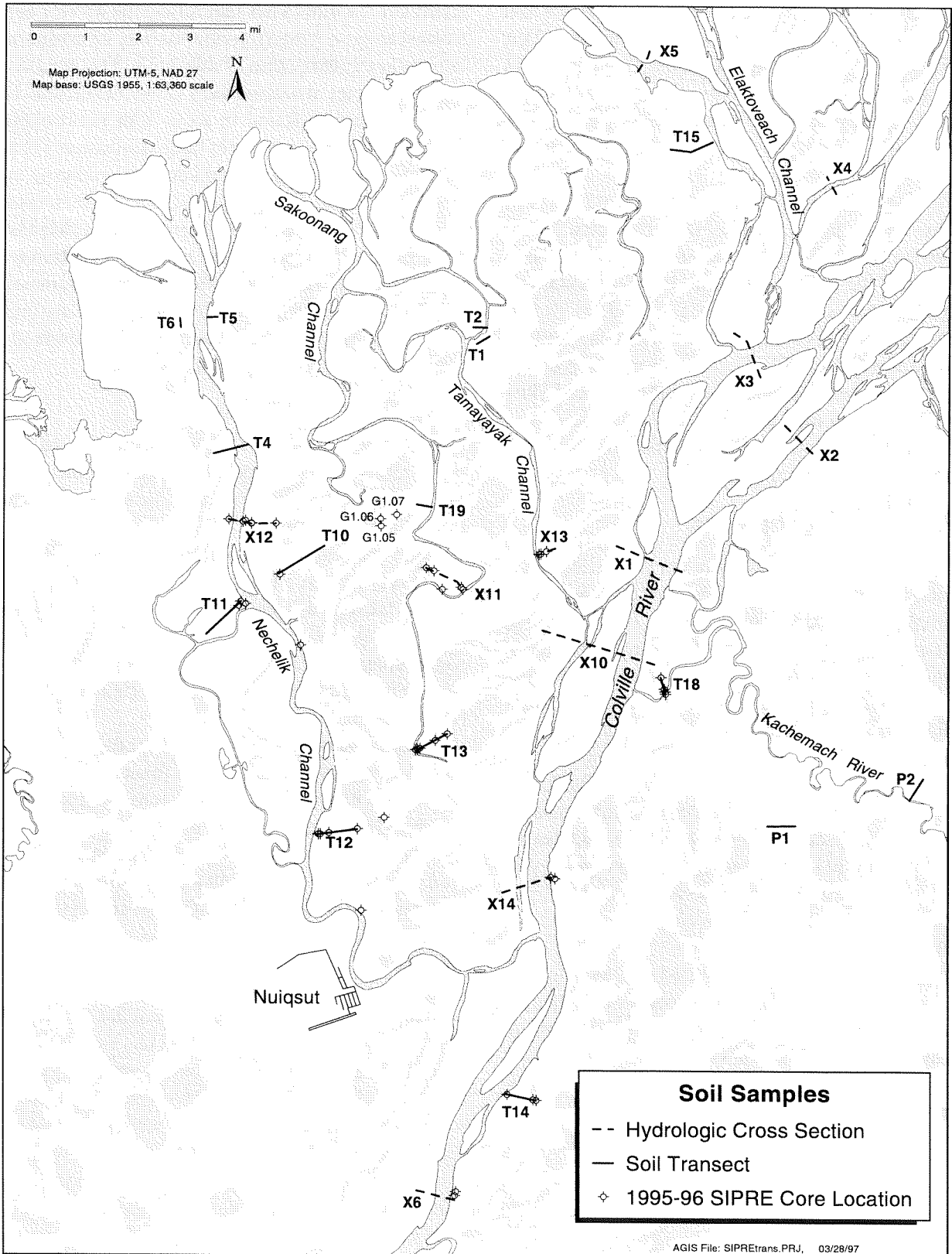


Figure 3-1. Map of soil sampling locations in 1992, 1995, and 1996.

bution, pH, and electrical conductivity (EC) by the Soil Testing Laboratory at Colorado State University (Fort Collins) following standard methods (Klute 1986). In 1995 and 1996, we measured water content and EC. Particle-size distributions were determined by Shannon and Wilson, Inc. in 1995 and by CSU Soil Testing Lab. In 1996.

To establish minimal ages for the older stratigraphic terrain units, samples were collected for radiocarbon dating from organic material (sedge peat) in some of the deeper profiles. In a few instances, fragments of wood stems were collected for dating. Laboratory analyses were performed by Beta Analytic, Inc. (Coral Gables, FL). Dates were reported by the laboratory as conventional radiocarbon years before 1950 AD and include the error (± 1 SD) associated with each analysis. We converted the dates to radiocarbon years before present (1996).

RESULTS AND DISCUSSION

In presenting and discussing our results, we focus on the patterns and processes that are responsible for the evolution of the landscape. First, we classify the types and patterns of materials (mineral sediments, organic matter, ice) that we observed in near-surface sediments at multiple spatial scales (lithofacies, stratigraphic terrain unit, and surface terrain unit) and we illustrate how these patterns are interrelated across representative toposequences. The classification of lithofacies and terrain units emphasized differences in materials that are related to fluvial, eolian, and marine processes, and to permafrost aggradation and degradation. Second, we compare the physical and chemical characteristics within these classes, with particular attention on ice characteristics. We then use the results to develop a conceptual model of the geomorphic evolution of the delta, which accounts for changes in sediment, organic matter, and ice accumulation. Finally, we discuss how the various patterns and processes affecting the evolution of the permafrost landscape may affect, or be affected by, oil development in the delta.

CLASSIFICATION AND MAPPING

Lithofacies

The texture and structure of sediments observed within the delta and Transportation Corridor were clas-

sified into 23 lithofacies that reflect the diverse depositional environments (riverine, marine, lacustrine, and eolian) in the study area (Table 3-1). The most common lithofacies in near-surface sediments included (1) layered organics, found in areas with rapid organic accumulation and infrequent flood deposition, (2) layered fines, in areas of frequent deposition during high flood stages, and (3) rippled fines with detrital organics, found in lateral accretion deposits along river channels. Other common lithofacies included massive organics; massive, turbated fines with organics; massive sands; and turbated, layered organics. Our interpretations of the depositional environments represented by the lithofacies are provided in Table 3-1.

Ice Structures

Eight primary ice structures (based on continuity of ice structures) were described for the delta (Table 3-2) and were further subdivided by secondary structural characteristics such as shape and size. This subdivision and combining some structures in composite structures, created a total of 102 combinations in the field. Because this created too many combinations for practical application, we reduce this variability by aggregating classes into the 8 simple primary structures (Figure 3-2) and 6 composite primary structures (Figure 3-3).

After grouping, the simplest relationships between ice structure and lithofacies were found in massive and inclined sands, which always had pore ice (nonvisible), and massive organics, which always had organic-matrix ice. In contrast, ice structures in massive fines were highly variable, including vein (a composite class dominated by lenticular ice with few vertical veins and layered ice), reticulate, ataxitic, and solid (sheet) ice. Lithofacies with higher clay contents, such as fines with clay, had more reticulate and ataxitic ice.

At four sites (bottom sections of X12.10, X14.3, T11.2, and Y3), we observed sheet ice, a term we used to describe a type of ice of unknown origin (Jorgenson and Shur 1995). These massive sheets of clear ice with trace amounts of suspended particles were 1-2 ft thick, although the true extent of this type of ice structure was not determined because it occasionally extended beyond the depth of our coring. The most plausible explanation for this ice structure is that sheet ice forms during permafrost development in tapped-lake basins.

Table 3-1. Classification and description of lithofacies observed in the Colville River Delta and adjacent coastal plain, Alaska, 1996. Structures less < 4 in. (10 cm) thick are not identified.

Lithoface class (and code)	Primary and secondary particle sizes	Sedimentary structure	Mechanism interpretation
Gravel, massive (Gm)	Clean gravel (little or no fines)	None visible	Longitudinal bars, lag deposits, sieve deposits
Gravel, horizontal (Gl)	Clean gravel	Horizontal layers or crudely stratified gravel	Longitudinal bars, lag deposits, sieve deposits
Sands-massive (Sm)	Medium-coarse sands	None visible, medium-coarse, light brown sands, may be pebbly	Uncertain
Sands, massive with trace gravel (Sgm)	Medium-coarse sands, loamy sands, with trace gravels.	None visible	Coastal plain, reworked coastal environment from coastal or thaw lake processes
Sands with trace gravel, massive, turbated (Sgmt)	Medium-coarse sands, loamy sands, with trace gravels.	Turbated, intermixed massive sand and organics inclusions	Coastal plain, wave-mixed or cryoturbated sediments.
Sand, layered (Sl)	Medium-coarse sands	Horizontally stratified layers	Planar bed flow (lower and upper flow regime) or eolian
Sands, inclined (Si)	Medium-coarse sands	Undifferentiated wavy-bedded, ripple, or crossbed stratified layers. Interpretation limited by small size of cores.	Lower flow regime and eolian sand
Sands with organics, inclined (Sdi)	Medium-coarse sands with interbedded detrital peat layers	Undifferentiated wavy-bedded, ripple, or crossbed structure	Lateral accretion deposits during flood stage
Sands, rippled (Sr)	Fine-medium sands	Ripples with variable internal structure, typically 3 cm high, 10-15 cm, internally graded,	Lower flow regime
Sands with organics, rippled (Sor)	Fine-medium-coarse sands with interbedded detrital peat layers	Ripples with variable internal structure	Lateral accretion deposits during flood stage in organic-rich landscapes
Fines, massive (Fm)	Silts and fine sands	None visible	Overbank deposition of sediments or eolian input
Fines with organics, massive (Fom)	Silts and fine sands with well-decomposed organics	None visible,	Soil formation in massive silts
Fines with organics, massive, turbated (Fomt)	Silts and fine sands with poorly decomposed organic inclusions	Disrupted organic and mineral inclusions due to cryoturbation	Compression and displacement of material during freezing and thawing .
Fines with trace gravel, massive, turbated (Fgmt)	Silts and fine sands with trace gravel	Massive, turbated inclusions	Cryoturbation in active layer
Fines, layered (Fl)	Silts and fine sands	Horizontally stratified layers	Proximal overbank deposition of sediments
Fines, rippled (Fr)	Silts and fine sands	Inclined beds or ripples	Lateral accretion deposits along riverbars formed during flood stage

PART III. Soil Stratigraphy and Permafrost Development

Table 3-1. Cont.

Lithoface class (and code)	Primary and secondary particle sizes	Sedimentary structure	Mechanism interpretation
Fines with organics, rippled (For)	Silts and fine sands with detrital organics	Inclined beds or ripples, interbedded detrital peat	Lateral accretion deposits along riverbars formed during flood stage
Fines with clay, massive (Fcm)	Clay-rich silts and fine sands	None visible to indistinct lamination	Slackwater deposits, lacustrine
Fines with clay, layered (Fcl)	Clay-rich silts and fine sands	Horizontally stratified layers	Overbank or tidal flat deposition at flood stage or high tide.
Fines with algae (Fa)	Benthic algal mat and other limnic material	None visible to horizontal lamination	Lacustrine sediments
Organic, massive (Om)	Undecomposed organics, includes trace silt or sand layers	None visible	Autochthonous organic matter, fluvial sedimentation is rare or lacking
Organic, layered (Ol)	Undecomposed organic and fine mineral layers	Horizontal bedding, some elluvial mineral redistribution in peat	Occasional overbank deposition of suspended sediments
Organic, layered, turbated (Olt)	Undecomposed organic and mineral layers	Disrupted inclusions or inclined bedding due to cryoturbation	Interbedded sediments deformed by ice-wedge compression

Table 3-2. Description of terms used for classifying ground ice on the Colville River Delta, Alaska, 1996.

Ice structure	Definition
Pore	Ice in minute holes, or pores, within mineral soil matrix that has an almost structureless appearance. May be visible (without handlens) or non-visible. Visual impression is that ice does not exceed original voids in soil. Forms where pore water freezes <i>in situ</i> .
Organic-matrix	Ice formed within organic matrix and has a structureless appearance. May be visible or non-visible. Mostly formed where pore water freezes <i>in situ</i> .
Vein	Isolated, thin lens, needle-like or sheetlike structures, or particles visible in the face of soil mass. Usually inclined and bisecting sedimentary structures. Differs from layered ice in that they are solitary and do not have a repeated, parallel pattern.
Lenticular	Lens-shaped, thin (generally < 0.5 mm), short bodies of ice within a soil matrix. The orientation is generally normal to the freezing front and usually reflects the structure of the sediments.
Layered	Laterally continuous bands of ice less than 10-cm thick. Usually parallel, repeating sequences that follow with sedimentary structure or are normal to freezing front. Thicker layers (>10 cm) are described as solid ice. Sparse: ice layers <5% of structure. Medium: ice layers 5–25% of structure Dense: ice layers 25–50% of structure.
Reticulate	Net-like structure of ice veins surrounding fine-grained blocks of soil. Ice occupies up to 50% of surface area. Trapezoidal: ice has distinct horizontal parallel veins with occasional diagonal, vertically oriented veins. Soil blocks have trapezoidal appearance due to fewer vertical veins than lattice-like ice. An incomplete form of latticelike reticulate ice. Latticelike: ice exhibits regular, rectangular or square framework. Foliated: irregular horizontally dominated ice giving soil a platy structural appearance.
Ataxitic	Ice occupies 50–99% of cross-sectional area, giving the soil inclusions a suspended appearance. Sparse: ice occupies 50–75% area, soil inclusions occupy 25–50% of area. Medium Inclusions: ice occupies 75–95% of area, soil inclusions occupy 5–25%. Dense Inclusions: ice occupies 96–99% of area, soil inclusions occupy 1–5%.
Solid	Ice (>10-cm thick) where soil inclusions occupy <1% of the cross-sectional area. Sheet ice: Cloudy or dirty, horizontally bedded ice exhibiting indistinct to distinct stratification. Wedge Ice: V-shaped masses of vertically foliated or stratified ice resulting from infilling of frost fissures. Best identified when large exposures or cross-sections are visible.

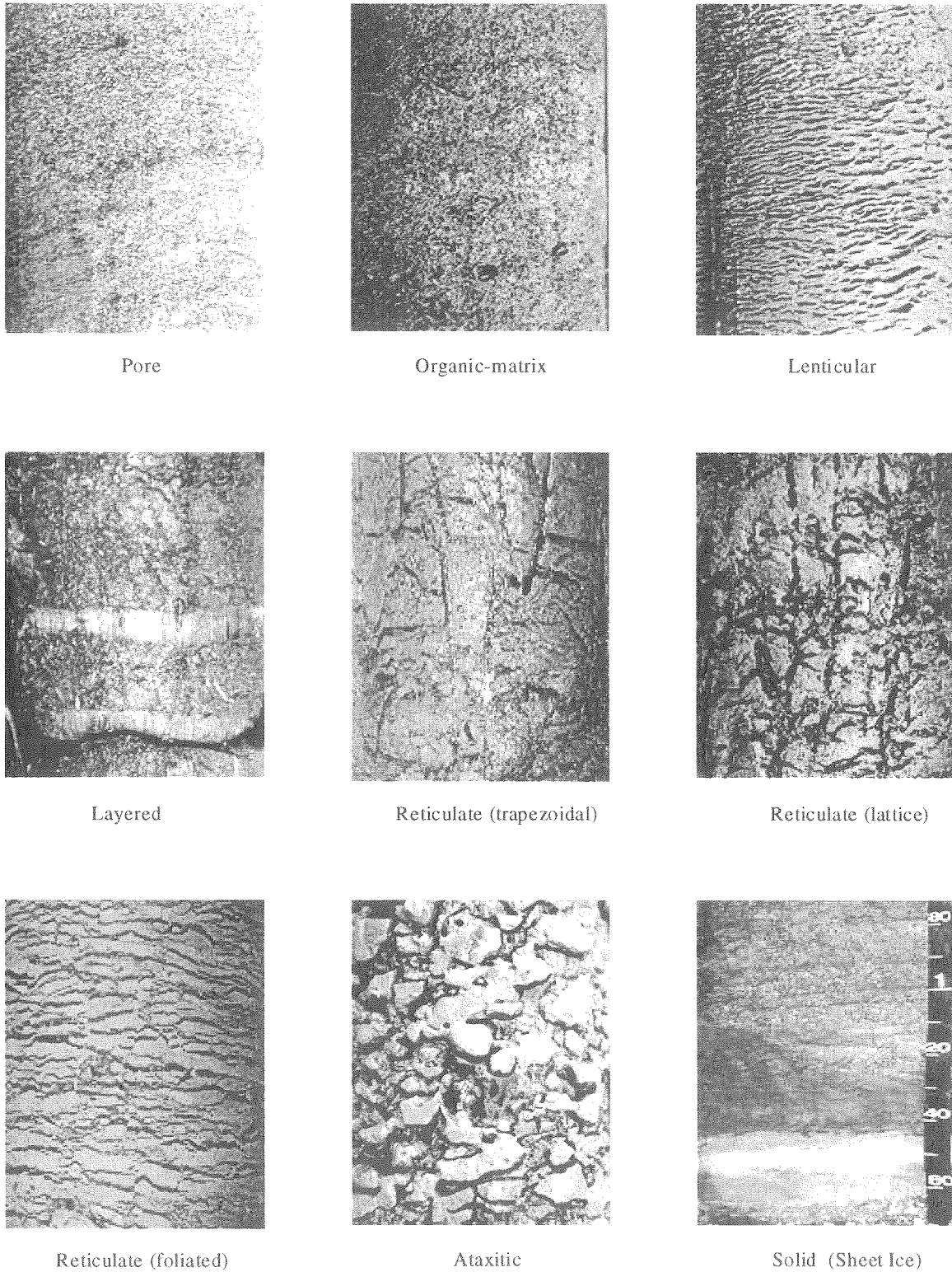
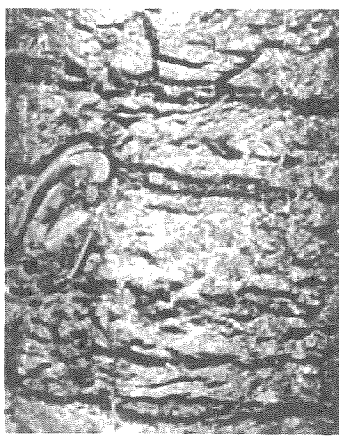


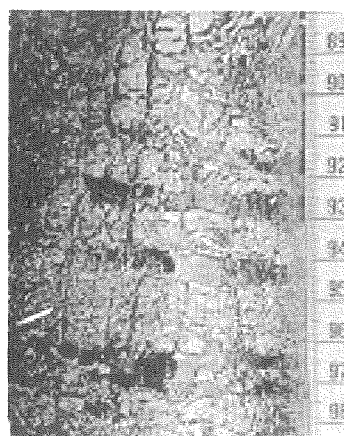
Figure 3-2. Photographs of simple ice structures found in soils in the Colville River Delta, Alaska, 1996.



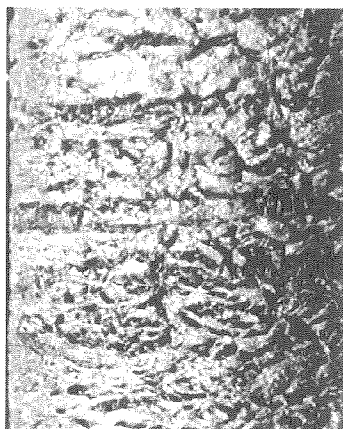
Lenticular-Pore



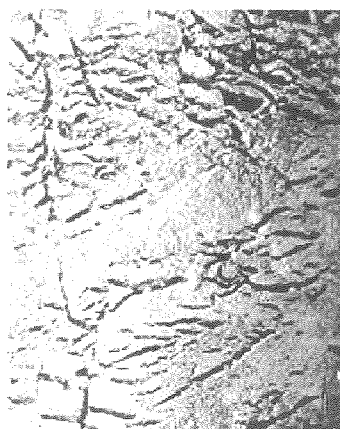
Layered-Lenticular



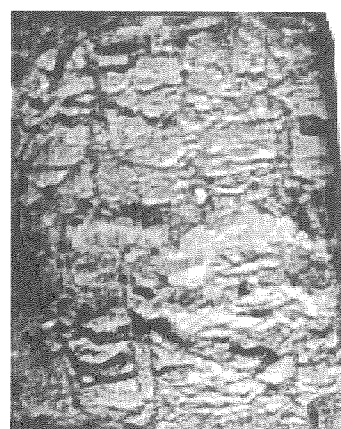
Reticulate-Layered



Vein-Layered
(includes Lenticular)



Vein-Lenticular



Ataxitic-Reticulate

Figure 3-3. Photographs of common composite ice structures found in soils in the Colville River Delta, Alaska, 1996.

Terrain Units

Twenty-one terrain units were identified within the delta and the adjacent (Transportation Corridor) (Table 3-3, Figure 3-4). Two of these units (solifluction deposits and loess) were too small or thin in extent to map. A map of terrain units (terrain units at the surface) revealed large differences in distribution of terrain units between the two areas (Figure 3-5). Terrain units that were common on the delta included: delta riverbed/riverbar deposits, high-water channels, active-floodplain cover deposits, inactive-floodplain cover deposits, abandoned-floodplain cover deposits, tidal flat deposits, eolian sand deposits, and ice-rich and ice-poor thaw basin deposits. In contrast, terrain units in the Transportation Corridor included meander-floodplain riverbed deposits, active-floodplain cover deposits, inactive-floodplain cover deposits, alluvial and alluvial-marine terraces, alluvial plain, and gravel and peat fill deposits.

Relationships Among Terrain Components

Most of the terrain components (lithofacies, ice structures, terrain units) occur in distinct associations and thus vary in similar patterns across the landscape (Figure 3-6). Lithofacies and ice structures were classified by visually independent characteristics (sediments versus ice) and the relationships between them reveal interrelated processes. In contrast, both lithofacies and terrain unit were based on sediment characteristics and the lithofacies were used in the definition of terrain units, so they are interrelated in part due to defining characteristics. The following section evaluates the interrelationships among lithofacies, ice structures, and terrain units by comparing changes across topographic sequences on the delta floodplain.

Topographic sequences noting changes in elevation, soils, surface-forms, and vegetation at selected locations within the delta are illustrated in Figures 3-7 through 3-12. Transect 12, located along the upper Nechelik Channel, includes a complete lateral bar sequence with a high-water channel and illustrates the dramatic difference in organic matter accumulation typical of abandoned-floodplain cover deposits (Figure 3-7). Cross Section N7.46 (12), located along the middle portion of the Nechelik Channel approximately one mile west of the Alpine 1 Exploratory Well Site, includes a complete floodplain sequence and a small

sand dune covered by abandoned-floodplain cover deposits (Figure 3-8). Transect 13, situated along the upper Sakoonang Channel, also provides a complete lateral bar sequence, but reveals how shallow (~3 ft) some abandoned-floodplain cover deposits can be (Figure 3-9). Cross Section S9.80 (11), near the proposed well sites adjacent to the Sakoonang Channel, represents a nearly complete sequence of landscape evolution; from a barren riverbed/riverbar deposit to an abandoned-floodplain cover deposit, including an inactive sand dune and a thaw lake that is eroding into the ice-rich sediments (Figure 3-10). Transect 19, also situated near one of the proposed drill sites, reveals accumulations of massive organics on both inactive- and abandoned-floodplain cover deposits and the position of the highest driftline associated with the 1989 flood (Figure 3-11). Transect 18, situated along the East Channel, again reveals the gradual accumulation of organic material at the surface away from the riverbank and illustrates the abrupt change in stratigraphy associated with the abandoned-floodplain cover deposits (Figure 3-12). Overall, consistent patterns in stratigraphy were observed across the toposequences. These patterns, as well as results from the analysis of sediment characteristics provided below, were used to develop a conceptual model of floodplain evolution (see section titled Conceptual Model of Floodplain Evolution on the Delta).

In addition to these general relationships, we examined the change in ice structures over time by comparing differences within a lithofacies across the common surface terrain units (Figure 3-13). Within the rippled fines with organics lithofacies, both pore and lenticular ice structures are dominant in the riverbed/riverbar deposit, whereas lenticular ice becomes more prominent in active-floodplain cover deposits. By the time the surface becomes an inactive-floodplain, rippled fines with organics have substantially more vein, reticulate, and ataxitic ice (Figure 3-14a). Within active-floodplain the layered-fines lithofacies, pore and lenticular ice was dominant during the stage, whereas within inactive-floodplains, the lithofacies have more well-developed ice structures (vein, reticulate, ataxitic ice). In contrast, the massive and inclined sands show no modification during floodplain evolution; they retain their pore ice structure. This indicates that fines deposited within lateral accretion deposits (riverbars) and active-floodplain cover deposits are the principal materials in which ice aggradation occurs. This brief

PART III. Soil Stratigraphy and Permafrost Development

Table 3–3. Descriptions of terrain units found within the Colville River Delta and adjacent coastal plain, Alaska, 1996.

Unit	Description
Solifluction Deposit	Unconsolidated fine-grained material, or rocky or gravelly fines, resulting from mass movement of saturated materials. Surface has lobe pattern from downslope movement. (not mapped)
Eolian Sand Deposit	Unconsolidated, wind-deposited accumulations of primarily very fine and fine sand. Surficial patterns associated with ice-aggradation generally are absent. These active sand dunes are being built by deposition of sand from adjacent sandbars and are prone to wind erosion, giving them distinctive, highly dissected patterns. Active dunes occur at the inner edge of extensive mudflats, the outer delta, and along the western and southwestern sides of river channel bars. Only distinct dunes were mapped, whereas sand sheets overlying other deposits were not.
Eolian Loess	Unconsolidated, wind-deposited accumulations of silt and very fine sand that form a blanket over other terrain units in the delta, such as abandoned floodplains and old terraces. (not mapped).
Delta, Riverbed/ Riverbar Deposit	Silty and sandy riverbed or lateral accretion deposits laid down from the bed load of a river in areas of channeled flow. Riverbed alluvium includes point bars, lateral bars, mid-channel bars, unvegetated high-water channels, and broad riverbed/sandbars exposed during low water. In general, texture of the sediments decreases in a seaward direction along the distributaries and in a bankward direction from the thalweg. Organic matter, including driftwood (mostly small willows), peat shreds, and other plant remains, usually is interbedded with the sediments. Only those riverbed deposits that are exposed at low water are mapped, but they also occur under rivers and cover deposits. Frequent flooding (every 1–2 yr) prevents the establishment of permanent vegetation.
Delta, High-water Channel	Riverbed deposits that occur in channels flooded only during periods of high flow. Because of river meandering, these channels no longer are active during low-flow conditions. Deposits in this unit are similar to those described for riverbed alluvium. These old channels show little surface polygonization indicative of ice-wedge development, although there infrequently are high-water channels that are older and have developed disjunct polygon rims. Very old channels that have distinct low-centered polygons are not included in this unit.
Delta, Active- Floodplain Cover Deposit	Thin (0.5–1 ft) fine-grained cover deposits (primarily silt) that are laid down over sandier riverbed deposits during flood stages. Deposition occurs sufficiently frequently (every 3–4 yr) to prevent the development of a surface organic horizon. Supra-permafrost groundwater generally is absent or occurs only at the bottom of the active layer during mid-summer. This unit usually occurs on the upper portions of point and lateral bars and supports riverine willow vegetation.
Delta, Inactive- Floodplain Cover Deposit	Fine-grained cover or vertical accretion deposits of a braided floodplain that are laid down over coarser riverbed deposits by streams at bank overflow (flood) stages. The surface contains a sequence (0.5–2 ft thick) of interbedded organic and silt layers near the surface, indicating occasional flood deposition. Under the organic horizons is a thick layer (1–5 ft thick) of silty cover deposits overlying riverbed deposits. Surface forms range from nonpatterned to disjunct and low-density, low-centered polygons. Lenticular and reticulate forms of segregated ice and massive ice in the form of ice wedges are common.
Delta, Abandoned Floodplain Cover Deposit	Peat, silt, or fine sand (or mixtures or interbeds of all three), deposited in a deltaic overbank environment by fluvial, eolian, and organic processes. These deposits generally consist of an accumulation of peat 2–6 ft thick that overlies cover and riverbed alluvium. Because these are older surfaces, eolian silt and sand may be common as distinct layers or as intermixed sediments. The surface layer, however, lacks interbedded silt layers associated with occasional flood deposition. Lenticular and reticulate forms of segregated ice and massive ice in the form of ice wedges are common in these deposits. The surface is characterized by high density, low-relief polygons and represents the oldest surface on the floodplain.
Meander Floodplain Riverbed Deposit	Sandy gravel, and occasionally sand, deposited as lateral accretion deposits in channels of active floodplains by fluvial processes. Subrounded to rounded pebbles and cobbles are common in the sandy gravel. Frequent deposition and scouring from flooding prevents the establishment of vegetation. The channel has a meandering configuration.

Table 3-3. (cont.).

Unit	Description
Meander Active-Floodplain Cover Deposit	Thin (0.5–1 ft), fine-grained cover deposits (primarily silt) that are laid down over sandy or gravelly riverbed deposits during flood stages. Deposition occurs sufficiently frequently (probably every 3–4 years) to prevent the development of a surface organic horizon. This unit usually occurs on the upper portions of point and lateral bars and supports riverine willow vegetation.
Meander Inactive-Floodplain Cover Deposit	Interbedded layers of peat and silty very fine sand material (0.5–2 ft thick), indicating a low frequency of flood deposition. Cover deposits below this layer generally consist of silt but may include pebbly silt and sand and usually are in sharp contact with underlying gravelly riverbed deposits. This unit has substantial segregated and massive ice, as indicated by the occurrence ice-wedge polygons.
Thaw Basin Deposit, Ice Poor	Thaw basin deposits, which are caused by the thawing of ground ice; they typically are fine-grained and organic-rich, and the stratigraphy of the original sediments has been deformed by the subsidence. On the terraces and coastal plain west of the delta, pebbly silt or fine sand is more common. The presence of nonpatterned ground or disjunct polygonal rims indicates that ground ice is low and that lake drainage has occurred recently. Ponds in these basin typically have irregular shorelines and are highly interconnected.
Thaw Basin Deposit, Ice Rich	Sediments similar to non-ice rich thaw lake deposits but having much more ground ice, as indicated by the development of low-centered or high-centered polygons. Waterbodies within these basins tend to be rectangular, to have smooth, regular shorelines, and to be poorly interconnected.
Delta Thaw Basin Deposit, Ice Poor	Deposits occurring in thaw lakes having a connection to a river or nearshore water (tapped lake); they occur only in deltaic environments. Most connections occur when a meandering distributary cuts through a lake's bank; once connected, the lake is influenced by changes in river level. During breakup, large quantities of sediment-laden water flow into the lake, forming a lake delta at the point of breakthrough. Sediments typically consist of fine sands, silts, and clays and typically are slightly saline.
Delta Thaw Basin, Ice-rich	Similar to the above unit, except that sediments are ice-rich, as indicated by the development of ice-wedge polygons. Typically, the sediments contain a sequence of a thick (1–2 ft) layer of interbedded silt and peat, fine-grained cover deposits, and silty clay lacustrine deposits. They still are subject to flooding
Alluvial Terrace Deposit	Fluvial gravelly sand, sand, silty sand, and peat. The old terraces were deposited at an earlier age and are not subject to flooding under the current regime. Deposits usually are overlain by eolian silt and sand and organic-rich thaw basin deposits. This unit has a high content of segregated and massive ice, as indicated by the presence of ice-wedge polygons and the abundance of thaw ponds.
Alluvial-Marine Terrace Deposit	A sequence of alluvial and marine terraces (A, B, and C of Rawlinson 1993) that have variable composition but generally consist of undifferentiated gravelly sand overlain by fluvial gravelly sand, silty sand, and organic silt. Stratified layers of marine gravelly sand, silty sand, silt and minor clay occur in some locations beneath the fluvial deposits. The deposits generally are overlaid by pebbly eolian sand and silt and organic-rich lacustrine deposits. This unit is not subject to flooding.
Alluvial Plain Deposit	Peat, eolian loess and sand, lacustrine sediments, and sandy gravel deposited by braided river processes on an alluvial plain. A typical sequence consists of 0.5–2 ft of peat or mixed sand and peat typical of lacustrine material, 4–7 ft of sand and pebbly fine sand (Beechey Sand), and thick beds (below 5–10 ft) of sandy gravel and gravel (Ugnuravik Gravel). The surface is ice-rich, as indicated by polygonal development and the prevalence of thaw lakes. Water depths in thaw lakes generally are 3–7 ft, indicating that ice contents are high and sediments are not thaw stable.
Tidal Flat Deposit	Areas of nearly flat, barren mud or sand that are periodically inundated by tidal waters. Tidal flats occur on seaward margins of deltaic estuaries, leeward portions of bays and inlets, and at mouths of rivers. Tidal flats frequently are associated with lagoons and estuaries and may vary widely in actual salinity, depending on how exposed the flat is to salt-water incursion and the rate of influx of fresh water.
Fill, Gravel and Peat	Gravel and sandy gravel that has been placed as fill for roads and pads in the village of Nuiqsit and the Kuparuk Oilfield. Peat fill ("peat road") includes a mixture of organic and fine-grained sediments that has been obtained by taking peat material from the active layer and piling it into a roadbed

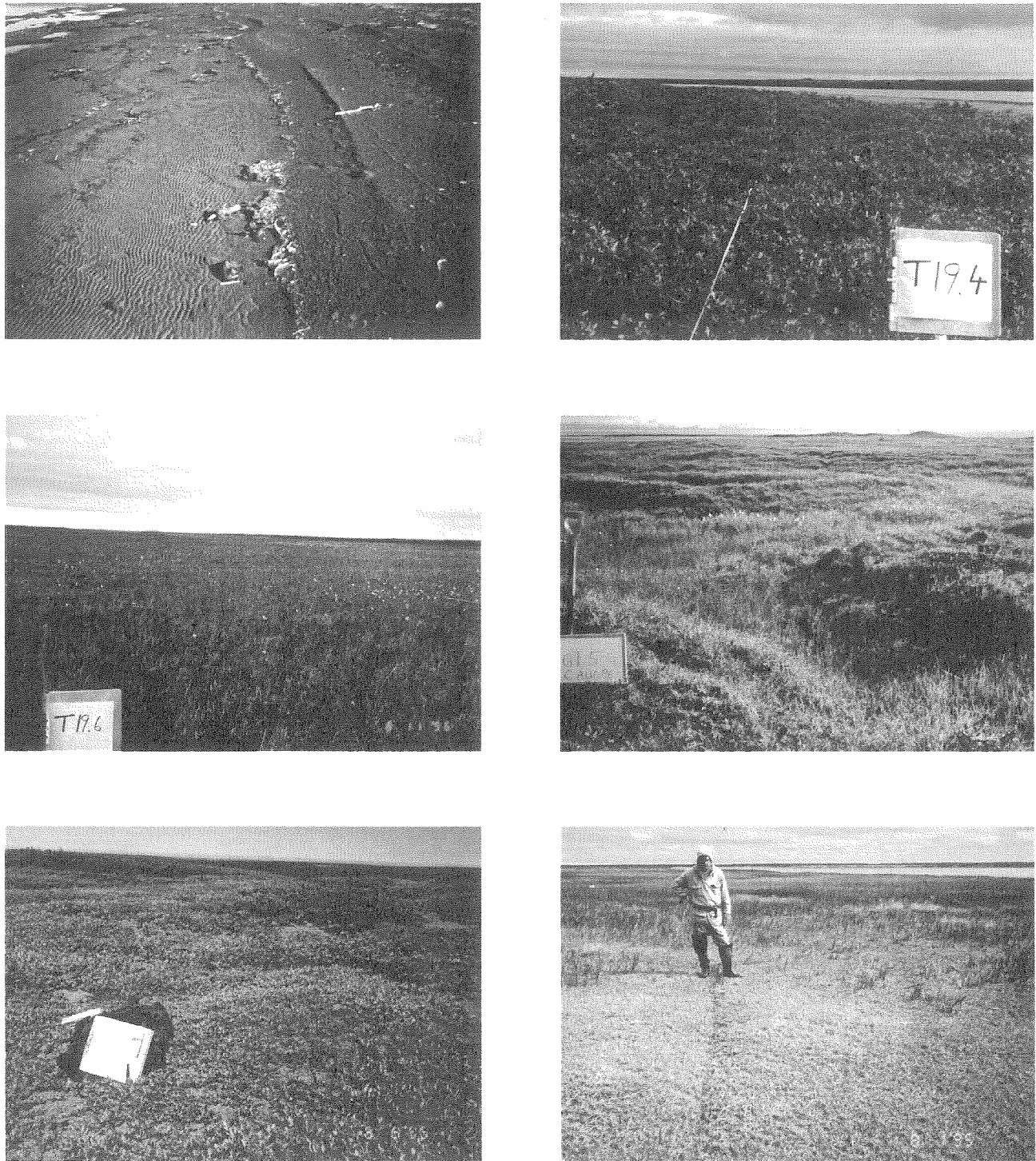
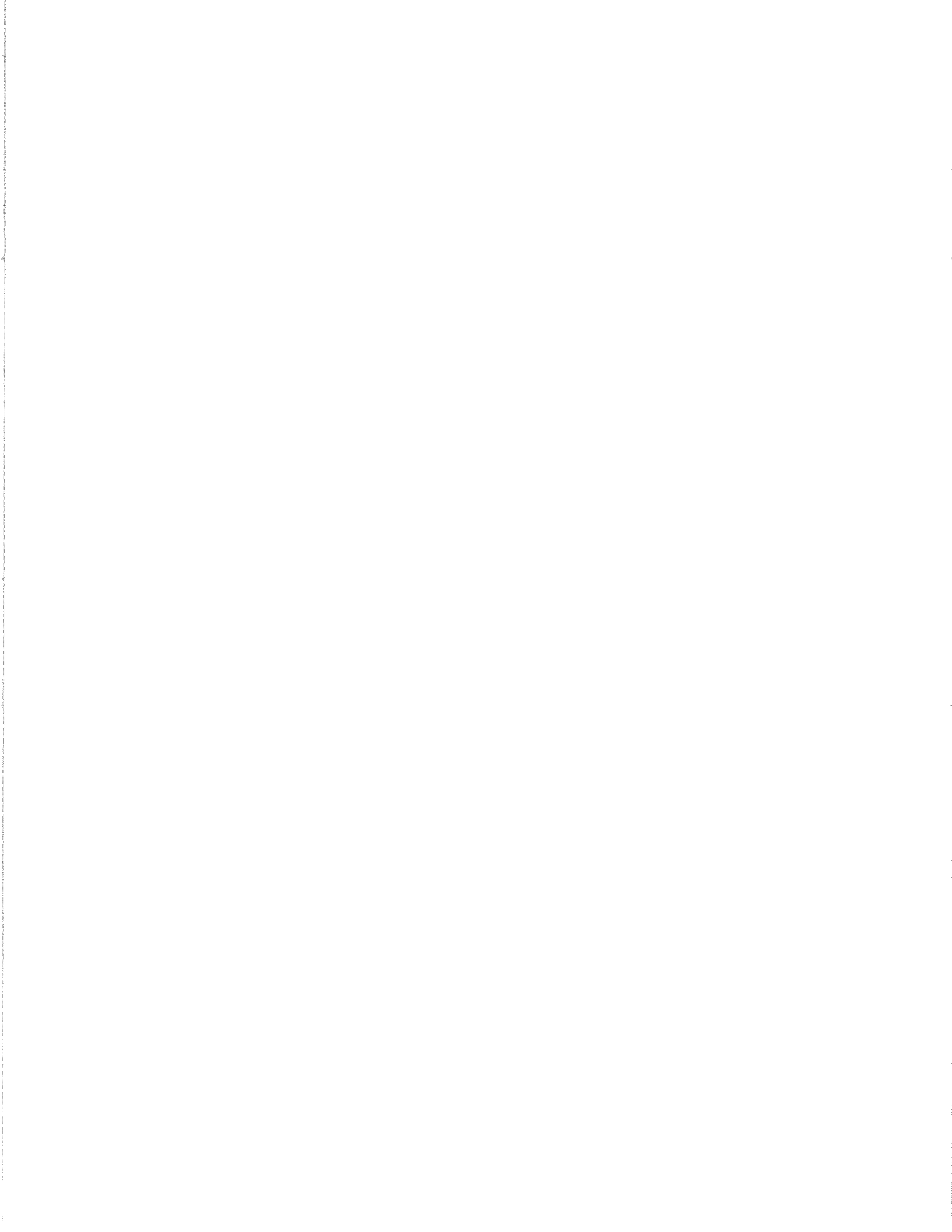
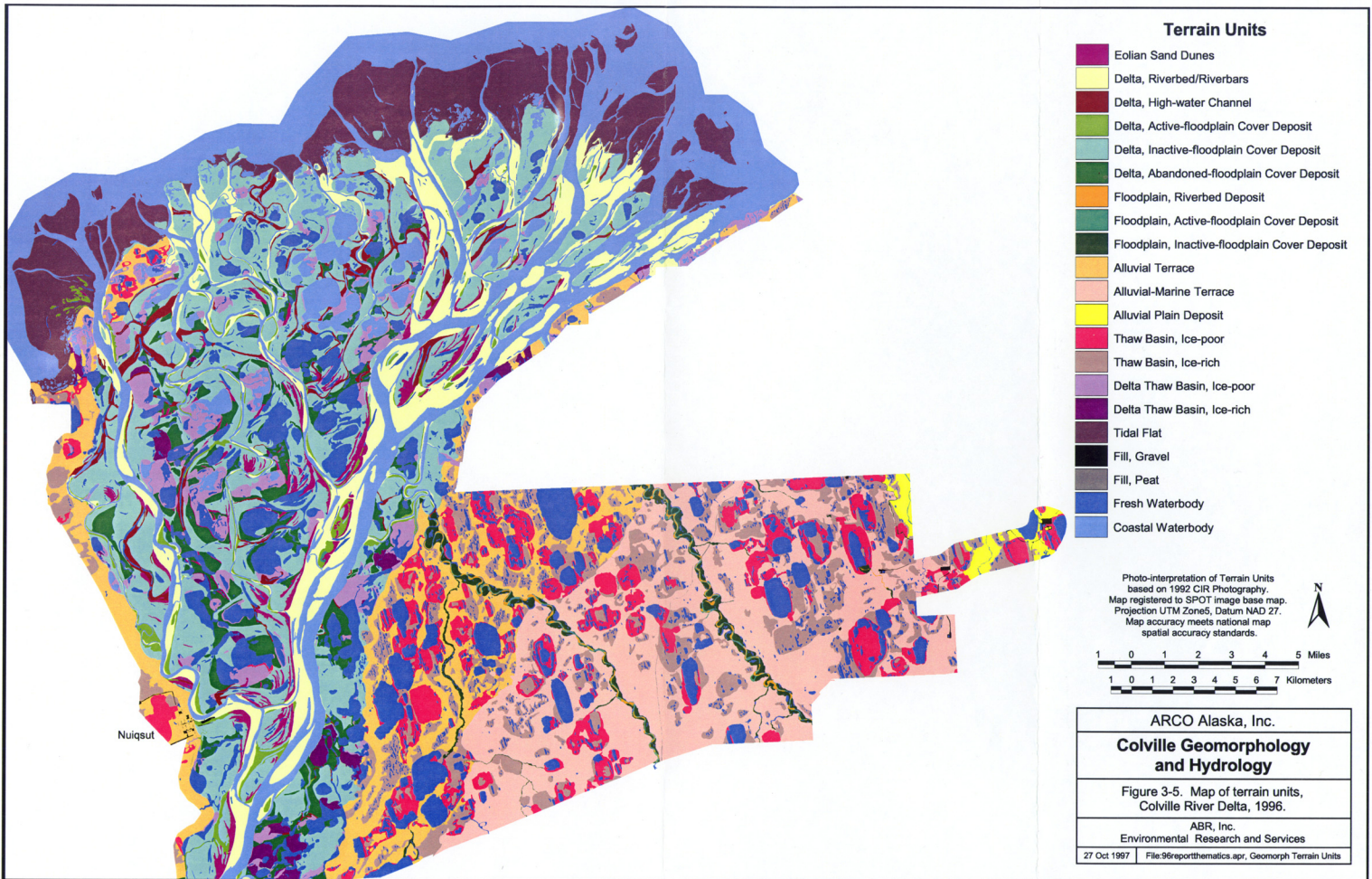


Figure 3-4. Photographs of typical depositional environments associated with lateral accretion deposits on riverbars (upper left), active-floodplain cover deposit (upper right), inactive-floodplain cover deposit (middle left), abandoned floodplain cover deposit (middle right), sand dunes (lower left), delta thaw lake deposits (lower right), Colville River Delta, Alaska, 1996.





Nuqsut

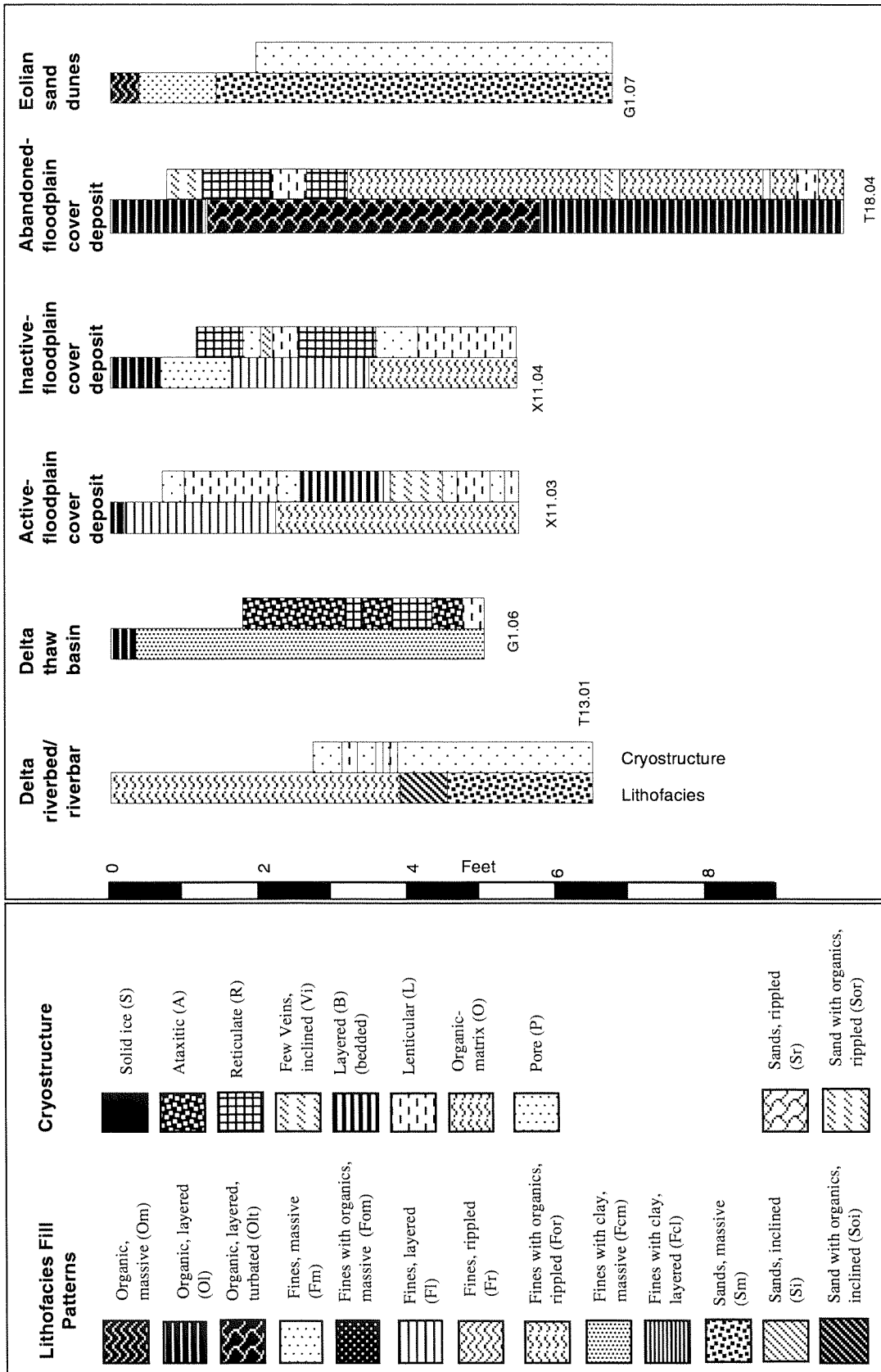


Figure 3-6. Representative soil profiles showing lithofacies and ice structures associated with six terrain units, Colville River Delta, 1996.

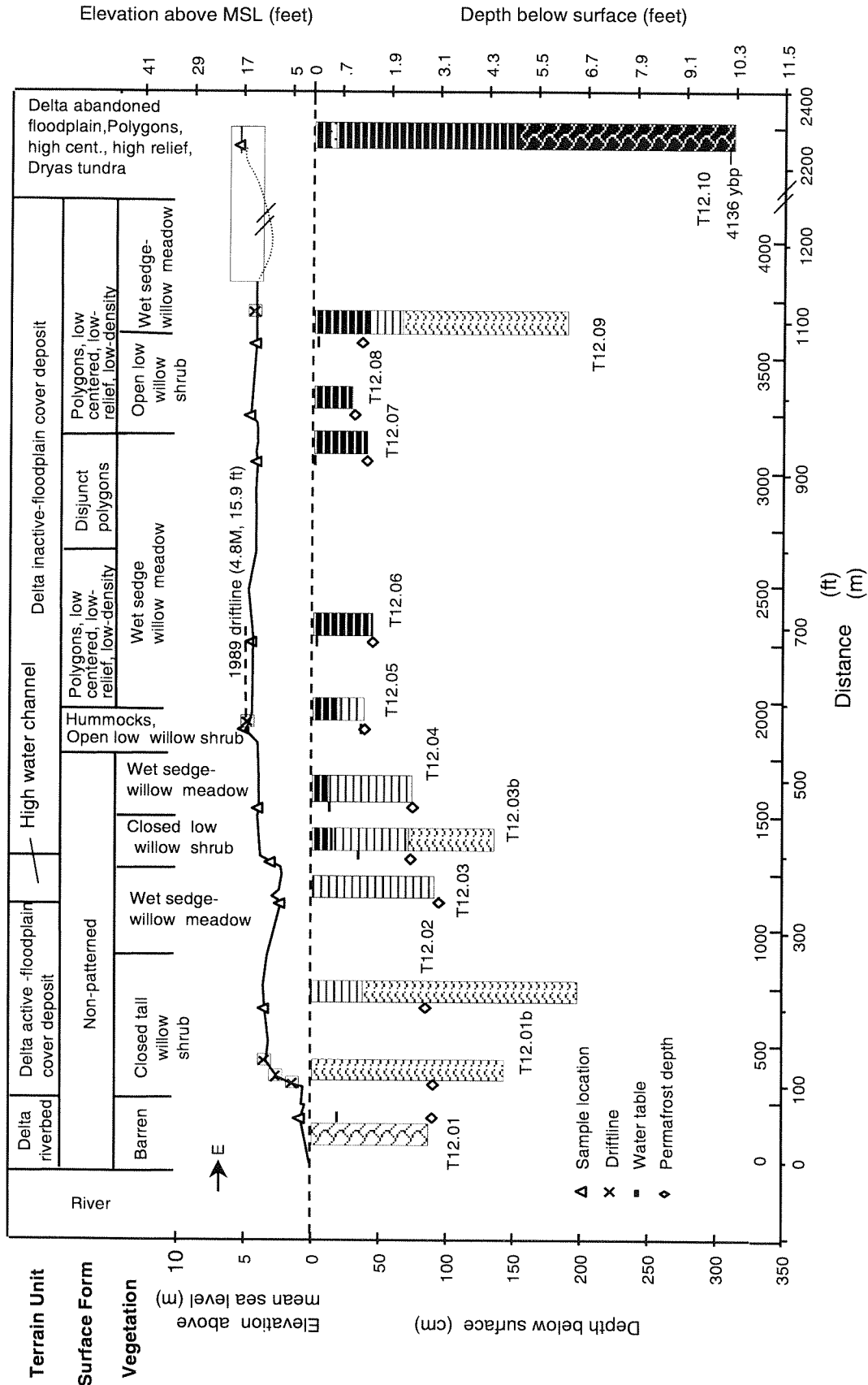


Figure 3-7. Soil stratigraphy along a terrain sequence (Transect 12) along the upper Nechelik Channel, Colville River Delta, 1996.

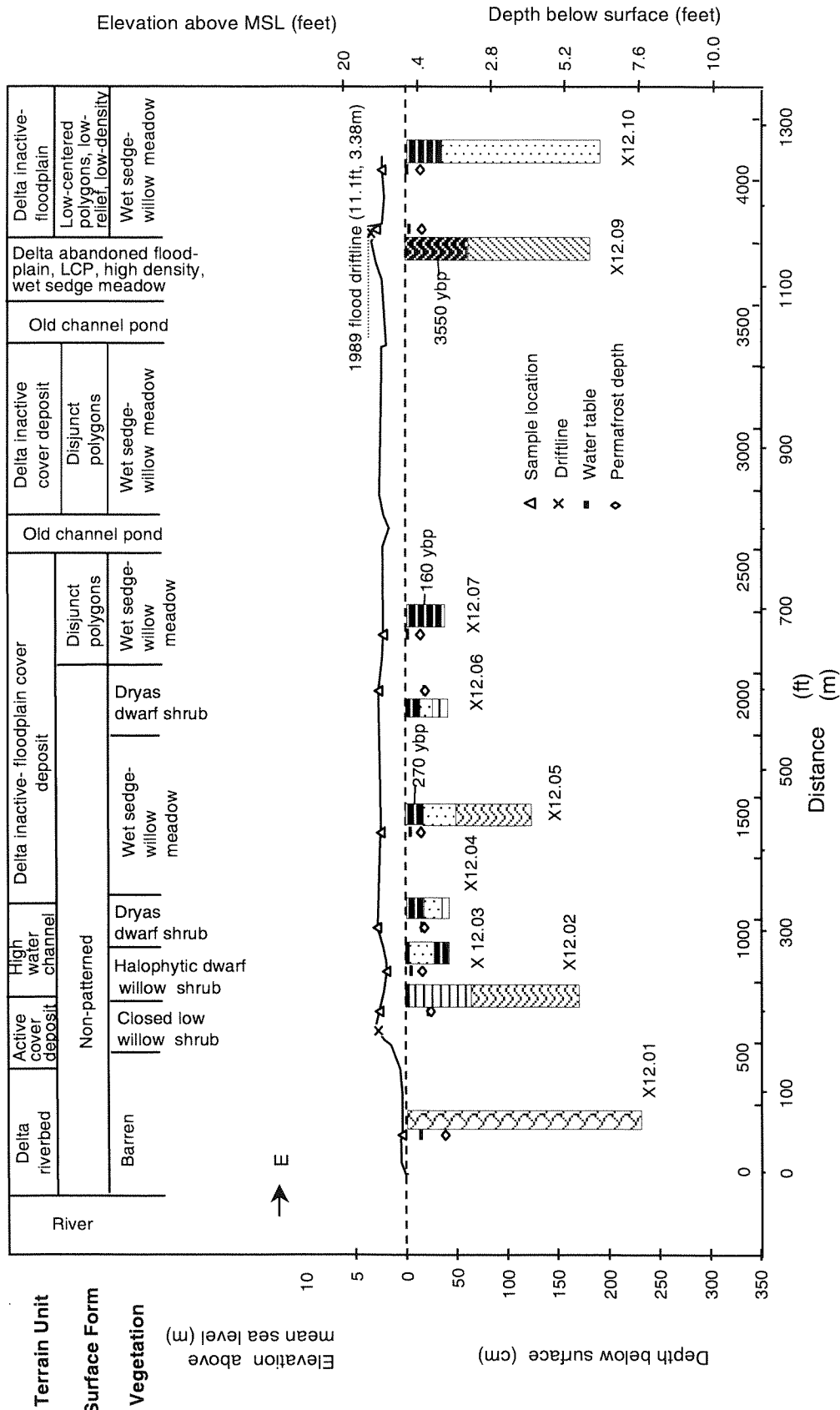


Figure 3-8. Soil Stratigraphy along a terrain sequence (Cross-section N7.46, 312) along the middle Nechehlik Channel, Colville River Delta, 1996.

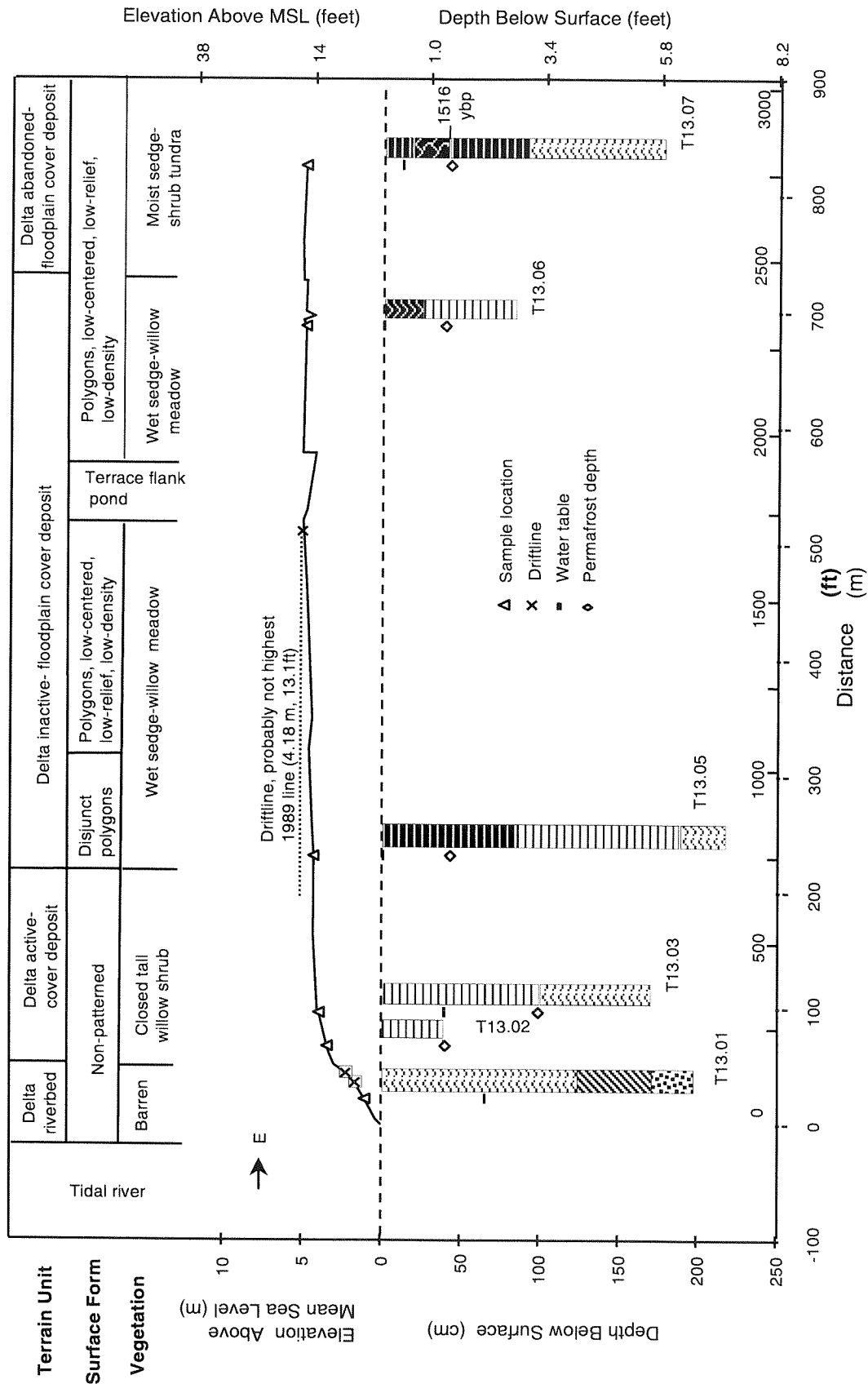


Figure 3-9. Soil stratigraphy along a terrain sequence (Transect 13) along upper Sakoonang Channel, Colville River Delta, 1996.

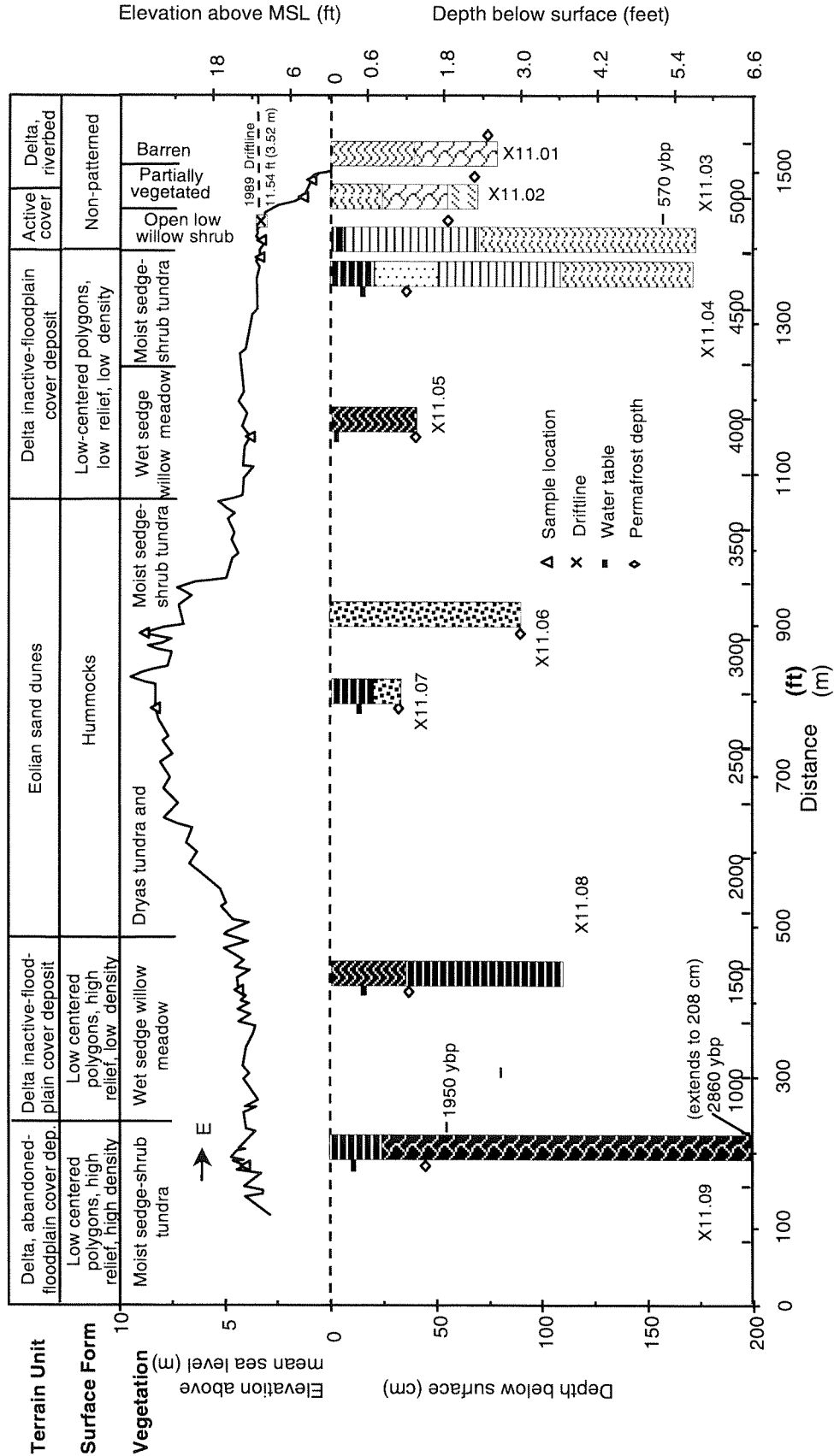


Figure 3-10. Soil stratigraphy along a terrain sequence (Cross-section S9.80, #11) along the middle Sakoonang Channel, Colville River Delta, 1996.

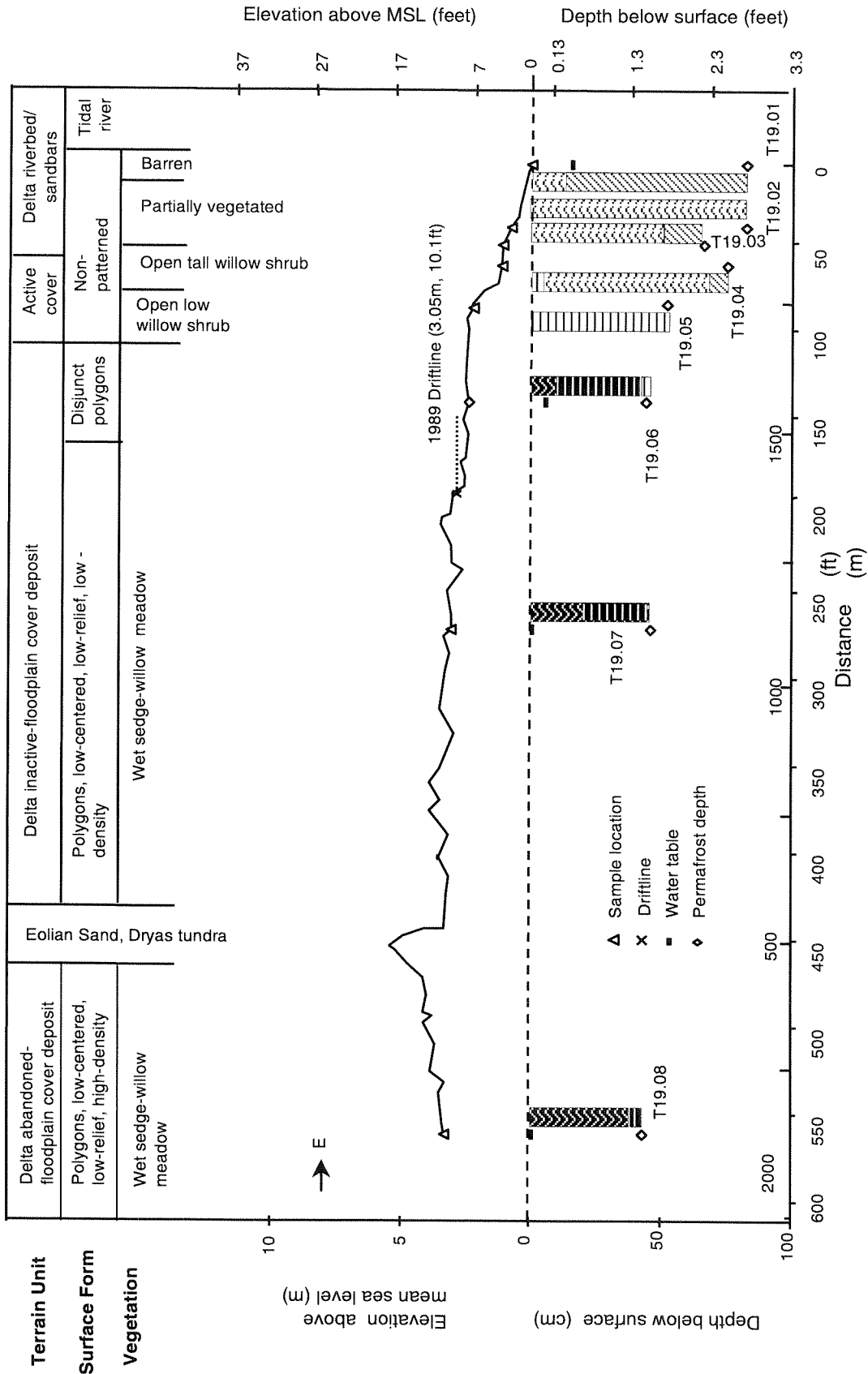


Figure 3-11. Soil stratigraphy along a terrain sequence (Transect 19) along the middle Sakoong Channel, Colville River Delta, 1996.

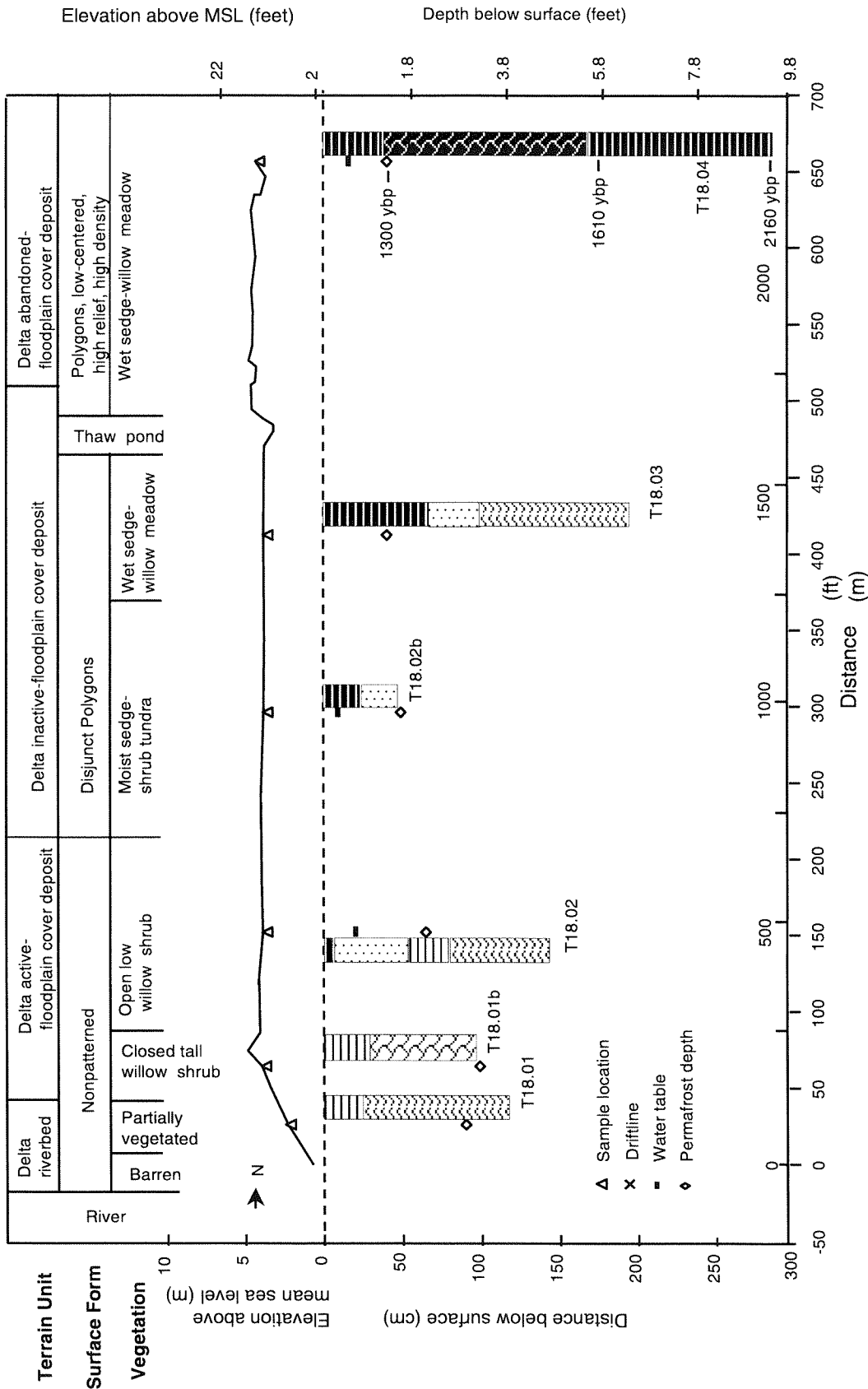


Figure 3-12. Soil stratigraphy along a terrain sequence (Transect 18) along the East Channel, Colville River Delta, 1996.

PART III. Soil Stratigraphy and Permafrost Development

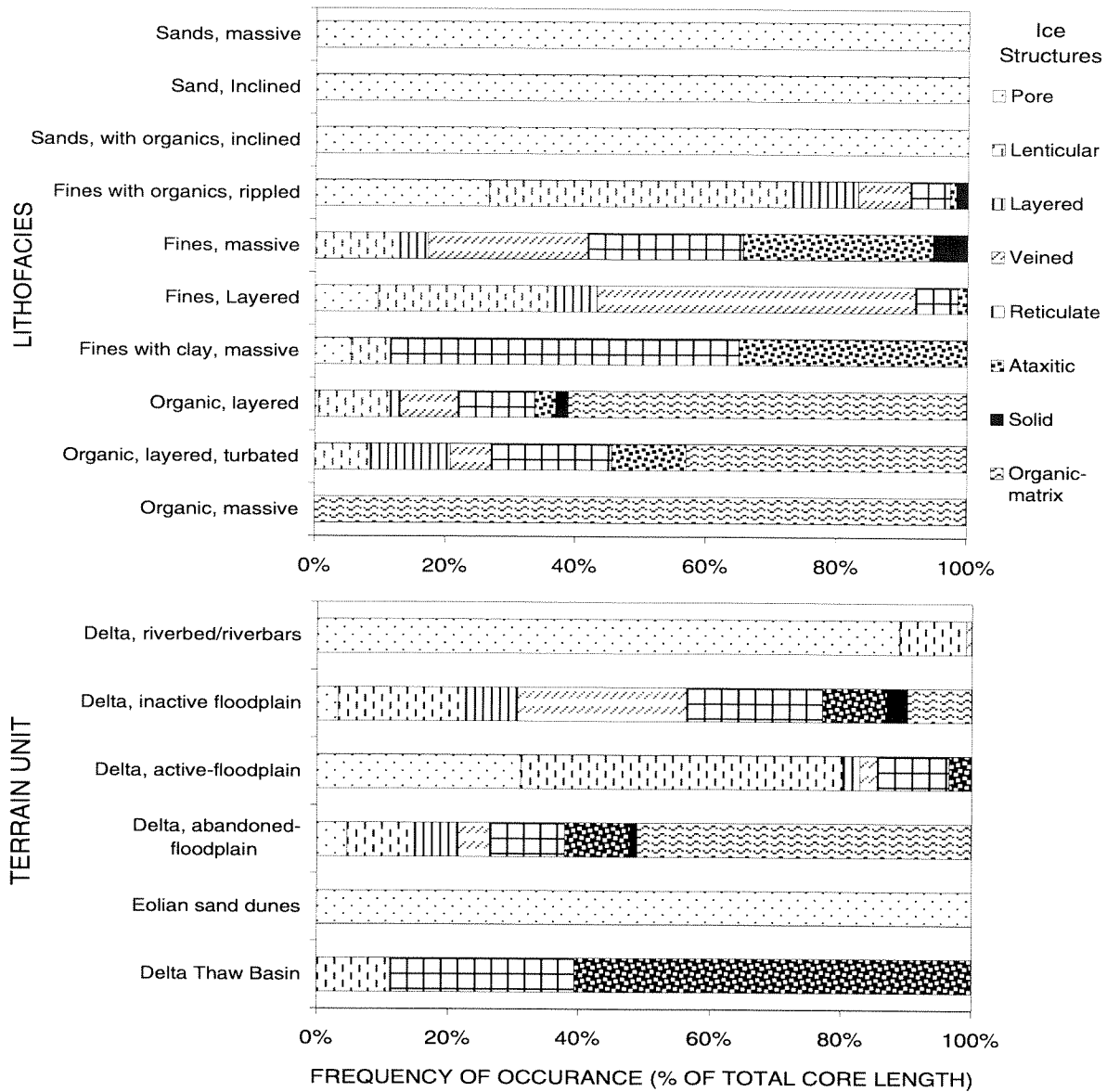


Figure 3-13. Frequency of occurrence (% of total core length) of ice structures by lithofacies (top) and map terrain unit for profiles that extend down to riverbed/riverbar sediments (below) of the Colville River Delta, 1996.

period of accumulation of fine-grained material along the margins of the river channels sets the stage for the remarkable process of aggradation and degradation of ice-rich permafrost.

The relative elevations of the ice structures also indicates that cryostructures evolve during floodplain evolution in response to changes in sediments and active layer process (Figure 14b). In general, there is a pattern of evolution from pore ice evolutionary sequence from pore ice (lowest on floodplain) to organic matrix ice (highest on floodplain). Ataxitic and Reticulate ice, however, depart somewhat from this trend. They are found at the upper portions of profiles of inactive and abandoned floodplains, in clay-rich thaw lake deposits at the bottom of some inactive-floodplain sequences, and at the bottom of some (2-3m depth) of organic-rich layers in abandoned floodplains. When analyzed within inactive-floodplains only, difference relative elevations among ice structures is more consistent (Figure 3-14b, bottom).

SEDIMENT CHARACTERISTICS

In the following analysis of the physical and chemical characteristics of sediments (particle size, salinity, organics, thaw depths, and ice) in the delta and the adjacent coastal plain, we compare differences in sediment characteristics among lithofacies, stratigraphic terrain units, and surface terrain units (according to the scale of geomorphic analysis that best accounts for variation in sediment characteristics). We also identify those factors that have contributed to changes in physical characteristics.

Particle Size

Among lithofacies, particle-size distribution was highly variable (Figure 3-15). Lithofacies with the highest sand content included massive and inclined sands, rippled fines, and massive, turbated organic fines (found on coastal plain deposits). Two lithofacies with unusually high sand contents include layered, clay-rich fines (presumably due to incorporation of sandy layers) and massive organics (presumably due to eolian sand input). In contrast, lithofacies with the highest clay content included massive, clay-rich fines and turbated, layered organics (presumably from slackwater deposition).

Among stratigraphic terrain units, sand percentages were highest in eolian sand, old terrace, and riverbed/riverbar deposits and lowest in inactive- and

abandoned-floodplain cover deposits (Figure 3-15). The mean percentage of clay was highest in the high water channel and inactive-floodplain cover deposits.

Changes in particle-size distribution reflect differences in flood frequency, duration, and magnitude, and in eolian input among terrain units. The high percentage of sand and low percentage of clay in delta riverbed samples indicate high-frequency, moderate-energy, depositional environments. In contrast, the higher percentage of clay in inactive-floodplain cover deposits indicates a low-velocity depositional environment.

The increase in the percentage of sand from inactive-floodplain to abandoned-floodplain cover deposits probably was due to eolian input, because sand grains tended to be evenly distributed through the organic matrix in abandoned floodplains, as opposed to occurring in distinct thin layers of silt, as would be seen in fluvial deposition. In addition, the greater age of the abandoned-floodplain cover deposits allowed greater accumulation of eolian material (even though the rate of eolian deposition may be similar between inactive- and abandoned-floodplain deposits).

Organic Matter Accumulation

Among surface terrain units, large differences were found in the mean thickness of the top organic horizon, reflecting differences in how much organic material has accumulated since the last significant deposition of sediments (Figure 3-16).

Autochthonous (*in situ*) accumulations of organic material (not including thin layers of drifted peat) were absent on riverbed/riverbar, tidal flat, and active-floodplain cover deposits. Mean thicknesses of organic accumulation since the last major depositional event were intermediate for inactive-floodplain cover deposits (0.1 ft) and abandoned-floodplain cover deposits (0.2 ft). In contrast, mean organic horizon thicknesses at the surface were much higher for abandoned-meander-floodplain cover deposits (0.6 ft), ice-poor (0.4 ft) and ice-rich (0.3 ft) thaw lake deposits, and alluvial (0.3 ft) and alluvial-marine (0.3 ft) terraces, which are all in the adjacent coastal plain.

The mean cumulative thickness of organic horizons (organic or organic with some silt) in the top 1 ft (a long-term indicator of the frequency of fluvial deposition), also showed large differences among riverbed/riverbar (0 ft), active-floodplain cover (0.1 ft), inac-

PART III. Soil Stratigraphy and Permafrost Development

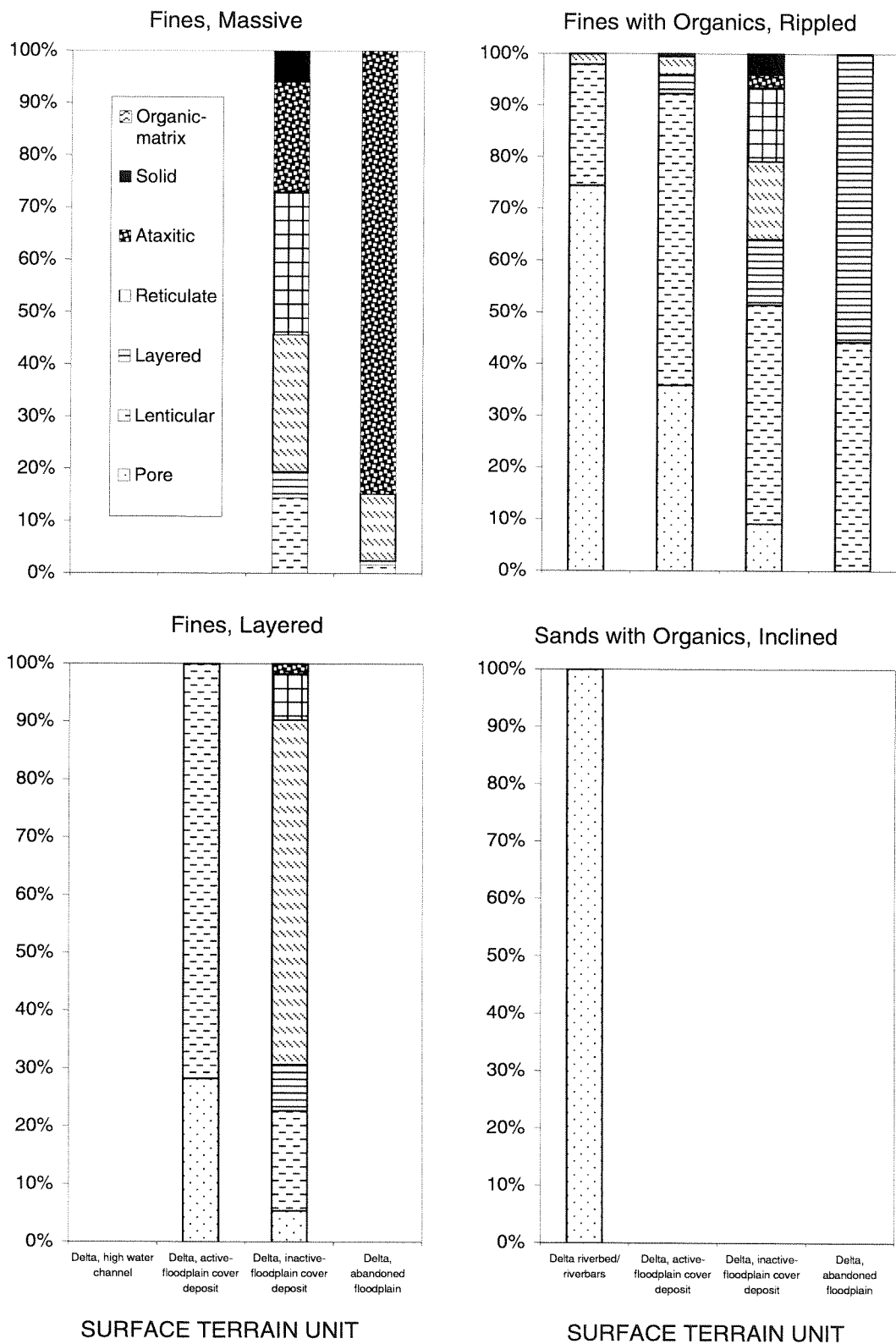


Figure 3–14a. Frequency of occurrence (% of observations) of ice structures by map terrain unit within a lithofacies allowing comparison of how structures change over time, Colville River Delta, 1996.

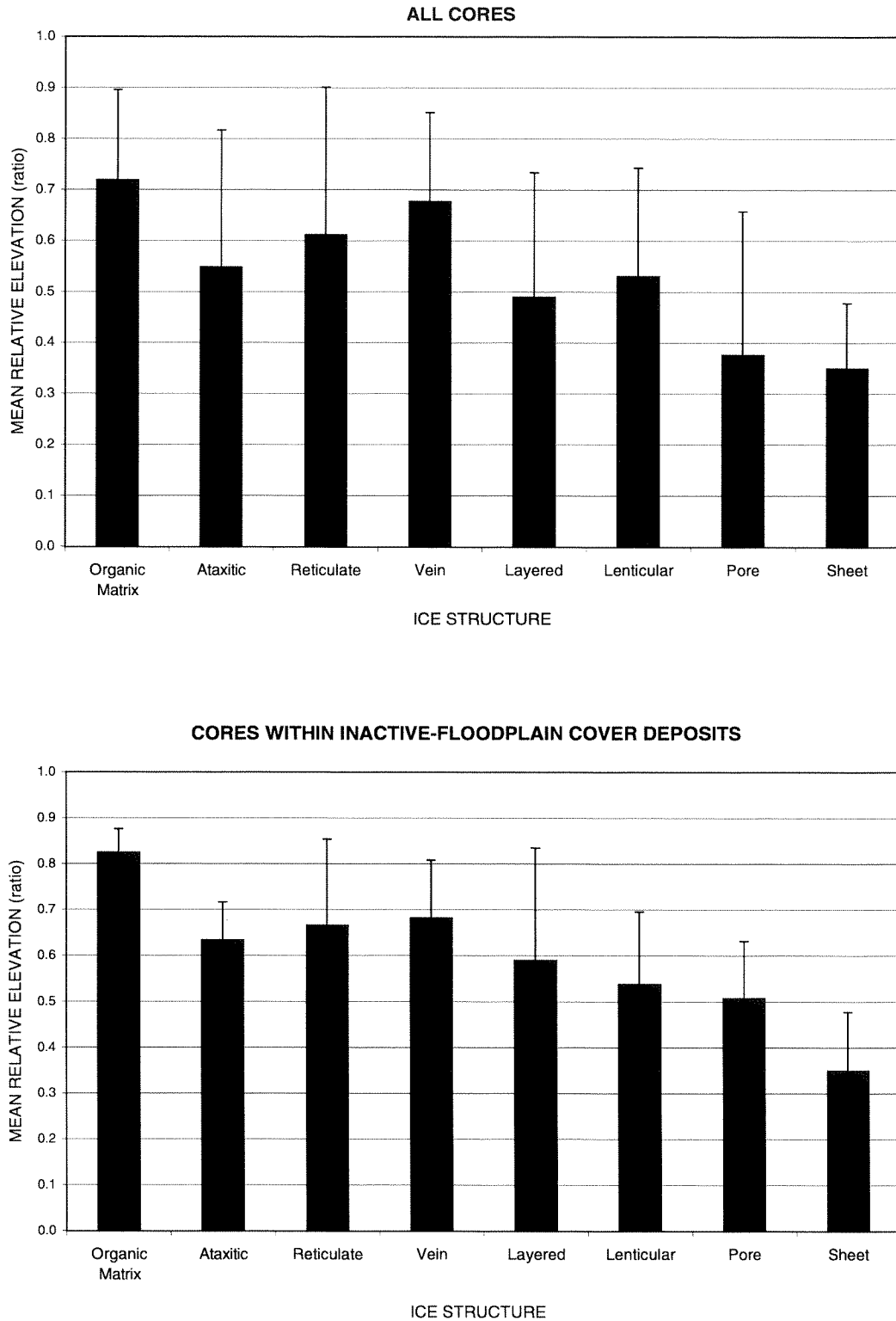


Figure 3-14b. Mean (\pm SD) relative elevations (relative to surface of inactive floodplain) or ice structures for terrain units (top) and within inactive-floodplain cover deposits, Colville River Delta, 1996.

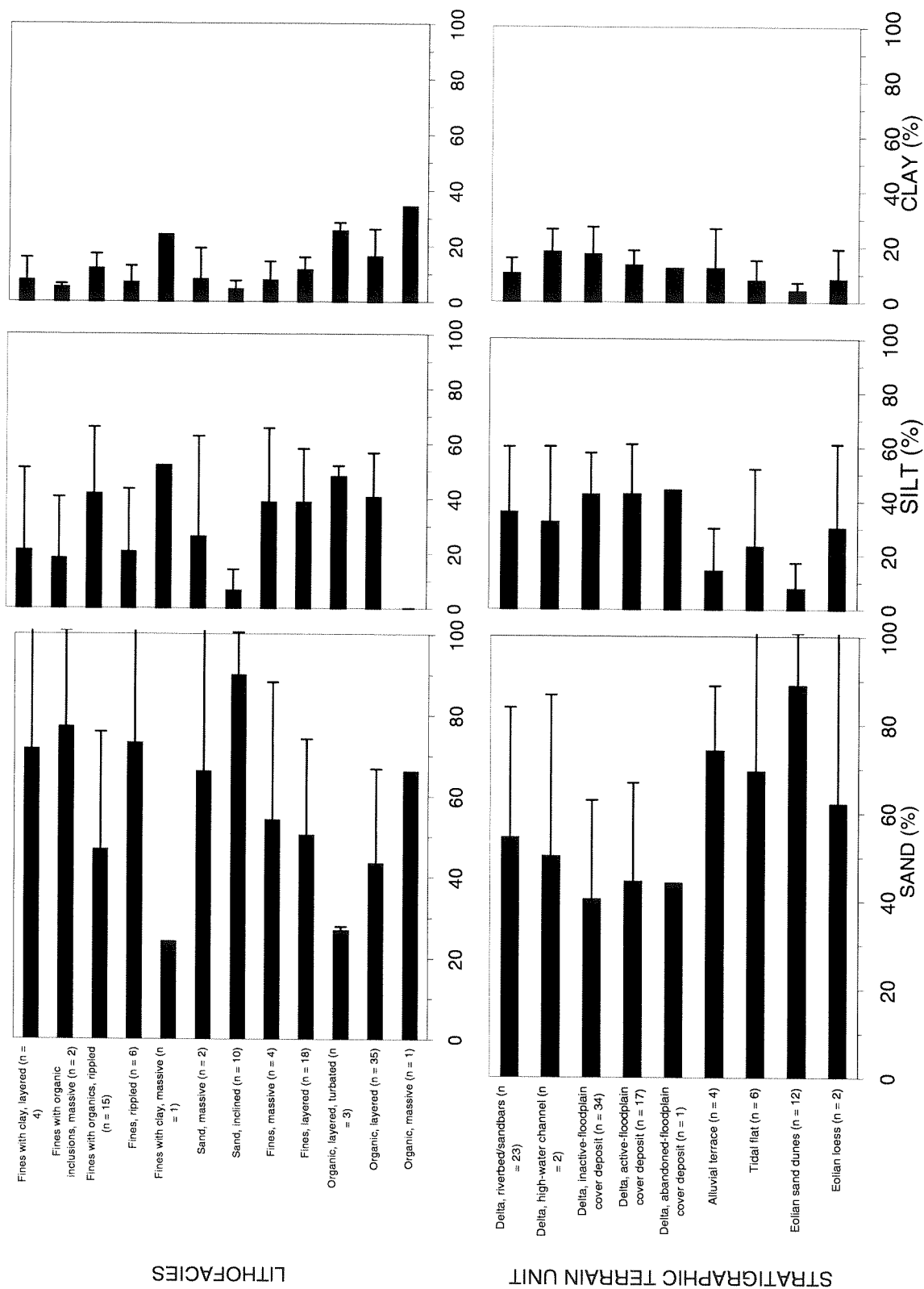


Figure 3-15. Mean (\pm SD) percentages of sand, silt, and clay of sediments associated with various lithofacies (top) and strata terrain units (bottom) on the Colville River Delta, 1996.

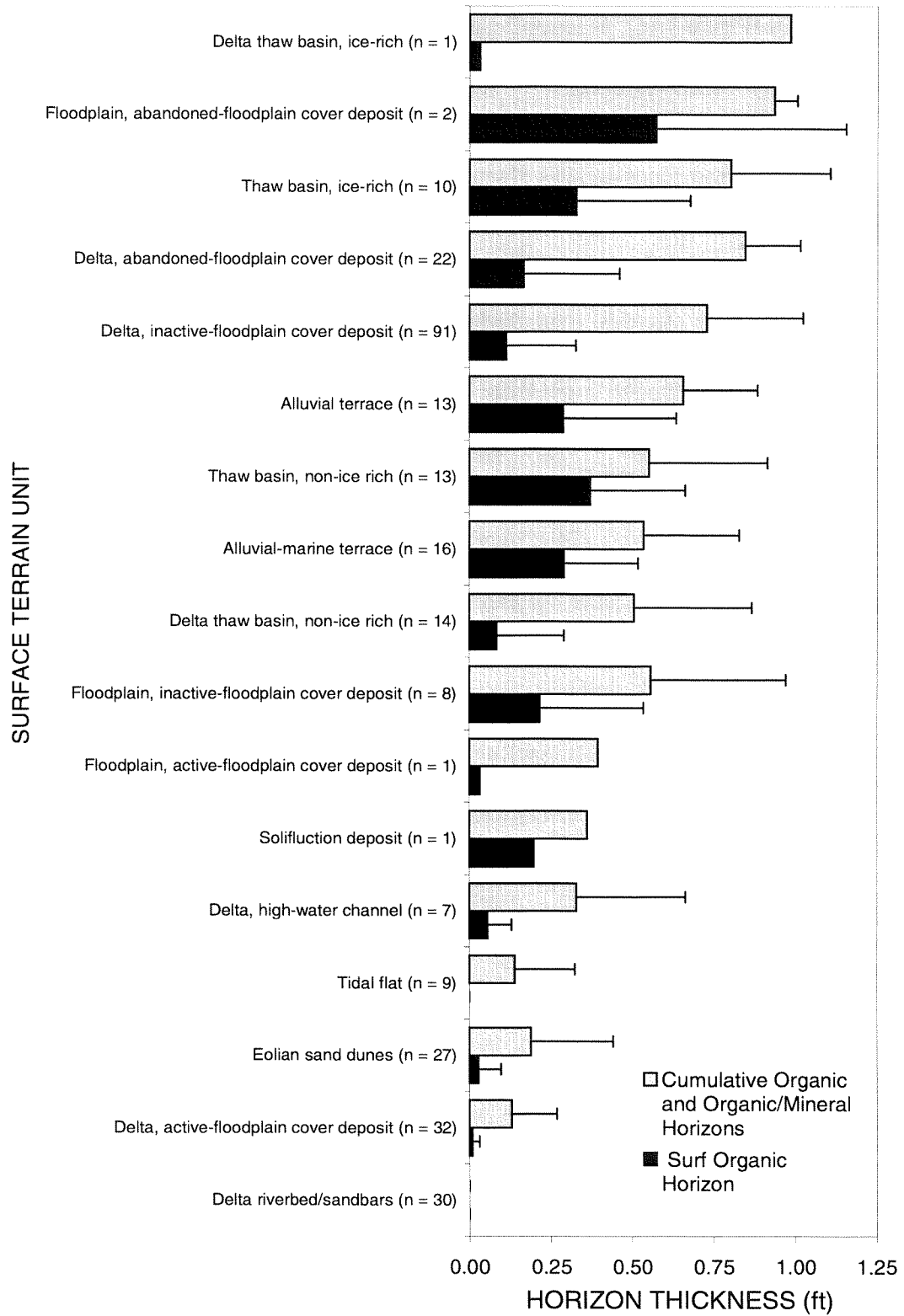


Figure 3–16. Mean (\pm SD) thickness of the surface organic horizon and cumulative thickness of organic (organic and organic-mineral combined) layers in top 1 ft (right) for soils associated with various surface terrain units on the Colville River Delta and the adjacent Transportation Corridor, 1996.

tive-floodplain (0.7 ft), and abandoned-floodplain cover (0.9 ft) deposits (Figure 3-16). Inactive-floodplain cover deposits were characterized by numerous interbedded organic and mineral layers near the surface, but most of the material was organic in origin. In contrast, abandoned-floodplain cover deposits were almost entirely organic or had minor amounts of sand of eolian origin (although layered organics were noted occasionally).

Salinity

Among lithofacies, mean electrical conductivity values (an indirect measure of salinity) was highest in clay-rich fines (6,473 $\mu\text{S}/\text{cm}$), inclined (1,757 $\mu\text{S}/\text{cm}$) and rippled sands (1,500 $\mu\text{S}/\text{cm}$), and rippled fines with organics (740 $\mu\text{S}/\text{cm}$) (Figure 3-17). These lithofacies typically were found at the lowest floodplain levels. In contrast, mean EC values were lowest in massive sands with trace gravels (74 $\mu\text{S}/\text{cm}$), turbated, massive fines with organics (86 mS/cm), and massive organics (278 $\mu\text{S}/\text{cm}$). The latter lithofacies typically were found in the at the highest levels of the floodplain on the delta or adjacent coastal plain.

Among stratigraphic terrain units, the highest mean EC values occurred in ice-poor delta thaw basins (7,465 $\mu\text{S}/\text{cm}$), ice-rich delta thaw basins (1,276 $\mu\text{S}/\text{cm}$), and delta riverbed/lateral accretion deposits (1,061 $\mu\text{S}/\text{cm}$) (Figure 3-17). In contrast, mean EC values were lowest in alluvial terrace (86 $\mu\text{S}/\text{cm}$), abandoned-floodplain cover deposits (90 $\mu\text{S}/\text{cm}$), and ancient coastal plain (165 $\mu\text{S}/\text{cm}$) deposits. Because distinct vertical gradients were evident in stratigraphic terrain units, EC was not summarized by surface terrain unit.

Thaw Depths

Among surface terrain units, mean thaw depths were greatest in delta riverbed/riverbar (2.4 ft), active-floodplain cover (2.1 ft), and eolian sand (2.4 ft) deposits (Figure 3-18). In contrast, mean thaw depths were shallowest in inactive-floodplain (1.4 ft) and abandoned-floodplain (1.2 ft) cover deposits and on alluvial (1.2 ft) and alluvial-marine (1.3 ft) terraces. Because thaw processes are limited to the surface, thaw depths were not analyzed by stratigraphic terrain unit or lithofacies.

Ice Accumulation

Among lithofacies, the mean volumetric percentage of ice determined from laboratory analysis was lowest in massive (43%) and inclined sands (49%), intermediate in layered (61%) and rippled (60%) fines, and highest in massive fines (72%), massive organics (77%), and layered organics (78%) (Figure 3-19). Ice volumes at saturation were assumed to be in the range of 40–48%, based on porosity of the silts and fine sands. Thus, volumes above this amount were considered to represent excess ice (above what the soil contains at saturation). The large differences in ice contents demonstrate that particle size and organic content exert large effects on ice development.

Among ice structures, mean ice volume ranged from 50% for pore ice to 80% for ataxitic ice (Figure 3-20). Ice structures with intermediate levels of development in the continuity of ice had intermediate mean ice volumes (70% for lenticular ice, 72% for reticulate ice). Overall, the ice structure classification appears to be better than visual estimates at partitioning the variability in ice volumes. We frequently had difficulty estimating ice volumes from visual examination of the amount of ice on the surface of the core.

Among surface terrain units, mean ice volumes were lowest in delta riverbed/riverbar deposits (42%) and eolian sand (48%), intermediate in active-floodplain cover deposits (60%), and highest in delta inactive-floodplain cover deposits (72%) and abandoned-floodplain cover deposits (79%) (Figure 3-21). These mean values appear to be reasonable estimates for near-surface sediments (6–10 ft), but probably are less reliable for the greater depths at which sandy sediments associated with riverbed/riverbars typically occur.

Among depths (terrain units combined), mean ice volumes differed little in the top 2–10 ft of soil (64–77%). The small differences among depths underscores the usefulness of stratifying the sediments by lithofacies or surface terrain unit.

We derived an indirect estimate of the amount of ice contributed by ice-wedge development through measurements of ice-wedge characteristics from aerial photographs and assumptions of wedge width and depth (Figure 3-22). When comparing differences in surface form, a large increase was evident in the density of ice wedges (expressed as linear ft of polygon rims/acre) from zero for nonpatterned ground on inac-

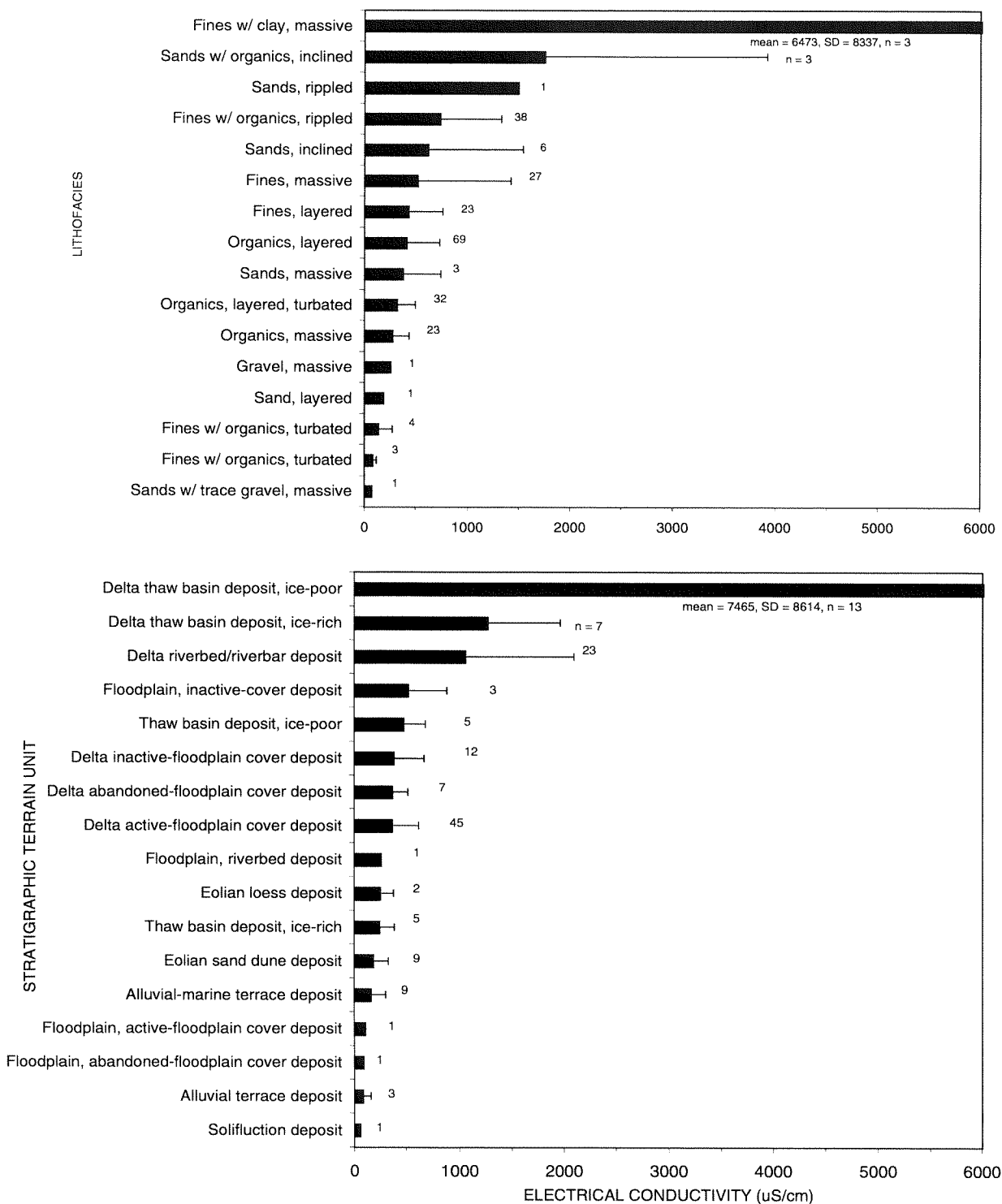


Figure 3-17. Mean (\pm SD) salinity (electrical conductivity) values for sediments associated with various lithofacies and stratigraphic terrain units on the Colville River Delta and the adjacent coastal plain, Alaska, 1996.

PART III. Soil Stratigraphy and Permafrost Development

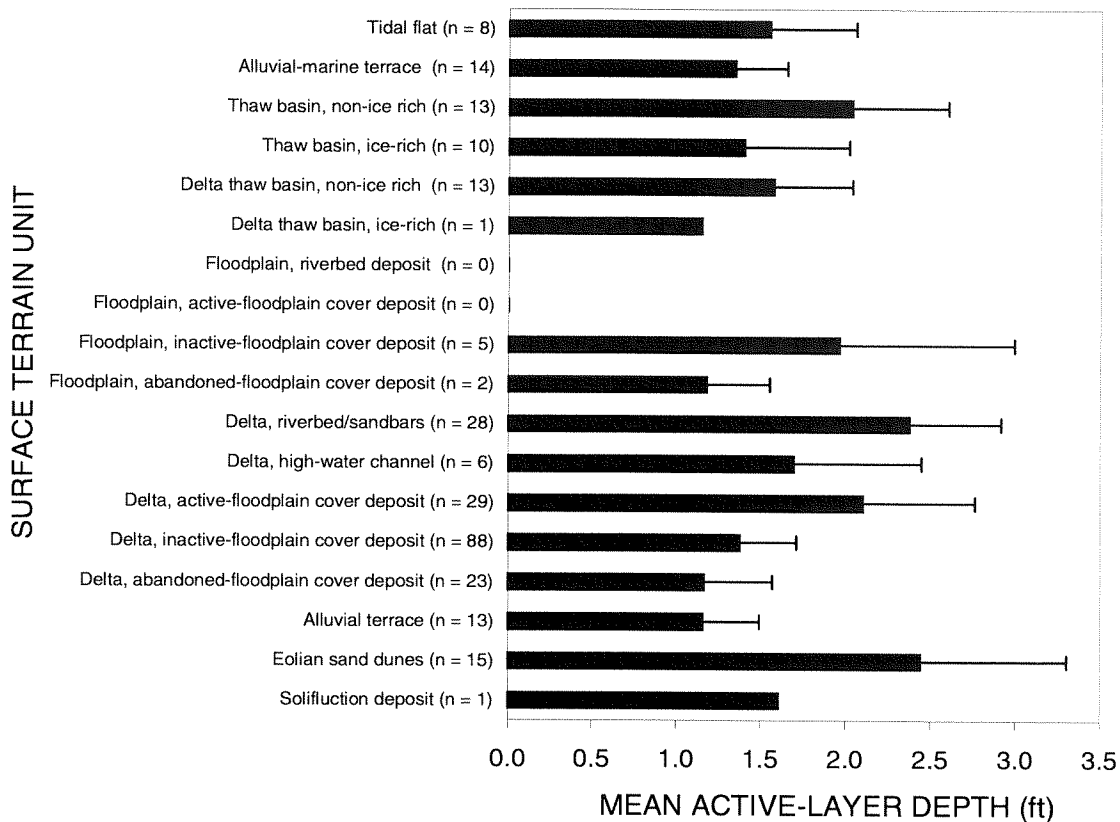


Figure 3-18. Mean (\pm SD) active-layer depths for various surface terrain units on the Colville River Delta and the adjacent Transportation Corridor, Alaska, 1996.

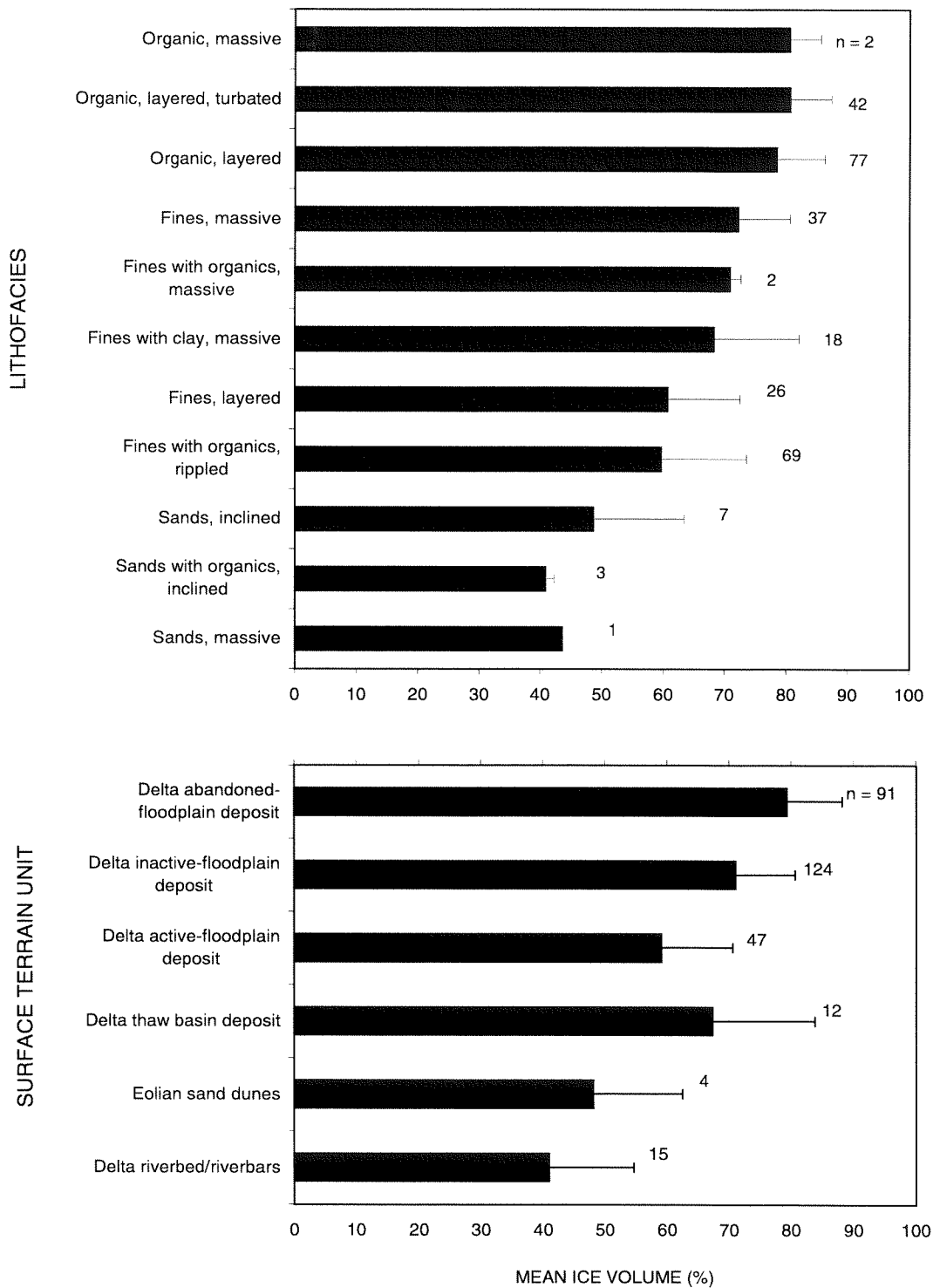


Figure 3-19. Mean (\pm SD) volumetric ice contents in near surface sediments grouped by lithofacies and surface terrain unit, Colville River Delta, Alaska, 1996.

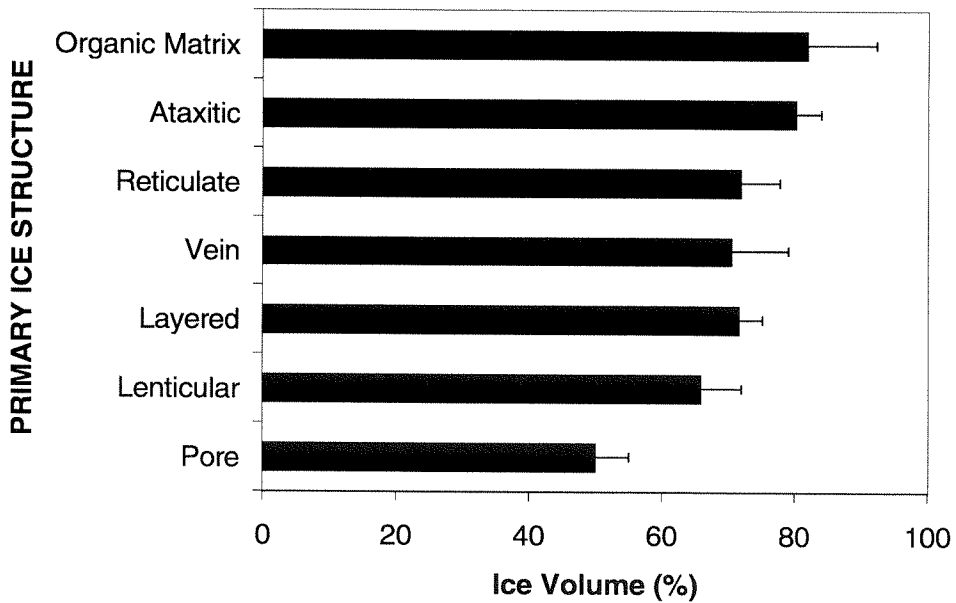
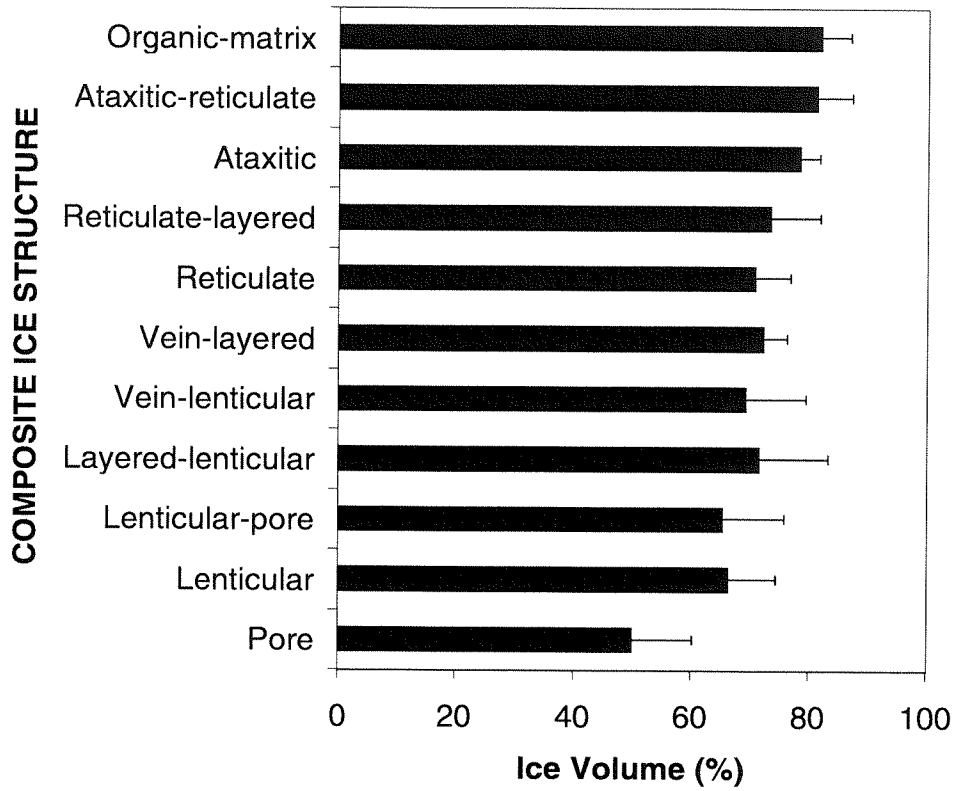


Figure 3-20. Mean (\pm SD) volumetric ice contents in near surface sediments grouped by composite and primary (dominant structure within composite) ice/structures, Colville River Delta, Alaska, 1996.

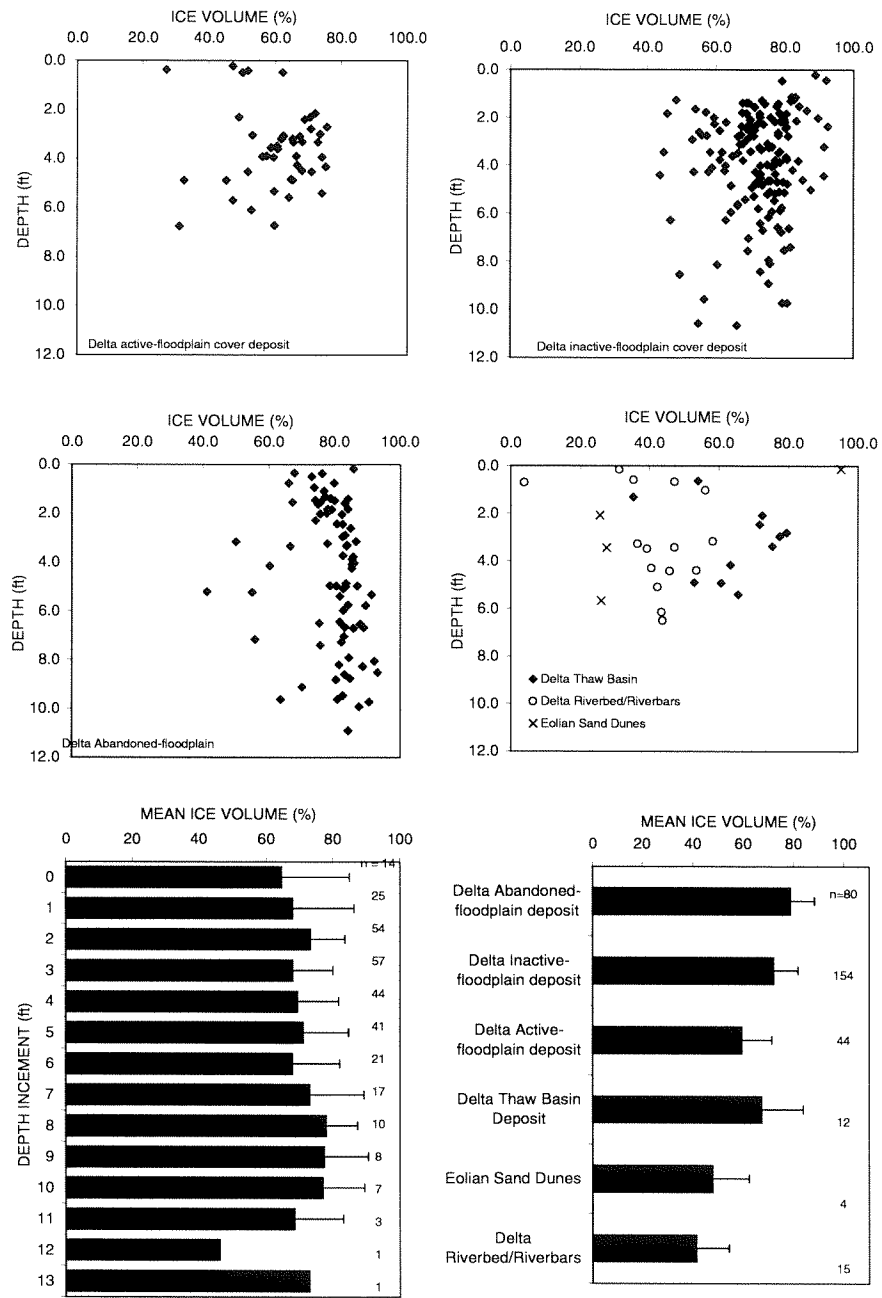
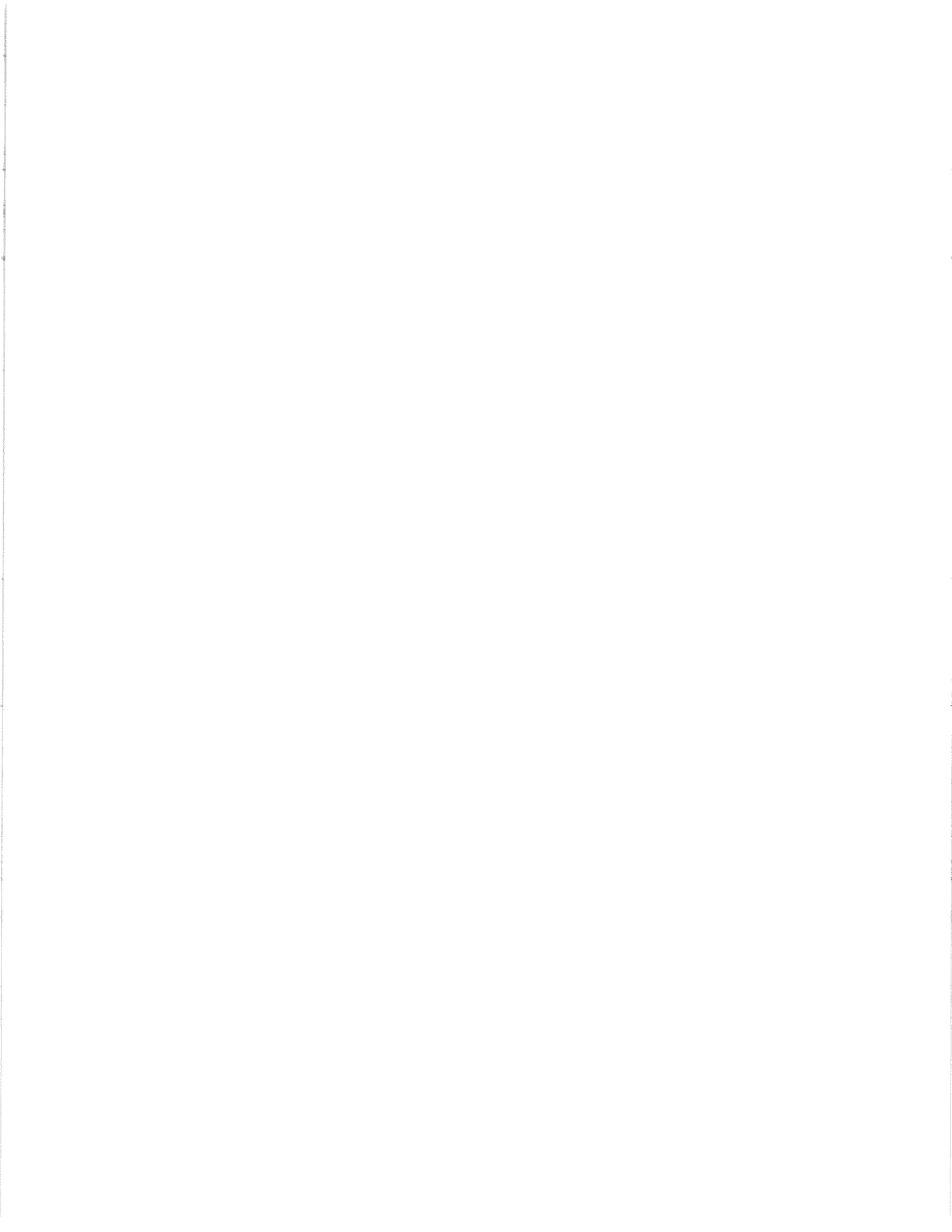


Figure 3-21. Volumetric ice contents by depth within stratigraphic terrain units (upper four graphs) and mean (\pm SD) contents summarized by depth (lower left), Colville River Delta, 1995.



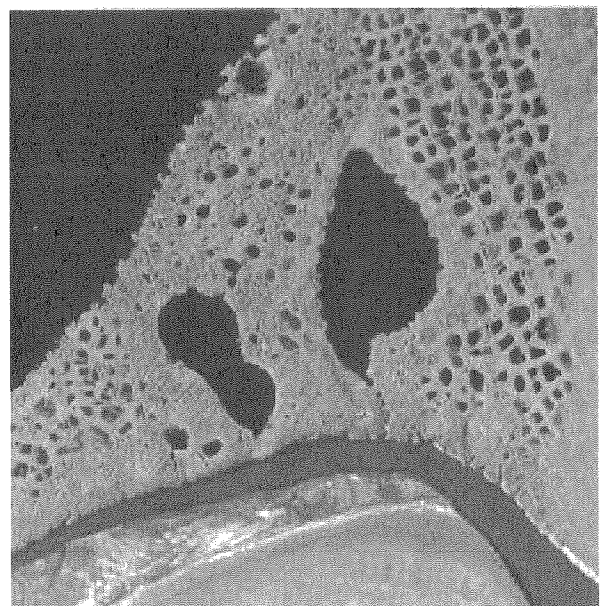


Figure 3-22. Aerial photographs of development of ice-wedge polygons associated with nonpatterned (upper left), disjunct polygons (upper right), low-density polygons (lower left), and high-density polygons (lower right), Colville River Delta, Alaska, 1996.

tive-floodplain cover deposits to 1,029 ft/acre for high-density, low-centered polygons on abandoned-floodplain cover deposits (Figure 3-23). The mean size of low-centered polygons decreased from 1,627 yd² (for occasional polygons that were closed) for disjunct polygons to 440 yd² for high-density polygons. Based on assumptions of dimensions of ice wedges within disjunct (1 ft wide, 7 ft deep), low-density (3 ft wide, 10 ft deep), and high-density polygon (8 ft wide, 13 ft deep), the volumetric percentage in the top 7 ft of permafrost increased from zero for nonpatterned ground to 19% for high-density polygons.

Although we did not systematically sample ice wedges and made only a few observations of wedge width and depth, we believe our estimates of the volumetric percentage of ice wedges are reasonable. Measurements made by one of us (Shur) in Russian deltas suggest that a range of 5–15% for the percent of the total volume contributed by ice wedges is typical. Our values are similar to these data. By comparison, the volumetric percentage of ice wedges was estimated to exceed 50% of the materials in the upper 3–7 ft of ground in the Mackenzie Delta (Pollard and French 1980).

Another indicator of very high ice contents in portions of the delta is the abundance and depth of thaw lakes. Most of the abandoned-floodplain cover deposits have been lost to thaw-lake processes, so only scattered remnants are now present (Figure 3-5). In addition, most thaw lakes in the central delta are 11–15 ft deep. Using these water depths to interpret how much excess ice was present in the deposits before they melted is problematic, however, because the elevations of the adjacent floodplain deposits surrounding the thaw lakes have increased over time, making the lakes deeper.

Overall Accumulation Rates

Using radiocarbon dating of active-layer samples and permafrost cores, large differences in accumulation rates were found among eolian (1.30 ft/100 yr), active-floodplain cover (0.87 ft/100 yr), inactive-floodplain cover (0.44 ft/100 yr), and abandoned-floodplain cover (0.14 ft/100 yr) deposits (Figure 3-24). We were unable to estimate the accumulation rates for riverbed/riverbar deposits because of a lack of organic material suitable for dating.

Because these rates also include accumulations of sediment, organic material, and ice, however, the ac-

tual amount contributed by sedimentation cannot be separated, although some generalizations can be made. Eolian deposits were composed almost entirely of mineral sediment. Active-floodplain cover deposits were mostly sediment, with lesser amounts of excess ice. Inactive-floodplain cover deposits had substantial amounts of ice, sediments, and organics. Abandoned-floodplain cover deposits mostly were ice and organic material. Our analysis of accumulation rates for eolian and active-floodplain cover deposits was hampered by small sample size because these deposits, along with riverbed/riverbars, usually lacked suitable material for radiocarbon dating.

CONCEPTUAL MODEL OF FLOODPLAIN EVOLUTION ON THE DELTA

By examining similarities in sediment characteristics, organic matter accumulation, and ice aggradation along terrain sequences, we have identified several general patterns and processes that affect floodplain evolution, which are similar to those described on arctic floodplains in Russia (Shur 1988). In the following discussion, we relate the trends we observed to landscape position and synthesize these into a conceptual model of floodplain evolution on the Colville delta. This conceptual model is a useful tool for improving our understanding of surficial materials and our ability to use terrain units to predict soil properties across the delta. Lastly, we discuss the implications of these patterns and processes for oil development on the delta.

Accumulation of Deltaic Deposits

Our analysis of stratigraphy revealed that the deltaic deposits were formed by four processes: (1) fluvial deposition of mineral material, (2) eolian deposition of mineral material, (3) accumulation of organic material derived from partially decomposed plants, and (4) accumulation of ice. The relative importance of these processes in the development of delta-floodplain deposits changes during the various phases of floodplain evolution from riverbed/riverbar deposits to abandoned-floodplain deposits (Figure 3-25). Eolian sand deposits are included because they are prominent features on the western side of most distributary channels, even though they are not a normal step in the evolutionary sequence of fluvial deposits.

The relative contribution of each process to a par-

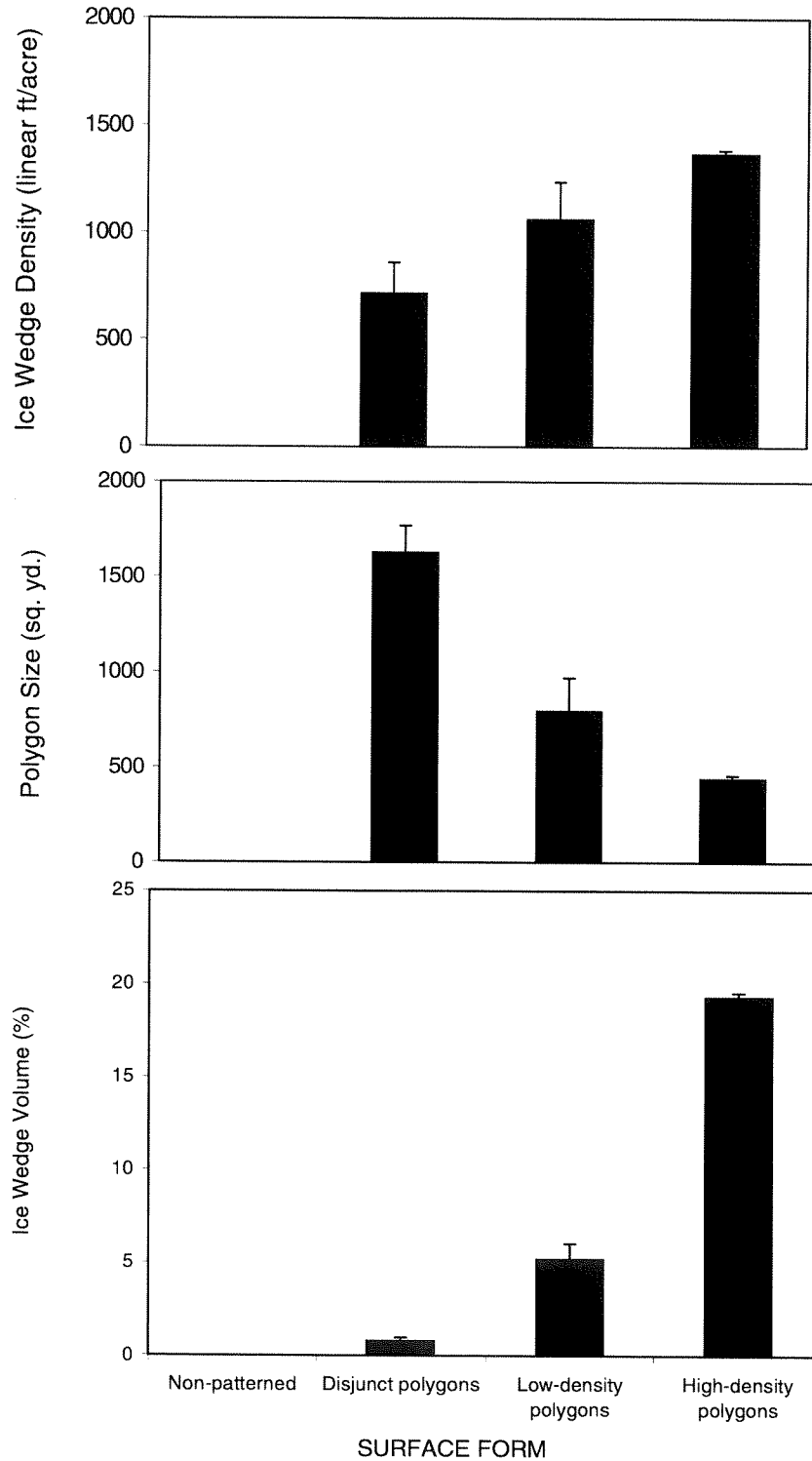


Figure 3-23. Mean (\pm SD) density of ice wedges (top graph), mean polygon size (middle graph), and estimated percent of the volume of the top 7ft, of permafrost occupied by ice wedges (bottom graph), Colville River Delta, Alaska, 1996.

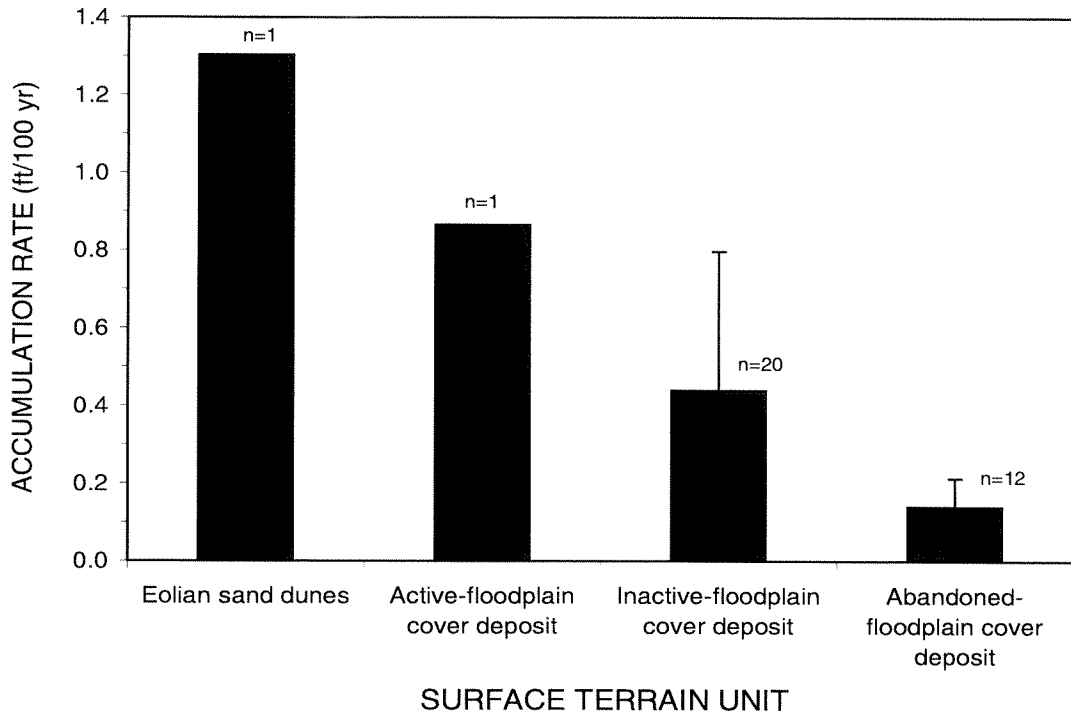


Figure 3-24. Mean (\pm SD) rates of accumulation of material (sediments, organics, and ice) for various surface terrain units on the Colville River Delta, 1996.

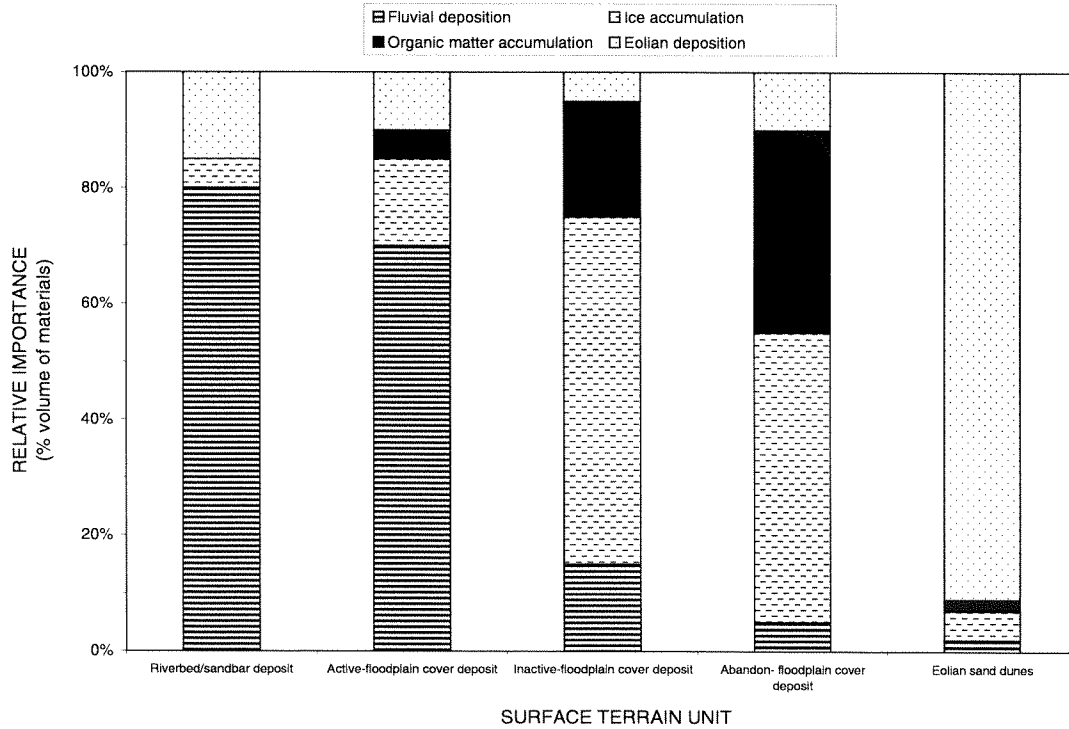


Figure 3-25. Relative importance of the processes of fluvial and eolian deposition, and organic matter and ice accumulation in common floodplain deposits on the Colville River Delta, 1996.

ticular phase of evolution is determined by its intensity relative to that of the other three processes. For example, we found higher percentages of sand in abandoned-floodplain cover deposits than in inactive-floodplain cover deposits. Although this difference could be attributed to higher eolian activity on abandoned floodplains, it is more likely due to lower rates of fluvial deposition and organic matter accumulation there (thus making eolian deposition relatively more important). The patterns resulting from interplay of the various processes are described below.

Permafrost Development and Thaw Stability on Deltaic Floodplains

In the Arctic, low air and soil temperatures and thin, high-density snow cover result in the formation of continuous permafrost on river deltas through a special type of permafrost formation called syngeneses (Shur 1988). The aggradation of ice during permafrost formation, and subsequent degradation of permafrost due to thermal instability, results in a wide range of deposits and surface forms that are characteristic of arctic deltas.

The formation of syngenetic permafrost in the delta is caused by the addition of new material at the soil surface, a decrease in active-layer thickness, and by the accumulation of ice below the active layer. Over the course of floodplain evolution, new material is added to the top of the active layer through deposition of fluvial sediment on the soil surface and accumulation of organic matter. The accumulation of organic material, increased saturation of the active layer, and changes in vegetation structure alter the thermal regime of the soils, causing the thickness of the active layer to decrease. This addition of new material and the decrease in active-layer thickness results in new mineral and organic material being incorporated in the top of the permafrost.

At the same time, ice is formed at the bottom of the active layer, because water freezes to the top of the cold permafrost during refreezing of the active layer in the fall. We hypothesize that this ice accumulates through three basic processes: freezing of pore water in the sediments to form pore ice and organic-matrix ice, horizontal freezing at the bottom of the active layer to form lenticular and layered ice, and vertical freezing in micro-contraction cracks (similar to ice-wedge development, but on a smaller scale) to provide the vertically oriented ice found in vein, reticulate, and

ataxitic ice. During some summers, not all of the ice produced the preceding fall thaws; over time, therefore, ice accumulates in the underlying sediments. This accumulation of sediments, organic matter, and ice causes the permafrost surface to rise over time.

Within this general framework of syngenetic permafrost formation, changes in the relative importance of formative processes (fluvial, eolian, organic) associated with the various phases of floodplain evolution are important to the structure and volume of the ice in the permafrost. Changes in the processes and the resulting patterns of material in the most common terrain units, are described below (Figure 3-26). Each of the deposits described represents a distinctive phase of floodplain evolution.

Delta Riverbed/Riverbar Deposits

Delta riverbed/riverbar deposits, which are situated in and along the margins of active channels, are frequently flooded (every 1-2 yr), resulting in scouring and fairly rapid rates of sediment accumulation. The sediments usually are composed of rippled sands or fines, which are typical of lateral accretion deposits, overlying massive or inclined (including cross-bedded) sands, which are typical of sandy bedforms. The inclusion of thin detrital peat layers, which become stranded on the surface by receding floodwaters, is a unique characteristic of these sediments. The coarse texture of the sediments and lack of vegetative cover, result in deep thaw layers (mean depth = 2.4 ft). Below the active layer, ice structures typically are dominated by nonvisible pore ice; ice contents are low (40-50%) because of the sandy texture of the sediments. In addition, the rapid rates of deposition move the active layer upward before much ice can be formed at the bottom of the active layer. Ice wedges are absent. Due to the frequent scouring and sediment deposition, the surface either is barren or has pioneering herbaceous vegetation.

Delta Active-floodplain Cover Deposits

Delta active-floodplain cover deposits occur on level, nonpatterned areas in narrow strips immediately adjacent to channels. Flooding is fairly frequent (every 3-4 yr), but the accumulation rate (0.87 ft/100 yr) of material (mostly sediment) is lower than that of riverbed/riverbar deposits. The sediments generally have layered (horizontally stratified silts and very fine sands) or massive fines overlying rippled fines with

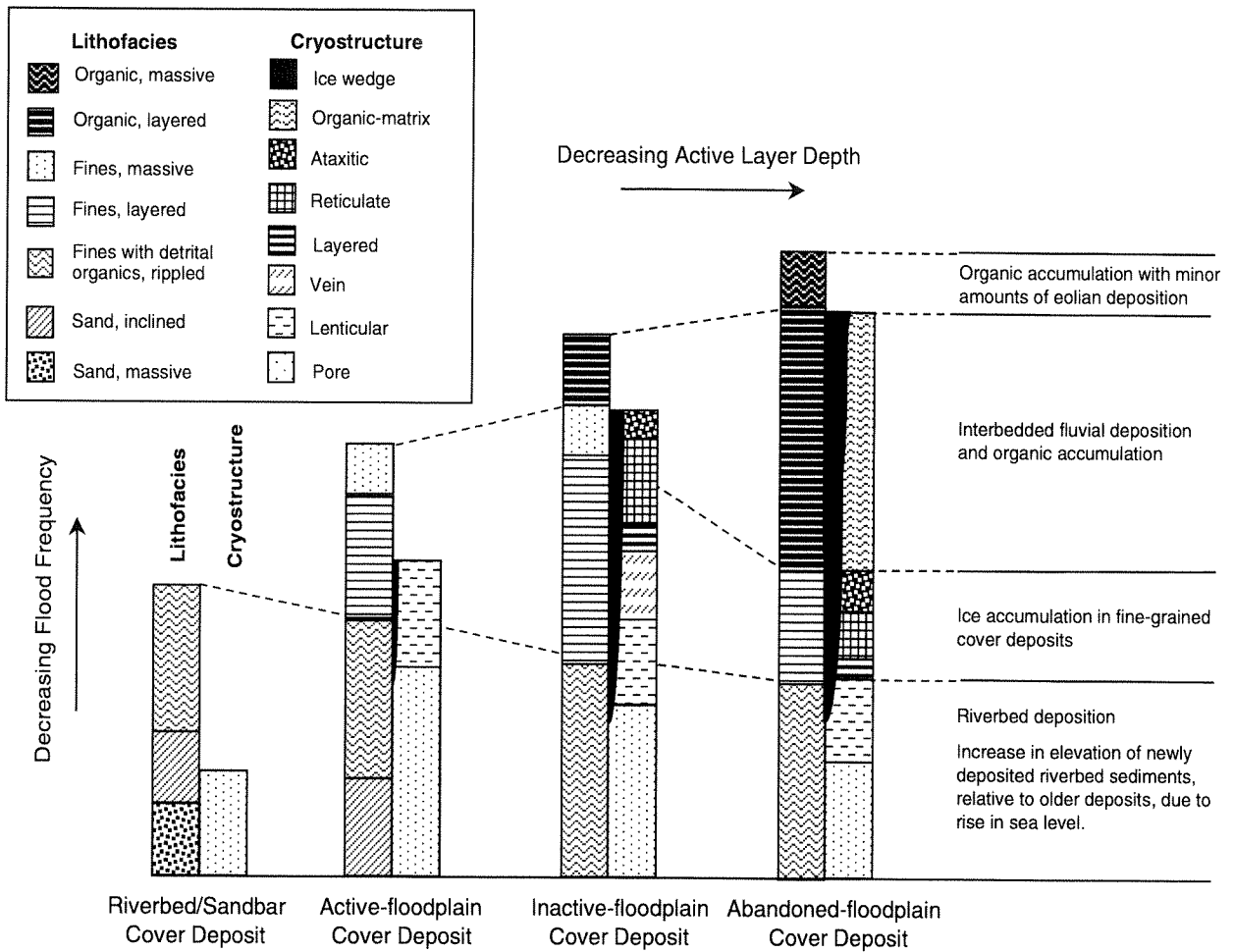


Figure 3–26. A conceptual model of changes in lithofacies, ice structures, and active-layer thicknesses during evolution of floodplain deposits on the Colville River Delta, Alaska, 1996.

interbedded silts, sands, and detrital peat layers associated with lateral accretion deposits. The active layer is relatively deep (2.1 ft) and well-drained. With increasing distance from channels, the active-cover deposits cross a transition zone where flood deposition is less frequent and thin (<0.5 in.) layers of moss occasionally form at the surface. The active layer frequently is saturated at depth (>12 in.) and the soils are mottled, indicating more reducing conditions. Below the active layer are layered fines and rippled fines with detrital organics that are dominated by lenticular ice structures, but which also include minor amounts of vein ice. Contraction cracks are evident on the ground surface, although polygon rims are not, indicating that ice wedges are in the initial stage of development. Well-drained soils near channels support vigorous growth of tall willows (*Salix alaxensis*), whereas seasonally saturated soils further from the river support growth of low willows (*Salix lanata*).

During the active-floodplain phase, approximately 2–4 ft of silty sediment can accumulate on top of the riverbed deposits, which in turn reduces the frequency of flooding. The accumulation of fine-grained sediments provides the primary material for ice aggradation during the next evolutionary phase (involving inactive-floodplain cover deposits). Eventually, the added sediments and migration of channels reduces the frequency of flooding to a point where peat starts to accumulate. Based on sedimentation rates and the lack of change in these deposits between 1955 and 1992 (Jorgenson et al. 1996), we estimate that this phase may persist for 100–300 yr. After this early phase of floodplain evolution, a large transition in permafrost development occurs on inactive-floodplain cover deposits.

Delta Inactive-floodplain Cover Deposits

Delta inactive-floodplain cover deposits occur immediately adjacent to the river along higher cutbanks and at greater distances from the river along point bars. Flood frequency (approximately every 5–25 yr) and sedimentation rates are substantially lower than on active-floodplain cover deposits, allowing build-up of organic material and creating distinctive interbedded layers of silt and peat. Layered organics (averaging 0.7 ft thick) generally are contained within the active layer but sometimes extend into the permafrost. The active layer remains saturated throughout the summer, resulting in anaerobic conditions and gleyed soils.

Thaw depths (mean = 1.4 ft) decrease substantially from the previous phase in response to changes in vegetation composition and changes in thermal properties of the soil. The sediments in the active layer, which were deposited during the previous phase, slowly join the permafrost. The upper layer of permafrost, which forms during this phase from the active layer of the previous phase, is extremely ice-rich (65–85% volume) and has distinctive ice structures, including layered, vein, reticulate, and ataxitic ice. The ataxitic and layered ice may represent periods when the active layer was static (with little sediment accumulation or change in active-layer thickness) and ice accumulated at the same place. This combination of distinctive ice structures in the upper horizon of permafrost, which is evident in both the Russian and North American Arctic, has been termed the “intermediate layer” (Shur 1988). When layered organics extend into the permafrost, organic-matrix ice (an amorphous type of ice generally visible within the loose, fibric organic matrix) is the dominant ice structure. The permanently saturated soils usually support wet sedge-willow meadows.

Accumulation of ice in inactive-floodplain cover deposits also includes other types of ice development, such as the formation of ice wedges and sheet ice. The formation of ice wedges begins near the end of the active-floodplain phase, and they eventually develop into large bodies of massive ice that form a continuous, low-density network of ice-wedge polygons in inactive-floodplain cover deposits. At this latter stage, ice wedges occupy approximately 5% of the volume of the top 7 ft of permafrost. In addition, massive formations of sheet ice (Shur and Jorgenson 1995), which probably formed in tapped-lake basins, occasionally are found near the bottom of inactive-floodplain cover deposits.

The decrease in thaw depth, change to saturated conditions, and reduced sedimentation occurring during this phase all contribute to the accumulation of ice at the top of the permafrost. The accumulation rate of materials (mostly ice, with some organics and sediments) is substantial (0.24 ft/100 yr). The total thickness of inactive-floodplain cover deposits ranges from 2.5 ft on new deposits to 9 ft on older deposits. As a result of ice accumulation, the thickness of the intermediate layer can become two or more times greater than the thickness of the active-floodplain cover deposit from which the intermediate layer formed (Shur 1988). Eventually, inactive-floodplain cover deposits

accumulate sufficient ice and organic material, along with minor amounts of fluvial and eolian material, that the ground surface rarely is flooded, at which point the deposit can be considered an abandoned-floodplain cover deposit. The time required to reach this transition is about 1500–2500 yr.

Delta Abandoned-floodplain Cover Deposits

Delta abandoned-floodplain cover deposits occur mostly in the central portion of the delta and represent the oldest portions of the delta landscape (with the exception of a few isolated old alluvial terraces). The deposits typically have deep (3–10 ft) accumulations of massive and layered organics that frequently have been deformed or turbated by formation of large ice-wedges. Eolian material occasionally is present also. Due to the accumulation of organic material and shallow thaw depths (mean = 1.2 ft), the active layer becomes almost entirely organic. Below the active layer, the massive organics usually have organic-matrix ice, while turbated, layered organics are dominated by organic-matrix ice and minor amounts of lenticular, layered, vein, reticulate, and ataxitic ice. The organic-rich sediments have extremely high ice contents (80–90%). Accumulation rates (0.08 ft/100 yr) of surface materials (mostly organics, ice, and trace amounts of eolian silt and sand) decrease sharply, however. The continued development of massive ice wedges creates a network of high-density, high-relief, low-centered polygons, in which the ice wedges occupy approximately 20% of the volume of the top 7 ft of permafrost. Because of the irregular topography resulting from polygon development, the surface typically supports a complex mosaic of wet sedge-willow and moist sedge-shrub meadows. At the latest stage of development, the centers of the polygons are raised sufficiently by organic matter and ice accumulation, to become high-centered polygons supporting moist sedge-shrub meadows.

We estimate that this phase occurs 2000–4000 yr after the active-floodplain cover phase. The abrupt differences in organic accumulation between inactive- and abandoned-floodplain cover deposits, however, indicate that the abandoned-floodplain cover deposits usually are remnant portions of old floodplains that have been undercut by meandering channels. The undercut portions are then filled in during lateral accretion from these cutbanks.

By the time the floodplain has evolved to the aban-

doned-floodplain stage, so much ice has accumulated in the sediments that the deposits become susceptible to thermal degradation and collapse, as indicated by the high areal extent of thaw lakes on inactive-floodplain and abandoned-floodplain cover deposits. Indeed, most of the abandoned-floodplain cover deposits apparently have been lost to melting because most remaining deposits exist as only narrow patches surrounding large thaw lakes in the central delta.

Delta Thaw Basin Deposits

Some thaw lakes eventually become tapped and drained by river channels. Due to breaching by channels and the resulting lower elevation of the exposed lake bottom, sediment deposition from flood water again becomes frequent. At this point the whole process begins again. The sediments usually are clay-rich and reticulate and ataxitic ice are common. There are very few locations in the delta, however, where tapped lakes have evolved all the way back to inactive-floodplain cover deposits. It appears that rates of channel migration usually prevents completion of a thaw lake cycle. Indeed, analysis of rates of landscape change indicates that most of the delta is reworked by erosion and deposition over a period of approximately 2000 years (Jorgenson et al. 1993).

External Factors

Complicating this analysis of evolutionary trends are the effects of sea level rise. Sea level has risen about 13 ft since 5000 yr ago, for an average rise of 0.26 ft/100 yr (Hopkins 1982). Recently, sea level has been rising worldwide at an average rate of 0.79 ft/100 yr (Peltier and Tushingham 1989). This increase in sea level is evident in soil profiles: the surface elevations of new riverbed deposits and of organic horizons in inactive floodplains are considerably higher than the elevations at which these deposits formed in older soil profiles. For example, at Cross Section S9.08 (X11), organic material dating to 2906 ybp was found at an elevation of 6.0 ft in an abandoned-floodplain cover deposit (core X11.09), whereas organic material now starts to accumulate at an elevation of approximately 11.5 ft. This difference indicates that sea level was approximately 5.5 ft lower 2900 years ago.

The rise in sea level probably is increasing the frequency of flooding on the higher floodplain steps, because the rate of sea level rise is faster than the rate of sediment accumulation on inactive-floodplain cover

deposits. For example, the current rate of increase in sea levels (0.79 ft/100 yr) is similar to the rate of material accumulation for active-floodplain cover deposits (0.87 ft/100 yr), but is substantially higher than the rates of accumulation for abandoned- and inactive-floodplain cover deposits (0.14–0.44 ft/yr).

Implications for Development

Every surficial deposit on the Colville delta is a potential foundation (base) for oil development facilities and transportation systems (roads and pipelines). Two terrain units—eolian sand and abandoned-floodplain cover deposits—are of particular interest because they occupy the highest elevations in the delta, and therefore are least subject to flooding. Eolian sand deposits have the best geotechnical properties, whereas abandoned-floodplain cover deposits have the most difficult properties to work with.

Eolian sand deposits generally are well-drained, have the lowest ice content in the area, and generally are not subject to flooding. Some ice wedges are present in sand dunes, but they are much smaller than the ice wedges in inactive- and abandoned-floodplain cover deposits. The uneven topography of the dunes poses the greatest disadvantage for facility siting. In addition, some dunes are still active, although most have been stabilized by vegetation cover.

Abandoned-floodplain cover deposits are extremely ice-rich as a result of well-developed segregated ice and wedge ice. The ice-rich intermediate layer, which is located under the active layer, is potentially subject to thaw settlement of 50% or more, and any increase in the depth of the active layer would initiate the settlement process. Thus, the thermal sensitivity of the active layer must be considered during the design of roads and pads. This sensitivity presents three potential problems.

First, the main principle of design on abandoned-floodplain cover deposits has to be protection of the existing permafrost table; the depth of the active layer under any structures (i.e., gravel fill) should not exceed the depth of the existing one. At present, this protection is commonly achieved on the North Slope by placement of foam insulation or sufficient gravel.

Second, when constructing facilities on abandoned-floodplain cover deposits, the vegetative cover and organic mat must be protected, because of the occurrence of well-developed ice wedges and the high density of low-centered polygons. The thermal regimes

of these features can easily be altered by damage to the insulating vegetation and surface organic layer. Disturbance of vegetation and organic soil by scraping or heavy dust deposition usually leads to complete (or at least deep) thawing of ice wedges. Once begun in one spot, thawing can propagate to adjacent ice wedges. Prevention of off-road traffic and minimization of on-road traffic during summer, as is common practice, will alleviate this problem.

Third, water may accumulate inside deep ice-wedge polygons as a result of impedance of surface runoff or impoundment of meltwater from snowdrifts adjacent to roads. The presence of standing water on the surface can alter the thermal regime (Jorgenson 1986), resulting in an increase in the active layer and partial thawing of the ice-rich permafrost over a long period (perhaps 25–100 yr).

The greatest advantage of the area for development is low permafrost temperatures. For the most part, the permafrost is very stable and mitigative measures can be used to minimize the potential problems associated with the high ice contents of inactive- and abandoned-floodplain cover deposits. On balance, we believe the benefits of siting facilities on abandoned-floodplain cover deposits to minimize problems with flood waters outweighs the potential risks of thaw settlement from developing on this ice-rich terrain.

PART IV. DRAINAGE NETWORK

BACKGROUND

Drainages in the Transportation Corridor were mapped to aid in oil spill contingency planning and spill response. During mapping, an emphasis was placed on identifying "micro-drainages" on slopes, such as "water-tracks" and nutrient-enhanced flow zones, that would help us identify flow directions in areas where topographic changes are minimal. In addition to the drainage network, thaw basins that provide topographic catchments were delineated to identify areas where spilled oil may be expected to pool.

METHODS

The delineation of the drainage network was done in conjunction with the ecological land classification effort that mapped terrain units, waterbodies, surface forms, and vegetation (Jorgenson et al. 1996). Waterbodies and thaw basins that were mapped during the ecological land classification were incorporated into the drainage network map. Waterbodies were classified by type (river, lake, ocean), salinity (fresh, brackish, marine), depth (<6 ft, 36 ft), presence of inflow/outflow streams (isolated, connected, tapped), and presence of islands; then, they were delineated on acetate overlays of 1:18,000-scale color-infrared and true-color aerial photography. Minimal polygon size for delineation of waterbodies was about 1 acre (0.5 ha). In addition, ice-poor and ice-rich thaw basins, which were terrain units delineated by the ecological land classification, also were transferred onto the drainage network map.

Drainages in the Transportation Corridor were classified with a system of stream ordering developed by Strahler (1952). In this system, (1) "fingertip" tributaries (first-order channels) combine to become a second-order channel below their confluence, (2) the confluence of two second-order channels creates a third-order channel, (3) two third-order channels join to create a fourth-order channel, and so on. A junction with a lower-order channel (e.g., a first-order with a second-order one) does not alter the designation of the higher-order stream.

Classification of first- and second-order channels on the poorly-integrated drainage network typical of

tundra on the Arctic Coastal Plain was problematic. We originally attempted to assign all beginnings of drainage lines on the USGS maps as second-order streams according to common practice for the Strahler system. The mapping on these USGS maps, however, was inconsistent, with some large channels missed and some indistinct channels included. Therefore, we instead classified the first- and second-order channels based on characteristics of the tundra and channel morphology. First-order channels were indistinct drainages identifiable by surface topography, surface forms (periglacial features), or vegetation that indicated ephemeral movement of water on the surface or within the seasonally active layer on top of the permafrost. We refer to these first-order channels as micro-drainages. In many instances these micro-drainages ended at the edges of thaw basins, because drainage patterns within the basins frequently were not clear.

During stream classification, many micro-drainages could join together before the channel became a second-order channel. This departure from normal stream-ordering procedures was made so that the numerous micro-drainages on the tundra could be delineated without regard to implications concerning the ordering of higher-order channels. In contrast to the micro-drainages, all second-order channels had a distinct channel or flow zone. Because second-order channels were distinct and could be identified consistently, second-order channels formed the basis for subsequent ordering of higher-order channels.

Many of the streams classified in 1995 flow north out of the Transportation Corridor, passing through a region whose habitats and drainages have not been classified. To facilitate oil spill contingency and response planning, in 1996 we delineated all such streams (second-order or greater) that originate within the Transportation Corridor downstream to their final drainage into the Colville River.

RESULTS AND DISCUSSION

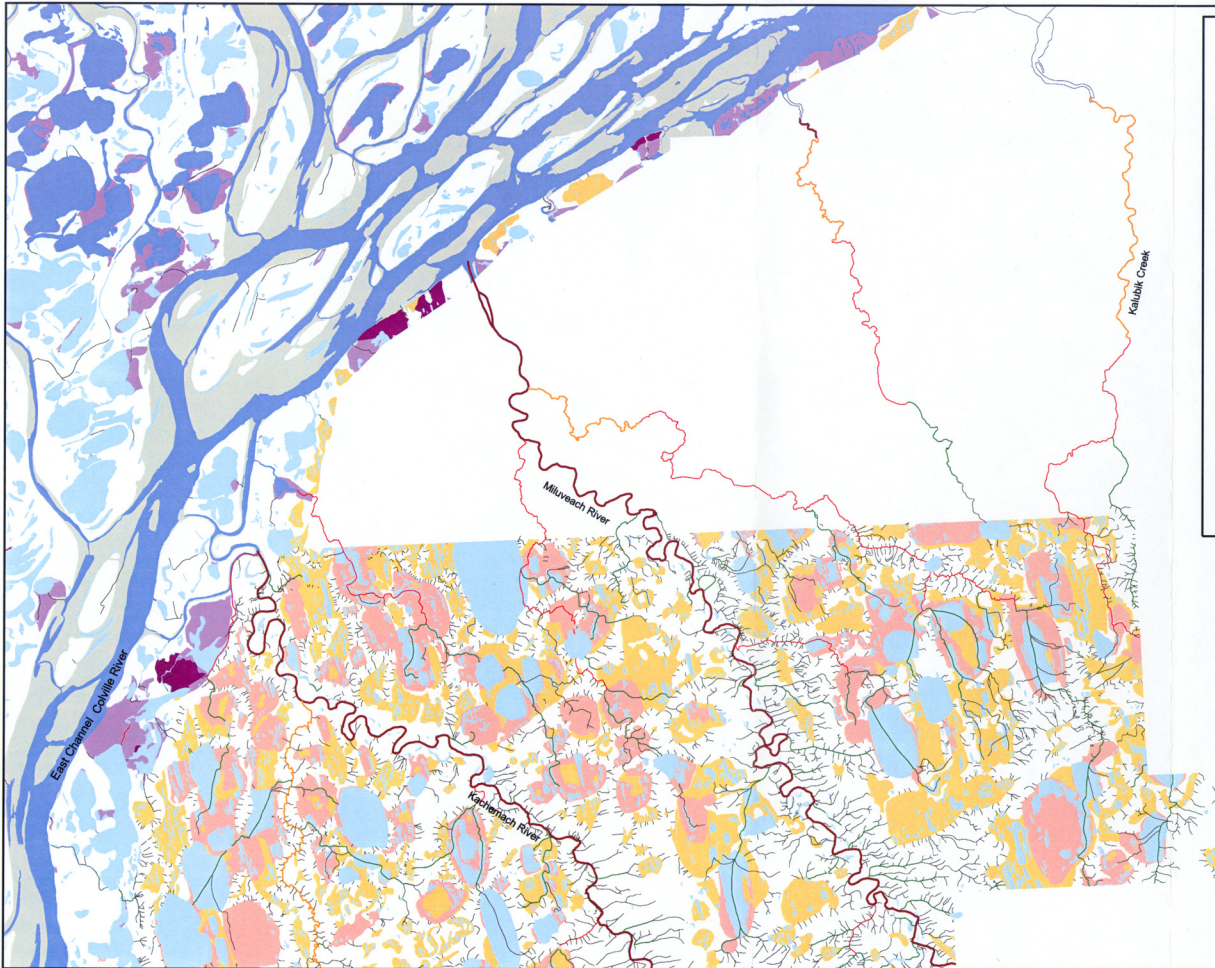
The map of the drainage network within the Transportation Corridor reveals a poorly integrated drainage system that is interrupted by numerous thaw basins (Table 4-1, Figure 4-1). Further, many of these thaw basins did not have a distinct outlet that could be mapped, and in some instances, the basins had multiple outlets. The two largest channels, the Miluveach and Kachemach rivers, were designated fifth-order

channels. Because it would have required mapping its entire watershed and because its stream order is not essential to this effort, the stream order for the Colville River was not determined. Descriptions of the various channel orders are presented in Table 4-1.

The map of the drainage network will help in contingency planning for oil spills by identifying where oil will flow at any point on the tundra and where the oil could be intercepted and contained. For small spills on the tundra, movement of oil would be expected to be minimal. For large spills, however, the thaw basins identified on this map would be useful for helping to contain and control large volumes of oil, thus preventing it from reaching larger streams, and alternately,

Table 4-1. Descriptions of stream orders for the drainage network in the Transportation Corridor adjacent to the Colville River Delta, 1996.

Stream Order	Description
First (micro-drainages)	Drainages are referred to as "micro-drainages" to indicate their indistinct and ephemeral nature. The micro-drainages denote areas on slopes and swales where water might flow across the tundra's surface during snowmelt or through the active layer during mid-summer. The distinguishing features were identified by topographic breaks across the slopes, as interconnected networks of ice-wedge polygons, or by enhanced growth of vegetation that indicates areas of subsurface water movement (e.g. "water-tracks").
Second	Seasonally active drainages that have a distinct, albeit small, channel incised in the tundra. These drainages primarily carry water during breakup and usually do not have flowing water during mid-summer. Second-order channels were classified more by their distinct channels with intermittent flow than by noting the confluences of first-order channels.
Third	Drainages that had a distinct, incised channel and that usually have water present in the channel during mid-summer. These streams probably have intermittent flow during the summer and have periods when the water may be still.
Fourth	Only one fourth-order stream was noted within the proposed Transportation Corridor. It is a small, beaded stream that probably has continuous low flow during the summer.
Fifth	Broad, gravelly riverbeds indicative of high flow during spring breakup and low flow during mid-summer. The meandering channels are bordered by high floodplain steps that receive occasional overbank flow, the floodplains are constrained by the adjacent alluvial/marine terraces, and the channels frequently alternate between pools and riffles. The Miluveach and Kachemach rivers were classified as fifth-order channels.



Basins and Waterbodies

- Thaw Basin, Ice-poor
- Thaw Basin, Ice-rich
- Delta Thaw Basin, Ice-poor
- Delta Thaw Basin, Ice-rich
- Delta, Riverbed/Riverbar
- Fresh Waterbody
- Coastal Waterbody

Stream Order

- First
- Second
- Third
- Fourth
- Fifth

Photo-interpretation of Drainage Network based on 1992 CIR Photography. Map registered to SPOT image base map. Projection UTM Zone5, Datum NAD 27. Map accuracy meets national map spatial accuracy standards.

N

1 0 1 2 3 4 Kilometers
1 0 1 2 3 Miles

ARCO Alaska, Inc.	
Colville Geomorphology and Hydrology	
Figure 4-1. Drainage Network for the Transportation Corridor, 1996.	
ABR, Inc. Environmental Research and Services	
27 Oct 1997	File:96reportthematis.apr, Drainages

PART V. DIGITAL ELEVATION MODEL USING SATELLITE RADAR DATA

BACKGROUND

Development of oil facilities within a complex fluvial environment such as the Colville River Delta requires high-resolution (2 ft) topographic information for engineering design, hydrologic modeling, and other environmentally related studies. For the delta as a whole, topographic information currently is limited to the resolution of the 1:63,360 scale U.S.G.S maps that have 25 ft contour intervals. The surface elevation for most of the delta, however, is less than 25 ft. The lack of topographic data has been partially addressed through surveying of the proposed pipeline alignments, surveying of cross-sections across channels and the adjacent floodplain, and by photogrammetric mapping of the facilities area. For most of the delta, however, detailed topographic data is lacking and acquisition of high-resolution topographic data for the entire area would be expensive.

To address this data gap, we evaluated the use of synthetic aperture radar (SAR) data acquired from satellites as a potentially much less costly approach to acquiring topographic data for the delta. In essence, this technique requires two SAR images of the same area from slightly different positions to form a stereo view of the ground (Li and Goldstein 1990). Recent developments of interferometric techniques have shown substantial promise using this remote sensing approach (Zebker et al. 1994).

The feasibility of this approach was enhanced by the acquisition of data by a tandem satellite mission over Alaska conducted by the European Space Agency using their Remote Sensing Satellites (ERS-1 and ERS-2). The tandem mission provided stereo coverage over most of Alaska and presented the opportunity to develop topographic information from the data. While stereo radargrammetry also can be performed using data from other sensors/platforms, airborne SAR and RADARSAT for example, we chose to use data obtained from the ERS satellites because it already has been acquired and there is better positional information regarding the orbits for these satellites.

Because this technology has not been evaluated over a range of terrain conditions, we performed a preliminary evaluation of the image processing approach to evaluate its potential accuracy and to identify potential problems with its use on arctic terrain, which is relatively flat but has high variability in terms of vegetation, soil moisture, waterbodies, soil types, and ice contents. We conducted an evaluation of only the preliminary interferogram to assess whether the vertical resolution is sufficient to warrant further image processing. There are several additional image-processing steps beyond the initial interferogram that would need to be done to create an actual digital elevation model. These additional steps are described below.

METHODS

We assessed the potential accuracy of the technique in a two step process. First, we identified suitable stereo pairs for analysis and used them to produce a preliminary interferogram that is proportional to elevation. Second, we assessed the potential accuracy by comparing interferogram values with ground survey data. We refer to this as potential accuracy because additional processing would need to be done to generate real elevation data, and this process can both correct and introduce error. These are described in more detail below.

PRELIMINARY IMAGE PROCESSING

This experiment used SAR data acquired by the ERS-1 and ERS-2 satellites. Because the two satellites are identical, stereo pairs can be formed either by repeat orbits of a single satellite or through a tandem operation using two satellites. According to principles inherent in the use of interferometric synthetic aperture radar (INSAR), a digital elevation model (DEM) can be created using ERS data only when the distance between the repeat or tandem orbits is within about 600 m. In addition, there are other constraints. The main repeat cycle of a single ERS satellite is 35 days, which is too long a temporal difference given the sensitivity of INSAR to temporal changes in ground conditions. Although ERS-1 had a short 3-day repeat cycle during fall 1991, spring 1992, and spring 1994 that reduced potential problems with temporal effects, there was no data coverage of the study area because of gaps between adjacent orbit paths. Due to these constraints

in using repeats orbits of one satellite, we used data from the ERS-1 and ERS-2 tandem operation, which was conducted from May 1995 until June 1996 and provided stereo images one day apart.

A search through the existing database of single-look SAR images, revealed a tandem pair of images acquired on 11 and 12 October 1995. The baseline (distance between tandem orbits) of the stereo pair was 116 m, which we considered adequate for DEM generation. Standard INSAR techniques (Li and Goldstein 1990) then were performed to generate an interferogram (Figure 5-1). The main steps include co-registration of the two single-look complex SAR images to sub-pixel accuracy, removal of fringes from a flat-earth model, and some preliminary fine-tuning. The result is an image that provides a representation (unitless values) of the topography of the area.

ASSESSMENT OF POTENTIAL ACCURACY

We evaluated the preliminary interferogram to assess what level of accuracy potentially could be obtained from the image. To assess the potential vertical resolution of the interferogram, we rectified the image to our base map for the delta. We then overlaid five of our cross-sections (E27.09, E20.56, N7.46, S9.80, E14.20) that had detailed survey information and extracted the interferogram values along the transects. Both the extracted index values (0–255) and the elevation data were plotted along the transects to identify areas of agreement and disagreement. This approach allowed us to evaluate the variation in the SAR data within a small geographic area and allowed us to ignore changes in calibration across the scene. The SAR data was subjectively scaled to provide a “best fit” to the elevation data.

RESULTS AND DISCUSSION

A visual inspection of the preliminary interferogram indicates that the SAR-derived data was able to resolve the more prominent features within the facilities area (Figure 5-2). Channels, lakes, and sand dunes are evident and generally conform to our interpretation of features evident on SPOT satellite images and aerial photographs. There was substantial noise, or erroneous data, produced from waterbodies, however. We attributed this to slight changes in ice accumulation during the one-day interval between acquisition of images during October.

When compared to elevations surveyed along five cross-sections, the plots indicate that the interferogram values could be calibrated to achieve accuracies within 3–6 ft (1–2 m) for most portions of the cross sections (Figure 5–3 and 5–4). The problem with waterbodies was particularly evident on the cross-sections. In addition, there were other anomalies that did not appear to be related to any particular terrain feature.

Based on this evaluation of the preliminary results, we concluded that while the approach potentially can achieve relatively high vertical resolution (3–6 ft, 1–2 m) at high horizontal resolution (41 ft, 12.5 m) over a large area, it is insufficient for engineering purposes on the delta which need a resolution of 2 ft or better. Therefore, we did not proceed with the additional steps required to produce an actual digital elevational model.

Some of the additional steps that would be required to produce an actual DEM include:

- 1) Rectifying and calibrating the image to fit the curvature of the earth and to compensate for distance from the sensor. Currently, areas farther away from the sensor appear higher than areas closer to the sensor. This could be corrected using existing algorithms.
- 2) An “unwrapping” procedure needs to be performed to remove breaks in sequences of index values (Goldstein et al. 1988) because the index values in the preliminary interferogram can go through multiple ranges of 0 to 255. For example, along a hill the index values will reach 255 and then start again at 0 as the image continues up a hill.
- 3) Interferogram values need to be calibrated to actual elevations by developing linear regression equations using ground survey data.
- 4) The large erroneous values associated with waterbodies need to be screened out. This can be done by overlaying a mask of areas of large amounts of change identified by contrasting the two stereo images. We have already produced such as mask, but its still needs to be used to screen the erroneous values.

Overall, a considerable amount of processing still needs to be done on the preliminary image. While these corrections likely would remove most of the

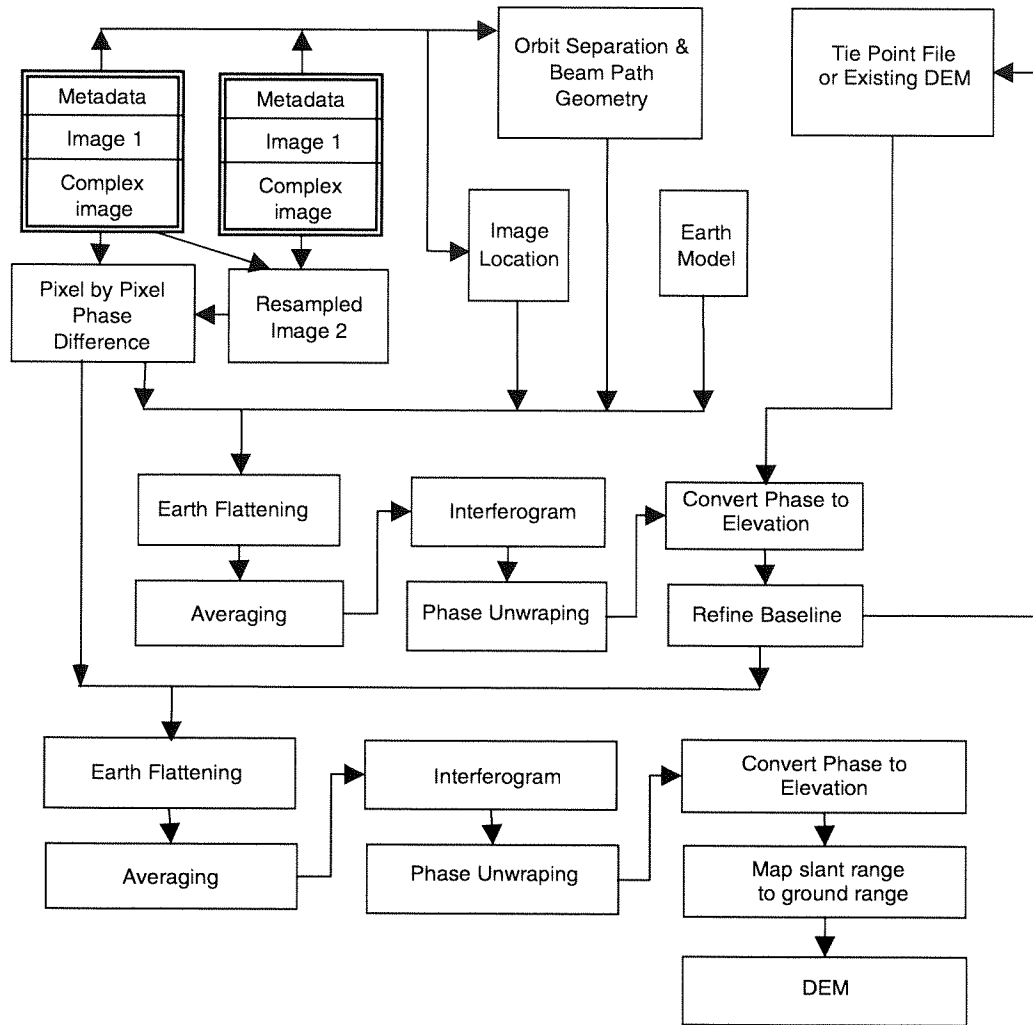
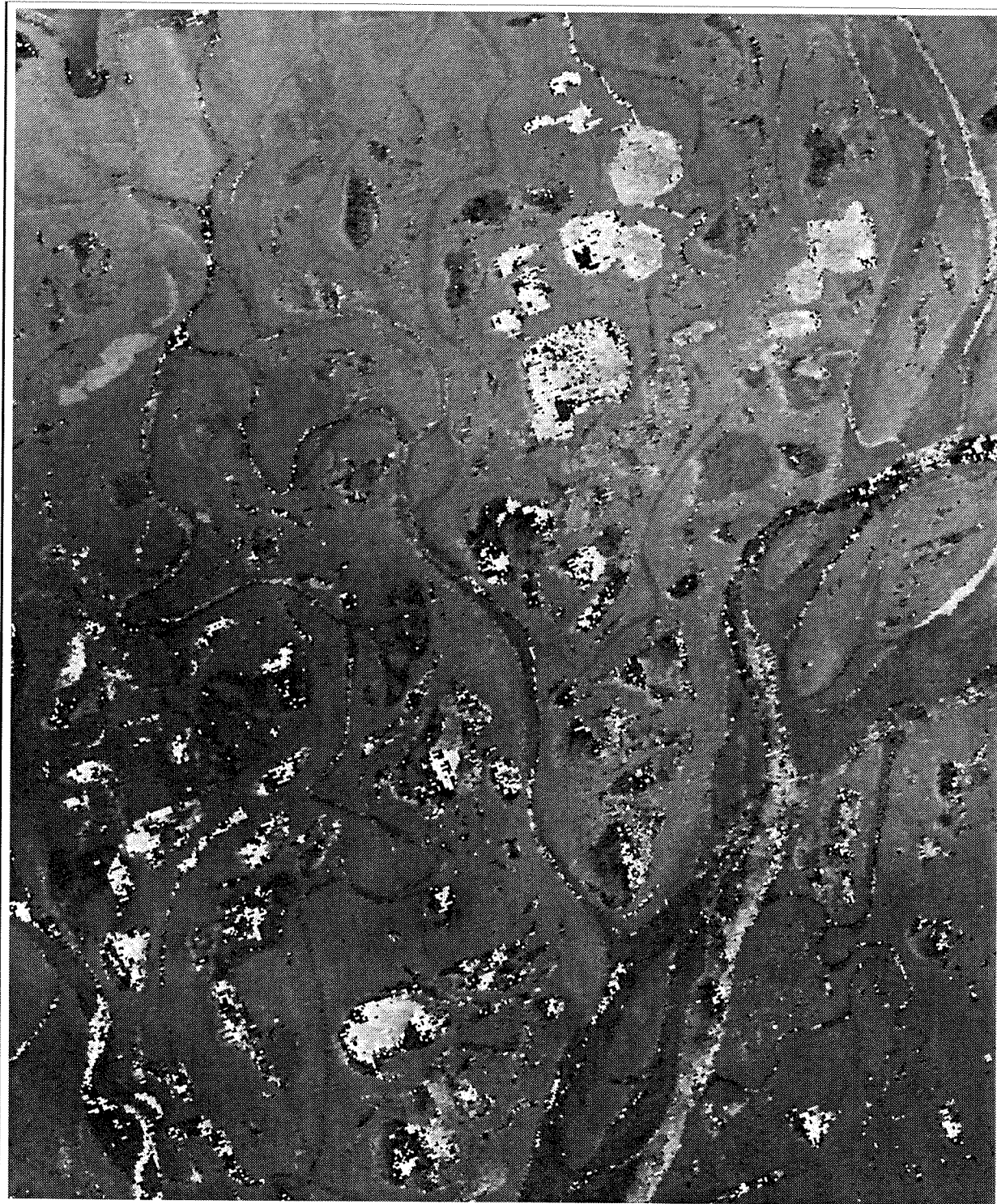
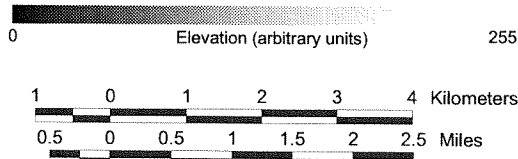


Figure 5-1. Image processing steps utilized for generation of digital elevation model (DEM) from synthetic aperture radar images.



Map Projection: UTM-5, NAD27
 ERS-1 and ERS-2 INSAR Image
 Image Date: October 11 & 12, 1995

Registration based on 1995
 SPOT base map, USGS control
 points and ground DGPS surveys.



ARCO Alaska, Inc.	
COLVILLE GEOMORPHOLOGY AND HYDROLOGY	
Figure 5-2. Interferogram from ERS-SAR images of the Alpine development area.	
ABR, Inc.	
Date: 03/25/97	File: Interferogram.apr

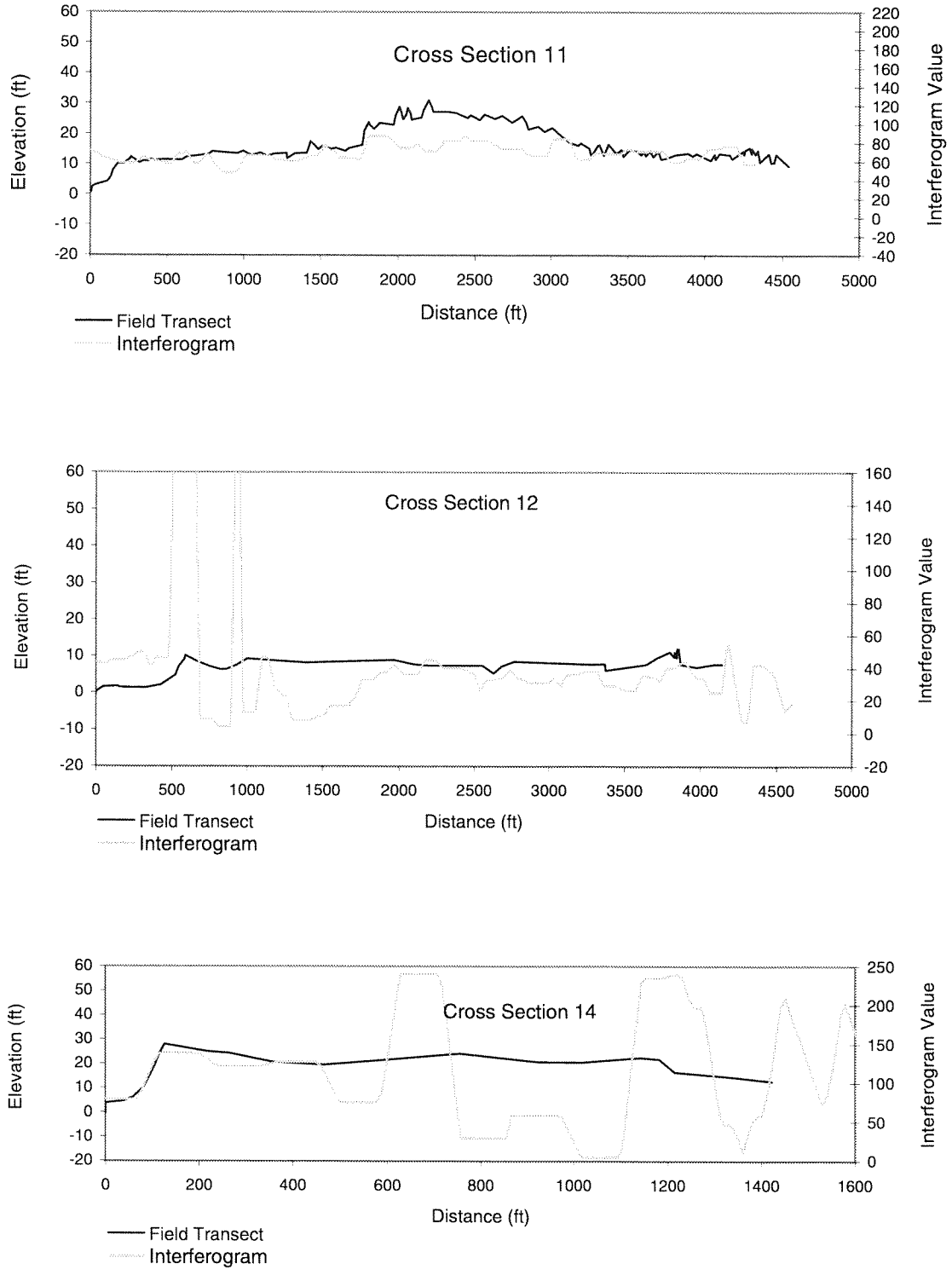


Figure 5-3. Comparison of ground elevations with interferogram index values generated from synthetic aperture radar imagery along Cross-sections 11, 12, and 14, Colville River Delta, Alaska, 1996.

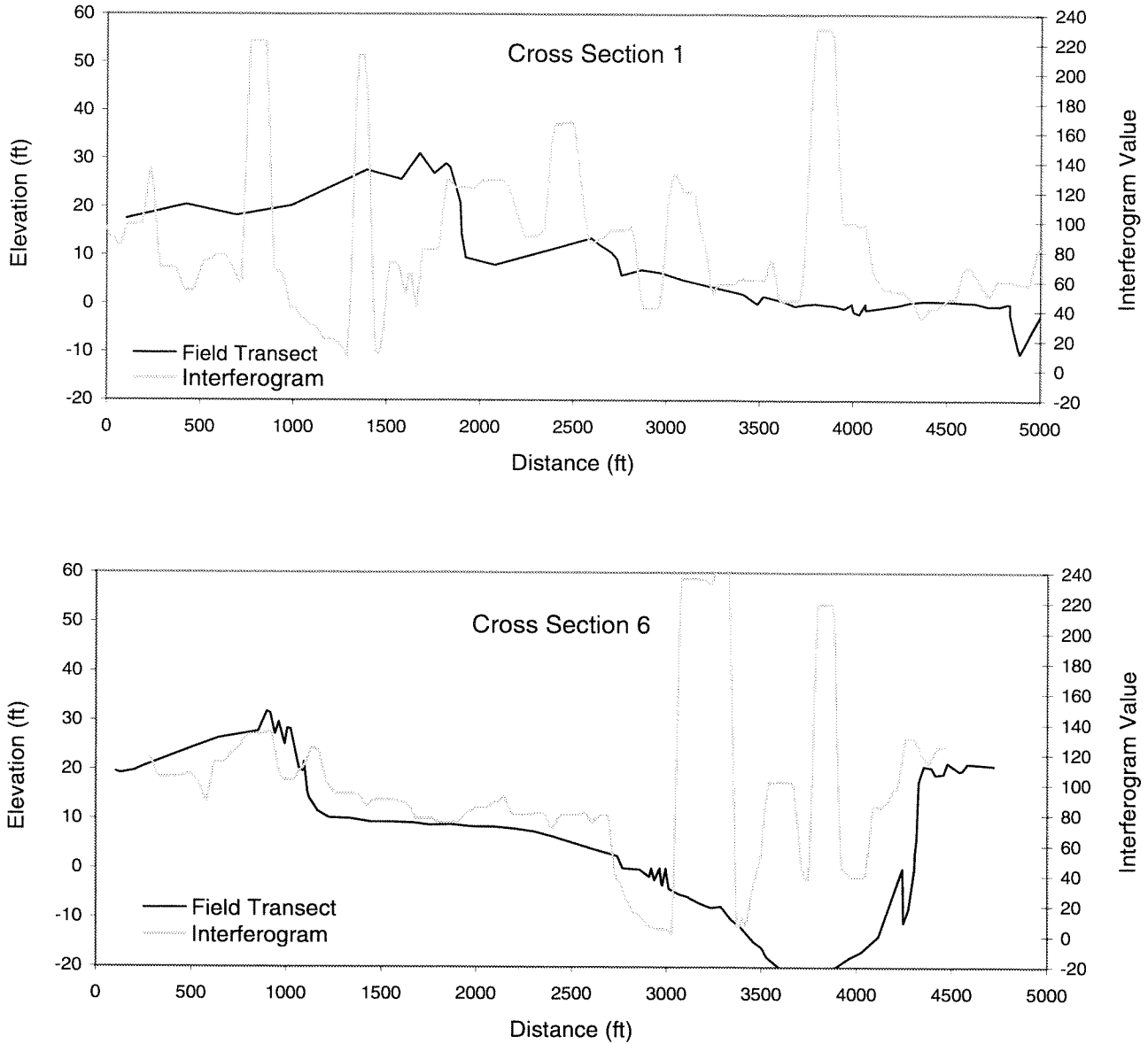


Figure 5-4. Comparison of ground elevations with interferogram index values generated from synthetic aperture imagery along two Cross-sections 1 and 6, Colville River Delta, 1996.

problems currently inherent in the data, there still would likely be small portions of the DEM that would have less accuracy than the potential accuracy of 3–6 ft (1–2m). Given that the potential accuracy still would be insufficient for the needs of the project, we decided to not continue further development of the DEM.

While the preliminary evaluation indicates that the data do not achieve the vertical resolution desired, there still is potential for achieving higher accuracy. First, there may exist a better set of tandem pairs in the ERS SAR database. During the initial search through the database, we identified several additional tandem pairs that are available for the study area. These data, however, probably are still in raw signal format and awaiting processing into single-look complex image format. This processing is needed before use with INSAR techniques. The images that we acquired were some of the first images released after calibration. Second, some of those pairs have baselines >200 m, which is twice that of the baseline of the pair that we used; thus, their use probably would improve the vertical precision and accuracy of the resulting DEM's by a factor of two. Third, a comparison of pairs taken in different seasons may lead to minimization of the temporal changes between tandem acquisitions. This refinement would result in a reduction of the noise level seen on the interferograms generated from data acquired during freeze-up conditions in October. Finally, the processing procedures and software could be improved. We estimate that these refinements would improve the current vertical accuracy by a factor of two.

SUMMARY AND CONCLUSIONS

The complex geomorphic and hydrologic processes on the Colville River Delta provide a challenging environment in which to develop oil resources. To help provide information essential for engineering design and evaluation of potential environmental impacts, this report presents the results from the fifth year of field studies and summarizes information from previous year's efforts.

FLOOD DISTRIBUTION

The distribution of flooding during spring breakup was mapped within five small study areas from 1992–1996. In 1996, when peak discharge (160,000 cfs) was the smallest that we observed over a 5-yr period, the amount of flooding ranged from 28% in the Alpine study area to 40% in the Tamayyak area in the central delta. When comparing differences among years, flooding in the Alpine study area ranged from 28% in 1996 to 69% in 1993, the year with the highest peak discharge (379,000 cfs). We attributed the frequent flooding observed near the proposed facilities to the occurrence of several low-lying thaw basins and the tapping of Nanuk Lake. When comparing differences among terrain units, delta riverbed/riverbar deposits were nearly entirely flooded (82–95%) every year, active-floodplain cover deposits were up to 47% flooded at the highest flood stage that we observed, and inactive- and abandoned-floodplain cover deposits had relatively low flooding, up to 16% and 17%, respectively.

We evaluated the use of synthetic aperture radar imagery from the RADARSAT satellite for monitoring flood distribution, because it can be acquired during all weather conditions and avoids the safety risks associated with acquiring aerial photography during marginal weather. When flooding mapped with RADARSAT imagery was compared with flooding mapped with color oblique aerial photography, the two methods had high agreement (94%). Based on these results, we recommend future monitoring be done using RADARSAT imagery.

PALEOFLOOD HYDROLOGY

Paleoflood indicators were used to assess the magnitude, distribution, and frequency of past flood events to help resolve some of the uncertainty associated with

which flood stage and discharge criteria should be used for the design of facilities for the Alpine Development. In particular, the study focused on paleoflood indicators (slackwater deposits and driftlines) from a large flood in 1989.

Field surveys in 1996 of soil stratigraphy at six distances along 19 transects; (92 sites total) revealed that sediments from the 1989 and other flood events formed distinctive deposits of fine-grained material interbedded with organic material. An analysis of factors affecting sediment distribution (distance from bank, terrain unit, and flood region) revealed that samples taken from >328 ft, within inactive-floodplain cover deposits, and within Flood Region 1 (along the East Channel), provided the best conditions for estimating the return period for the 1989 flood. On inactive-floodplains, the mean rank of the size of the deposits attributed to the 1989 flood (in comparison to other flood deposits) was 2.7 over a mean time period of 308 years, for a mean return period of 128 years (\pm 32 yr, 95% confidence interval).

Driftlines associated with the 1989 event were surveyed at 27 locations; 15 of which were judged to be good indicators of the peak stage. Near the proposed Alpine facilities, the mean elevation of four nearby good driftlines was 10.6 ft (maximum of 11.2 ft). Slackwater deposits were not found within the top 1 ft of organic material at locations above these driftlines, whereas, deposits related to the 1989 flood were found at sites 1–2 ft below these driftlines. Based on the water-surface elevations from a two-dimensional hydrologic model that provided the best fit with the driftline elevations, the peak discharge associated with the 1989 flood was estimated to be approximately 775,000 cfs.

SOIL STRATIGRAPHY AND PERMAFROST DEVELOPMENT

Studies on soil stratigraphy and permafrost development in the delta conducted in 1992, 1995, and 1996 investigated the nature and distribution of surficial deposits in the delta to provide information for facility siting, engineering design, and analysis of potential impacts from development. Initial classification and mapping of terrain units was completed in 1992. In 1995 and 1996, we further investigated the stratigraphy of near-surface materials near the proposed facilities and along numerous toposequences in the delta. After detailed classification and analysis of the

microscale and macroscale differences in soil properties across this complex landscape, we synthesized the patterns and processes we observed into a simplified conceptual model of floodplain evolution. We then used this conceptual model as the basis for assessing the environmental and engineering constraints for development in the delta.

The texture and structure of sediments (mineral sediments, organic matter, and ice) were classified into 23 lithofacies (repeating assemblages of texture and structure), 8 primary ice structures (based on continuity and shape), and 21 terrain units (three-dimensional structural elements related to depositional processes). Large differences in particle-size distribution, organic-matter accumulation, salinity, active-layer depths, ice volume, and material accumulation rates were found among these microscale and macroscale classes.

These differences in sediment characteristics were related to formative processes (fluvial, eolian, marine, and organic) and organized into a conceptual model of the evolution of terrain units across the deltaic landscape. Delta riverbed/riverbar deposits have massive or crossbedded-sandy sediments that accumulate rapidly due to frequent flooding (every 1–2 yr), have no organic matter buildup, and have low ice contents (40–50%). Active-floodplain cover deposits have layered or massive fines on top of sandier riverbed materials, still have rapid material (mostly sediment) accumulation rates (0.87 ft/100yr) due to slightly less-frequent flooding (every 3–4 yr), lack organic matter buildup, and have intermediate ice volumes (60–70%) associated with the development of lenticular and pore ice. Inactive-floodplain cover deposits have interbedded mineral and organic layers indicative of infrequent flooding (every 5–25 yrs), much lower material (mostly ice and organics) accumulation rates (0.24 ft/100yr), and have high ice contents (70–80%) associated with development of vein, reticulate, ataxitic, and wedge ice. Abandoned-floodplain cover deposits have massive or layered organic accumulations at the surface due to very infrequent flooding (every 25–150 yrs), very low material (mostly organics and ice) accumulation rates (0.08 ft/100yr), and have very high ice contents (80–90%) associated with organic-matrix ice and wedge ice. By this stage of floodplain evolution, sediments in the abandoned-floodplain cover deposits have accumulated so much ice they become unstable and prone to thaw-lake development. Tapping of thaw lakes by meandering channels can drain the lakes and

the lower surface is subject again to the processes described above. In addition to these deposits, eolian sand deposits frequently form downwind (southwest) of active channels.

Eolian sand deposits and abandoned-floodplain cover deposits are of particular interest for development because they occupy the highest elevations in the delta and, therefore, are least subject to flooding. The eolian sand deposits have the best geotechnical properties because they have low ice contents (40–50%). In contrast, abandoned-floodplain cover deposits present difficulties because they are extremely ice rich and their surfaces are sensitive to disturbance, both from direct effects related to the physical disruption of the organic mat at the surface, and from indirect effects associated with impoundment of water in the high-relief, high-density, low-centered polygons associated with this terrain type.

DRAINAGE NETWORK

Drainages within the Transportation Corridor were mapped in 1995 to aid in oil spill contingency planning and spill response. The map was updated in 1996 to include drainages downstream from, but originating in, the Transportation Corridor that also may be affected by oil spills.

DIGITAL ELEVATION MODEL

We conducted a preliminary evaluation of the use of synthetic aperture radar (SAR) imagery acquired by satellites (ERS-1 and ERS-2) for creating a digital elevation model of the delta. An interferometric technique, using two SAR images of the same area from slightly different positions taken on 11 and 12 October 1995, was used to create an interference pattern proportional to surface elevations. We assessed the accuracy of the preliminary interferogram at five cross sections surveyed in 1992 and 1995 and estimated the potential accuracy of the technique to be 3–6 ft. Numerous processing steps still need to be performed, however, to create an actual digital elevation model. Because our preliminary evaluation indicated that the interferometric technique using these images would not provide the level of resolution desired (2 ft), we halted final processing until further notice. It is possible that higher resolution still could be obtained, either from other images with wider separation and/or from images taken on dates that do not have the problems associated with freeze-up.

LITERATURE CITED

- Aldrich, J. W., and C. Malcovish. 1983. A review of scour multiplication factors for gravel-bed rivers. Unpublished report prepared for Alberta Environmental Research Trust, Calgary, AB, Canada, by Hydrocon Engineering Ltd., Calgary, AB, Canada. 33 p.
- Arnborg, L., H. J. Walker, and J. Peippo. 1967. Suspended load in the Colville River, Alaska, 1962. *Geografiska Annaler* 49A: 131-144.
- Arnborg, L., H. J. Walker, and J. Peippo. 1966. Water discharge in the Colville River, 1962. *Geografiska Annaler* 48A: 195-210.
- Baker, V. R. 1987. Paleoflood hydrology and extraordinary flood events. *Journal of Hydrology* 96: 77-99.
- Baker, V. R., R. C. Kockel, and P. C. Patton. 1988. *Flood Geomorphology*. John Wiley & Sons, New York.
- Blench, T. 1969. *Mobile-bed fluviology*. University of Alberta Press, Edmonton, AB, Canada. 300 p.
- Black, R. F. 1964. Gubik Formation of Quaternary age in northern Alaska. U. S. Geological Survey, Prof. Pap. 302-C. 91 p.
- Brierley, G. J. 1991. Floodplain sedimentology of the Squamish River, British Columbia: relevance of element analysis. *Sedimentology* 38: 735-750.
- Cannon, P. J., and S. E. Rawlinson. 1979. The environmental geology and geomorphology of the barrier island-lagoon system along the Beaufort Sea Coastal Plain from Prudhoe Bay to the Colville River. Pages 209-248 in National Oceanic and Atmospheric Administration, Environmental assessment of the Alaskan Continental Shelf, Annual reports of principal investigators, April 1978 to March 1979. National Oceanic and Atmospheric Administration, v. 10.
- Cannon, P. J., and S. E. Rawlinson. 1981. Environmental geology and geomorphology of the barrier island-lagoon system along the Beaufort Sea Coastal Plain from Prudhoe Bay to the Colville River. Pages 357-444 in National Oceanic and Atmospheric Administration Environmental assessment of the Alaskan Continental Shelf. National Oceanic and Atmospheric Administration, Final Report 34 (1985).
- Cannon, P. J., and T. W. Mortensen. 1982. Flood hazard potential of five selected arctic rivers Arctic Coastal Plain. Report prepared for North Slope Borough Coastal Management Program, Barrow, AK, by Mineral Industries Research Lab, Univ. of Alaska, Fairbanks, 56 p.
- Carter, L. D. 1981. A Pleistocene sand sea on the Alaskan Arctic Coastal Plain. *Science* 211: 381-383.
- Carter, D. L., and J. P. Galloway. 1982. Terraces of the Colville River Delta region, Alaska. Pages 49-52 in W. L. Coonrad, ed., *The United States Geological Survey in Alaska: Accomplishments during 1980*. U.S. Geological Survey, USGS Circular 884.
- Carter, D. L., and J. P. Galloway. 1985. Engineering-geologic maps of northern Alaska, Harrison Bay Quadrangle. U. S. Geological Survey, Open File Rep. 85-256. 47 p.
- Carter, L. D., J. K. Brigham-Grette, and D. M. Hopkins. 1986. Late Cenozoic marine transgressions of the Alaskan Arctic Coastal Plain. Pages 21-26 in J. A. Heginbottom, and J. S. Vincent, eds. *Correlation of Quaternary deposits and events around the margin of the Beaufort Sea: Contributions from a joint Canadian-American workshop, April 1984*. Geological Survey of Canada, Open File Report 1237.
- Carter, L. D., C. A. Repenning, L. N. Marinovich, J. E. Hazel, D. M. Hopkins, K. McDougall, and C. W. Naeser. 1977. Gubik and pre-Gubik Cenozoic deposits along the Colville River near Ocean Point, North Slope, Alaska. Pages B12-B14 in K. M. Blean, ed. *The United States Geological Survey in Alaska: Accomplishments during 1976*. U. S. Geological Survey, Circular 751-B.

- CH2M HILL, Inc. 1994. Paleoflood hydrology: an assessment of the methodology based on 1993 flood data for the Salt and Verde Rivers, Arizona. Unpubl. rep. prepared for the Salt River Project, Phoenix, AZ, by CH2M HILL, Inc., Tempe, AZ. 35 p.
- Chang, H. H. 1988. Fluvial processes in river engineering. John Wiley & Sons, NY. 432 p.
- Craig, J. D., and G. P. Thrasher. 1982. Environmental geology of Harrison Bay, northern Alaska. U. S. Geological Survey, Open-File Rep. 82-35. 25 p.
- Davidian, J. 1984. Computation of water-surface profiles in open channels. U. S. Geological Survey, Washington, D. C. Techniques of Water Resources Investigations, Book 3, Chapter A15. 48 p.
- Divoky, G. 1983. The pelagic and nearshore birds of the Alaska Beaufort Sea. U. S. Dept. of Comm., Juneau, AK. NOAA-OCEASP Final Rep. 114 p.
- EarthInfo. 1993. USGS Peak Values, 1993 (revised). Boulder, CO. (CD-ROM)
- Everett, K.R. 1980. Distribution and properties of road dust along the northern portion of the haul road. Chapter 3 in J. Brown and R. L. Berg, eds. Environmental engineering and ecological investigations along the Yukon River-Prudhoe Bay haul road. CRREL report 80-19. U.S. Army Cold Regions Research Engineering Laboratory, Hanover, NH. 203 p.
- Foster, D. S. 1988. Quaternary acoustic stratigraphy between the Colville River and Prudhoe Bay, Beaufort Sea Shelf, Alaska. U. S. Geological Survey, Open-File Rep. 88-0276. 108 p.
- Gilliam, J. J., and P. C. Lent. 1982. Caribou/Waterbird impact analysis workshop. Proceedings of the National Petroleum Reserve in Alaska (NPR-A). U. S. Alaska State Office, Bureau of Land Manage., Anchorage, AK. 29 p.
- Helmericks, J. 1996. Personal communications of September 15, 1995 and January 2, 1996. Golden Plover Lodge, Colville River, AK.
- Henderson, F. M. 1966. Open channel flow. Macmillan Publishing, Inc., New York. 521 p.
- Hopkins, D. M. 1982. Aspects of the paleogeography of Beringia during the late Pleistocene. Pages 3-28 in D. M. Hopkins, J. Matthews, C. E. Schweger, and S. B. Yount, eds., Paleocology of Beringia. Academic Press, New York.
- Hopkins, D. M., and R. W. Hartz. 1978. Coastal morphology, coastal erosion, and barrier islands of the Beaufort Sea, Alaska. U. S. Geological Survey, Open-File Rep. 78-1063. 54 p.
- Hupp, C. R. 1988. Plant ecological aspects of flood geomorphology and paleoflood history. Pages 335-356 in V. R. Baker, R. C. Kockel, and P. C. Patton, eds. Flood Geomorphology. John Wiley & Sons, Inc., New York.
- Interagency Advisory Committee on Water Data. 1982. Guidelines for determining flood flow frequency. U. S. Geological Survey, Office of Water Data Coordination, Washington, DC. Bulletin 17B.
- Jones, S. H., and C. B. Fahl. 1994. Magnitude and frequency of floods in Alaska and conterminous basins of Canada. U. S. Geological Survey, Anchorage, AK. Water-Resources Investigations Report 93-4179. 122 p.
- Jorgenson, M. T. 1986. Biophysical factors affecting the geographic variability of soil heat flux. M.S. Thesis, Univ. of Alaska, Fairbanks, AK. 109 p.
- Jorgenson, M. T., J. W. Aldrich, J. G. Kidd, and M. D. Smith. 1993. Geomorphology and hydrology of the Colville River Delta, Alaska, 1992. Unpublished annual report prepared for ARCO Alaska Inc., Anchorage, AK, by Alaska Biological Research, Inc., Fairbanks, AK. 79 p.
- Jorgenson, M. T., J. W. Aldrich, and C. J. Hammond. 1994a. Geomorphology and hydrology of the Colville River Delta, Alaska, 1993. Unpublished annual report prepared for ARCO Alaska Inc., Anchorage, AK, by Alaska Biological Research, Inc., Fairbanks, AK. 36 p.

Literature Cited

- Jorgenson, M. T., J. W. Aldrich, and C. J. Hammond. 1994b. Geomorphology and hydrology of the Colville River Delta, Alaska, 1994. Unpublished data report prepared for ARCO Alaska Inc., Anchorage, AK, by Alaska Biological Research, Inc., Fairbanks, AK. 9 p.
- Jorgenson, M. T., J. E. Roth, E. R. Pullman, R. M. Burgess, M. Reynolds, A. A. Stickney, M. D. Smith, and T. Zimmer. 1997. An ecological land survey for the Colville River Delta, Alaska, 1996. Unpubl. rep., for ARCO Alaska, Inc., Anchorage, AK, by ABR, Inc., Fairbanks, AK. 160p.
- Jorgenson, M. T., and Y. L. Shur. 1995. Sheet ice associated with polygons in the Colville River Delta. Page F244 in Proceedings of 1995 Fall Meeting, American Geophysical Union, Washington, DC. (abstract).
- Katasonov, E. M. 1969. Composition and cryogenic structure of permafrost. Pages 25–36 in Permafrost investigations in the field. National Research Council of Canada, OT. Technical Translation 1358.
- Klute, A., ed. 1986. Methods of soil analysis: Part 1. Physical and mineralogical methods. Amer. Soc. of Agron., Madison, WI. 1188 p.
- Kreig, R. A., and R. D. Reger. 1982. Air-photo analysis and summary of land-form soil properties along the route of the Trans-Alaska pipeline system. Alaska Division of Geological and Geophysical Surveys, Geol. Rep. 66. 149 p.
- Lewellen, R. I. 1977. A study of Beaufort Sea coastal erosion, northern Alaska. Pages 491–527 in Environmental Assessment of the Alaskan Continental Shelf, annual reports of principal investigators for the year ending March, 1977. U. S. National Oceanic and Atmospheric Administration, v. 15.
- Lounsbury and Associates, Inc. 1995. Colville River Survey Report. Unpubl. rep. prepared for ABR, Inc., Fairbanks, AK, by Lounsbury and Associates, Anchorage, AK.
- Maidment, D. R. 1993. Handbook of Hydrology. McGraw-Hill, Inc., New York.
- Miall, A. D. 1978. Lithofacies types and vertical profile models in braided river deposits: a summary. *Fluvial Sedimentology* 5: 597–604.
- Miall, A. D. 1985. Architectural-element analysis: a new method of facies analysis applied to fluvial deposits. *Earth Sciences Review* 22: 261–308.
- Miller, D. L., and W. T. Phillips. 1996. Geotechnical exploration, Alpine Development Project, Colville River, Alaska. Unpubl. rep. prepared for by ARCO Alaska, Inc., Anchorage, AK, by Duane Miller and Associates, Anchorage, AK. 36 p.
- Moulton, L. J. 1986. Colville River 1985–1986 under-ice temperatures and salinity monitoring. Unpublished progress report No. 1 prepared for ARCO Alaska, Inc., Anchorage, AK, by Entrix.
- Moulton, L. J. 1995. The 1994 Endicott Development Fish Monitoring Program, Volume II: the 1994 Colville River fishery. Unpublished final report prepared for BP Exploration (Alaska) Inc., Anchorage, AK, and North Slope Borough, Barrow, AK, by MJM Research, Bainbridge Island, WA.
- Murton, J. B., and H. M. French. 1994. Ice structures in permafrost, Tuktoyaktuk coastlands, western arctic Canada. *Can. J. Earth Science* 31: 737–747.
- Naidu, A. S., and T. C. Mowatt. 1975. Depositional environments and sediment characteristics of the Colville and adjacent deltas, northern arctic Alaska. Pages 283–309 in M. L. S. Broussard, ed., Delta models for exploration. Houston Geological Society, TX.
- National Wetlands Working Group. 1988. Wetlands of Canada. Environment Canada, Montreal, Quebec. Ecological Land Classification Series, No. 24. 452 p.
- Neill, C. R. 1973. Guide to bridge hydraulics. University of Toronto Press, Toronto, ON, Canada. 191 p.

- NOAA-OCSEAP. 1983. Sale 87. Harrison Bay synthesis. U. S. Dept. Comm., National Oceanic and Atmospheric Administration, Outer Continental Shelf Environmental Assessment Program, Juneau, AK. 81 p.
- Parametrix, Inc. 1996. Alpine Development Project Environmental Evaluation Document. Unpubl rep. for by Parametrix, Inc., Kirkland, WA.
- Peltier, W. R., and A. M. Tushingham. 1989. Global sea level rise and the greenhouse effect: might they be connected. *Science* 244: 806–810.
- Philainen, J. A., and G. H. Johnston. 1963. Guide to a field description of permafrost. Associate Committee on Soil and Snow Mechanics, National Research Council, OT. Tech. Memo. 79.
- Pollard, W. H., and H. M. French. 1980. A first approximation of the volume of ground ice, Richards Island, Pleistocene Mackenzie Delta, Northwest Territories, Canada. *Can. J. Earth Sciences* 17: 509–516.
- Rawlinson, S. E. 1993. Surficial geology and morphology of the Alaskan Central Arctic Coastal Plain. Alaska Div. Geol. and Geophys. Surv., Fairbanks, AK. Report of Investigations 93–1. 172 p.
- Reed, J. C., and J. E. Sater. 1974. The coast and shelf of the Beaufort Sea. Arctic Institute North America, Washington, D.C. 648 p.
- Reimnitz, E., S. M. Graves, and P. W. Barnes. 1985. Beaufort Sea coastal erosion, shoreline evolution, and sediment flux. U. S. Geological Survey, Open-File Report 85–380. 66 p.
- Reimnitz, E., S. M. Graves, and P. W. Barnes. 1988. Map showing Beaufort Sea coastal erosion, sediment flux, shoreline evolution, and the erosional shelf profile. U. S. Geological Survey, Denver, CO. Misc. Invest. Series Map I-1182-G.
- Rothe, T. C., C. J. Markon, L. L. Hawkins, and P. S. Koehl. 1983. Waterbird populations and habitat analyses of the Colville River delta, Alaska, 1981 summary report. U. S. Fish and Wild. Serv., Anchorage, AK. Special Studies Prog. Rep. 67 p.
- Schell, D., and G. Hall. 1972. Water chemistry and nutrient regeneration process studies. Pages 3–28 in P. J. Kinney, and others, eds. Baseline data study of the Alaskan arctic aquatic environment. University of Alaska, Fairbanks, AK. Institute of Marine Science Report R72–3.
- Searcy, C., K. Dean, and W. Stringer, 1995. Merging remotely sensed data with geophysical models, *Polar Record*, 31 (178), p. 297–304.
- Shannon and Wilson, Inc. 1996b. 1996 Colville River Delta channel assessment, Colville River Delta, North Slope, Alaska. Unpubl. rep. prepared for Michael Baker Jr., Inc., Anchorage, AK, by Shannon & Wilson, Inc., Fairbanks, AK. 9 p. w/ app.
- Shannon and Wilson, Inc. 1996a. 1996 Colville River Delta spring breakup and hydrologic assessment North Slope, Alaska. Unpubl. rep. prepared for Michael Baker Jr., Inc., Anchorage, AK, by Shannon & Wilson, Inc., Fairbanks, AK. 16 p.
- Shannon and Wilson, Inc. 1996c. Flood-frequency analysis for the Colville River North Slope, Alaska. Unpubl. rep. prepared for Michael Baker Jr., Inc., Anchorage, AK, by Shannon & Wilson, Inc., Fairbanks, AK. 11 p.
- Shur, Y. L. 1988. The upper horizon of permafrost soil. Pages 867–871 in K. Senneset, ed., *Proceedings of the Fifth Intern. Conf. on Permafrost*. Tapir Publishers, Trondheim, Norway.
- Simons, Li & Associates. 1982. Engineering analysis of fluvial systems. Simons, Li, and Associates, Fort Collins, CO.
- Simpson, S. G., J. Barzen, L. Hawkins, and T. Pogson. 1982. Waterbird studies on the Colville River delta, Alaska, 1982 summary report. U. S. Fish and Wild. Serv., Anchorage, AK. Special Studies Prog. Rep.

Literature Cited

- Soil Survey Division Staff (SSDS). 1993. Soil survey manual. U. S. Department of Agriculture, Washington, D.C. Handbook No. 18. 437 p.
- Strahler, A. N. 1952. Dynamic basis of geomorphology. Geological Society of America Bulletin 63: 923-938.
- University of Alaska (Fairbanks UAF). 1972. Baseline study of the Alaska arctic aquatic environment. Institute of Marine Science, University of Alaska, Fairbanks, AK. Report R72-3. 275 p.
- U. S. Army Corps of Engineers. 1992. Hydrologic design package for flood control channels (SAM Ver. 3.04). Unpublished draft computer program manual. U. S. Army Corps of Engineers, Waterways Experiment Station, Vicksburg, MS.
- U. S. Geological Survey. 1978. Water resources data for Alaska, water year 1977. Water Resources Division, Anchorage, AK.
- U. S. Geological Survey. 1980. Water resources data for Alaska, water year 1979. Water Resources Division, Anchorage, AK.
- U. S. Geological Survey. 1981. Water resources data for Alaska, water year 1980. Water Resources Division, Anchorage, AK.
- U. S. Geological Survey. 1982. Water resources data for Alaska, water year 1981. Water Resources Division, Anchorage, AK.
- U. S. Geological Survey. 1994. Water resources data for Alaska, water year 1993. Water Resources Division, Anchorage, AK. 373 p.
- U. S. Geological Survey. 1995. Water resources data for Alaska, water year 1994. Water Resources Division. Anchorage, AK. 289 p.
- Viereck, L.A., C.T. Dyrness, A.R. Batten, and K.J. Wenzlick. 1992. The Alaska vegetation classification. U.S. Department of Agriculture, Forest Service, Pacific Northwest Research Station, Portland, Oregon. General Technical Report PNW-GTR-286. 278 p.
- Walker, D. A., and W. Acevedo. 1987. Vegetation and a Landsat-derived land cover map of the Beechey Point Quadrangle, Arctic Coastal Plain, Alaska. CRREL Rep. 87-5, U.S. Army Corps of Engineers, Cold Reg. Res. and Eng. Lab., Hanover, NH. 63 p.
- Walker, D. A., K. R. Everett, P. J. Webber, and J. Brown. 1980. Geobotanical atlas of the Prudhoe Bay region, Alaska. U. S. Army Corps of Engineers, Cold Regions Research and Engineering Lab., Hanover, NH. Lab. Rep. 80-14. 69 p.
- Walker, H. J. 1966. Permafrost and ice-wedge effect on riverbank erosion. Pages 164-171 in International Conference on Permafrost, 1963, Proceedings. National Academy of Sciences, National Research Council Publication 1287, Washington, D.C.
- Walker, H. J. 1973a. Salinity changes in the Colville River Delta, Alaska, during breakup. Pages 514-527 in Proceedings of the Snow and Ice in Hydrology Conference. Banff, AB, Canada.
- Walker, H. J. 1973b. Morphology of the North Slope. Pages 49-92 in Proceedings of the 25th Anniversary Celebration of the Naval Arctic Research Laboratory. Arctic Institute of North America, Arlington, VA. Technical Paper No. 25.
- Walker, H. J. 1974. The Colville River and the Beaufort Sea: Some interactions. Pages 513-540 in J. C. Reed, and J. E. Sater, eds., The coast and shelf of the Beaufort Sea. Arctic Institute of North America, Washington, DC.
- Walker, H. J. 1976. Depositional environments in the Colville River Delta. Pages C1-C22 in, T. P. Moller, ed., Recent and ancient sedimentary environments in Alaska. Alaska Geological Society, Anchorage.
- Walker, H. J. 1978. Lake tapping in the Colville River Delta. Pages 233-238 in Proceedings of the Third International Conference on Permafrost, Edmonton, AB. National Research Council of Canada, OT, Canada.

- Walker, H. J. 1983a. Colville River Delta, Alaska, guidebook to permafrost and related features. Alaska Division of Geological and Geophysical Surveys, Fairbanks, AK. Guidebook 2 for Fourth International Conference on Permafrost. 34 p.
- Walker, H. J. 1983b. The Colville River Delta. Section G: The delta's distributaries. Unpublished report prepared for North Slope Borough, Barrow, AK. 41 p.
- Walker, H. J. 1994a. Environmental impact of river dredging in arctic Alaska (1981-89). *Arctic* 47: 176-183.
- Walker, H. J. 1994b. Nechelik Channel investigations—1994. Unpublished report prepared for North Slope Borough, Barrow, AK, by Louisiana State University, Baton Rouge, LA.
- Walker, H. J., and L. Arnborg. 1966. Permafrost and ice-wedge effect on riverbank erosion. Pages 164-171 *in* Proceedings, Permafrost International Conference, 1963, Lafayette, IN. National Academy of Sciences, Washington, DC, National Research Council Publication 1287.
- Walker, H. J., and Y. Matsukara. 1979. Barchans and barchan-like dunes as developed in two contrasting areas with restricted source regions. Pages 43-46 *in* Annual Report. Institute of Geoscience, Tsukuba, Japan.
- Walker, H. J., and J. M. McCloy. 1969. Morphologic changes in two arctic deltas. Arctic Institute of North America, Arlington, VA. Research Paper No. 49. 91 p.
- Walker, H. J., and H. M. Morgan. 1964. Unusual weather and river bank erosion in the delta of the Colville River, Alaska. *Arctic* 17: 41-47.
- Washburn, A. L. 1973. *Periglacial Processes and Environments*. Edward Arnold, London. 320 p.
- Williams, J. R., L. D. Carter, and W. Yeend. 1978. Coastal Plain deposits of NPR-A. Pages B20-B22 *in* The United States Geological Survey in Alaska: Accomplishments during 1977. U. S. Geological Survey, Circular 772-B.

APPENDICIES

APPENDIX A. DATA TABLES AND FIGURES FOR PART I.

APPENDIX B. DATA TABLES FOR PART II.

APPENDIX C. DATA TABLES AND FIGURES FOR PART III.

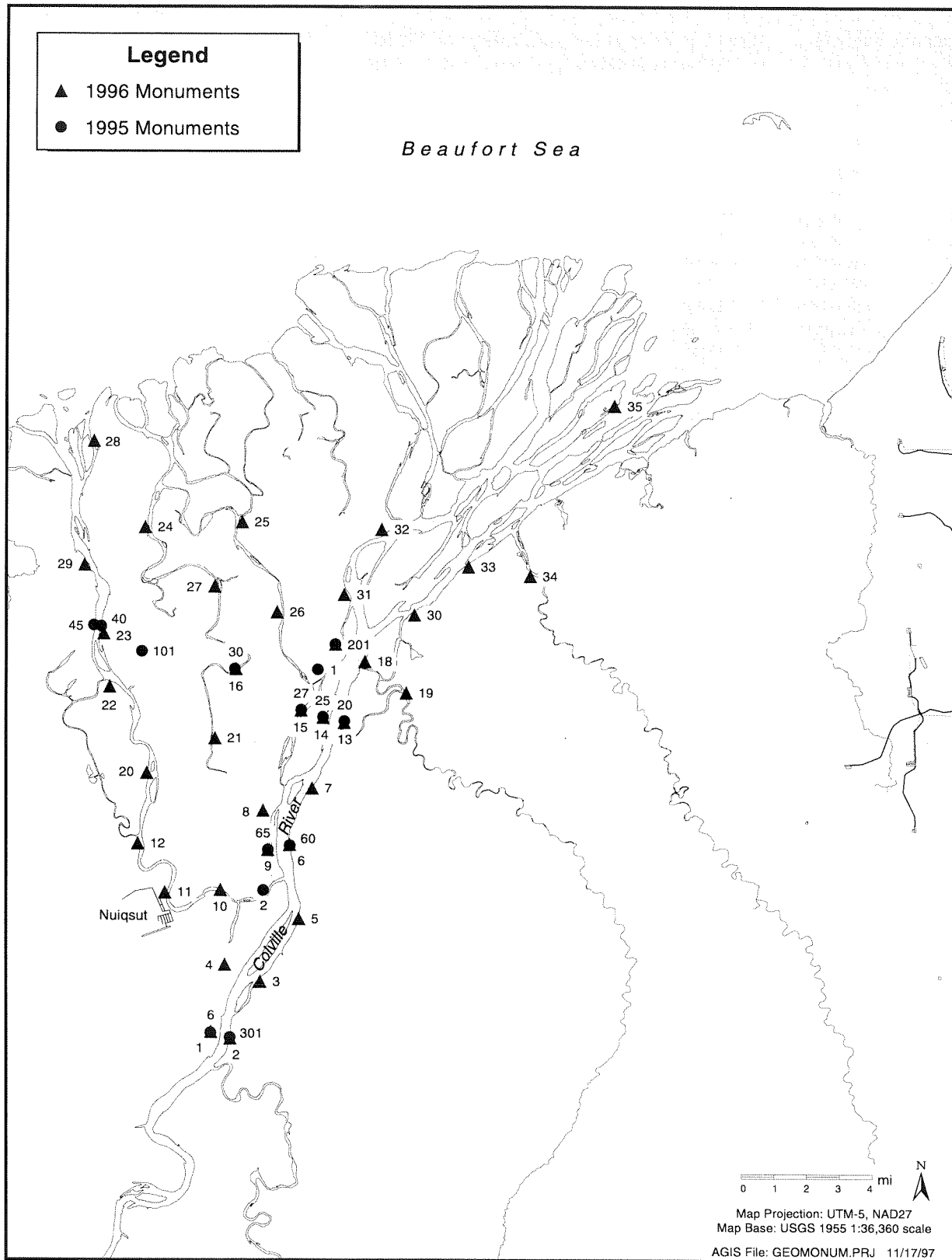
Appendix Table A-1. Data file listing for geodetic control points on the Colville River Delta, Alaska, 1996.

Monument ID	Reference	1992 Elevation		Reference	1995 Elevation		Reference	1996 Elevation		Coordinates UTM NAD27	
		ft	m		ft	m		ft	m	Easting	Northing
TBM1A	RIVER						RIVER				
TBM2B	DUNE	2.98	0.91				DUNE	2.54	0.78		
TBM3B	DUNE	2.19	0.67				DUNE	1.75	0.53		
TBM4A	SALVO	6.62	2.02				SALVO	7.29	2.22		
TBM5A	SALVO	3.8	1.16				SALVO	4.47	1.36		
6P				RIVER	30.473058	9.29	MON 1	29.48	8.99	578097.37	7785484.23
20P				RIVER	15.15748	4.62	MON 13	14.95	4.56	584657.14	7800683.94
25P				RIVER	22.769029	6.94	MON 14	23.09	7.04	583602.89	7800890.78
27P				RIVER	21.128609	6.44	MON 15	20.61	6.28	582532.91	7801226.98
30P				RIVER	12.335958	3.76	MON 16	12.03	3.67	579286.96	7803227.13
40P				RIVER	10.137795	3.09	MON 23	9.72	2.96	572765.03	7805303.65
45P				RIVER	7.9724409	2.43				572387.95	7805349.71
60P				RIVER	18.864829	5.75	MON 6	18.11	5.52	581981.87	7794620.50
65P				RIVER	27.919948	8.51	MON 9	26.97	8.22	580909.87	7794405.08
1B (Alpine)				RIVER (?)	7.480315	2.28				574739.57	7804077.36
1CP				RIVER	28.576115	8.71	MON 17	28.45	8.67	584206.70	7804431.83
1P				RIVER	21.948819	6.69	MON 2	20.83	6.35	579044.82	7785259.80
MON 1							BSPMSL	27.72	8.45	578116.20	7785556.78
MON 2							BSPMSL	21.29	6.49	579063.39	7785238.91
MON 3							BSPMSL	20.66	6.30	580526.80	7787999.69
MON 4							BSPMSL	18.59	5.67	578788.52	7788832.77
MON 5							BSPMSL	15.41	4.70	582420.17	7791063.86
MON 6							BSPMSL	18.30	5.58	581973.20	7794681.84
MON 7							BSPMSL	14.95	4.56	583076.36	7797427.33
MON 8							BSPMSL	26.69	8.14	580665.78	7796346.29
MON 9							BSPMSL	25.03	7.63	580900.34	7794438.05
MON 10							BSPMSL	17.42	5.31	578580.02	7792484.26
MON 11							BSPMSL	27.04	8.24	575867.72	7792353.37
MON 12							BSPMSL	14.60	4.45	574546.22	7794735.87
MON 13							BSPMSL	13.75	4.19	584644.52	7800647.01
MON 14							BSPMSL	20.52	6.25	583601.78	7800878.92
MON 15							BSPMSL	19.49	5.94	582530.17	7801231.44
MON 16							BSPMSL	12.12	3.70	579352.88	7803253.76
MON 17							BSPMSL	26.28	8.01	584217.65	7804455.40
MON 18							BSPMSL	12.12	3.69	585648.78	7803615.17
MON 19							BSPMSL	11.58	3.53	587670.29	7802084.92
MON 20							BSPMSL	19.17	5.84	574989.57	7798187.26
MON 21							BSPMSL	12.40	3.78	578319.56	7799874.81
MON 22							BSPMSL	10.13	3.09	573181.47	7802381.20
MON 23							BSPMSL	9.53	2.90	572890.12	7804984.93
MON 24							BSPMSL	8.40	2.56	574903.87	7810159.23
MON 25							BSPMSL	10.46	3.19	579635.78	7810412.47
MON 26							BSPMSL	14.07	4.29	581353.26	7806017.44
MON 27							BSPMSL	10.66	3.25	578301.21	7807265.91
MON 28							BSPMSL	3.67	1.12	572390.42	7814347.44
MON 29							BSPMSL	8.03	2.45	571943.45	7808327.98
MON 30							BSPMSL	10.10	3.08	588079.51	7805887.42

Appendicies

Appendix Table A-1. (cont.)

Monument ID	Reference	1992 Elevation		Reference	1995 Elevation		1996 Elevation		Coordinates UTM NAD27			
		ft	m		ft	m	ft	m	Easting	Northing		
MON 34								BSPMSL	13.44	4.10	593787.70	7807776.08
MON 35								BSPMSL	5.57	1.70	597898.71	7816076.55
KINIK		22		22				BSPMSL	22.82	6.96		
FORK		47.9	14.6	47.9	14.6			BSPMSL	47.38	14.44	580685.16	7792443.15
DUNE		36	11	36	10.97			BSPMSL	35.56	10.84	589870.40	7809298.56
RIVER		41.99	12.8	41.99	12.8			BSPMSL	41.80	12.74	583353.85	7803197.43
SALVO		18	5.49	18	5.486			BSPMSL	18.67	5.69	587052.45	7815937.41



Appendix Figure A-1. Location of geodetic control monuments, Colville River Delta, Alaska, 1996.

Appendix Table B-1. Data file listings for soil profile and SIPRE core locations along sediment transects, Colville River Delta, Alaska, 1996.

Site ID	Latitude	Longitude	Site ID	Latitude	Longitude
G1.01	70.341244	-150.974831	P2.07	70.268996	-150.529511
G1.02	70.351047	-150.981858	P2.08	70.269883	-150.526164
G1.03	70.350329	-150.975425	P3.01	70.276243	-150.151898
G1.04a	70.347666	-150.949274	P3.02	70.276915	-150.150130
G1.05	70.341976	-150.952216	P3.03	70.277380	-150.148338
G1.06	70.343950	-150.952285	P3.04	70.277754	-150.145868
G1.07	70.344888	-150.939265	P3.05	70.277775	-150.143234
G2.01	70.269066	-150.865511	P3.06	70.277833	-150.141233
G2.02	70.271332	-150.855317	P3.07	70.277857	-150.135994
G2.03	70.271018	-150.850861	P3.08	70.277853	-150.134002
G2.04	70.275939	-150.858023	P3.09	70.278057	-150.132166
G2.05	70.277770	-150.884662	T1.01	70.391510	-150.859580
G2.18	70.391470	-150.872967	T1.02	70.391210	-150.862363
G2.25	70.395044	-150.880183	T1.03	70.391199	-150.862952
G2.26	70.399241	-150.876219	T1.04	70.391196	-150.863433
G2.27	70.393853	-150.861285	T1.05	70.391095	-150.864005
G3.01	70.279414	-150.977792	T1.06	70.390829	-150.864967
G3.02	70.282274	-150.976820	T1.07	70.390746	-150.865537
G4.01	70.254691	-150.664452	T1.08	70.390651	-150.865921
G4.02	70.255957	-150.702153	T1.09	70.390088	-150.868384
G4.23	70.364588	-151.055106	T1.11	70.389599	-150.870224
G5.01	70.316342	-150.281499	T2.14	70.393964	-150.864559
G5.02	70.317941	-150.286958	T2.15	70.394069	-150.866685
G5.03	70.317590	-150.285114	T2.16	70.393975	-150.869314
G6.01	70.248102	-150.204277	T2.17	70.394085	-150.872588
G6.02	70.250145	-150.211005	T4.01	70.364244	-151.069890
G6.03	70.251831	-150.210962	T4.02	70.364191	-151.072482
G6.32	70.393300	-151.122757	T4.03	70.364238	-151.074318
G6.33	70.390977	-151.128900	T4.04	70.363506	-151.078868
G11.29	70.321311	-151.058148	T4.05	70.362652	-151.083749
G11.30	70.321902	-151.040603	T5.06	70.398890	-151.085291
G11.31	70.294265	-151.002329	T5.07	70.398936	-151.083683
G12.24	70.346972	-151.072824	T5.08	70.398973	-151.082878
G12.25	70.344576	-151.079472	T5.09	70.398890	-151.081016
G12.26	70.340798	-151.047614	T5.10	70.398973	-151.080366
G12.27	70.341597	-151.045966	T5.11	70.398872	-151.077651
G12.28	70.332223	-151.066781	T6.12	70.398641	-151.107678
P1.01	70.258810	-150.652093	T6.13	70.398786	-151.107744
P1.02	70.258600	-150.648348	T6.14	70.398755	-151.108228
P1.03	70.258530	-150.644401	T6.15	70.398107	-151.108074
P1.04	70.258571	-150.640654	T6.16	70.396410	-151.107083
P1.05	70.258592	-150.635423	T6.17	70.398802	-151.108491
P1.06	70.258582	-150.629877	T10.01	70.330245	-151.034852
P2.01	70.264385	-150.538084	T10.02	70.330475	-151.032886
P2.02	70.264970	-150.538279	T10.03	70.331471	-151.027144
P2.03	70.265417	-150.537482	T10.04	70.332075	-151.024955
P2.04	70.265637	-150.534562	T10.05	70.332075	-151.024955
P2.05	70.266203	-150.532608	T10.06	70.335768	-151.020630
P2.06	70.267081	-150.531892	T10.07	70.337287	-150.997307
T11.01	70.323218	-151.065288	X2.04	70.363668	-150.623062
T11.03	70.321949	-151.067378	X2.05	70.363203	-150.621782

Appendix Table B-1. (cont.)

Site ID	Latitude	Longitude	Site ID	Latitude	Longitude
T10.15	70.330009	-151.033730	X2.03	70.364265	-150.624807
T11.06	70.317978	-151.082842	X3.02	70.387874	-150.654515
T11.07	70.314712	-151.093738	X3.04	70.389649	-150.662779
T12.01	70.260529	-151.011471	X3.05	70.390257	-150.664686
T12.01b	70.260578	-151.009449	X3.06	70.381954	-150.649106
T12.02	70.260604	-151.007722	X3.07	70.381574	-150.648883
T12.02	70.260604	-151.007722	X3.08	70.379927	-150.647097
T12.03	70.260709	-151.004261	X3.09	70.379247	-150.646561
T12.03B	70.260836	-151.001170	X3.10	70.379082	-150.646313
T12.04	70.260868	-150.999230	X3.11	70.378656	-150.645988
T12.05	70.260939	-150.997498	X3.12	70.378220	-150.644917
T12.06	70.261026	-150.994835	X4.01	70.429349	-150.584540
T12.07	70.261197	-150.988448	X4.03	70.429816	-150.585234
T12.08	70.261315	-150.985411	X4.04	70.430328	-150.585923
T12.09	70.261599	-150.978748	X4.05	70.430870	-150.586233
T12.09	70.261599	-150.978748	X4.06	70.427301	-150.581678
T12.10	70.264441	-150.957046	X4.07	70.426750	-150.580726
T13.01	70.282144	-150.929859	X4.08	70.426530	-150.580378
T13.01	70.282144	-150.929859	X5.02	70.464222	-150.726731
T13.02	70.282189	-150.929084	X5.03	70.465826	-150.725077
T13.03	70.282305	-150.928275	X5.04	70.466039	-150.724919
T13.03	70.282305	-150.928275	X5.05	70.467460	-150.723017
T13.05	70.282553	-150.926443	X5.08	70.460601	-150.734883
T13.05	70.282553	-150.926443	X6.06	70.162434	-150.912950
T13.06	70.284518	-150.914021	X6.08	70.162382	-150.912374
T13.06	70.284518	-150.914021	X6.11	70.162200	-150.910569
T13.07	70.286189	-150.904178	X6.12	70.164932	-150.939697
T13.07	70.286189	-150.904178	X6.13	70.165298	-150.943465
T14.03	70.189686	-150.866154	X6.13b	70.164217	-150.909705
T14.05	70.188028	-150.846013	X11.01	70.324007	-150.887585
T14.06	70.187838	-150.843705	X11.02	70.324007	-150.887585
T18.01	70.294784	-150.729341	X11.03	70.324460	-150.887964
T18.01B	70.295109	-150.729595	X11.04	70.325032	-150.889317
T18.02	70.295345	-150.729784	X11.05	70.326469	-150.892497
T18.02	70.295345	-150.729784	X11.06	70.327301	-150.896991
T18.03	70.296178	-150.730357	X11.07	70.328297	-150.902322
T18.03	70.296178	-150.730357	X11.08	70.329677	-150.910782
T18.04	70.299285	-150.732673	X11.09	70.330563	-150.916791
T18.04	70.299285	-150.732673	X11.10	70.324637	-150.904667
X1.05	70.333460	-150.756461	X12.01	70.344371	-151.061983
X1.06	70.334076	-150.760549	X12.02	70.344592	-151.060044
X1.07	70.334532	-150.762630	X12.03	70.343803	-151.059186
X1.08	70.335160	-150.766930	X12.04	70.343847	-151.057476
X2.01	70.365356	-150.627909	X12.05	70.343840	-151.055185
X2.02	70.364627	-150.625699	X12.06	70.343648	-151.055603
X12.07	70.343596	-151.049133	X13.05	70.333765	-150.820225
X12.09	70.343741	-151.055141	X13.05	70.333765	-150.820225
X12.10	70.343604	-151.035808	X13.06	70.334568	-150.813107
X12.11	70.345092	-151.073214	X14.01	70.246662	-150.822636
X13.01	70.333060	-150.826454	X14.03	70.247139	-150.825716
X13.01	70.333060	-150.826454	X14.01a	70.244716	-150.854828
X13.03	70.333121	-150.824849	X14.02a	70.244331	-150.857838
X13.03	70.333121	-150.824849	X14.03a	70.244023	-150.859913
X13.04	70.333497	-150.822492	X14.04a	70.243797	-150.862005
X14.05a	70.243499	-150.864131	Y2	70.322500	-151.061948
Y1.00	70.239932	-150.977746	Y3	70.310982	-151.018979

Appendicies

Appendix Table B-1. (cont.)

POINT_ID	LAT (NAD27)	LONG (NAD 27)	POINT_ID	LAT (NAD27)	LONG (NAD 27)
S1.100	70.162991	-150.910501	S8.200	70.304073	-150.740635
S1.2	70.163019	-150.913107	S8.243	70.304053	-150.739487
S1.20	70.163014	-150.912619	S8.50	70.304138	-150.744632
S1.200	70.162962	-150.907854	S9.100	70.324518	-150.719564
S1.50	70.163005	-150.911828	S9.2	70.324892	-150.721937
S1.500	70.162875	-150.899987	S9.20	70.324823	-150.721500
S10.100	70.326844	-150.715396	S9.200	70.324136	-150.717144
S10.150	70.326714	-150.714116	S9.400	70.323372	-150.712312
S10.2	70.327096	-150.717906	S9.50	70.324709	-150.720774
S10.20	70.327049	-150.717445	S12.20	70.221284	-150.967981
S10.50	70.326973	-150.716676	S11.2	70.222087	-150.961375
S2.100	70.165624	-150.908755	S11.20	70.222248	-150.961433
S2.2	70.165655	-150.911356	S11.50	70.222516	-150.961525
S2.20	70.165649	-150.910877	S11.100	70.222965	-150.961682
S2.200	70.165594	-150.906105	S12.2	70.221126	-150.967873
S2.50	70.165640	-150.910080	S12.50	70.221547	-150.968162
S2.500	70.165501	-150.898268	S12.100	70.222053	-150.968512
S3.100	70.189942	-150.862904	S13.2	70.286957	-150.996421
S3.2	70.190071	-150.865479	S13.20	70.286963	-150.995939
S3.20	70.190047	-150.865005	S13.50	70.286972	-150.995139
S3.200	70.189810	-150.860278	S13.100	70.286987	-150.993806
S3.360	70.189600	-150.856078	S13.170	70.287009	-150.991940
S3.50	70.190010	-150.864220	S14.2	70.294497	-150.995767
S4.100	70.196832	-150.844905	S14.20	70.294605	-150.995409
S4.2	70.197563	-150.846361	S14.50	70.294786	-150.994812
S4.200	70.196085	-150.843422	S14.100	70.295086	-150.993816
S4.29	70.197362	-150.845959	S14.200	70.295685	-150.991836
S4.415	70.194481	-150.840229	S16.180	70.309908	-151.012187
S4.56	70.197160	-150.845557	S16.2	70.309752	-151.016873
S5.100	70.244510	-150.822586	S16.20	70.309769	-151.016396
S5.2	70.244540	-150.825194	S16.50	70.309795	-151.015597
S5.20	70.244534	-150.824715	S16.100	70.309839	-151.014268
S5.200	70.244477	-150.819928	S17.2	70.322089	-151.061350
S5.50	70.244527	-150.823921	S17.200	70.321650	-151.066534
S5.500	70.244380	-150.812030	S17.20	70.322051	-151.061816
S6.100	70.246225	-150.823281	S17.50	70.321984	-151.062594
S6.2	70.246254	-150.825887	S17.100	70.321874	-151.063888
S6.20	70.246248	-150.825410	S18.2	70.323568	-151.065185
S6.200	70.246194	-150.820622	S18.20	70.323514	-151.065637
S6.50	70.246240	-150.824611	S18.50	70.323423	-151.066391
S6.500	70.246102	-150.812696	S18.100	70.323271	-151.067649
S7.100	70.297893	-150.749275	S18.200	70.322968	-151.070165
S7.150	70.297875	-150.747949	S19.2	70.348543	-151.069636
S7.2	70.297928	-150.751889	S19.20	70.348523	-151.070094
S7.20	70.297922	-150.751409	S19.50	70.348490	-151.070890
S7.50	70.297912	-150.750608	S19.100	70.348435	-151.072218
S7.500	70.297744	-150.738587	S19.200	70.348325	-151.074874
S8.100	70.304117	-150.743299	S19.500	70.347996	-151.082840
S8.2	70.304160	-150.745911	S20.2	70.352364	-151.068312
S8.20	70.304153	-150.745434	S20.20	70.352325	-151.068773

Appendix Table B-1. (cont.)

S20.50	70.352262	-151.069554
S20.100	70.352157	-151.070855
S20.200	70.351947	-151.073457
S20.500	70.351317	-151.081263

Appendicies

Appendix Table B-2. Results from multi-factor analysis of variance for 1989 flood deposits, Colville River Delta, Alaska, 1996

Source	Sum of squares	df	Mean square	F	Sig.	Noncent. Parameter	Observed Power (alpha =.05)
Corrected model	27.718 ^b	3	9.239	1.854	.148	5.562	.454
Intercept	658.968	1	658.968	132.219	.000	132.219	1.000
ITU	2.025	1	2.025	.406	.527	.406	.096
Flood region	25.729	1	25.729	5.162	.027	5.162	.607
ITU * Flood region	4.277	1	4.277	.858	.358	.858	.149
Error	269.131	54	4.984				
Total	1082.750	58					
Corrected Total	296.849	57					

^b. R squared = .093 (adjusted R squared= -.043)

Appendix Table B-3. Results from multi-factor analysis of variance for total mineral accumulation, Colville River Delta, Alaska, 1996.

Source	Sum of squares	df	Mean square	F	Sig.	Noncent. Parameter	Observed Power (alpha = .05)
Corrected model	25.246 ^b	3	8.415	.673	.574	2.018	.179
Intercept	507.634	1	507.634	40.567	.000	40.567	1.000
ITU	8.543	1	8.543	.683	.414	.683	.127
Flood region	10.371	1	10.371	.829	.368	.829	.144
ITU * Flood region	11.599	1	11.599	.927	.341	.927	.156
Error	500.543	40	12.514				
Total	1096.750	44					
Corrected Total	525.790	43					

^b. R squared = .048 (adjusted R squared= -.023)

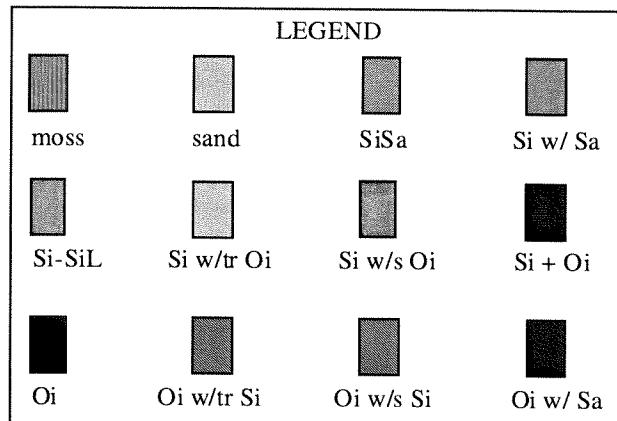
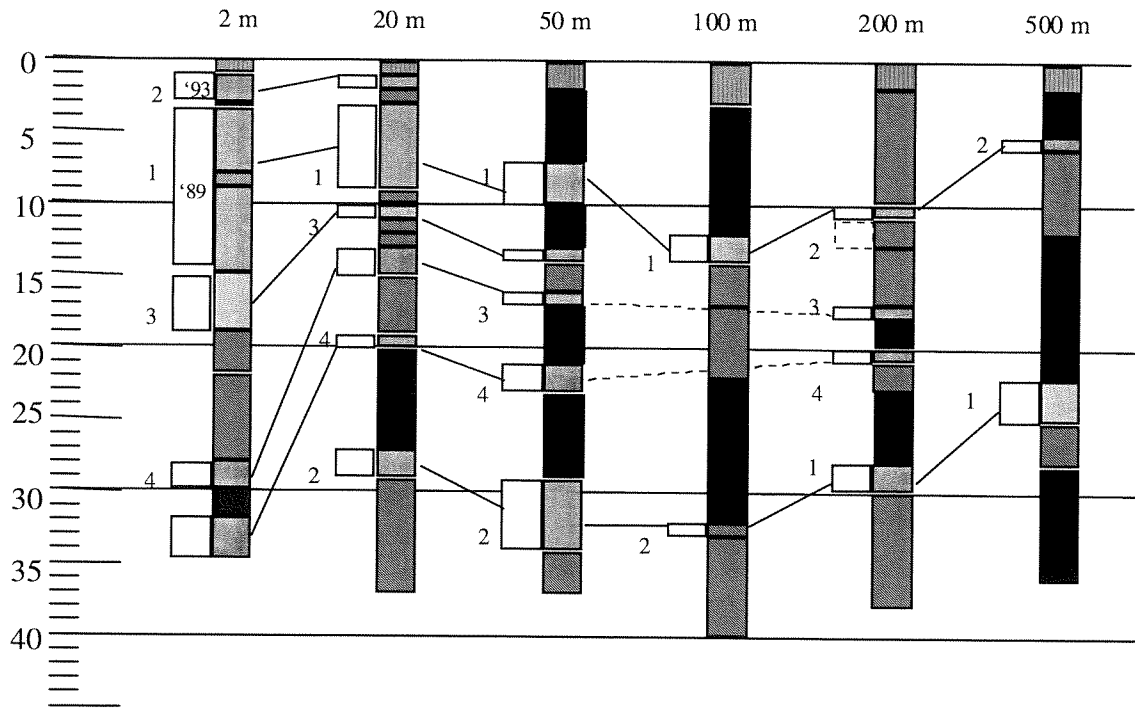
Appendix Table B-4. Results from a multi-factor analysis of variance for ranking of flood deposits, Colville River Delta, 1996.

Source	Sum of squares	df	Mean square	F	Sig.	Noncent. Parameter	Observed Power (alpha =.05)
Corrected model	17.536 ^b	3	5.845	6.106	.002	18.317	.940
Intercept	222.900	1	222.900	232.832	.000	232.832	1.000
ITU	2.3 *10-2	1	2.3 *10-2	.024	.878	.024	.053
Flood region	11.343	1	11.343	11.849	.001	11.849	.918
ITU * Flood region	1.579	1	1.579	1.650	.207	1.650	.240
Error	34.464	36	.957				
Total	302.000	40					
Corrected Total	52.000	39					

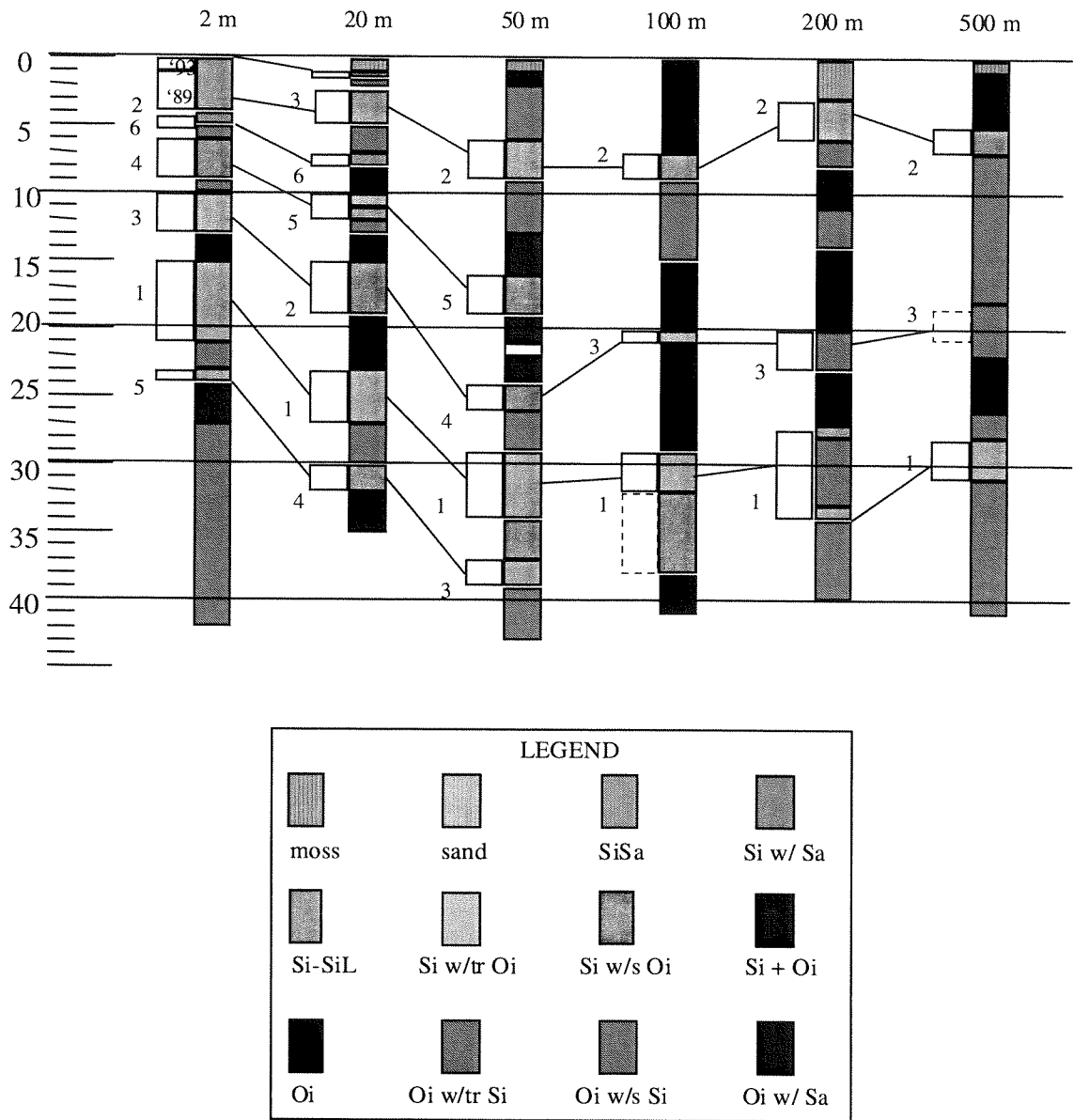
^b. R squared = .337 (adjusted R squared = -.282)

Appendix Table B-5. Data file listing for samples with radiocarbon aging, Colville River Delta, 1996.

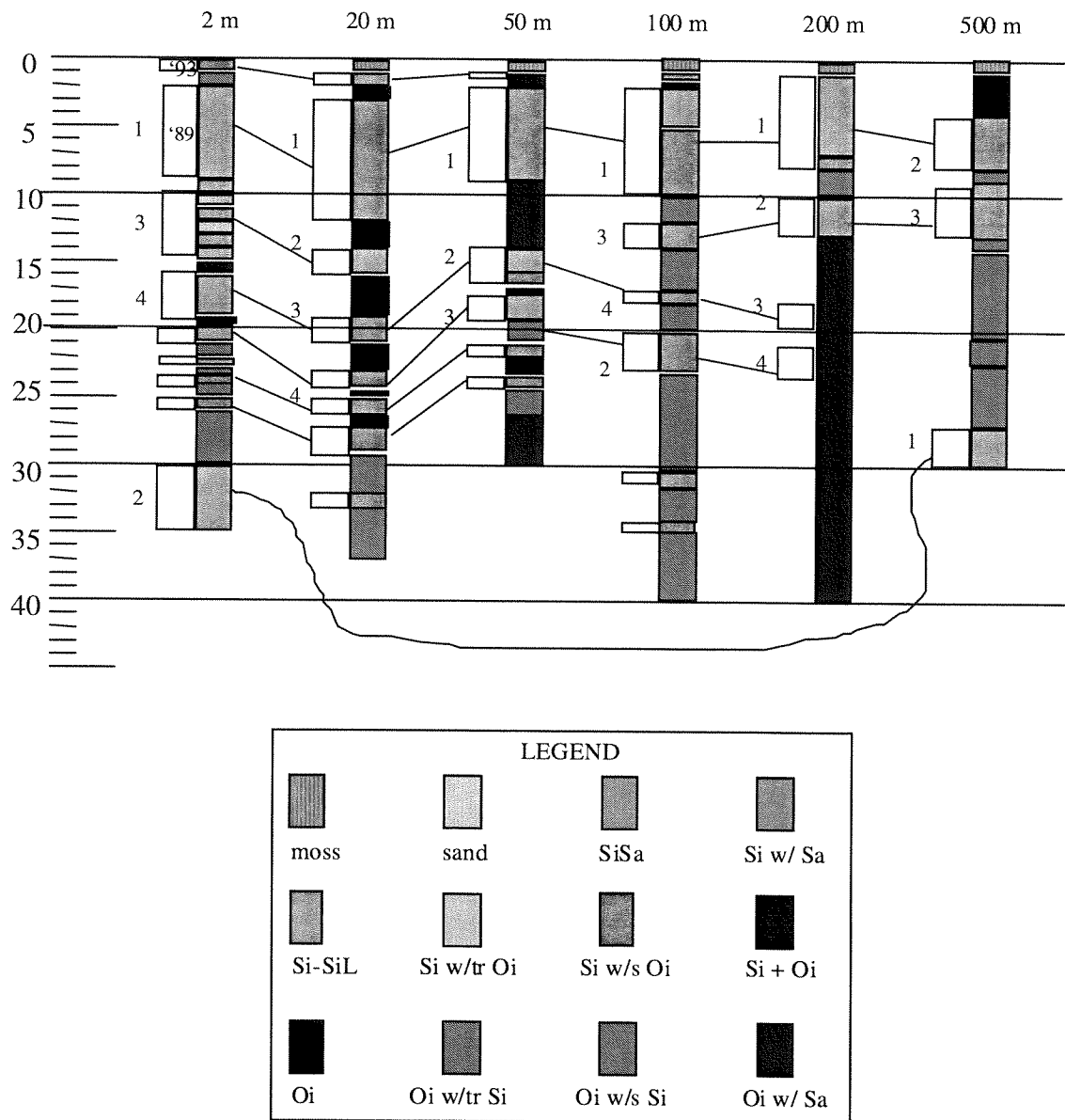
CORE	Mid-Depth (cm)	Conventional Date before 1996	Cal. Age - Yrs before 1996	Cal. Age - Ave. of Intercepts	Cal. Age.- Lower 95%	Cal. Age - Upper 95%	Accumulation Rate (cm/yr)	Accumulation Rate (ft/100 years)
S1.100	55	126		none	1685	1930	0.44	1.43
S1.500	39	196	205	1791	1650	1950	0.20	0.65
S1.500	55	746	706	1290	1235	1400	0.07	0.24
S3.50	41	146	98	1898	1665	1950	0.28	0.92
S3.100	55	346	423	1573	1425	1665	0.16	0.52
S3.500	55	296	341	1655	1475	1950	0.19	0.61
S7.100	49.5	596	586	1410	1295	1460	0.08	0.27
S8.200	35.5	436	521	1475	1425	1650	0.08	0.27
S9.100	55	1476	1356	640	530	705	0.04	0.12
S9.500	55	876	771	1225	1040	1290	0.06	0.21
S18.50	37.5	136		none	1665	1950	0.28	0.90
G1.5	43	2216	2186	-190	-385	-20	0.02	0.06
T12.10	42.5	1136	1016	980	855	1035	0.04	0.12
T13.7	44.5	1576	1441	555	370	670	0.03	0.09
T18.4	45	1346	1301	695	635	885	0.03	0.11
X13.5	50	686	646	1350	1235	1440	0.07	0.24
X13.7	47	796	721	1275	1165	1400	0.06	0.19
X14.2	47	846	776	1220	1030	1290	0.06	0.18
X6.12	55	206	205	1791	1640	1950	0.27	0.88
X6.13B	32	1156	1026	970	770	1040	0.03	0.09
T14.06	40.5	996	956	1040	990	1225	0.04	0.13
X11.3	162.5	616	591	1405	1295	1445	0.26	0.87
X11.9a	57.5	1996	1926	70	-115	245	0.03	0.09
X12.5	16.5	316	346	1650	1425	1950	0.05	0.17
X12.7	28	206	205	1791	1650	1950	0.14	0.45
X12.9	62	3596	3886	-1890	-2035	-1690	0.02	0.06
X14.3a	62.5	1106	1001	995	895	1030	0.06	0.19
G4.23(N23a)	12.5	386	423	1573	1440	1665	0.03	0.11
G11.30(N30a)	82.5	1166	1036	960	785	1020	0.07	0.23
G2.27(T27)	88.5	1696	1581	415	250	555	0.05	0.17
T4.05(N5)	32	396	421	1575	1435	1665	0.08	0.27
T2.16(T16)	27	466	541	1455	1415	1640	0.06	0.19
T1.09(t9)	27	296	341	1655	1495	1950	0.09	0.30
G4.04(LS2)	129.5	326	346	1650	1470	1680	0.40	1.30
G4.03(LS1.1)	75.5	1046	961	1035	960	1250	0.07	0.24
T4.04(N4)	4.5	173		ND	ND		0.03	0.09
Y1a	40	146	99	1897	1665	1950	0.27	0.90
T1.01(TC1)	13	106		None	1675	1940	0.12	0.40



Appendix Figure B-1. Profiles of vertical sediment distribution along Transect S1, Colville River Delta, Alaska, 1996.



Appendix Figure B-2. Profiles of vertical sediment distribution along Transect S3, Colville River Delta, Alaska, 1996.



Appendix Figure B-3. Profiles of vertical sediment distribution along Transect S5, Colville River Delta, Alaska, 1996.

Appendix Table C-1. System for classifying ground ice structures observed on the Colville River Delta, 1996.

Continuity	Primary Bedding Property or Shape	Secondary Pattern or Shape	Size
Pore (P)	Nonvisible (n) Visible (v)		Very fine (<0.5 mm) (v) Fine (0.5 - <1 mm) (f) Medium (1-3 mm) (m) Coarse (3-5 mm) (c) Large (>5 mm)(l)
Organic-matrix (O)	Nonvisible (n) Visible (v)		Same as above
Crustal (C)	Entire (e) Partial (p)		Same as above
Vein (V)	Vertical or inclined (v) Irregularly oriented (i)		Same as above (thickness)
Lenticular (L)	Horizontal (h) Inclined (i) Crossbedded (c) Grouped (g)	Planar (p) Wavy (w)	Same as above (thickness)
Layered or Bedded (B) (<10 cm thick)	Sparse (<5%) (s) (density of layers) Medium (5-25%)(m) Dense (25-50%)(d)	Planar (p) Wavy (w) Curved (c)	Same as above (thickness)
Reticulate (R)	Trapezoidal (prismatic) (t) Lattice (regular, blocky) (l) Foliated (platy) (f)		Width of inclusions Fine (<5 mm) Medium (5-10 mm) Coarse (>10 mm)
Ataxitic (A)	Sparse (50-75% ice) (s) Medium (75-95% ice) (m) Dense (95-99% ice) (d)	Round (r) Angular (a) Blocky (b)	Same as above
Solid (S) (>10 cm thick)	Clear (c) Opaque (o) Dirty (<1% soil particles) (d) Porous (p) Columnar (r) Sheet, horizontally stratified (h) Wedge, vertically stratified (w)		

Appendix Table C-1. (cont.)

Class	Definition
Pore	Ice in minute holes, or pores, within mineral soil matrix that has an almost structureless appearance. May be visible (without handlens) or non-visible. Visual impression is that ice does not exceed original voids in soil. Forms where pore water freezes <i>in situ</i> .
Organic-matrix	Ice formed within organic matrix and has a structureless appearance. May be visible or non-visible. Mostly formed where pore water freezes <i>in situ</i> .
Crustal	Ice coating or rind around, or on the bottom of, a rock clasts or wood fragments.
Vein	Isolated, thin lens, needle-like or sheetlike structures, or particles visible in the face of soil mass. Usually inclined and bisecting sedimentary structures. Differs from layered ice in that they are solitary and do not have a repeated, parallel pattern.
Lenticular	Lens-shaped, thin (generally < 0.5 mm), short bodies of ice within a soil matrix. The orientation is generally normal to the freezing front and usually reflects the structure of the sediments.
Layered	Laterally continuous bands of ice less than 10 cm thick. Usually parallel, repeating sequences that follow with sedimentary structure or are normal to freezing front. Thicker layers (> 10 cm) are described as solid ice. Sparse: ice layers <5% of structure. Medium: ice layers 5-25% of structure Dense: ice layers 25-50% of structure.
Reticulate	Net-like structure of ice veins surrounding fine-grained blocks of soil. Ice occupies up to 50% of surface area. Trapezoidal: ice has distinct horizontal parallel veins with occasional diagonal, vertically oriented veins. Soil blocks have trapezoidal appearance due to fewer vertical veins than lattice-like ice. An incomplete form of latticelike reticulate ice. Latticelike: ice exhibit regular, rectangular or square framework. Foliated: irregular horizontally dominated ice giving soil a platy structural appearance.
Ataxitic	Ice occupies 50-99% of cross-sectional area, giving the soil inclusions a suspended appearance. Sparse: ice occupies 50-75% area, soil inclusions occupy 25-50% of area. Medium Inclusions: ice occupies 75-95% of area, soil inclusions occupy 5-25%. Dense Inclusions: ice occupies 96-99% of area, soil inclusions occupy 1-5%.
Solid	Ice (>10 cm thick) where soil inclusions occupy <1% of the cross-sectional area. Clear Ice: no visible inclusions. Opaque Ice: cloudy or milky appearance. Dirty Ice: Individual soil grains, granules, or rock clasts visible but occupy <1% of area. Porous: ice contains numerous, interconnected voids, usually resulting from melting between air bubbles or along crystal interfaces from presence of salt or other materials in water. Though porous, the mass is firm or rigid. Columnar Ice: Ice that has melted or irradiated into long columnar crystals, very loosely bonded together. Stratified ice: Unspecified ice exhibits obvious banding or striations due to differences in color or sediment. Sheet ice: Cloudy or dirty, horizontally bedded ice exhibiting indistinct to distinct stratification. Wedge Ice: V-shaped masses of vertically foliated or stratified ice resulting from infilling of frost fissures. Best identified when large exposures or cross-sections are visible.

Appendix Table C-2. Integrated terrain units for ecological land classification system of the Colville River Delta, 1996.

Code	Class	Code	Class
TERRAIN UNIT		SURFACE-FORM	
DEPOSITS		0	N Nonpatterned
330	Cs Solifluction deposit	2	Pd Polygons, disjunct
380	Es Eolian sand dunes	3	Pf Polygons, flat-centered
411	Fdrl Delta, riverbed/riverbars (412)	5	Pill Polygons, low-cent., low-relief, low-dens.
413	Fdrh Delta, high-water channel	6	Pllh Polygons, low-cent., low-relf, high-dens.
415	Fdca Delta, active-floodplain cover deposit	7	Plhl Polygons, low-cent., high-relf, low-dens.
416	Fdci Delta, inactive-floodplain cover deposit	8	Plhh Polygons, low-cent., high-relf., high-dens
417	Fda Delta, abandoned-floodplain cover deposit	9	Pm Polygons, mixed high and low
441	Fpr Floodplain, riverbed deposit	11	Phl Polygons, high-centered, low-relief
443	Fpca Floodplain, active-floodplain cover deposit	12	Phh Polygons, high-centered. high-relief
444	Fpci Floodplain, inactive-floodplain cover deposit	17	Tm Mixed pits and polygons
452	Fpa Floodplain, abandoned-floodplain cover dep.	21	Fh Hummocks
545	Fto Alluvial terrace (ancient floodplain)	23	Ff Frost scars
595	FGp Alluvial plain deposit (undifferentiated fluvial)	31	Mud Mounds, undifferentiated, dense
816	Ltn Thaw basin, non-ice rich	35	Mpi Pingos
817	Lti Thaw basin, ice-rich	39	Ms Strang
818	Ltdn Delta thaw basin, non-ice rich	62	Ek Dunes, streaked
819	Ltdi Delta thaw basin, ice-rich	81	Dw Water tracks
860	Mp Alluvial-marine terrace	85	Db Streambank
862	Mt Tidal Flat	96	Si Islands Present
872	Hfg Fill, gravel	97	Sm Water with highly polygonized margin
874	Hfp Fill, peat (peat roads)	98	L Cliff or Bluff
		101	Cb Basin Complex
WATERBODIES (with original mapping codes)		VEGETATION	
905	Rt River, tidal	0	B Barren (<5% vegetated)
910	Rl River, lower perennial	10	P Partially Vegetated (Hairgrass, Elymus)
918	Rb River, thermokarst (beaded stream)	221	Stcw Closed tall willow shrub
922	Ldi Deep isolated lake	231	Stow Open tall willow shrub
922/96	Ldi Deep isolated lake w/ islands	242	Slcw Closed low willow shrub
922/97	Ldip Deep isolated lake, with polygonal marg.	260	Slow Open low willow shrub (can include sedges)
925	Ldir Deep isolated lake., riverine	270	Sdd Dryas dwarf shrub (also w/ sedge or lichens)
930	Ldc Deep connected lake	295	Sdwh Halophytic dwarf willow shrub (coastal)
930/96	Ldc Deep connected lake with isl.	314	Hmt Mesic tussock tundra
930/97	Ldc- Deep connected lake w/ polyg. margins	320	Hmss Mesic sedge-shrub tundra (dryas/willow)
941	Lsi Shallow isolated pond	328	Hmsk Salt-killed mesic meadow
941/96	Lsi Shallow isolated pond with isl.	334	Hwsw Wet sedge-willow meadow (also w/o willow)
941/97	Lsi Shallow isolated pond w/ poly margins	336	Has Fresh sedge marsh
416/7/336	Lsi Shallow isolated w/ deep poly centrs	337	Hag Fresh grass marsh
943	Lsir Shallow isolated pond, riverine	345	Hwhg Halophytic grass wet meadow
948	Lsid Shallow isolated pond, dune depression	346	Hwhs Halophytic sedge wet meadow
950	Lsc Shallow connected pond	348	Hwhk Salt-killed wet meadow
950/96	Lsc Shallow connected pond with isl.	411	Cby Basin wetland complex, young
950/97	Lsm Shallow connected pond w/ poly margins	412	Cbo Basin wetland complex, old
963	En Nearshore water		
983a	Etdl Deep Tapped Lk w/ low-water connection	EXAMPLE OF CODING SYSTEM	
984	Etdh Deep Tapped Lk w/ high-water conn.	Landform, Surface-form, Vegetation	
986	Etsl Shallow Tapped Lk w/ low-wat conn.	412/6/331 or 941/96/337	
987a	Etsh Shallow Tapped Lk w/ high-water conn.		
989	Ep Brackish ponds (Tidal affected)		
989/97	Epp Brackish ponds w/ polygonized margin		
996	Hl Sewage lagoon		
997	Hr Reserve pit		